
THE UNIVERSITY
*of* EDINBURGH

# The CX3CR1/CX3CL1 Axis Drives the Migration and Maturation of Oligodendroglia in the Central Nervous System

Catriona Ford

Thesis Submitted for the Degree of Doctor of Philosophy

The University of Edinburgh

2017

# Abstract

In the central nervous system, the axons of neurons are protected from damage and aided in electrical conductivity by the myelin sheath, a complex of proteins and lipids formed by oligodendrocytes. Loss or damage to the myelin sheath may result in impairment of electrical axonal conduction and eventually to neuronal death. Such demyelination is responsible, at least in part, for the disabling neurodegeneration observed in pathologies such as Multiple Sclerosis (MS) and Spinal Cord Injury. In the regenerative process of remyelination, oligodendrocyte precursor cells (OPCs), the resident glial stem cell population of the adult CNS, migrate toward the injury site, proliferate and differentiate into adult oligodendrocytes which subsequently reform the myelin sheath.

Existing research indicates that OPC migration is directed by chemomigratory signals released from the site of injury and that the absence of OPCs is a feature of some MS lesions, suggesting that increased recruitment of OPCs to injury sites might improve remyelination, eventually leading to treatments of patient pathologies. I hypothesized that as yet undiscovered migration cues for OPCs might be released at sites of demyelination, diffuse through the CNS tissue, activate distal OPCs and guide them back to sites of demyelination.

In this thesis, I performed bioinformatics analysis of gene expression arrays and identified upregulated cell surface receptors on OPCs activated in a cuprizone model, and upregulated secreted factors in whole lesion sites from an LPC induced MS type injury model and a Spinal Cord Injury model. I then optimised the X-celligence system for the quantification of OPC migration in response to secreted factors identified in my bioinformatics screen. By combination of these techniques with immunofluorescent staining I discovered novel expression of the cell surface receptor CX3CR1 on OPCs, increased expression of the corresponding ligand CX3CL1 in both MS type injury and Spinal Cord Injury, increased directional migration of OPCs in response to low concentrations of CX3CL1, and increased maturation of OPCs into adult oligodendrocytes at high concentrations of CX3CL1.

Taken together these results propose a system in which an increasing gradient of CX3CL1 released from the site of injury directs the recruitment, then maturation of OPCs, making CX3CL1 a master regulator of OPC led CNS regeneration.

# Lay Summary

In the brain and spinal cord, the neurons which relay electrical signals are protected and insulated by the myelin sheath which is made by support cells known as oligodendrocytes. Loss of the myelin sheath can lead to the death of neurons which prevents the brain from sending signals properly and can cause disability in conditions like Multiple Sclerosis (MS) and Spinal Cord Injury.

For lost myelin to be replaced repair brain cells scattered throughout the brain and spinal cord must migrate into the injury site, change into adult oligodendrocytes and make new myelin sheaths. In conditions like MS and Spinal Cord Injury this repair process does not always work properly because the repair stem cells do not find their way to the area needing repaired.

The purpose of my project was to find a way to recruit more of these repair stem cells into injury sites. By analysing online databases, I identified chemical signals released at the site of injury and studied cells cultured in a dish to find out if adding these chemical signals increased repair, stem cell migration or the maturation of repair stem cells into oligodendrocytes.

I found a protein called CX3CL1 which made the repair stem cells migrate and mature more quickly and it is hoped that we might be able to develop CX3CL1 into a drug to treat MS and Spinal Cord Injury in the future.

# Declaration

The work for this doctoral thesis was conducted at the Scottish Centre for Regenerative Medicine at the University of Edinburgh. I declare that the research described within this thesis is my own work and that this thesis was composed by myself unless otherwise specified in the text or the acknowledgements.

Neither this dissertation nor part thereof has been submitted for academic merit at another educational institution.

Catriona Ford, January 2017

# Acknowledgements

Accomplishment of the body of work which makes up this thesis would not have been possible without the support of a number of others.

I would firstly like to sincerely thank my primary supervisor Professor Anna Williams for her insight, guidance and unwavering support throughout my experimental work and thesis writing. I would also like to thank my secondary supervisor Dr Simon R Tomlinson for his supervision and support throughout the bioinformatic component of the project, and my thesis committee Professor Lesley Forrester and Professor Charles ffrench-Constant.

In addition, this project would not have been possible without the wit and wisdom of both past and present members of the Williams and Tomlinson labs, in particular Dr Rikesh Rajani, Elitsa Peeva, Amanda Boyd, Misuzu Hashimoto, Claire Fournier, Dr Sowmya Sekizar, Dr Eva Borger, Sonja Rittchen, Silvie Ruigrok, Thomas Carr, Dr Florian Halbritter, Dr Jonathan Manning, Alison McGarvey, Anastasia Kousa, James Ashmore and Will Bowring.

I would also like to thank the Medical Research Council for funding my scholarship, and the Scottish Centre for Regenerative Medicine for hosting my project.

Finally, I would also like to thank my family and friends for their constant interest (feigned or otherwise!) and encouragement and my partner Duncan Godwin, not only for his positivity and endless reassurance through the difficult times, but also for the crash courses in Java/Javascript and remote controlled Lego cars.

**Contents**

Chapter 1

# Introduction

In the adult central nervous system (CNS), the process of remyelination is central to regenerative tissue repair. Successful remyelination requires the presence of oligodendrocyte precursor cells (OPCs) at sites of injury. OPCs at the injury site have the capacity to differentiate into adult oligodendrocytes and subsequently repair the myelin sheath, thus restoring protection, trophic support and increased conduction velocity to the axons. Inefficient remyelination results in impaired conduction of neural impulses and possible axonal destruction leading to the symptoms typical of neurodegenerative disorders such as Multiple Sclerosis (MS). Remyelination is known to be insufficient in MS and previous research (including in the Williams' group) has shown that some MS lesions are either deficient or devoid of OPCs (Boyd et al., 2013a; Chang et al., 2002; Lucchinetti et al., 1999), due to a lack of OPC migration into lesion sites. In order to effectively contribute to remyelination, OPCs, which are distributed throughout the uninjured CNS, must become activated and migrate to the site of injury by following chemomigratory cues. Therefore, identification of chemical signals which improve the recruitment of OPCs to sites of injury may later lead to the development of regenerative therapies for pathologies such as MS.

At the outset of this PhD project, I hypothesized that these chemomigratory stimuli were present after demyelinating injury during remyelination and could be recognised by their ability to increase OPC migration *in vitro*. To test this hypothesis, in this thesis:

1) I identified possible modulators of OPC migration by bioinformatic analysis of microarray data from demyelinating injury.

2) I optimised the X-celligence Real-Time Cell Analysis (RTCA) system for the specific requirements of the analysis of directional cell migration in OPCs.

3) I identified the secretion of the chemokine fractalkine/CX3CL1 at the lesion site and the expression of its only known receptor CX3CR1 on OPCs and showed increased directional OPC migration at low concentrations of CX3CL1 and increased differentiation of OPCs into adult oligodendrocytes at a high concentration of CX3CL1.

In my introductory chapter, I will discuss the biology of OPCs and myelination, as well as the relevance of the regenerative process of remyelination in the context of demyelinating diseases in humans.

## 1.1 Myelin

### 1.1.1 Myelin and the Propagation of Electrical Impulses

In the mature central nervous system, the electrically conductive axonal tracts of neurons are wrapped by spiralling layers (Geren and Schmitt, 1954) of oligodendrocyte membrane, providing insulation and made of a complex of proteins and lipids known as myelin. The presence of a distinguishable white or "marrow-like" substance associated with the outside of nerve fibres was first documented as early as the 16$^{th}$ to 17$^{th}$ centuries (reviewed in Boullerne, 2016). The term "myelin" is derived from the Greek *myelos* meaning marrow, and was first used in 1854 by the German pathologist Rudolph Virchow (Virchow, 1854).

### 1.1.2 Myelin Composition

Myelin is a diverse composite made up of 70% lipids and 40% proteins. Of the protein content up to 30% is made up of myelin basic protein (MBP), 50% proteolipid protein (PLP), 4% 2',3'-Cyclic nucleotide 3'-phosphodiesterase (CNP), 1%(CNS)/0.1%(PNS) myelin associated glycoprotein (MAG) and the remainder by myelin oligodendrocyte glycoprotein (MOG) and small amounts of other proteins (Baumann and Pham-Dinh, 2001).

The high lipid content of myelin gives myelin rich regions of the CNS a whitish appearance in formaldehyde fixed tissue. Consequently, these areas which are around 40 – 50% myelin by dry weight (Baumann and Pham-Dinh, 2001), are known as the white matter in contrast to the sparsely myelinated grey matter. While the grey matter regions are chiefly functionally associated with processing and cognition, containing the neuronal cell bodies, the primary function of the white matter regions is to transport neuronal signals between the different grey matter regions. White matter regions include the Corpus Callosum through which the two cerebral hemispheres are connected, and the white matter tracts in the spinal cord containing the long axons of spinal cord neurons which relay information to and from to the brain.

### 1.1.3 Myelin Function

Within the nervous system, information is relayed through the propagation of electrical impulses along axonal tracts, however the escape of electrons from the nerve fibres

retards conduction velocity. In non-myelinated nervous systems, conduction velocity is improved by increasing axonal diameter, as exemplified by the super axons observed in organisms such as crustaceans, insects and cephalopods.

In other organisms with highly developed nervous systems including mammals, conduction velocity is improved through the insulator process of myelination. In contrast to the axonal tracts themselves, myelin is not electrically conductive and is therefore able to prevent the dissipation of electrical signals into the nervous system parenchyma.

Each axon is wrapped by multiple segments of myelin sheath known as internodes which are periodically interrupted by brief unmyelinated breaks known as the nodes of Ranvier. Electrical signals travelling along myelinated tracts appear to "jump" between nodes of Ranvier via the process of saltatory conduction (derived from the Latin *saltare*, to leap or hop), which was first described in the mid-20$^{th}$ century, first reported by Tasaki in 1939 and corroborated by Huxley and Stämpfli in 1949. However, the electrical impulse only appears to jump between the nodes of Ranvier because of the high conduction velocity it is able to achieve as it is relayed through the myelinated internodes.

This concerted direction of electrical impulses by myelin improves the efficiency with which neuronal signals can be propagated over long distances. Accordingly, the development of myelin is of great evolutionary significance because the increase in the distance over which nerve impulses could be efficiently propagated facilitated the adaption of large complex nervous systems in larger organisms such as mammals.

While both the central nervous system(CNS) and peripheral nervous system(PNS) propagate electrical impulses along the axons of neurons, there is a significant divergence in the format of their myelin and the cell types which produce it.

In the PNS, myelination is carried out by the myelinating Schwann cells. Each Schwann cell forms a close relationship with a single axon and produces only one myelin internode so that each axon is wrapped by multiple Schwann cells each separated by a node of Ranvier. Conversely, in the CNS myelination is carried out by the oligodendrocytes which have the capacity to produce multiple internodes and wrap as many as 40 axons concurrently (discussed in Baumann and Pham-Dinh, 2001).

### 1.1.4 Adult Oligodendrocytes are Unable to Regenerate

Both Schwann cells and oligodendrocytes are glial cell types, which besides increasing electrical impulse conduction velocity, perform the dual functions of providing trophic support to the neurons and protecting axons from destruction.

In the context of regeneration following a destructive insult, there are differences in functionality between the Schwann cells and oligodendrocytes. In PNS injury, adult Schwann cells retain their developmental plasticity and revert back to a stem cell like state, allowing for their capacity to proliferate, migrate along axon tracts and replace lost myelin (reviewed, Jessen and Mirsky, 2016).

In contrast, once individual oligodendrocytes have wrapped their associated axons, they appear to be unable to form new myelin sheaths beyond the end of the developmental stage (Crawford et al., 2016). Thus, myelin sheaths lost via mechanical injury or inflammatory attack cannot be replaced by existing oligodendrocytes. Oligodendrocytes also provide trophic support to the neurons. through the production of factors which promote neuronal survival (Bankston et al., 2013). The loss of oligodendrocytes and myelin sheaths therefore, have pathological implications because, without the insulation of protective myelin, axons are unable to efficiency conduct electrical impulses, lack trophic factors provided by oligodendrocytes, and are at greater risk of destruction.

## 1.2 Development

### 1.2.1 Myelination in Development

During the development of the human CNS, magnetic resonance imaging (MRI) has revealed that the essential process of myelination begins during gestation and extends well beyond early adult life (reviewed Baumann and Pham-Dinh, 2001; Boulanger and Messier, 2014). A 2012 study using histological examination of the myelinated fibre density in the somatosensory, motor and visual cortices of post-mortem human tissue from birth, childhood, adolescence and adulthood showed that full myelination in these regions was not complete until well into the third decade (Miller et al., 2012). More recently, it has also been shown that myelin continues to be laid down and remodelled over lifetimes, contributing to the plasticity of the adult CNS (O'Rourke et al., 2014; Young et al., 2013).

This prenatal onset of myelination is dependent on the presence of newly differentiated oligodendrocytes which are derived from stem cell like progenitor cells.

### 1.2.2 Oligodendrocytes are the Terminally Differentiated Progeny of Increasingly Lineage Restricted Precursors

Mature oligodendrocytes can be found throughout the adult CNS, however there has been significant debate in the literature as to where and when oligodendrocytes and their precursors first arise in the developmental CNS (discussed at length in Naruse et al., 2016a; Richardson et al., 2006).

Oligodendrocytes ultimately trace their lineage back to the neuroepithelial cells of the embryonic neural tube which have the capacity to produce both neurons and glia as progeny. The dorsal region of the neural tube develops into the adult brain while the ventral portion matures into the spinal cord (reviewed in Grabel, 2012). A subset of neuroepithelia differentiates into the more lineage restricted neural stem cells (NSCs) of which all oligodendrocytes are progeny.

NSCs have the plasticity to differentiate into neurons, astrocytes and oligodendroglia during development (McKay, 1997; Rao, 1999) and persist in neurogenic niches in the adult CNS, generating new neurons in areas such as the olfactory bulb and dentate gyrus of the hippocampus (Gage, 2000; Yamaguchi et al., 2016). NSCs perform their diverse functions at different temporal stages of CNS development, proliferating in the early embryo, differentiating into neurons in the mid embryonic period and producing oligodendroglia in the late embryonic stage and postnatally (Naruse et al., 2016a).

Oligodendrocyte precursor cells are an intermediate cell type between NSCs and oligodendrocytes and similar to NSCs, are found in the adult as well as developmental CNS (Crawford et al., 2014; Dawson et al., 2003). The precise developmental timings of the differentiation of OPCs into adult oligodendrocytes are yet to be clearly defined, in part because the explosive proliferation of OPCs immediately prior to differentiation into oligodendrocytes, making lineage tracing experiments difficult (Naruse et al., 2016a; Raff et al., 1998). Developmental OPC dynamics are further complicated by controlled OPC cell death, concurrent with the process of myelination. In a recent study, in myelinating organotypic cerebellar cortex slices, OPC numbers were found to be curtailed by endogenous release of the neurotransmitter GABA (Hamilton et al., 2017).

### 1.2.3 Developmental OPCs First Arise in Late Gestation to Early Neonatal Phase

To investigate the true origins of OPCs in development, it was necessary to examine the behaviour of the NSCs from which OPCs originate in finer detail. During development, multipotent nestin expressing NSCs may leave the cycle of self-renewal in order to

become lineage committed fully differentiated cell types (Alvarez-Buylla et al., 2001; Okano and Temple, 2009). In order to pinpoint the exact timing of differentiation of NSCs into OPCs, in a recent study by Naruse and colleagues used Cre-LoxP reporter systems to permanently green fluorescent protein (GFP) label cells expressing the NSC marker nestin or the oligodendroglial lineage marker oligodendrocyte transcription factor 2 (Olig2) in separate mice at three developmental time points (Naruse et al., 2016b). Cells labelled as nestin positive at E12 or E16 were found to produce few oligodendroglia when cortices were imaged at P30, however, over 80% of cells labelled as nestin positive at P10 were detected as oligodendroglia at P30 (although the actual number of cells is not given in the paper).

Taken together, these findings suggest that NSCs which are destined to become oligodendrocytes cease expression of nestin and begin expression of Olig2 between just before E16.5 and P10. Thus, OPCs (intermediates between NSCs and oligodendrocytes), arise in the period from late gestation to the early neonatal stage.

### 1.2.4 CNS Patterning in Development

While the timely emergence of OPCs is essential to CNS development, the spatial distribution of oligodendroglial lineage cells within the embryo is also of immense importance. By the conclusion of the developmental stage, OPCs and adult oligodendrocytes have become distributed throughout the CNS, a process which is regulated by the orchestration of complex extracellular signals and intracellular responses.

The CNS is derived from the neural tube, the dorsal portion forming the telencephalon which becomes the cortex, and the ventral portion forming the developing spinal cord. It was once thought that all oligodendroglial precursors arose in the mid-line of the ventral regions of both the nascent brain and spinal cord, before migrating outwards to reach the rest of the developing CNS tissue. However, more recent evidence has supported additional dorsal sources of OPCs in both CNS structures and contribution of both dorsally and ventrally derived OPCs to the adult OPC and oligodendrocyte population reviewed in Naruse et al., 2016a; Richardson et al., 2006).

During the development of the CNS, the first positions of OPCs are dictated by the location of the NSCs from which they as derived. The positioning and differentiation of NSCs is directed by concentration gradients of morphogens which restrict them to the dorsoventral and anteroposterior axes (Hitoshi et al., 2002; Mehler, 2002; Shimogori et

al., 2004; Zappone et al., 2000). Significant signalling molecules include sonic hedgehog (Shh) which is indispensable for ventral patterning of both the developing spinal cord and telencephalon (Dessaud et al., 2008; Echelard et al., 1993; Fuccillo et al., 2004; Jessell, 2000; Sousa and Fishell, 2010; Yu et al., 2013), while Wnts and bone morphogenetic proteins (BMPs) are released from spinal cord roof plate and cortical hem in the telencephalon thus directing dorsal patterning (Chizhikov and Millen, 2005; Liem et al., 1997; Muroyama et al., 2002; Shimogori et al., 2004, 2004).

### 1.2.5 Origins of OPCs in the Developing Spinal Cord

#### 1.2.5.1 Historical Ventral Perspective on OPC Origins – Spinal Cord

There are two known sources of OPCs in the developing spinal cord, the historically established ventral source in the ventral motor neuron progenitor (pMN) domain and the more recent discovery of an OPC source in the more dorsal p0 domain. The idea of single ventral source for OPCs in the developing spinal cord was brought into question by the identification of glial restricted precursors (GRPs) (which demonstrated the potential to become oligodendrocytes or astrocytes but not neurons *in vitro*), in both ventral and dorsal regions of the embryonic spinal cord (Rao et al., 1998).

Developmental oligodendroglia have been shown to express the established OPC marker platelet derived growth factor receptor alpha (PDGFrα) as early as E12. These PDGFrα+ OPCs arise in the pMN domain of the spinal cord, which contains specific neural precursor cells which are first destined to produce motor neurons but undergo a later fate change to produce OPCs (Richardson et al., 2000) (see **figure 1.1 b)i-b)iv**).

Secretion of Shh from the floorplate of the notochord plays a pivotal role in the patterning of the developing ventral spinal cord (He and Lu, 2013) and the generation of OPCs and oligodendrocytes. The developing spinal cords of mice deficient in either Shh or two of its downstream target transcription factors NK2 Homeobox 6.1 (Nkx6.1) and NK2 Homeobox 6.2 (Nkx6.2), have been shown to be devoid of Olig2+ OPCs (Cai et al., 2005; Vallstedt et al., 2005) (see **figure 1.1 b)iii-iv** and **c)iii-iv**).

Another major player in the generation of OPCs in the ventral spinal cord is the basic helix-loop-helix (bHLH) transcription factor Olig2. Despite its widespread use as an oligodendroglial marker, the protein is also expressed by pMN neural precursors and is indispensable for the differentiation of motor neurons (Lu et al., 2000; Takebayashi et al., 2000; Zhou et al., 2000).

Olig2 knockout mice fail to produce either motor neurons or oligodendroglia in the spinal cord and perish within hours of birth (Lu et al., 2002; Takebayashi et al., 2002). There is evidence that the fate choice between motor neurons and oligodendroglia may be driven by phosphorylation of Olig2. Phosphorylation of the Olig2 bHLH domain results in the differentiation of motor neurons while dephosphorylation of Olig2 alters its range of binding partners and results in the generation of OPCs (Li et al., 2011). Thus, Shh and Olig2 are the major drivers of the differentiation of OPCs from the pMN domain in the spinal cord.

#### 1.2.5.2 Dorsal Origin of OPCs in the Spinal Cord

The historical view that OPCs were generated only in the ventral embryonic spinal cord has been challenged by contradictory reports of an OPC source in the dorsal spinal cord. Explants taken from both the ventral and dorsal regions of E11 spinal cord are capable of producing O4 positive oligodendroglia in *in vitro* culture, although this process is less rapid in dorsal explants (Sussman et al., 2000) (see **figure 1.1 a)ii, b)ii** and **c)ii**). The inability of the intermediate portion between the dorsal and ventral regions to produce O4 positive progeny rules out the possibility of invasion of progenitors from the ventral to dorsal region. Similarly to ventrally derived OPCs, the generation of oligodendroglia by cultured explants was shown to be Shh dependent.

In their 2005 study, Cai and colleagues used an elegant system using knock outs of Nkx6 proteins to demonstrate a second dorsal origin of OPCs in the developing spinal cord (Cai et al., 2005). Nkx6.1 and Nkx6.2, which are both downstream of Shh and upstream of Olig2, have been found to be functionally redundant in the differentiation of motor neurons (Vallstedt et al., 2001). Knock-out of both Nkx6.1 and Nkx6.2 resulted in the complete abolition of Olig2 expression at E10.5 and E12, however expression of Olig2 in Nkx6 double mutant could be detected in the dorsal region at E13.5 to E15.5 and throughout the spinal cord at E18.5 (see **figure 1.1 b)ii** and **c)ii**). Other markers of OPCs such as PDGFrα and SRY-Box 10 (Sox10) which are detectable throughout the spinal cord from E13.5 onward, had similarly delayed patterns of expression in Nkx6 double mutants with no detectable expression in either gene at E13.5 and E15.5 but expression throughout the spinal cord in both genes at E18.5. Co-localisation of Olig2 and dorsal neuronal marker paired box protein 7 (Pax7) antibody in wild type mice, confirmed the dorsal source of OPCs in the developing spinal cord *in vivo*.

In contrast to the Sussman and colleagues explant study, Cai and colleagues found the generation of OPCs from the dorsal spinal cord to be independent of Shh signalling, this corresponds with earlier studies which found the spinal cord to be dorsalized and lacking in ventral regions in Shh knock-out mice (Chiang et al., 1996; Pierani et al., 1999) (see **figure 1.1 b)iii-b)iv** and **c)iii-c)iv**). Whether or not the dorsal source of oligodendroglia is Shh dependent is thus rendered somewhat irrelevant from a functional perspective, since the absence of sonic hedgehog signalling is incompatible with life.

Further evidence for a dorsal source of oligodendroglia in the spinal cord is also supported by evidence from studies using Cre/loxP reporter systems in which the Cre recombination was placed under the control of the promotor for dorsally expressed genes, developing brain homeobox 1 (Dbx1), genetic screened homeobox protein 2 (Gsh2) or murine msh homeobox 3 (Msx3) (Fogarty et al., 2005; Tripathi et al., 2011). Co-expression of OPC markers such as Olig2 and Sox10 with these dorsal markers in the developing spinal cord corroborates a dorsal origin for a proportion of spinal cord OPCs and subsequent oligodendrocytes.

As summarised in **figure 1.**1, the evidence for both ventral and dorsal origins of OPCs in the spinal cord indicates that spinal cord oligodendroglia are derived from at least two regions, and that their genesis may be Shh dependent or independent. Regardless of the exact location of their origin, OPCs migrate out from the central ventral-dorsal line to dissipate throughout the spinal cord white matter by the end of development. This ability to migrate is central to the importance of OPCs, an ability which is also retained by the OPCs in the adult brain.

Catriona Ford



| Developmental Stage | Normally Developing Spinal Cord | Explants from Wild Type Spinal Cord at E11 | Nkx6.1/Nkx6.2 Double Mutant Knock-out | Shh Knock-out |
|---|---|---|---|---|
| **a)** E11 | **i)** 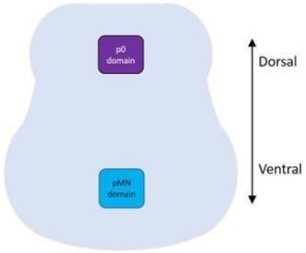 | **ii)** 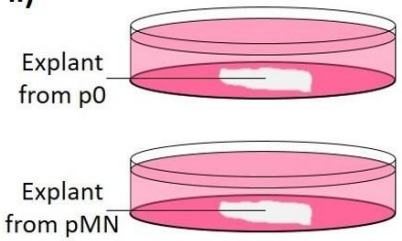 | **iii)** 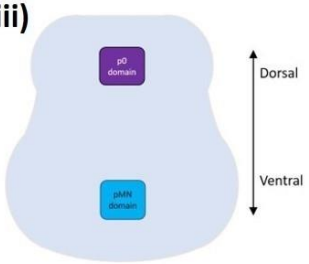 | **iv)** 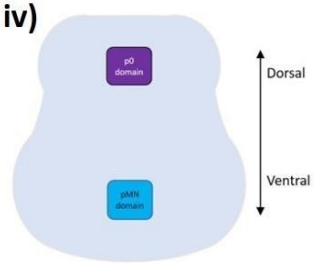 |
| **b)** E12 | **i)** 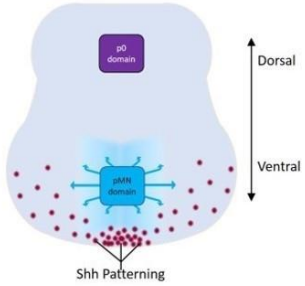 | **ii)** 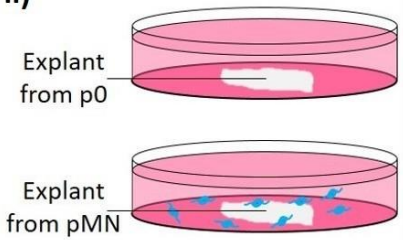 | **iii)** 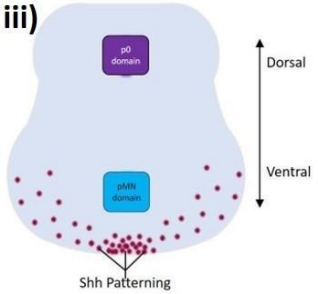 | **iv)** 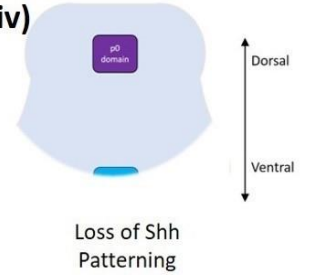 |
| **c)** E13.5-E15.5 | **i)** 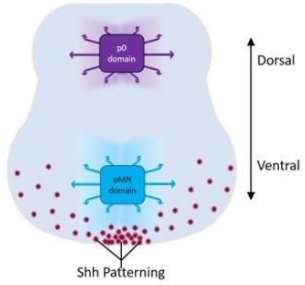 | **ii)** 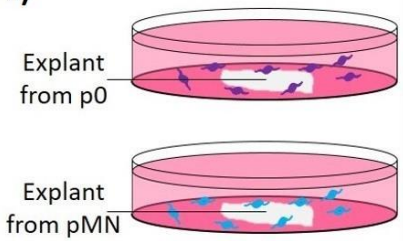 | **iii)** 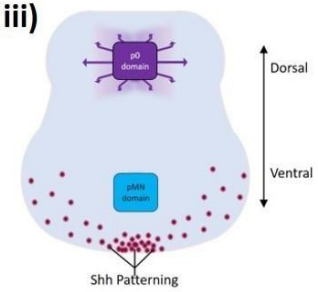 | **iv)** 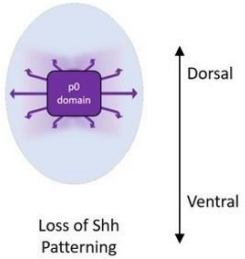 |

**Figure 1.1 OPCs arise in both the dorsal p0 domain and ventral pMN domain in the developing spinal cord.** At E11, in **a)i)** normally developing spinal cord , **a)ii)** freshly dissected dorsal p0 and ventral pMN explants, **a)iii)** Nkx6.1/Nkx6.2 double mutant knock-outs and **a)iv)** Shh knock-outs, OPCs are yet to arise and there is no evidence of OPCs in either the p0 or pMN domains. By E12, in **b)i)** normally developing spinal cord, Shh emanating from the floor plate of the notochord induces the emergence and dissemination of OPCs from the ventral pMN domain (illustrated as blue arrows) **b)ii)** At E12 OPCs (illustrated in blue) are observed to emerge from ventral pMN domain explants (dissected at E11 and cultured until E12), while no such OPCs emanate from equivalent p0 explants **b)iii)** As a result of the absence of Nkx6.1 and Nkx6.2 (downstream targets of Shh signalling), the developing spinal cord does not fully respond to Shh patterning, and no OPCs arise from either the dorsal p0 or ventral pMN domains **b)iv)** In the complete absence of Shh, at E12, no OPCs arise and the spinal cord becomes dorsalised **c)i)** By E13.5-E15.5, in normally developing spinal cord, OPCs are seen to emanate from both the ventral pMN domain (represented as blue arrows) and the dorsal p0 domain (represented as purple arrows) **c)ii)** Similarly, OPCs can be seen to arise from both p0 (purple) and pMN(blue) derived cultured explants **c)iii)** At E13.5-E15.5, in the absence of Nkx6.1 and Nkx6.2, OPCs fail to arise from the ventral pMN region, but do arise from the dorsal p0 region, indicating an additional Shh independent dorsal origin for spinal cord OPCs **c)iv)** This dorsal origin is confirmed by the emergence of OPCs from the p0 region of dorsalised Shh knock-out spinal cord. (figure adapted from Naruse et al., 2016a)

### 1.2.6 Origins of OPCs in the Developing Brain

#### 1.2.6.1 OPCs in the Developing Brain

As in the spinal cord, in the telencephalon (the developmental pre-runner of the cerebrum), OPCs arise first in the ventral portion which goes on to become the basal ganglia, and later in the dorsal portion which later forms the cerebral cortex. As shown in **figure 1.2a)**, OPCs first emerge at around E12 in the ventral ventricular and sub ventricular zones from the medial ganglionic eminence (MGE) to anterior entopeduncular area (AEP) under the direction of the morphogen Shh (Bulfone et al., 1993; Kessaris et al., 2001; Naruse et al., 2016b; Woodruff et al., 2001) . Generation of OPCs in the ventral telencephalon is dependent on Shh signalling and knock-out of NK2 Homeobox 2.1 (Nkx2.1) a critical upstream inducer of Shh, blocks the timely generation of PDGFrα positive OPCs in the ventral forebrain (Tekki-Kessaris et al., 2001).

Traditionally, cortical OPCs were thought to arise only from Nkx2.1 expressing precursors by this Shh dependent ventral mechanism, and while some of these ventrally

derived OPCs do migrate to the cortex (Kessaris et al., 2006; Nakahira et al., 2006), more recent evidence supports additional dorsally derived Shh independent sources. In the more dorsal cortical region in which Shh expression does not occur at any time, colonisation of the region by PDGFrα positive OPCs occurs by E17.5 to E20.5 in both wild-type and Nkx2.1 knockout mice (Tekki-Kessaris et al., 2001). This Shh independent OPC patterning in the developing telencephalon can be explained by the occurrence of three waves of OPC generation.

#### 1.2.6.2 OPCs Arise in Three Sequential Waves in the Developing Forebrain

Following the first wave of ventral OPC emergence (**figure 1.2a)**), a second wave of OPCs can be detected from E15.5 emanating from the MGE towards the more dorsal subventricular zones (**figure 1.2c)**), while a third wave colonise as far as the most dorsal regions of the developing cortex from around birth to early neonatal life (**figure 1.2e)**) (Kessaris et al., 2006).

Each wave of OPC generation is orchestrated by patterning of a different morphogen, a phenomenon elegantly documented in a 2006 study using inducible Cre fate mapping systems to visualise PDGFrα positive OPCs derived from precursor cell expressing either Nkx2.1, Gsh2 or Empty Spiracles Homeobox 1 protein (Emx1) between E12.5 and P2 (Kessaris et al., 2006). Experiments using Nkx2.1 reporter mice recapitulated the established view of an initial wave of Shh dependent OPC emergence from Nkx2.1 expressing precursors from around E12.5 some of which migrate to the cortical region (**figure1.2b)**). This was followed by a second wave beginning at around E15, in which OPCs derived from Gsh2 positive precursors emanate dorsally from the lateral ganglionic eminence (LGE) (**figure1.2d)**), and finally by a third wave, from P0 to P2 consisting of the emergence of OPCs from Emx1 positive precursors in the most dorsally located developing cortex (**figure1.2f)**). This process culminates in extensive coverage of the majority of cortical regions by OPCs derived from all three waves.

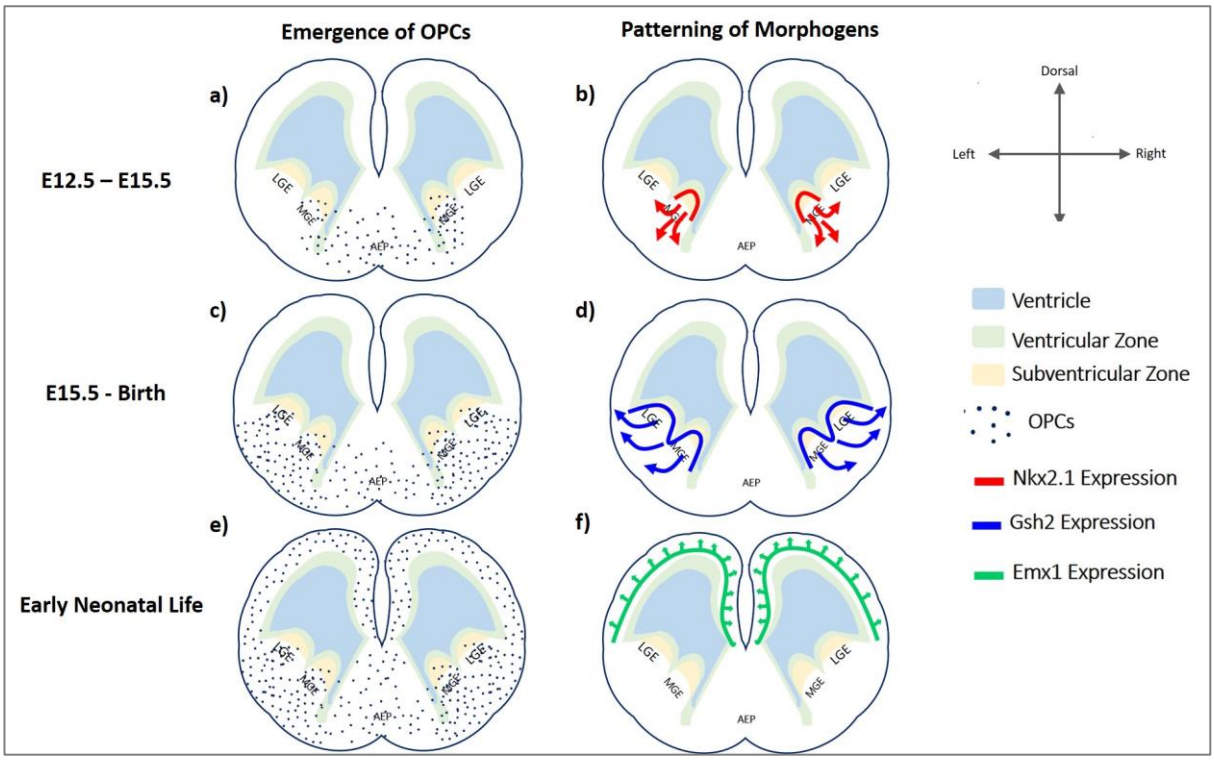


**Figure 1.2 OPCs in the developing telencephalon emerge in three waves.** Distribution of OPCs in the telencephalon at **a)** E12-E15.5, **c)** E15.5-birth and **e)** Early neonatal life. OPCs arising at: E12.5-E15.5 are derived from Nkx2.1 positive precursors emanating from the MGE **b)**, E15.5-birth are derived from Gsh positive precursors emanating dorsally from the MGE and LGE **d)**, Early neonatal life are derived from Exm1 positive precursors **f)**, figure adapted from Naruse et al., 2016a.

### 1.2.7 Origins of OPCs in the Developing Optic Nerve

In addition to the spinal cord and brain, another region of the developing CNS which has provided insight into the activities of nascent oligodendroglia is the developmental optic nerve. As shown in **figure 1.3**, in a similar fashion to the developing spinal cord and telencephalon, optic nerve OPCs arise from progenitor cells under the direction of Shh secreted by retinal ganglion cells (RGCs) (Merchán et al., 2007), this time in the proximal preoptic area which is located most dorsally from the retina between the third ventricle and the optic chiasm (Gao and Miller, 2006; Ono et al., 1997). OPCs can first emerge at the proximal end of the nerve at E14.5 from whence they dissipate out in a gradient from the optic chiasm toward the retina, so that they are homogeneously distributed over the whole optic nerve by E17.5 (Spassky et al., 2002).

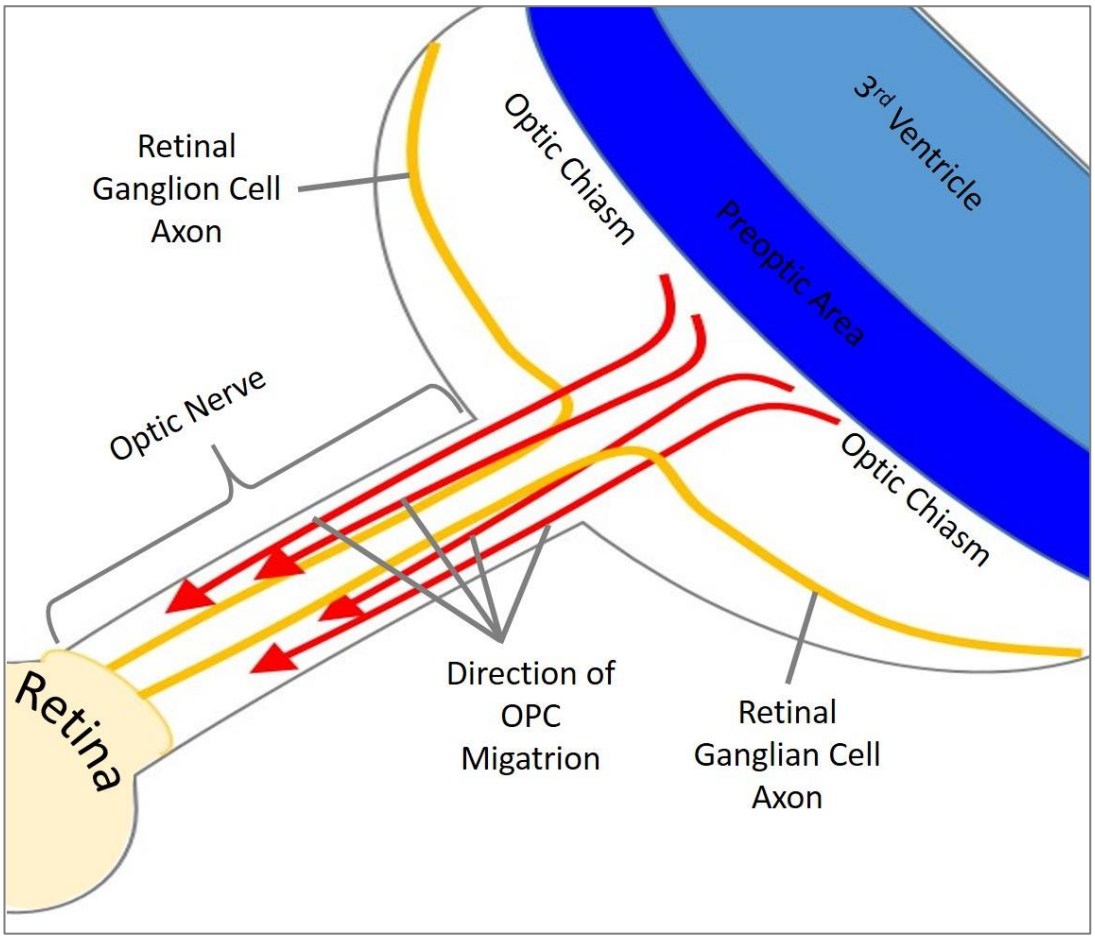


**Figure 1.3 Directional Migration of OPCs in the Developmental Optic Nerve** At around E.14.5 OPCs emerge in the Preoptic Area, under the direction of Shh secreted by the Retinal Ganglion Cells. OPCs then migrate from the Optic Chiasm to the Retina until they become dispersed in a gradient throughout the Optic Nerve by E17.5.

Regardless of their spatio-temporal origins and direct precursors, by the end of the developmental stage, OPCs migrate throughout the CNS, some differentiating into adult oligodendrocytes and the rest remaining at the precursor stage forming the resident adult glial stem cell population. While the emergence of OPCs from their precursors is vital for the establishment of a OPC population, migration of developmental OPCs from their origin to their diverse final spatial and functional destinations in the adult CNS is equally indispensable for mature CNS viability.

### 1.2.8 Developmental Migration of OPCs is Orchestrated by Chemomigratory Molecules

During the developmental stage, many OPCs migrate some distance from their site of emergence to their eventual terminus. This migratory behaviour has been shown to be the result of environmental factors rather than an intrinsic property of the OPCs themselves since OPCs transplanted from one region of the CNS to another adopt the migratory patterns of the recipient region as opposed to the donor region (Olivier et al., 2001). Directional migration or chemotaxis of OPCs is modulated via stimulation of their cell surface receptors by a variety of different factors including mitogens, chemokines, secreted growth factors and adhesion molecules in the extracellular matrix (ECM) (reviewed in de Castro et al., 2013). These chemical cues can be broadly split into two subtypes: chemoattractants which attract OPCs forwards and chemorepellants which repel OPCs preventing them from veering off track.

Chemomigratory factors for developmental OPCs are presented to the cell surface receptors in a number of different ways. Some, operate via contact-mediated mechanisms in which factor of interest is chemically bound to a surface with which the migrating OPC must make physical contact (reviewed de Castro and Bribián, 2005). Examples include extracellular matrix proteins such as Laminin, Fibronectin, Tenascin-C and Merosin (de Castro and Bribián, 2005; Frost et al., 1996; Garcion et al., 2001; Kiernan et al., 1996, 1999; Niehaus et al., 1999; Payne et al., 1996; Saga et al., 1992), transmembrane Semaphorins (classes 4, 5, 6 and 7) (Cohen et al., 2003), Neuregulins (Canoll et al., 1996; Milner et al., 1997), Ephrins (Prestoz et al., 2004) and Integrins(Milner et al., 1996, 1996; Niehaus et al., 1999; Tiwari-Woodruff et al., 2001).

Other factors are secreted molecules with the ability to disperse through the CNS parenchyma which contact OPCs independently from the cell types which secrete them. Examples include the ubiquitous PDGFα (Armstrong et al., 1990b; Dubois-Dalcq and Murray, 2000; Fruttiger et al., 1999; Milner et al., 1997; Simpson and Armstrong, 1999; Zhang et al., 2004), FGF-2 (Armstrong et al., 1990b; Bansal et al., 1996; Dubois-Dalcq and Murray, 2000; Milner et al., 1997; Osterhout et al., 1997; Simpson and Armstrong, 1999), Epidermal Growth Factor (EGF) (Fricker-Gates et al., 2000), Hepatocyte Growth Factor (HGF) (Yan and Rivkees, 2002), Vascular Endothelial Growth Factor (VEGF) (Zhang et al., 2003), Netrin-1 (Jarjour et al., 2003; Spassky et al., 2002; Sugimoto et al., 2001; Tsai et al., 2003), class 3 Semaphorins (Cohen et al., 2003; Ricard et al., 2001; Spassky et al.,

2002; Sugimoto et al., 2001) and Chemokine (C-X-C) Motif Ligand 1 (CXCL1) (Tsai et al., 2002).

### 1.3 Multiple Sclerosis

One of the diseases where remyelination of axons is important is Multiple sclerosis (MS). MS is a CNS disease with both inflammatory and degenerative neuropathology and was first documented in 1868 by Jean-Martin Charcot (Clanet, 2008). It is a leading cause of disability in young adults and has one of the highest incidences of non-traumatic neurological disorders worldwide (Browne et al., 2014). Despite improvements in both patient care and support services, between 2008 and 2013 the global prevalence of MS increased from 2.1 million to 2.3 million patients. Some of this augmentation in patient numbers can be attributed to earlier diagnosis and reporting and improved patient longevity (Browne et al., 2014). Scotland has one of the highest incidences of MS worldwide with 8.55 cases per 100,000 population (mean national incidence rate 2010 – 2015) (statistics from The Scottish MS Register 2016, http://www.msr.scot.nhs.uk/Reports/Main.html ). This reflects a worldwide trend in which cases of MS are most common in populations of European origin, distant from the equator. Such populations have a 0.1–0.2% lifetime risk of developing MS (Compston et al., 2005). While there is variability in the incidence and prevalence of MS across Europe (Kingwell et al., 2013), Europe is recognised as being a region of high MS incidence, with a reported incidence of ≥ 30/100,000 (Kurtzke, 2000) across the continent, which amounts to more than half the global population of known MS patients (Browne et al., 2014). In more northern regions of both Europe and North America prevalence has been reported at 0.1-0.2%, while yearly incidence is reported as 5-6 per 100,000 of the population (Goodin, 2016a; Wynn et al., 1990).

The underlying causes of MS are as yet poorly understood: the disease has not been exclusively linked to a single factor and appears to be multifactorial in its aetiology (Goodin, 2016a). While the disease does not follow a standard Mendelian inheritance pattern, in northern regions the siblings of MS probands have an increased risk of developing MS and monozygotic twins have a >200 fold increased risk (Ebers et al., 1995; Mumford et al., 1994; Willer et al., 2003), indicative of a strong genetic component. However, in southern populations the genetic link is weaker with the proband-wise concordance rate for monozygotic twins half of that in the north (French Research Group on Multiple Sclerosis, 1992; Islam et al., 2006; Ristori et al., 2006), suggestive of the

contribution of other aetiological components such as environmental factors and epigenetics.

Neurological symptoms associated with MS include deficits in vision, sensory perception and muscular weakness and balance (Noseworthy et al., 2000), all of which are the external manifestations of CNS damage. Multiple Sclerosis is characterised by the appearance of plaques of demyelination in the white matter, although it is now known that demyelination also occurs in the grey matter. White matter plaques can be identified by magnetic resonance imaging.

The pathologies associated with MS are the downstream result of the destructive attack of T-cells perpetrated against CNS components, most strikingly against myelin. Markers of MS in patients include the presence of oligoclonal immunoglobulin G in the cerebral spinal fluid (CSF), and gadolinium enhancing lesions in the CNS tissue during magnetic resonance imaging, indicative of inflammation as well as degeneration in the blood brain barrier (BBB) (Stys et al., 2012).

MS is primarily identified, by the demyelinating lesions in the brain and spinal cord, resulting from the immune attack (Sriram, 2011; Wu and Alvarez, 2011). These lesions can be classified into several subtypes. Acute plaques represent the earliest stages of formation of the lesion and are hallmarked by inflammatory infiltration and the distribution of Major Histocompatibility Class II (MHCII) expressing microglia and macrophages containing lipids and actively involved in the stripping of myelin from the axons(reviewed Frohman et al., 2006). Chronic plaques represent long term damage, and have regions of reduced cell density and glial scarring and distinct lesion borders. Chronic active plaques exhibit actively occurring damage at their borders. Chronic active lesion borders feature inflammation, microglia, macrophages astrocytes and perivascular cuffing, and some remyelinating may occur (reviewed Frohman et al., 2006). In chronic silent plaques, the demyelination and axonal destruction has already taken place, and no inflammation occurs at the border or elsewhere in the lesion. Chronic silent plaques are also devoid of remyelination or OPCs and feature the complete loss of oligodendrocytes and reduced density of axons (reviewed Frohman et al., 2006). In shadow plaques, the demyelination resulting from inflammatory damage has already been repaired by remyelination and myelin appears thinner than in normal appearing white matter (reviewed Frohman et al., 2006).

## 1.4 Regeneration

### 1.4.1 The Role of OPCs in the Normal Adult CNS

In the adult CNS, undifferentiated OPCs persist in their niche in the sub-ventricular zone (SVZ) (neural cell precursor derived OPCs) and are also found scattered throughout the adult CNS (parenchymal OPCs) making up 5-10% of the overall cell load.

Until recently, parenchymal OPCs were thought to be almost completely responsible for regeneration by OPCs, however more recent evidence has suggested greater involvement of OPCs derived from neural precursor cells in the SVZ. In their 2014 study, Kilpatrick and Merson et al., used in vivo genetic fate mapping to discover the contribution of the two OPC types to the repair of cuprizone induced demyelination in the corpus callosum of mice (Xing et al., 2014).

Two Cre transgenic mouse lines were used: Nestin-CreERT2 labelled OPCs derived from neural precursor cells in the SVZ (nestin being a marker of neural precursor cells) and Pdgfra-CreERT2 was used to label parenchymal OPCs, both transgenic lines were crossed with a fluorescent Cre reporter strain. In this way the fluorescence of regenerating OPCs were related back to the OPCs origin. Neural precursor derived OPCs were found to significantly contribute to the number of myelin forming oligodendrocytes present during the repair of cuprizone induced demyelination (a 23 fold increase in the presence of SVZ/neural precursor derived OPCs in the corpus callosum 6 weeks after injury, as compared to uninjured controls), and the myelin of such cells was found to be thicker than myelin produced by parenchymal OPCs (Xing et al., 2014).

The behaviour of OPCs in the uninjured CNS is still somewhat mysterious although there is evidence that they are a dynamic cell type capable of proliferation and migration (Dawson et al., 2003; Hughes et al., 2013).

OPCs have also been found to make synapses with neurons (Bergles et al., 2000; Orduz et al., 2015). Neurons use synapses to transmit electrical or chemical signals from one cell to another, and contrary to the traditional view that synapses only existed between neurons, neurons are now known to use synapses to communicate with glia. In a 2000 study, Bergles et al., showed that the stimulation of excitatory neuronal axons in the hippocampus, resulted in internal currents within OPCs. This process being mediated by the interaction of the neuron derived neurotransmitter alpha-amino-3-hydroxy-5-methyl isoxazole propionic acid (AMPA), and AMPA receptors on the surface of OPCs at synapses (Bergles et al., 2000).

In a more detailed 2015 study, Angulo et al., found OPCs to make complex synaptic networks with interneurons, specifically through the targeting of neuronal subdomains rich in GABAA receptors with γ2 subunits by NG2+ OPCs. These fast spiking interneurons formed a complex web of interactions with OPCs, with microcircuit complexity peaking at pre-natal day 10, immediately prior to the differentiation of OPCs into oligodendrocytes (Orduz et al., 2015). This suggests that the oligodendrogenesis may be initiated by neuronally derived signals, although further research would be required to verify this possibility.

While the differentiation of OPCs into adult oligodendrocytes has been extensively studied in development and regeneration (as will be discussed in depth in later sections of this thesis), there I also evidence the OPCs play an active role in the turnover of myelin in uninjured adult tissue. Proliferating and maturing OPCs have been found to make up 5-20% of the total oligodendroglia in the uninjured adult CNS in mice (Kang et al., 2010; Rivers et al., 2008; Young et al., 2013), and there is variability in the pattern of myelination of neuronal axons by adult oligodendrocytes in different regions of the adult brain and there is evidence of the persistence of unmyelinated neurons (Olivares et al., 2001; Tomassy et al., 2014). This variability in myelination, and incidence of unmyelinated axon tracts, allows for the optimisation of myelin coverage and thickness throughout adult life (reviewed in Mount and Monje, 2017).

Similar to neuronal plasticity, increasing evidence shows myelination to be a dynamic process in which myelin thickness and coverage of axons is varies with the activity and functions of the neurons being insulated (reviewed in Mount and Monje, 2017). In a 2012 study, Makinodan et al., showed social isolation in juvenile mice, to result in thinning of myelin sheaths in the medial prefrontal cortex (Makinodan et al., 2012). Another recent study found that the acquisition of motor skills in adult mice results in the generation of new OPCs and oligodendrocytes. Mice lacking a functional myelin regulatory factor (Mrf) gene – thus unable to generate new OPCs and oligodendrocytes, were unable to develop and retain new motor skills (McKenzie et al., 2014). The emerging picture is one of more general myelination of neuronal axons during development, followed by the tailoring of myelin dynamics to neuronal activity throughout adult life.

While the modification of adult myelination could represent a future avenue of for potential regenerative treatments, the migration of OPCs into regions of the adult CNS

requiring replacement or modulation of myelin is beneficial. PDGFα and FGF2 have long been known to be effectors of chemoattraction in OPCs derived from the adult and postnatal brain (Armstrong et al., 1990a; Decker et al., 2000; McKinnon et al., 1993; Milner et al., 1997; Zhang et al., 2004)

### 1.4.2 The Role of OPCs in Regeneration

In the adult CNS, OPCs are best known for their pivotal role in the regenerative process of remyelination. As previously mentioned, existing adult oligodendrocytes are unable to replace lost myelin sheaths, in light of this, OPCs are the primary source of new oligodendrocytes (Tripathi et al., 2010; Zawadzka et al., 2010) and might be best thought of as the resident glial stem cell population of the CNS, a pool of precursors from which new oligodendrocytes are generated.

As previously mentioned, in the uninjured CNS, the axons of neurons are protected and nurtured by the myelin sheath produced by oligodendrocytes, and quiescent OPCs are scattered throughout the CNS parenchyma (see **figure 1.4a)**)(Franklin and ffrench-Constant, 2008). Following demyelinating injury, distress signals, including chemoattractants for OPCs are released from the injury site (see **figure 1.4b)**). Chemoattractants form a gradient emanating from the lesion site which contact distal OPCs and direct them towards the lesion site (see **figure 1.4c)**). As previously mentioned, in developmental myelination, OPC migration precedes OPC proliferation which occurs directly prior to differentiation into adult oligodendrocytes (Raff et al., 1998) and it may be that the sequence of events is similar in remyelination. OPCs optimally placed in the vicinity of demyelinated axons differentiate into mature oligodendrocytes (see **figure 1.4d)**), ready to reform the myelin sheath, restoring protection and trophic support to the axon (see **figure 1.4e)**), thus preventing neurodegeneration(Franklin and ffrench-Constant, 2008).

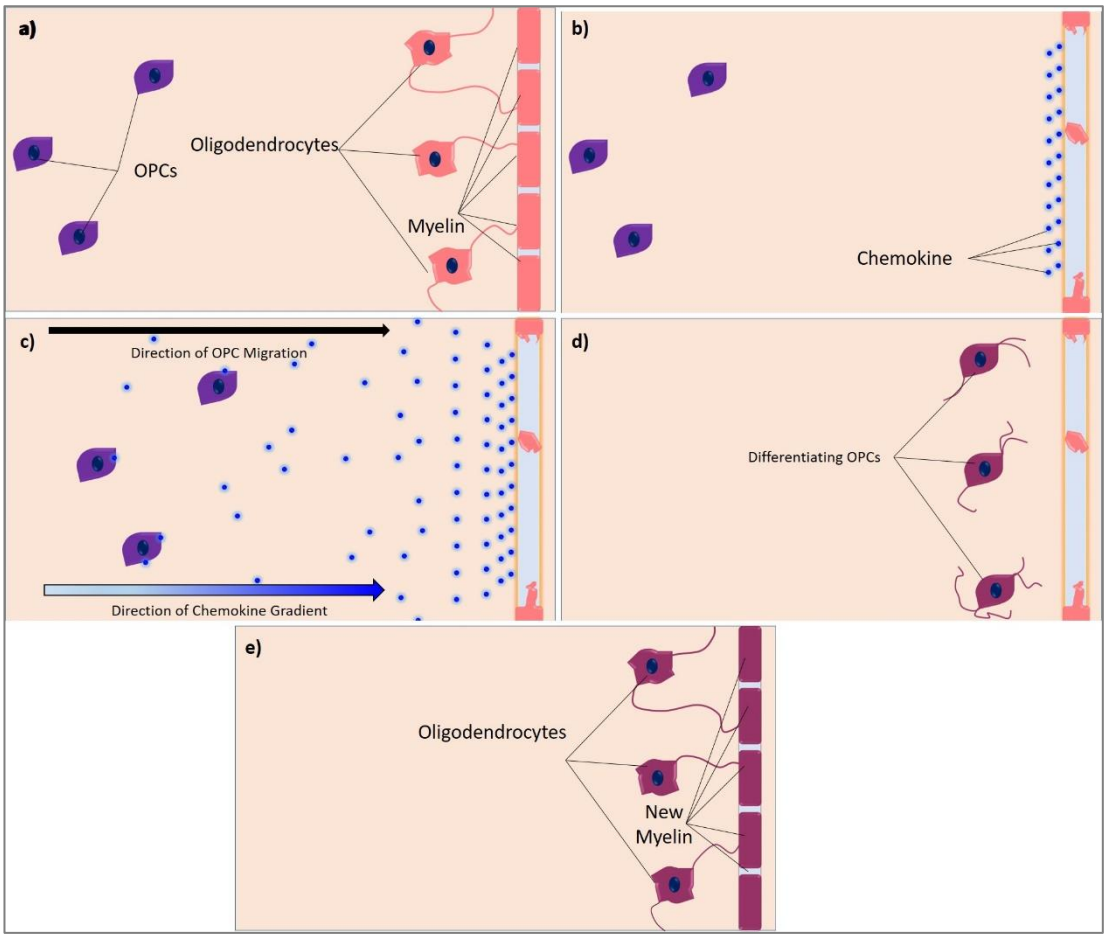


**Figure 1.4 Remyelination a)** In the healthy CNS, the axons of neurons are protected and supported by the myelin sheath formed by oligodendrocytes, quiescent OPCs are distributed throughout the CNS tissue **b)** Following a demyelinating insult resulting in the destruction of myelin an the loss of oligodendrocytes, chemical distress signals including OPC chemokines, are released from the lesion site **c)** OPC chemokines form a liquid gradient emanating from the lesion site, which directs OPCs towards the site of demyelination **d)** OPCs in proximity to the denuded axon begin to differentiate **e)** OPCs fully differentiate into new mature oligodendrocytes, which replace the lost myelin sheaths restoring protection and trophic support to the axon

### 1.4.4 Models of Demyelination

In the study of the regenerative process of remyelination a number of models have been developed which recapitulate various aspects of MS pathology. In the Experimental Autoimmune Encephalomyelitis (EAE) model, a myelin proteins such as myelin basic protein (MBP), myelin oligodendrocyte glycoprotein (MOG) or proteolipid protein (PLP) are used as antigens in conjunction with an adjuvant to boost the immune response, to immunise rodent models (Pachner, 2011). This causes an episode of inflammatory attack in the CNS resulting in demyelination and paralysis followed by full recovery, this

recapitulates the short inflammatory episodes experienced by MS patients in the relapsing and remitting phase of the disease.

Another widely used model of remyelination, is cuprizone induced global demyelination. Cuprizone is a toxin which is administered to rodents by feeding and results in demyelination of highly myelinated tracts in the white matter over a period of weeks and cessation of cuprizone treatment is followed by effective remyelination(Blakemore and Franklin, 2008; Blakemore and Patterson, 1978; Ludwin, 1978). The cuprizone model recapitulates the latter stages of MS progression in which demyelination leads to neurodegeneration, and is also an excellent model for the study of the process of remyelination.

Focal demyelinating lesions can also be induced by toxin treatment. Injection of the demyelinating agent lysophosphatidyl choline (LPC) into the brain or spinal cord, induces the formation of a small region of demyelination. This model is used to recapitulate the formation of contained demyelinated plaques in MS patients (Woodruff and Franklin, 1999). Following injection of LPC, it takes 28 days for full remyelination to occur, and the focal nature of the lesion formed makes an attractive model to study the infiltration of OPCs and microglia into the lesion from out with the region of demyelination.

### 1.4.3 Failure of OPC Differentiation Contributes to Failure of Remyelination

The process of remyelination has been found to be more effective in murine models than in humans, and is inefficient in MS patients. This failure in remyelination may be attributed to the failure of OPCs to differentiate into mature myelinating oligodendrocytes and a number of factors have been found to inhibit OPC differentiation in animal models.

LINGO-1 has been shown to inhibit the differentiation of OPCs in the spinal cord of EAE mice (Mi et al., 2005), and the treatment of OPCs with a LINGO-1 antagonist, resulted in increased OPC differentiation and remyelination following induction of focal demyelinating lesions using LPC (Mi et al., 2009). Wnt signalling has also been found to negatively impact OPC differentiation through the signal transducer β-catenin. Transgenic mice over expressing β-catenin were found to exhibit delayed OPC differentiation and hypomyelination in development and Wnt activity was detected in human MS lesions. Other examples of negative regulator include FGF-2, Hyaluronan and BMPs.

In contrast, other factors have also be found to increase the differentiation of OPCs. In their 2011 study, Huang, Jarjour et al., discovered increased expression of RXR-γ during remyelination and showed that OPCs express RXR-γ and that loss of RXR-γ resulted in impaired OPC differentiation in LPC induced lesions (Huang, Jarjour et al., 2011).

Another factor found to improve OPC differentiation is CXCL12, which has two functionally distinct receptors, both of which are expressed by OPCs. Stimulation of the G-protein coupled receptor CXCR4 by CXCL12, initiates an intracellular signalling cascade, culminating in the alteration of gene expression. In contrast CXCR7, scavenges CXCL12, thus reducing the binding of CXCL12 to CXCR4. It has been demonstrated that agonism of CXCR4 and antagonism of CXCR7, increase OPC differentiation in demyelinating injury (Williams et al., 2014).

### 1.4.4 Inefficient Recruitment of OPCs to Demyelinating Lesions Contributes to the Inhibition of Remyelination and is Orchestrated by Chemomigratory Regulators

Lack of remyelination in MS lesions, could also be the result of inefficient migration of OPCs into sites of demyelination. There is some debate as to the contribution of OPC migration as opposed to proliferation during remyelination. Irradiation sufficient to kill all dividing cells in the spinal cord has been shown to impede remyelination and this has been suggested as evidence that loss of proliferation is responsible for blocking remyelination(Blakemore and Patterson, 1978). However, since more recent evidence shows that non-activated OPCs in uninjured adult tissue are still actively dividing cells (Hughes et al., 2013), it is clear that irradiation would kill these quiescent OPCs, thus stopping migration as well as proliferation.

It has also been postulated that improvement of OPC recruitment to lesion sites has no effect on the efficacy of remyelination. In a 2004 study, the gene for platelet derived growth factor alpha (PDGFα), a known chemoattractant for OPCs, was placed under the control of the glial fibrillary acidic protein (GFAP) gene promoter (Woodruff et al., 2004). The authors found that following lysophosphatidylcholine (LPC) induced demyelinating injury there was no improvement in remyelination in GFAP-PDGF-A mice as compared to control wild-type mice. However, figures within the paper show clearly that GFAP expression is limited to the periphery of the lesion and does not penetrate the central lesion where demyelination is most pronounced. It can therefore be concluded that far from proving that increased migration of OPCs into lesion sites has no effect on remyelination, the results show that misdirection of OPCs to the periphery of the lesion

rather than to the demyelinated axons does not improve remyelination. Thus, highlighting the importance of nuanced directional chemokinetic signalling in the recruitment of OPCs.

#### 1.4.4.1 Semaphorin-3F is a Chemoattractant for OPCs and Semaphorin-3A is a chemorepellent for OPCs following demyelination

Previous research in the Williams and Lubetzki labs found some MS lesions, particularly chronic active lesions, to be completely devoid of OPCs (Boyd et al., 2013a). These studies also showed that the addition of OPC chemorepellent Semaphorin-3A (Piaton et al., 2011; Williams et al., 2007) to LPC induced sites of focal demyelination in the corpus callosum of mice, resulted in decreased OPC recruitment and remyelination. In contrast the addition of OPC chemoattractant Semaphorin-3F (Piaton et al., 2011; Williams et al., 2007), had exactly the opposite effect, increasing both OPC recruitment and remyelination(Boyd et al., 2013a).

#### 1.4.4.3 FGF8 is a Chemoattractant for OPCs Following Demyelination

Fibroblast growth factor 8 (FGF8) is necessary for CNS development at the embryonic stage, but is not known to be expressed in the adult CNS. OPCs were found to migrate towards FGF8 soaked heparin beads in Matrigel cultures and transplanted FGF8 soaked heparin beads in cuprizone induced demyelination, increasing the expression of NG2 and MBP(Cruz-Martinez et al., 2014).

#### 1.4.4.4 Netrin-1 is a Chemorepellant for OPCs Following Demyelination

The developmental OPC chemorepellent Netrin-1 (Jarjour et al., 2003), has been shown to occur in chronic demyelinatinating MS plaques (Bin et al., 2013). In their 2014 study, Tepavčević et al., discovered that in the early stages of demyelination in human MS lesions, astrocytes express Netrin-1 and OPCs express Netrin-1 receptors Deleted in Colorectal Cancer (DCC) and Unc5A. Conversely, in LPC induced focally demyelinated lesions which fully remyelinated, Netrin-1 expression was not detected until after OPC recruitment. OPCs were shown to migrate away from Netrin-1 in *in vitro* trans-well migration assays. The addition of Netrin-1 functional blocking antibodies to LPC induced lesions increased OPC numbers in the lesion site, and increased expression of Netrin-1 by lentiviral induction during the early stages of LPC lesion induction, when OPCs should be migrating, resulted in a decrease in OPC recruitment to the lesion site (Tepavčević et al., 2014). There is also evidence that the chemorepellent function of Netrin-1 results in the expulsion of OPCs from the sub-ventricular zone following demyelinating injury, thus

releasing OPCs to migrate into demyelinated lesions in the Corpus Callosum (Cayre et al., 2013).

#### 1.4.4.5 Prostacyclin is a Chemoattractant for OPCs Following Demyelination

Another factor which has been found to increase OPC migration following demyelinating injury is prostacyclin (prostaglandin-I2, PGI2). The prostacyclin receptor (IP receptor) was shown to be expressed by OPCs and OPCs were found to migrate up a gradient of prostacyclin analogs in trans-well assays *in vitro* (Takahashi et al., 2013). Expression of the IP receptor was also found in MS brain autopsy tissue, and administration of an IP receptor antagonist, reduced the number of OPCs migrating and ultimately reduced MBP expression in LPC induced demyelinating lesions in the spinal cord.

#### 1.4.4.6 FGF-2 is a Chemoattractant and Anosmin-1 is a Chemorepellant for OPCs in Demyelinating Lesions

In the developing CNS, FGF-2 is a chemoattractant for OPCs, while Anosmin-1 is a chemorepellent, both factors acting on OPCs by binding to the cell surface receptor FGFR-1 (Bribián et al., 2006, 2008). In a 2011 study, Clemente et al., reported the expression of FGF-2 in the active lesions and periplaque of chronic lesions in post mortem human MS tissue. In the same tissue, the authors also reported the upregulation of Anosmin-1 in chronic lesiona, and its absence in active lesions. It was also found that OPCs isolated from the cerebral cortices of adult mice migrated towards FGF-2 and away from Anosmin-1(Clemente et al., 2011).

#### 1.4.4.7 CCL2 is a Chemoattractant for OPCs Following Demyelination

In a recent study, the chemokine CCL2 was found to be upregulated in OPCs isolated from cuprizone demyelinated brains, and also during LPC induced focal demyelination (Moyon et al., 2015). *In vitro* studies showed that OPCs migrated up a gradient of CCL2 and videomicroscopy revealed that OPC non-directional OPC motility was also increased in response to CCL2. Transplantation of OPC like CG4 cells overexpressing CCL2, migrated away from the site of injection in the Corpus Callosum and CCL2 was shown to be expressed by the OPCs in human active MS plaques.

| Factor | Receptor on OPCs | Effect on OPCs | References |
|---|---|---|---|
| Anosmin-1 | FGFR1 | Chemorepellant | (Clemente et al., 2011; Murcia-Belmonte et al., 2016) |
| CCL2 | N/A, CCL2 expressed by OPCs themselves | Increased Migration/Motility | (Moyon et al., 2015) |
| FGF-2 | FGFR1 | Chemoattractant | (Clemente et al., 2011) |
| Netrin-1 | Unc5a, DCC | Chemorepellant | (Tepavčević et al., 2014,) |
| PDGFα | PDGFRα | Chemoattractant | (Redwine and Armstrong, 1998; Zhang et al., 2004) |
| prostacyclin (prostaglandin-I2, PGI2). | prostacyclin receptor (IP receptor) | Chemoattractant | (Takahashi et al., 2013) |
| Semaphorin-3A | Neuropilin-1 | Chemorepellant | (Piaton et al., 2011; Williams et al., 2007) |
| Semaphorin-3F | Neuropilin-2 | Chemoattractant | |

**Table 1.1 Summary of known modulators of OPC migration in demyelinating lesions**

As summarised in **table 1.1**, a variety of factors which modulate the migration of OPCs in demyelinating injury have already been identified. However, I hypothesized that other, perhaps more potent chemoattractants might be as yet undiscovered. In this thesis, I describe how the search for novel modulators of OPC migration led me to discover and validate a master regulator of OPC led regeneration, augmenting not only OPC migration, but also OPC maturation.

# Chapter 2

# Materials and Methods

## 2.1 Bioinformatic Methods

All data was analysed using the statistical computing software R version 3.3.2 "Sincere Pumpkin Patch" (R Core Team, 2016), with the aid of the microarray specific packages downloaded from Bioconductor (Gentleman et al., 2004), Limma (Ritchie et al., 2015) and Affy (Gautier et al., 2004). The Illumina specific Beadarray (Dunning et al., 2007) was used to parse the Illumina beadchip array data from Huang, Jarjour et al., 2011, and Ggplot2 (Wickham, 2009) was used to generate the Principal Component Analysis plots. See **Appendix 3** for full R code

Selection of genes by adjusted pvalue was performed in Microsoft Excel using the following formula:

```
=AND(B2>I$2,C2>I$2,D2>I$2,E2>I$2,F2>I$2,G2>I$2)
```

This formula returns TRUE if all the pvalues are greater than 0.05 and returns false if any of them are above 0.05.

Pearson correlation coefficitents for used for analysis of correlation with PDGFα were also calculated in Microsoft Excel using the following formula: `=CORREL(C$1820:H$1820, C2:H2)`

### 2.2 Wet Laboratory Procedures

Details regarding all reagents, kits and antibodies used in the methods for this thesis can be found in **chapter 2.2.9**.

All experiments were carried out in line with Home Office guidelines, under personal licence IF27165BD (Catriona Ford) and project licence 60/4524 (Anna Williams).

#### 2.2.1 - Animal housing and husbandry

All oligodendrocyte precursor cells (OPCs) used in this thesis were extracted from wild type Sprague Dawley rats housed at the University of Edinburgh.

#### 2.2.2 – Termination

For OPC extraction, the animals were terminated at postnatal day 0-2 by an intraperitoneally administered overdose of Euthatal (150mg/kg).

#### 2.2.3 Preparation of primary rat OPCs from neonatal brain tissue

The shake-off method for the culture of rat OPCs was first developed by McCarthy and de Vellis in their 1980 study, which included the characterisation of OPCs produced using

this method. Using both light and electron microscopy to characterise the cells in the cultures by morphology, the authors found post shake-off oligodendroglial cultures to be of around 98% purity, with isolated clumps of contaminating astrocytes, a result confirmed by both enzymatic and pharmacological characterisation (McCarthy and de Vellis, 1980).

The shake-off method used in this thesis, is the method described in Milner and ffrench-Constant's 1994 publication, in which in addition to being shaken-off, mixed glial cultures were further refined by a 20 minute incubation period in petri dishes post shake-off (Milner and ffrench-Constant, 1994). During this step, contaminating microglia adhere to the petri dish, leaving a near pure OPC population in the culture media. By morphological analysis, the authors found the culture to be greater than 95% oligodendroglial cells. After 4 hours in culture, immunostaining for the oligodendrocyte specific marker GalC, found less than 10% of the cell population to be oligodendrocytes, making the culture more than 90% OPCs. Further characterisation of markers expressed by OPCs in this culture can be found in **figure 4.16b)** and **figure 5.5**.

This method of primary OPC isolation is as follows:

P0-P2 Sprague Dawley rat brains were dissected into ice-cold MEM, the midbrain, hindbrain and meninges were removed leaving the cerebral cortices which were pooled in 1ml ice cold MEM, before mincing with fine scissors.

A papain enzyme mix of papain (1.2U/ml), L-cysteine (0.24mg/ml in MEM) and DNaseI Type IV (40µg/ml in PBS) in 1ml MEM was pre-warmed for 10 minutes at 37°C to activate the papain, before sterile filtration and addition to minced cortices in 1ml MEM. Cortices were then digested at 37°C for 1 hour.

Digested cortice suspension was diluted tenfold in OPC media (Dulbecco's modified Eagle medium (DMEM) with 10% FBS, 1% pen/strep) to stop digestion, spun down (5 minutes at 1000 RPM), half of the medium removed then triturated gently 3-4 times with a 19-gauge needle followed by 3-4 times with a 23-gauge needle to remove any clumps.

The cell pellet was resuspended in OPC media (1.5 brains in 10ml per flask) and plated onto T75 vented-top flasks (straight necked to avoid loss of cell culture during shake-off step) coated with poly-D-lysine (PDL; 5µg/ml in water; minimum 1 hour coating at 37oC I 7.5% $CO_2$).

Mixed glial cultures were cultured at 37°C and 7.5% $CO_2$ for a period of 10 days and replenished with fresh OPC media after 3-5 days and then every 2-3 days.

Following 10-14 days in culture, the vented cap of the flasks was sealed with parafilm (to circumvent the absence of $CO_2$ concentration control functionality on the shaker) and the

flasks containing mixed glial cultures were fixed to an orbital shaker using autoclave tape and shaken at 240 RPM and 37°C for 1 hour. After 1 hour, the media was replaced in order to remove the loosely attached microglia. Fresh media was added and the flasks were then reaffixed to the orbital shaker and shaken in the same way for a further 16-18 hours to isolate OPCs from the basal cell monolayer.

Following shake-off, flasks were removed from the shaker and media (containing shaken-off OPCs) was removed and distributed among 10cm plastic petri dishes and incubated at 37°C and 7.5% $CO_2$ for a period of 20-25 minutes (this step eliminates any remaining microglia which become adhered to the plastic). Media and non-adhered cells (OPCs) were transferred to 50ml falcon tube and centrifuged for 5 minutes at 1000 RPM, yielding a population of OPCs, 95% of which can be potentially be differentiated into adult oligodendrocytes in culture (Milner and Ffrench-Constant, 1994).

The supernatant was aspirated and discarded, and the cell pellet was resuspended in 5ml culture medium, gently triturated 6-10 times through a 21-gauge needle, passed through a 70µm cell strainer, counted and incubated in Sato medium (DMEM with 1% pen/strep. 1% ITS supplement, 16µg/ml putrescine, 400ng/ml L-thyroxine, 400ng/ml Tri-iodothyroxine, 60ng/ml progesterone, 100µg/ml BSA (fraction V)) at 37°C in 7.5% $CO_2$ for up to 4 hours until required for other experimental procedures.

### 2.2.4 Culture of post shake-off rat OPCs

#### *2.2.4.1 Culture of post shake-off rat OPCs on glass coverslips*

Post shake-off OPCs in Sato media in 50ml falcon tubes were spun down and resuspended at a density of 50,000 OPCs per 20µl droplet of Sato media per PDL coated coverslip in a 24 well plate. After 20 minutes at 37°C and 7.5% $CO_2$ (allowing time for OPCs to adhere to the coverslips), coverslips were topped up with 500µl Sato media per well. OPCs were then cultured for up to 50 hours and the media was not changed during this period.

#### *2.2.4.2 Culture of post shake-off rat OPCs in 324 well plates*

Post shake-off OPCs in Sato media in 50ml falcon tubes were spun down and resuspended at a density of 1000 OPCs per 25µl of Sato media. 25µl of OPCs in Sato media were then seeded into per PDL coated 384 well plates. After 15-20 minutes at room temperature (allowing time for OPCs to adhere to the bottom of the wells), wells were topped up with 25µl Sato media per well. OPCs were then cultured for up to 18 hours and the media was not changed during this period.

*2.2.4.3 Culture and assay of post shake-off rat OPCs in X-celligence RTCA CIM plates*

X-celligence plates were separated into their two parts by unclipping and 160µl of PDL was added to each well of the lower chamber. Upper chambers were then reattached and 50µl of PDL was added to each well of the upper chamber. X-celligence plates were incubated at 37°C and 7.5% $CO_2$ for 1 hour. All PDL was aspirated from the upper chamber of X-celligence plates and plates were separated by unclipping, before all PDL was aspirated from lower chamber.

Following PDL coating, 160µl of Sato media only or Sato media impregnated with the factor being tested was added to each lower chamber, and the upper chambers were reattached and 50µl of Sato media was added to each upper chamber. X-celligence plates were then incubated in the X-celligence machine at 37°C and 7.5% $CO_2$ for 1 hour.

In the X-celligence RTCA 2.0 software, the experimental notes tab was populated with information regarding the experiment name, purpose and unique X-celligence plate device part numbers, and the layout tab with cell type, cell number, factor name and concentration. The schedule tab was set up with an initial step of sweeps = 1, interval = 1 and duration = 0, a second step of sweeps = 100, interval = 15 minutes and duration = 24 hours and 45 minutes (i.e. 1 sweep every 15 minutes well beyond the end point of the experiment), and a final step of sweeps = 1, interval = 1 and duration = 0 with the Auto box ticked to ensure the machine idles at the end of the experiment.

After 1 hour of incubation, the X-celligence RTCA software was used to take the baseline electrical impedance of the underside of the membrane in the absence of cells.

Post shake-off rat OPCs (prepared according to the methods in 2.2.1to 2.2.3) were resuspended at a concentration of 250,000 OPCs per 100ul Sato media. 100µl of Sato media containing (250,000 cells) was then added to each of the upper chambers. X-celligence plates were incubated in the X-celligence machine at 37°C and 7.5% CO2 for 30 minutes to acclimatise before beginning software protocol.

Immediately after 30 minutes, using the X-celligence RTCA software, a second sweep measuring the electrical impedance of the underside of the membrane was performed to ascertain the nominal level of electrical impedance at the beginning of the experiment when cells are first added. Further electrical impedance sweeps of the underside of the membrane were performed at 15 minute intervals thereafter as the cells migrate through the permeable membrane.

*2.2.4.3 Arrest of OPC proliferation by treatment with the proliferation inhibitor mitomycin C*

Post shake-off rat OPCs (prepared according to the methods in **2.2.1**to **2.2.3**), were resuspended in Sato media containing mitomycin C at a concentration of 5µg/ml and incubated at 37°C and 7.5% $CO_2$. After a period of two hours, OPCs were spun down in a centrifuge for 5 minutes at 1,000 RPM, after which the media was aspirated and OPCs were resuspended in fresh Sato media, ready for use in further experiments.

## 2.2.5 – Fluorescent Immunocytochemistry (ICC)

*2.2.5.1 ICC of OPCs on glass coverslips and 384-well plates*

Cells were fixed for 10 minutes in 4% paraformaldehyde (PFA; diluted in phosphate buffered saline (PBS)), then washed with PBS (3 x 5 minutes). Cells were blocked for 1-1.5 hours at room temperature on a rocker in blocking solution (10% heat inactivated horse serum (HIHS), 0.1% triton in PBS) Cells were then incubated with blocking solution diluted primary antibodies, for 1-1.5 hour at room temperature on a rocker. Cells were then washed in PBS (3 x 2 minutes) before incubation with secondary antibodies, diluted in PBS, for 1 hour at room temperature on a rocker. Cells were washed with PBS (3 x 2 minutes), stained with Hoechst for 1 minute and washed again with PBS (rinse then 2 minutes) before mounting with Fluoromount in the case of OPCs on glass coverslips, or the wells were filled with PBS in the case of OPCs grown in 384-well plates.

*2.2.5.1 ICC of OPCs on X-celligence RTCA CIM plates*

Following the conclusion of an X-celligence RTCA CIM experiment, X-celligence plates were unclipped, all media was aspirated and 160µl of 4% PFA was added to each of the lower chambers and 100µl of 4% PFA was added to each of the upper chambers. Plates were fixed with PFA for a period of 5 minutes, before all PFA was aspirated and upper and lower chambers with washed in PBS (3 x 2 minutes), stained with Hoechst for 1 minute and washed again with PBS (rinse then 2 minutes) Cells were blocked for 1-1.5 hours at room temperature on a rocker in blocking solution (10% heat inactivated horse serum (HIHS), 0.1% triton in PBS) Cells were then incubated with blocking solution diluted primary antibodies, for 1-1.5 hour at room temperature on a rocker. Cells were then washed in PBS (3 x 2 minutes) before incubation with secondary antibodies, diluted in PBS, for 1 hour at room temperature on a rocker. Cells were washed with PBS (3 x 2 minutes), stained with Hoechst for 1 minute and washed again with PBS (rinse then 2 minutes).

Membranes (including the electrodes and cells) were extracted by running a scalpel around the membrane and carefully peeling it off in a single piece for each plate (see **figure 4.20**). Extracted membranes were then cut to size using scissors and mounted onto glass slides using Fluoromount.

### 2.2.6 Western Blot

#### *2.2.6.1 Extraction of proteins from cells*

OPC media was aspirated from the wells of a 24 well plate in which OPCs were cultured at a density of 50,000 OPCs per well. Approximately 50µl of radioimmunoprecipitation assay (RIPA) buffer with 1% protease inhibitor (PI). OPCs were scraped into the buffer using a bent pipette tip and the resultant suspension was transferred to a centrifuge tube. This was centrifuged at 13,000 RPM for 10 minutes at 4°C and the supernatant collected.

#### *2.2.6.2 - Quantification of total protein*

Protein levels were quantified using a bicinchoninic acid assay (BCA assay), using solutions from a Pierce BCA protein assay kit. BCA working solution was prepared according to the manufacturers instructions, and 200µl added to each well of a 96-well plate (flat bottomed). 10µl of sample was then added to each relevant well, and 9 wells were also used for a BSA standard curve (2000µg/ml, 1500µg/ml, 1000µg/ml, 750µg/ml, 500µg/ml, 250µg/ml, 125µg/ml, 25µg/ml, and 0µg/ml in RIPA). The plate was incubated at 37°C for 30 minutes and then allowed to cool to RT. The absorbance was measured using an Omega Plate Reader for each well at 562nm. The protein concentration of each sample was then computed by comparison to the standard curve plotted for BSA samples.

#### *2.2.6.3 Western Blotting*

Protein lysates from OPC samples were diluted in RIPA and 4 x Laemmli buffer (8% sodium dodecyl sulphate (SDS), 40% glycerol, 20% β-mercaptoethanol, 0.4% bromophenol blue, 0.25M Trizma hydrochloride) at 5µg of protein in 20µl in 1x Laemmli buffer. Then, protein lysates from samples were boiled at 95°C for a period of 10 minutes and loaded into a Pierce ready-cast 4-20% Tris-HEPES gels, in a gel tank containing HEPES running buffer (Pierce). These samples were then run with a protein ladder (Bio-Rad) for 1.5 hours at 100 Volts. The gel was then extracted and placed into a transfer cassette with a polyvinylidene fluoride (PVDF) membrane (activated in methanol). Gels were transferred in transfer buffer (20mM Trizma base, 150mM glycine, 20% methanol in water) for a period of 2 hours at 400 Amps. Following transfer, the membrane was

extracted from the cassette, washed in TBST (tris buffered saline (TBS; 20mM Trizma base, 150mM sodium chloride, 2.7mM potassium chloride in water) + 0.1% tween; PBST (PBS + 0.05% tween)) before blocking with 4% BSA in TBST for 1 hour on a rocker at room temperature. The membrane was then probed with primary antibodies diluted in blocking solution on a rocker at 4$^{o}$C overnight. The membrane was washed with TBST (3 x 10 minute washes) before incubation with secondary antibodies in blocking solution for 1 hour at RT on a rocker. Following secondary antibody administration, the membrane was washed in TBST and treated with ECL substrate for a period of 5 minutes. The excess was then dabbed off and the membrane was then imaged using a LiCor scanner.

### 2.2.7 TUNEL Assay

OPCs were grown overnight on glass coverslips as detailed in **chapter 2.2.4.1,** and TUNEL assay was carried out according to the manufacturers' Protocol for Cells on Coverslips included in the manual for the Click-iT TUNEL Alexa Fluor 647 Imaging Assay (Thermo Fischer Scientific).

### 2.2.8 Imaging, analysis and statistics for wet laboratory procedures

#### *2.2.8.1 Imaging*

Fluorescent images were captured using Leica SPE confocal microscope system, Leica SP8 confocal microscope system, the Zeiss Axio Observer inverted fluorescent microscope system and the Operetta High-Content Imaging System (PerkinElmer).

#### **2.2.8.2 - Image analysis**

Immunostained images generated using the Leica SPE, Leica SP8 or Zeiss Axio Observer microscopy systems were quantified using ImageJ FIJI software (open source). Cells were counted using the Cell Counter plugin. ICC images were blinded before quantification.

Immunostained images generated using the Operetta High-Content Imaging System (PerkinElmer) were captured using Harmony High-Content Analysis software (PerkinElmer) and quantified using Columbus Image Data Storing and Analysis System software (PerkinElmer).

#### *2.2.8.3 - Statistics*

*In* vitro data was visualised as graphs produced and with statistics calculated using GraphPad Prism software. All data is presented as mean +/- standard error of the mean

(SEM), comparing at least three biological repeats (data from OPCs from at least 3 different litters of rat pups) each time. Numbers of technical and/or biological repeats are stated in the results sections and in each graphical figure. Due to the fact that all the comparisons made were between two groups, significance was computed using a Students t-test, either paired (where the control and experimental conditions were run in parallel for each biological replicate) or unpaired.

### 2.2.9 Materials

*2.2.9.1 Culture dishes and plastics*

| **Name** | **Company** | **Product code** |
|---|---|---|
| 13mm round coverslips | VWR International | 631-0149 |
| 24-well plates | Costar (Corning) | 3524 |
| 70µm cell strainer | Fisher Scientific | 11597522 |
| Vented T75 flasks (OPCs) | Falcon (Corning) | 353110 |
| 384-well plates | | |
| X-celligence RTCA CIM plates | ACEA Biosciences | 05665825001 |
| Oris Assay Plates | | |
| 6.5mm Transwells with 8.0µm Pore Polycarbonate Membrane Insert, Sterile | Corning | **CLS3428-24EA** |

*2.2.9.2 Cell culture solutions*

| **Name** | **Company** | **Product code** |
|---|---|---|
| Dnase I type IV | Sigma-Aldrich | D5025 |
| Dulbecco's modified Eagle medium | Gibco (now Thermo Fisher Scientific) | 41966-029 |
| Dulbecco's phosphate buffered saline | Sigma-Aldrich | D8537 |

| | | |
|---|---|---|
| Fetal bovine serum | Gibco (now Thermo Fisher Scientific) | 10270106 |
| Heat inactivated horse serum | Gibco (now Thermo Fisher Scientific) | 26050 |
| HEPES | Gibco (now Thermo Fisher Scientific) | 15630-049 |
| ITS | Sigma-Aldrich | I3146 |
| L-cysteine | Sigma-Aldrich | C7477 |
| Minimum Essential Medium | Gibco (now Thermo Fisher Scientific) | 32360 |
| Papain, suspension | Worthington Biochemical Corporation | LS003127 |
| Penicillin/streptomycin | Gibco (now Thermo Fisher Scientific) | 15140 |
| Poly-d-lysine | Sigma-Aldrich | P6407 |
| Mitomycin C from Streptomyces caespitosus | Sigma-Aldrich | M4287-5X2MG |

*2.2.9.2 Recombinant Proteins*

| **Name** | **Species** | **Company** | **Product Code** |
|---|---|---|---|
| CX3CL1 | Rat | R&D Systems | 537-FT-025/CF |
| CXCL12 | Rat | Source BioScience | ABC2919 |
| Lipocalin-2 (LCN2) | Rat | R&D Systems | 3508-LC-050 |
| Netrin-1 | Mouse | R&D Systems | 1109-N1-025/CF |
| Platelet Derived Growth Factor-α (PDGFα) | Human | PeproTech EC Ltd | 100-13A-100ug |
| Semaphorin-3A (Sema3A) | Mouse | R&D Systems | 5926-S3-025/CF |

*2.2.9.2 Primary Antibody dilutions*

| Name | Species | Dilution | Company | Catalogue |
|---|---|---|---|---|
| 24p3r | Rabbit | 1:500 | Sigma-Aldrich | SAB3500306-100UG |
| CX3CR1 | Rabbit | 1:500(ICC), 1:1000(Western Blot) | Abcam | ab8021 |
| CXCR4 | Rabbit | 1:100 | Abcam | ab2074 |
| CXCR7 | Mouse | 1:500 | Abcam | ab72100 |
| Ki67 | Rabbit | 1:200 | Abcam | ab9160 |
| Ki67 | Rabbit | 1:200 | Abcam | ab16667 |
| MBP | Rat | 1:300 | AbD Serotec (a Bio-Rad company) | MCA409S |
| NG2 | Mouse | 1:200 | Merck Millipore (formerly Chemicon) | MAB5384 |
| NG2 | Rabbit | 1:200 | Merck Millipore (formerly Chemicon) | AB5320 |
| Olig2 | Goat | 1:20 | R&D Systems | AF2418 |
| PCNA | Mouse | 1:200 | Dako | M0879 |

*2.2.9.3 Secondary Antibody dilutions*

| Species | Host | Type | Dilution | Company | Category number |
|---|---|---|---|---|---|
| Goat | Donkey | Alexa Fluor 555 | 1:250 | Invitrogen (now Thermo Fisher Scientific) | A12432 |

| | | | | | |
|---|---|---|---|---|---|
| Mouse | Donkey | Alexa Fluor 488 | 1:1,000 | Invitrogen (now Thermo Fisher Scientific) | A21202 |
| Mouse | Donkey | Alexa Fluor 647 | 1:1,000 | Invitrogen (now Thermo Fisher Scientific) | A31571 |
| Rabbit | Donkey | Alexa Fluor 488 | 1:1,000 | Invitrogen (now Thermo Fisher Scientific) | A21206 |
| Rabbit | Donkey | Alexa Fluor 568 | 1:1,000 | Invitrogen (now Thermo Fisher Scientific) | A10042 |
| Rabbit | Donkey | Alexa Fluor 647 | 1:1,000 | Invitrogen (now Thermo Fisher Scientific) | A31573 |
| Rat | Donkey | DyLight 549 | 1:1,000 | Stratech Scientific | 712-505-153 |
| Rat | Donkey | DyLight 650 | 1:1,000 | Abcam | ab102263 |

*2.2.9.4 List of kits and other chemicals used*

| **Reagent** | **Company** | **Product code** |
|---|---|---|
| 10x Phosphate buffered saline | Gibco (now Thermo Fisher Scientific) | 70011-036 |
| 4-20% Tris-HEPES gels | Thermo Fisher Scientific | 25224 |
| BCA protein assay kit | Pierce (now Thermo Fisher Scientific) | 23228 + 23224 |
| Click-iT® TUNEL Alexa Fluor® 647 Imaging Assay | Thermo Fisher Scientific | C10247 |
| ECL femto kit | Thermo Fisher Scientific | 34094 |
| ECL substrate | Thermo Fisher Scientific | 80196 |
| Ethanol | VWR International | 20821.33 |
| Euthatal | Merial | |
| Fluoromount | Southern Biotech | 0100-01 |
| HEPES running buffer | Pierce (now Thermo Fisher Scientific) | 10230064 |
| Hoechst | VWR International | BTIU40045 |
| Kaleidoscope protein ladder | Bio-Rad | 1610375 |
| Methanol | Fisher Scientific | M/3900/17 |
| Paraformaldehyde | Sigma-Aldrich | P6148 |
| Potassium chloride | Fisher Scientific | P/4280/53 |
| Protease inhibitor | Calbiochem | 539134 |
| SDS | Sigma-Aldrich | 5030 |
| Triton x-100 | Fisher Scientific | BP151 |

Chapter 3

# Bioinformatic Analysis of Gene Expression Array Data from *in vivo* Models of Demyelination

### 3.1 Introduction

The aim of the PhD project described in this thesis, was to identify novel migration factors for OPCs in demyelinating injury. Two well characterized models of demyelinating injury, are focal demyelinating injury using lysophosphatidylcholine, (LPC) and cuprizone induced global demyelination.

In their 2011 study, Huang, Jarjour et al. induced focal demyelinating lesions in the caudal cerebellar peduncle of rats by injection of LPC, as a model of focal plaques of demyelination found in the CNS of human MS patients. RNA from the entire injury site was extracted 5, 14 and 28 days after injury, and analysed using whole genome gene expression microarrays. The authors hypothesized that factors driving OPC differentiation were likely to be most highly expressed at 14 days post lesion, and identified RXR-γ as being highly expressed at 14 days post lesion, compared to 5 days post lesion. Further experimentation showed that RXR-γ was expressed by oligodendroglial lineage cells and that loss of RXR-γ resulted in impaired OPC differentiation in LPC induced lesions. In this way, the gene expression array data set generated for focal demyelinating lesions was used to identify a novel regulator of OPC biology, the differentiation factor RXR-γ.

Hypothesising that modulators of OPC migration should be secreted at the lesion site following injury, I reanalysed this data set and searched for possible OPC migratory factors. From the whole genome data, I selected only the secreted factors, before narrowing this list down to only the secreted factors which correlated with PDGFα, a known chemoattractant for OPCs (Zhang et al., 2004). However, the number of PDGFα correlating secreted factors far exceeded the number which could be comfortably be tested for their effects on OPCs *in vitro*.

In order to discover information which would allow me to cut down my list of factors, I searched the bioinformatic gene expression data repositories the Gene Expression Omnibus (GEO, https://www.ncbi.nlm.nih.gov/geo/) and the Sequence Read Archive (SRA, https://www.ncbi.nlm.nih.gov/sra), for further genome wide expression data relating to demyelinating injury.

Although a number of transcriptomic data sets relating to OPCs have been published, I narrowed my search to include only transcriptomic data sets from OPCs in

demyelinating injury models. For this reason I did not reanalyse some well-known OPC transcriptome data sets.

In their 2006 study, Golman et al., used Affymetrix microarrays to compare the transciptome of immunomagnetically sorted human OPCs to the transcriptome of the unsorted white matter from which they were derived (Sim et al., 2006). Although this study established the pathways regulating the biology of OPCs in human white matter, the study did not investigate the unique transcriptomic environment of demyelinating injury. In a further study, the Goldman lab transplanted human OPCs into the non-myelinated brains of neonatal shiverer (MBP knock-out) mice (Readhead and Hood, 1990), and for the first time showed that human OPCs were highly migratory (Sim et al., 2011). While this study again utilised Affymetrix microarrays to classify the subtype of OPCs used for transplantation, no transcriptomic data relating to demyelinating injury was produced.

Other well known OPC transcriptomic data sets include the Barres RNA-Seq databases. These databases make available the results of RNA-Seq analyses of both mouse (Zhang et al., 2014) and human (Zhang et al., 2016) brain cells, isolated by cell type. As with the studies from the Goldman lab above, although the Barres databases represent and ground-breaking resource for the analysis of gene expression in OPCs and other cell types, the data relates only to uninjured tissue. Thus, the data in these studies was not suitable for investigating the behaviour of OPCs in demyelinating injury.

In this way, I discovered the data from Moyon et al., 2015, which was uploaded to GEO prior to the publication of the article in the Journal of Neuroscience. In this study, gene expression arrays were generated using RNA from neonatal OPCs, adult OPCs (from 2 month old mice), and adult oligodendrocytes isolated from healthy mouse brains. In addition the authors also included data from OPCs from mouse brains globally demyelinated using cuprizone (known as Activated OPCs).

The authors used their gene expression array data, to show that OPCs from demyelinated brains had a more similar gene expression profile to neonatal OPCs than either adult OPCs from healthy brains or adult oligodendrocytes. These Activated OPCs were also shown to have a higher propensity for migration and differentiation than OPCs from uninjured brains.

Reasoning that genes highly expressed in both Activated OPCs and during remyelination were likely to be important for remyelination, the authors identified genes which were highly expressed in both Activated OPCs as compared to OPCs from uninjured brains, and at 5 days post lesion (when OPC recruitment is likely to occur) as compared to 14 days post lesion. Amongst the genes they identified using this method, were interleukin-1β (IL1β) and chemokine (C-C motif) ligand 2 (CCL2), both of which are associated with innate immune system signalling. The authors then went on to show that both IL1β and CCL2 increase the directional migration of OPCs *in vitro*, and that migration in OPC like cells transplanted into neonatal mouse brains, could be increased by overexpression of CCL2. These results demonstrated that the combination of the two data sets could be used to identify new chemomigratory factors for OPCs.

From the outset, I had hypothesized that factors attracting OPCs into the heart of MS lesions would be secreted at the lesion site, before diffusing into the CNS parenchyma, forming a gradient of the factor, which would contact distal OPCs by binding to cell surface receptors expressed by the OPCs. I therefore reanalysed the data from Moyon et al., 2015, and selected cell surface receptors which were significantly upregulated in Activated OPCs as compared to OPCs from healthy tissue. I then checked this list of cell surface receptors against the list of secreted factors I had generated from the Huang, Jarjour et al., 2011 data, to identify known ligand-receptor pairs.

In the following chapter I will describe the computation methods with which I carried out my analysis of the two data sets. I will also report the results of these bioinformatic analyses and finally explain how I created an online resource to make the data accessible for other researchers.

All data was analysed using the statistical computing software R version 3.3.2 “Sincere Pumpkin Patch” (R Core Team, 2016), with the aid of the microarray specific packages downloaded from Bioconductor (Gentleman et al., 2004), Limma (Ritchie et al., 2015) and Affy (Gautier et al., 2004). The Illumina specific Beadarray (Dunning et al., 2007) was used to parse the Illumina beadchip array data from Huang, Jarjour et al., 2011, and Ggplot2 (Wickham, 2009) was used to generate the Principal Component Analysis plots. See **Appendix 3** for full R code.

### 3.2 Illumina Data - Expression of Secreted Factors in a rat *in vivo* Model of Focal Demyelination

#### 3.2.1 Illumina Bead Chip Array Design and Data Parsing

The data from Huang, Jarjour et al., 2011, was reported as having been generated using the Illumina ratRef-12 v1.0 expression beadchip. However, on inspection of the Illumina IDs for the probe sequences used on the array, I found that the Illumina IDs used in this experiment did not match any of the IDs on the Illumina ratRef-12 v1.0 chip and instead matched the IDs on the Illumina ratRef-12 v1.5.0.34 expression bead chip (GEO Accession: GPL8031). It can therefore be safely assumed that the data was in fact run on this newer version of the beadchip, rather than the older version reported in Huang, Jarjour et al., 2011.

As shown in **Table 3.1**, the data set consisted of three time-points after the induction of focal demyelinating injury using LPC, 5 days post lesion, 14 days post lesion and 28 days post lesion, and replicates from three separate rats were used for each condition.

| Data Type | GEO Numbers of Replicates |
|---|---|
| 5 Days Post Lesion, Focal demyelination induction in the rat cerebellar peduncle by LPC injection | 1.GSM610956<br>2.GSM610957<br>3.GSM610958 |
| 14 Days Post Lesion, Focal demyelination induction in the rat cerebellar peduncle by LPC injection | 1.GSM610959<br>2.GSM610960<br>3.GSM610961 |
| 28 Days Post Lesion, Focal demyelination induction in the rat cerebellar peduncle by LPC injection | 1.GSM610962<br>2.GSM610963<br>3.GSM610964 |

Table 3.1. Data sets from Huang Jarjour *et al*., 2011 (GEO Accession Number GSE24821)

An important difference between Illumina bead arrays and other popular gene expression microarray technologies, is that while in other array types probes are fixed to the 2 dimensional array surface, Illumina beadArrays are made up of 3-micron silica beads, each coated with hundreds of thousands of copies of a specific oligonucleotide corresponding to a particular genomic sequence (Dunning et al., 2007). In other array platforms, transcript probes are identified by their physical location on the array surface (Fodor et al., 1991; Holloway et al., 2002; Schena et al., 1995). In contrast, in the case of Illumina beadchips, the oligonucleotide coated beads self-assemble at random into wells on the array platform (Michael et al., 1998) and therefore cannot be identified by their physical position on the array. A consequence of this approach is that the randomly distributed oligonucleotide beads must be identified and matched to their associated transcript sequence before any analysis can take place. This decoding step is achieved using sequential hybridisation of fluorescently labelled oligonucleotide sequences to unique identifying sequences present on each bead (Gunderson et al., 2004).

To investigate the data sets from Huang, Jarjour et al., 2015, I retrieved the pre-analysed data from the Gene Expression Omnibus (GEO, accession number GSE24821). The available files included raw bead intensities from each of the 3 replicates for the 3 conditions (see **Table 3.1**). The data available for this experiment was in the bead summary level format, indicating that background correction, as well as the calculation of mean intensities for beads for the same transcript sequence, had already taken place.

Having retrieved the data from GEO, I parsed the mean intensity for each set of beads with the same probe sequence (bead group) into an R object using the Illumina beadchip specific beadarray package (Dunning et al., 2007).

### 3.2.2 Primary data inspection, Quality Control and Normalisation

Having parsed the data into R, I inspected the quality of data by generating quality control plots. As shown in **Figure 3.1**, the mean bead group intensities for each probe were extremely similarly distributed across all nine arrays making up this data set.

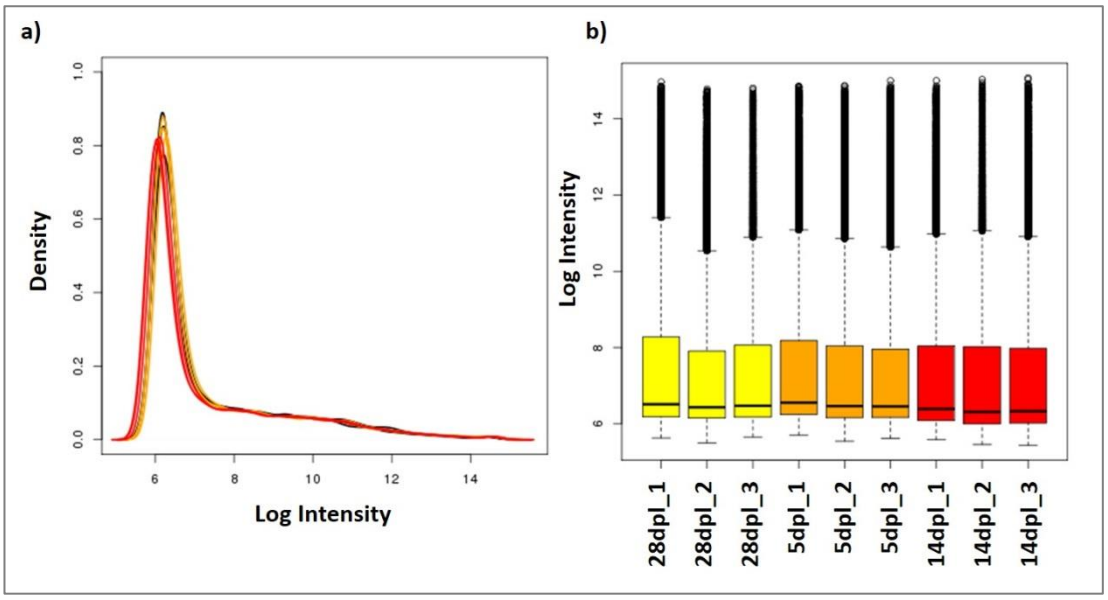


**Figure 3.1 Pre-normalisation quality control plots for Illumina data.** 5dpl samples are represented in red, 14dpl samples in orange and 28dpl samples in yellow **a)** Density and **b)** box plots showing an extremely similar pattern of raw log intensity across all the arrays in the data, without normalisation.

I then used MA plots to explore the distribution of log intensities in more depth. In an MA plot, the difference in expression for each transcript between two arrays (M) is plotted against the average expression of each transcript on the two arrays (A). Each transcript is represented with a single dot on the plot, and the distribution of points on the plot is used to visualise the variation between the two arrays.

As shown in **Figure 3.2 a)**, when an MA plot is generated for two replicate arrays for the same condition, in this case 28dpl replicate 1 and 28 dpl replicate 3, the vast majority of points are evenly distributed around M≈0 with the loess line at M≈0 across the range of average intensities and few outlying points. In **Figure 3.2 b)**, an MA plot for the arrays for 28 dpl replicate 3 and 5 dpl replicate 1 was generated, points are similarly evenly distributed around M≈0 with the loess line nearly horizontal across M≈0. In this plot, more outlying points are evident, but this is to be expected within a normal distribution for arrays representing different time-points.

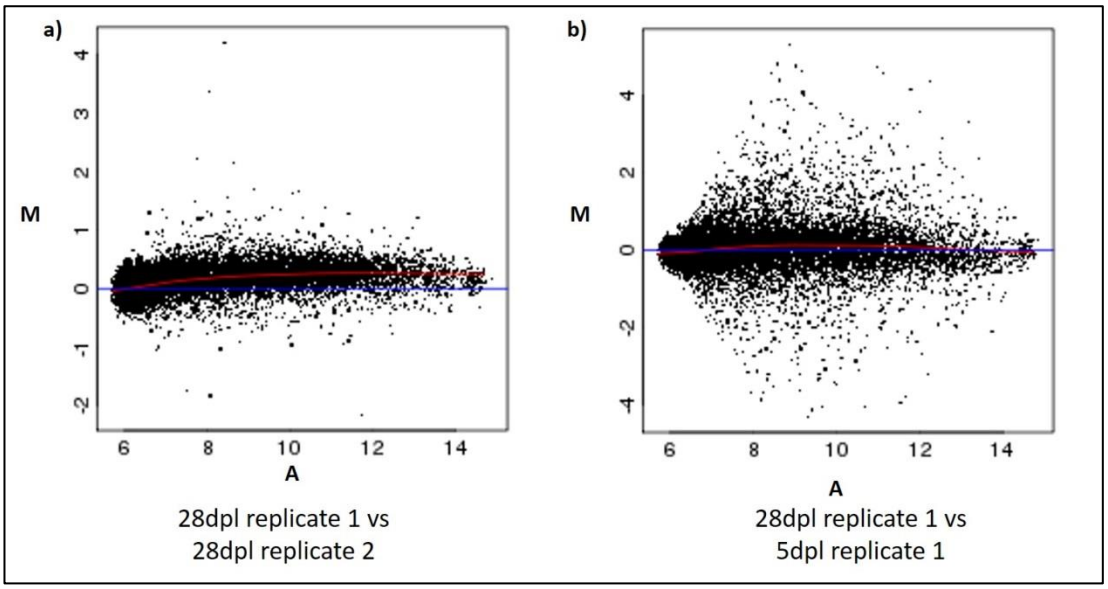


**Figure 3.2 Example MA plots: The log ratio (M) of the pixel intensities for two microarray samples is plotted against the average pixel intensity (A) of each probe pre-normalisation. IQR=Interquartile Range, Local Regression line denoted in red.** The difference in expression for each transcript between two arrays (M) is plotted against the average expression of each transcript on the two arrays (A) **a)** 28 dpl replicate 1 vs 28 dpl replicate 3, two replicate arrays for the same time-point show high correlation between the arrays with the majority of bead group intensities grouped around M≈0, the loess line at M≈0 across the whole range of intensities and few outliers. **b)** 28 dpl replicate 1 vs 5 dp replicate 2, arrays representing two different time-points showing an expected level of correlation with the majority of bead group intensities grouped around M≈0, the loess line at M≈0 across the whole range of intensities. A greater proportion of outliers are evident, representative of the biological differences between the two time-points.

Consistent with the plots in **figure 3.1,** this shows that the data is similarly distributed with no significant discrepancies to be mediated, although normalisation is still necessary to more evenly align the array distributions.

Having established that the data was of high quality and suitable for analysis, I normalised the data using an Illumina bead array specific method from the beadarray R package. This method featured quantile normalisation alone, because, as previous mentioned, the background correction step was carried out by the original authors before I accessed the data.

### 3.2.3 Hierarchical Clustering and Principal Component Analysis

To visualise how similar the 9 arrays in the data set were to one another, I used hierarchical clustering by Pearson's correlation coefficient to establish the relationships between the different arrays. As shown in **figure 3.3,** hierarchical clustering of the arrays using Pearson's correlation coefficient separates the samples by time-point, as would be expected. It also shows that there is higher correlation between the two later post-lesion time-points at 14 dpl and 28 dpl, and the earlier time-point at 5 dpl.

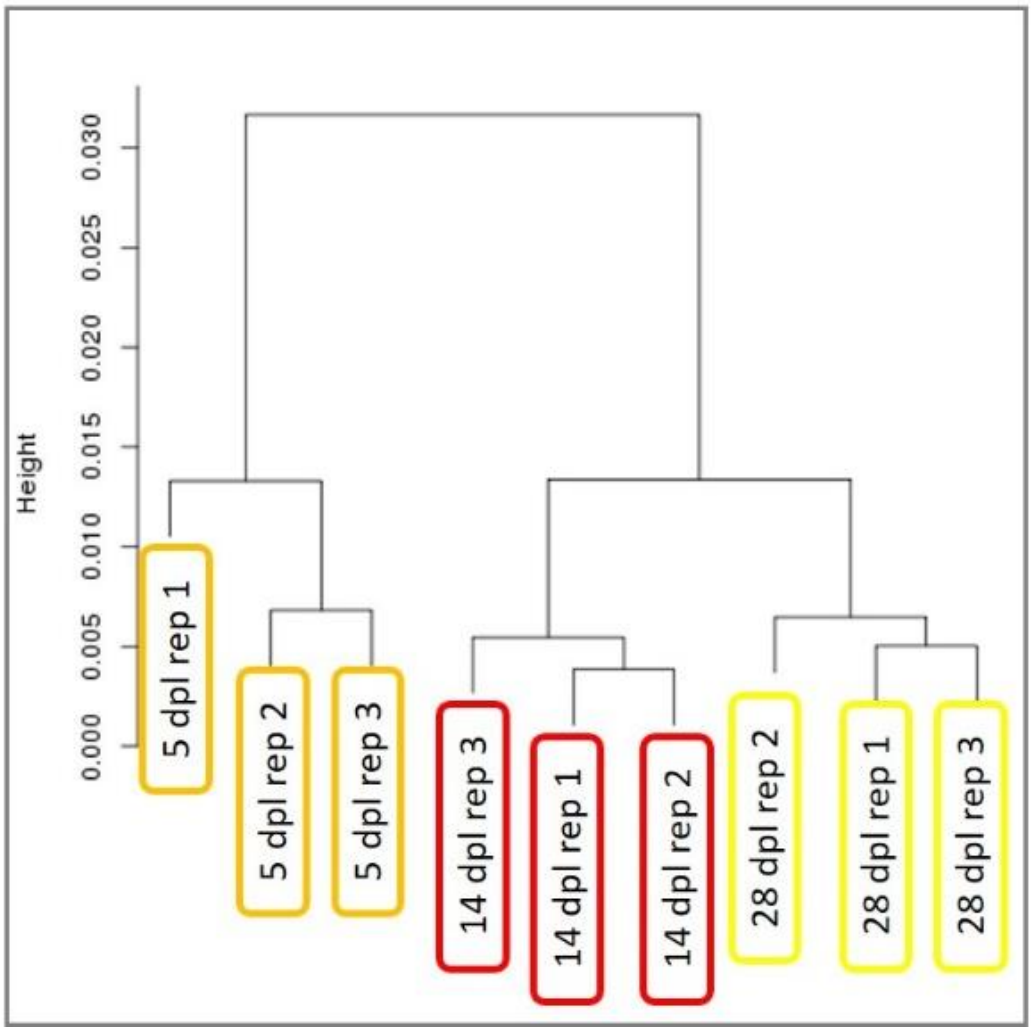


**Figure 3.3** Hierarchical clustering using Pearson's correlation coefficient groups arrays from Huang, Jarjour et al 2011 dataset by post-lesion time-point, with the 14 dpl and 28 dpl more closely correlated with one another than with 5dpl

Another technique which can be used to visualise the relationship between the arrays is Principal component analysis (PCA). This technique emphasises variation and can be

used to identify strong patterns in the data. In the case of gene expression array data, the covariance of each transcript in each array against every other transcript in every other array is constructed into a multi-dimensional covariance matrix. PCA then identifies the directions (known as principal components) in this matrix in which the data varies most strongly. The variation between the arrays which can be accounted for by each principal component, can then be visualised on a 3-dimensional plot.

As shown in **figure 3.4**, PCA of the Huang, Jarjour et al., 2011 dataset groups the replicates for each time point together, although there is close association between the 14 dpl and 28 dpl time-points with the 5 dpl time-point more distantly correlated. The contributions of the individual principal components can be found in **appendix 1**, along with the genes whose variation is captured most by each principal component.

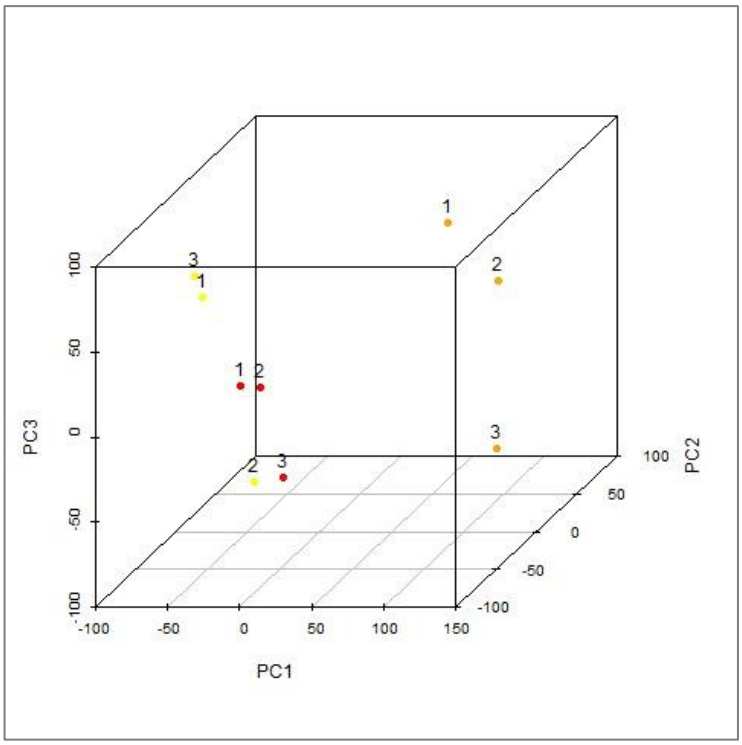


**Figure 3.4 3-D Scatterplot of Principal Component Analysis of Huang, Jarjour et al., 2011 Data** Orange dots=5dpl, red dots=14dpl, yellow dots=28dpl, numbers refer to the individual replicates (see **table 3.1**). Principal Component Analysis groups arrays from Huang, Jarjour et al 2011 dataset by post-lesion time-point, with the 14 dpl and 28 dpl more closely correlated with one another than with 5dpl less closely associated.

The differences in the groupings of the arrays by hierarchical clustering versus principal component analysis are a function of the difference between the two approaches. In essentials, the hierarchical clustering algorithm, groups data sets by similarity, while principal component analysis takes the opposite approach of separating data sets by their variation. Principal component analysis is designed to capture as much of the variation between the data sets as possible, however it also reduces the dimensionality of the data, in doing so, some of the weaker effects in the data are filtered out, leaving only the components with the strongest separating effects on the data set. A caveat of hierarchical clustering is that this method will find groupings in the data, even if no strong separating effect is present.

Thus, as shown in the hierarchical clustering dendrogram in **figure 3.3**, ranking of the arrays in the Huang, Jarjour et al., 2011 data by similarity, results in the grouping of the arrays by experimental condition. In contrast, in the principal component analysis in **figure 3.4**, the strongest diverging effect in the data set (principal component 1), separates the 5 days post lesion arrays from the 14 and 28 days post lesion arrays, more strongly than from one another. The principal component analysis suggests that there is more similarity in the 14 and 28 days post lesion, which is also reflected in the hierarchical clustering. This is a biological possibility given that by these later timepoints, the inflammatory infiltration characteristic of early injury has subsided, giving way to regeneration.

These results show that post-normalisation, the arrays separate into a pattern that could have been predicted based on the experimental design. This shows that normalisation was successful and the data is of high quality and suitable for differential expression analysis.

### 3.2.4 Differential Expression Analysis of Huang/Jarjour Data

Having produced arrays of quantile normalised expression values for the whole dataset, the next step in my analysis was to discover which genes were differentially expressed at the different time-points. I performed differential analysis and the statistical analyses required to accompany it using the limma package available for R.

I applied limma in two stages: firstly I created a model matrix specifying which arrays represent replicates for the same timepoint and applied it to the data thus allowing mean expression values for every probe for each timepoint to be calculated.

The second phase of the limma analysis was the application of the contrast matrix designating which conditions were to be compared to one another. Since there were only three timepoints available, I compared each timepoint to every other timepoint. Contrasts between conditions were calculated as $\log_2$ fold changes and the statistical tests were carried out to give the outputs listed in **table 3.2**. Briefly, for each gene in each contrast a moderated t-statistic was calculated which measured the difference between the two time-points by units of standard deviation, the resulting t-value was moderated across all the genes using a Bayesian model. The p-value for each gene was then adjusted for multiple testing to give the false discovery rate (Benjamini and Hochberg, 1995).

| **Statistical Analysis Outputs** | **Description** |
|---|---|
| $\text{Log}_2$ fold change | Difference in mean expression values between the two groups |
| Moderated t-statistic | Difference between the two groups by units of standard deviation, higher values indicate bigger differences between the two groups, the ratio of the Log2 fold change to its standard error. |
| p-value | t-value moderated across all genes using a Bayesian model, the probability that the observed difference between groups is real, does not account for multiple-testing |
| Adjusted p-value | p-value adjusted for multiple testing using the false discovery rate developed by Benjamini and Hochberg (Benjamini and Hochberg, 1995) |
| Log odds score | Log odds of differential expression for this gene (Smyth, 2004) adjusted for multiple testing assuming that 1% of genes are differentially expressed |

**Table 3.2 Statistical outputs from differential expression analysis using Limma**

To eliminate genes with no significant variance in any of the contrasts between timepoints, I excluded features without an adjusted p-value of ≤0.05 for at least one contrast from further analysis. In this way, from the 22,226 features on the array I found only 4,814 (21.66%) which were differentially expressed between at least two timepoints.

### 3.2.5 Selection of Secreted Factors Using Ensembl Biomart

My overall aim in analysing this dataset was to search for factors emanating from sites of demyelinating injury, which might modulate OPC behaviour. For this reason, having identified the significantly differentially expressed genes, I utilised the Ensembl Biomart tool (Herrero et al., 2016, Ensembl release 84, http://www.ensembl.org/biomart/martview/84ae73fe2c935c797186934eba30f2e9) to obtain a list of all the genes on the Illumina ratRef-12 v1.5.0.34 expression bead chip whose proteins were known to be secreted.

In the Ensembl Biomart web interface, I selected Ensembl Genes 84 database and the Rat Genes (Rnor_6.0) dataset. On the Attributes tab, I selected Gene ID, Transcript ID and Associated Gene Name as outputs from the GENE dropdown list and signal peptide from the list of Transmembrane and Signal domains as an output from the PROTEIN DOMAINS AND FAMILIES dropdown list. This produced a list of all 3891 rat genes listed as having a protein signal domain indicative of extracellular secretion.

I then matched my differentially upregulated gene list to this signal peptide list and identified 3614 significantly differentially upregulated genes with a signal peptide in their corresponding proteins.

### 3.2.6 Selection of Factors by Expression Pattern Using Correlation Analysis

With so many secreted factors identified, an approach curtailing this list to only those factors most likely to impact OPC biology was necessary. I reasoned that secreted factors which augment OPC migration were likely to be similarly expressed in a similar pattern to PDGFα, which is a known chemoattractant for OPCs (Zhang et al., 2004).

As illustrated in **figure 3.5a)**, PDGFα expression steadily rises in expression intensity from the 5 days post lesion time point to the 28 days post lesion time point. Reasoning that other novel regulators of OPC biology might follow a similar pattern of expression, I

next performed a correlation analysis to discover factors whose expression pattern correlated with both PDGFα. **Figure 3.5b)**, plots the Log2 fold changes in PDGFα expression for all the possible contrasts for the 3 time-points.

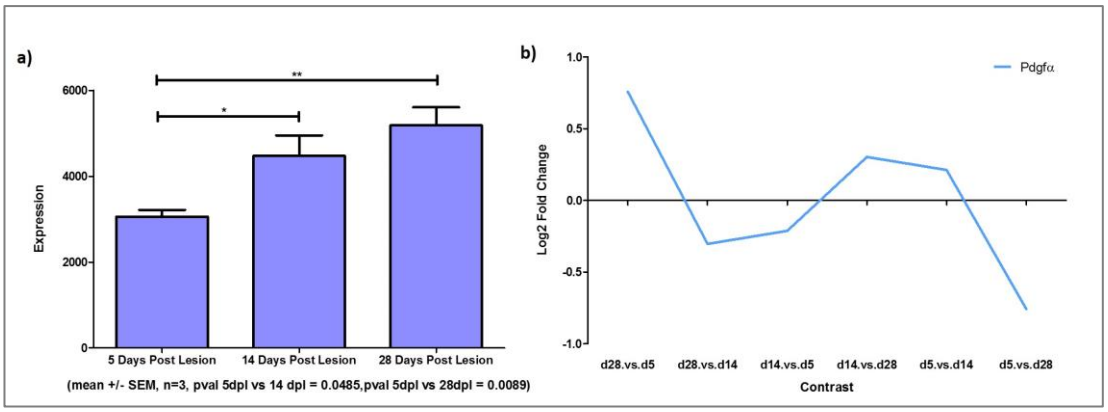


**Figure 3.5 Experssion of PDGFα in Huang, Jarjour et al., 2011 data a)** Normalised expression of PDGFα across the 3 time-points, there is a significant increase in expression of PDGFα between 14 dpl and 5dpl, and a further more significant increase in expression between 28 dpl and 5 dpl (both by unpaired t-Test) **b)** Pattern of $Log_2$ fold change in PDGFα between the 6 possible contrasts for the 3 time-points, all Log2 fold changes have an adjusted pvalue ≤0.05.

To give the maximum number of data points for the correlation analysis, I analysed the $log_2$ fold change between the means of each time-point for contrasts between all conditions (28 days post lesion vs 5 days post lesion, 28 days post lesion vs 14 days post lesion, 14 days post lesion vs 5 days post lesion, 14 days post lesion vs 28 days post lesion, 5 days post lesion vs 14 days post lesion and 5 days post lesion vs 28 days post lesion).

In order to identify other factors which followed a similar pattern of expression, I calculated the Pearson's correlation coefficient for each secreted factor compared with PDGFα. From the secreted factors, I selected only those which had a correlation coefficient of >0.85 with PDGFα. Using this method, I identified 410 factors with correlating expression patterns, as demonstrated in **figure 3.6**. Interestingly, among the secreted factors identified was Lingo-1, reported to be a negative regulator of OPC differentiation (Mi et al., 2005) and CXCL12 which has been shown to act as a proliferation and differentiation factor for OPCs (Patel et al., 2012). This supports my hypothesis that other modulators of OPC biology would be expressed in a similar post injury temporal pattern to known PDGFα.

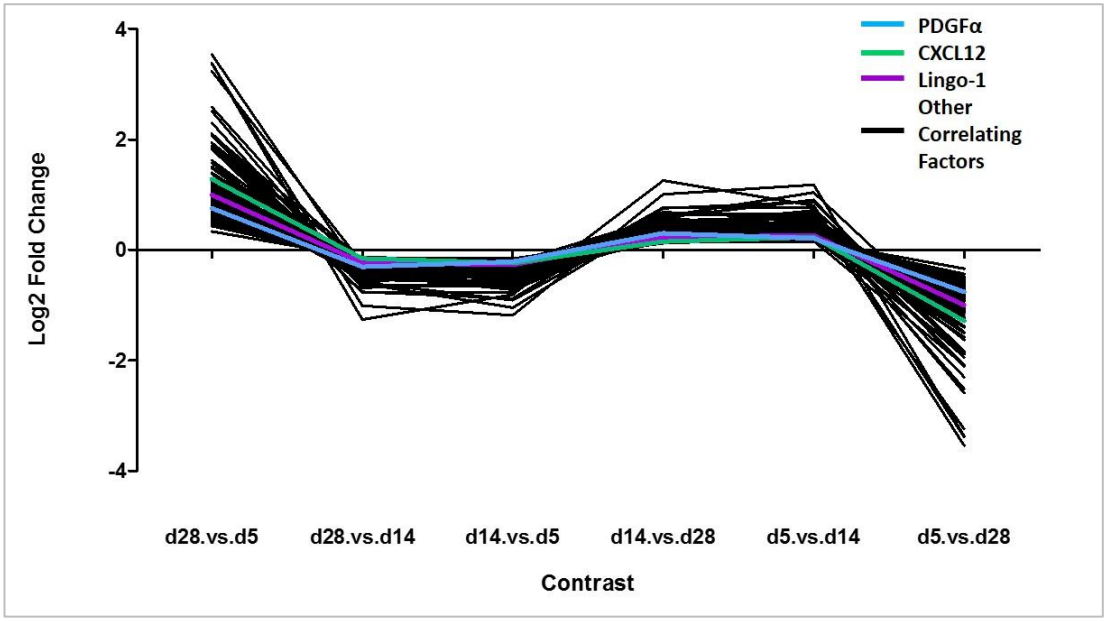


**Figure 3.6 Expression Pattern of Secreted Factors with a Correlation with PDGFα of >0.85.** Expression patterns of all 288 features from the Huang/Jarjour *et al*., 2011 study with an adjusted p-value of <0.05 in at least 1 contrast, and Pearson's Correlation of >0.85 with PDGFα. Interestingly, another known OPC modulators LINGO-1 which is a negative regulator of OPC differentiation (Mi et al., 2005) and CXCL12(Patel et al., 2012) a proliferation and differentiation factor for OPCs are also expressed in a correlating pattern.

A full list of the 410 correlating factors and their statistics can be found in **appendix 2**.

In summary, of the 22,226 probes represented on the complete array, I found only 4,814 with statistically significant differences in expression between two or more timepoints (with a p-value of ≤0.05). Of these 4,814, I found only 3,614 with a known signal domain according to the Ensembl Biomart database, of which only 410 correlated with the temporal expression pattern of PDGFα. Since this was a reasonably small number of potential targets, I did not reduce the list further based on absolute expression value or fold change between timepoints, at this stage. Further reduction of this list of potential targets was achieved using the data from the Moyon et al., 2015 data, which will be described in **Chapter 3.3**.

With 410 correlating secreted factors identified, I next set out to reduce this number by identifying only those secreted factors which had receptors which were expressed by migratory OPCs. In the next section, I will explain how I analysed the data from Moyon et al., 2015 and used it to identify cell surface receptors expressed by migratory OPCs.

### 3.3 Identification of Upregulated Cell Surface Receptors in Regeneratively Activated OPCs

#### 3.3.1 Moyon et al., 2015 Experimental Design

As summarised in **Table 3.2,** in their 2015 paper, Moyon *et al*. ran samples of purified mouse activated OPCs, non-activated OPCs, neonatal OPCs, adult OPCs and adult oligodendrocytes on Agilent 026655 Whole Mouse Genome Microarrays (GPL11202 GEO). These arrays have 39,430 biological features derived from Entrez Gene RNAs and 10 replicate probes for each biological feature along with 12 x10 ERC control probes and 32x10 E1A spike in control probes. All probes are 60mer in length and arrays were prepared using Agilent sureprint technology.

(http://www.genomics.agilent.com/article.jsp?crumbAction=push&pageId=1520, last accessed 15/12/2015)(2015)

| Sample Type | Preparation | Animal Line | GEO Numbers of Replicates |
|---|---|---|---|
| **Neonatal oligodendrocyte precursor cells (nOPCs)** | Isolation from P1 – P5 mouse brain by Fluorescence-activated cell sorting (FACS) (Piaton et al., 2011) | PDGFαR:GFP hemizygous mice (Moyon et al., 2015) RRID:IMSR_JAX:007669 | 1.GSM1186197<br>2.GSM1186198<br>3.GSM1186199 |
| **Adult oligodendrocyte precursor cells (aOPCS)** | Isolation from 2month old mouse brain by Fluorescence-activated cell sorting (FACS) | PDGFαR:GFP hemizygous mice (Klinghoffer et al., 2002) RRID:IMSR_JAX:007669 | 1.GSM1186193<br>2.GSM1186194<br>3.GSM1186194<br>4.GSM1186195 |
| **Adult Oligodendrocytes (aOLs)** | Isolation from 2month old mouse brain by Fluorescence-activated cell sorting (FACS) | PLP-GFP mice (Spassky et al., 2001) | 1.GSM1186200<br>2. GSM1186201<br>3. GSM1186202<br>4. GSM1186203 |
| **Activated adult oligodendrocyte precursor cells (Activated aOPCs)** | Isolation from 2 month old mouse brain precedently treated with 0.2% cuprizone for 5 weeks by Fluorescence-activated cell sorting (FACS) (Piaton et al., 2011) | PDGFαR:GFP hemizygous mice (Klinghoffer et al., 2002) | 1.GSM1186204<br>2. GSM1186205<br>3. GSM1186206<br>4. GSM1186207 |
| **Non-activated adult oligodendrocyte precursor cells (Nonactivated aOPCs)** | Isolation from 2 month old mouse brain by Fluorescence-activated cell sorting (FACS) (Piaton et al., 2011) | PDGFαR:GFP hemizygous mice (Klinghoffer et al., 2002) | 1.GSM1186208<br>2. GSM1186209<br>3. GSM1186210 |

Table 3.2. Data sets from Moyon *et al*., 2015 (GEO Accession Number GSE48872)

### 3.3.2 Primary Data Inspection, Quality Control and Difference in Intensity Distribution Between Arrays Issue

To visualise the data sets from Moyon *et al*., 2015, I retrieved the pre-analysed data from the Gene Expression Omnibus (GEO, accession number GSE48872) and read the mean foreground and background pixel intensities for all probe spots into the statistical analysis environment R.

Having read the mean pixel intensities for the Agilent microarrays into an R data frame, I visualised the distribution of pixel intensities using density plots and box plots (**Figure 3.7**). The density plots (**Figure 3.7a)**) and boxplots (**Figure 3.7d)**) for the foreground features reveal that the data sets can be divided into two distinct groups based on their distributions of pixel intensities.

The first pixel intensity group with higher median log pixel intensities of around 10 comprising all the replicates for activated OPCs and non-activated OPCs will henceforth be described as **Intensity Group A (figure 3.7 b), e))**, and the second with lower median log pixel intensities of around 8 comprising all the replicates for neonatal OPCs, adult OPCs and adult oligodendrocytes, will henceforth be described as **Intensity Group B (figure 3.7 c), f))**. Such a discrepancy in the distributions of log intensities between samples represents a confounding inconsistency in the data which is unlikely to be biological.

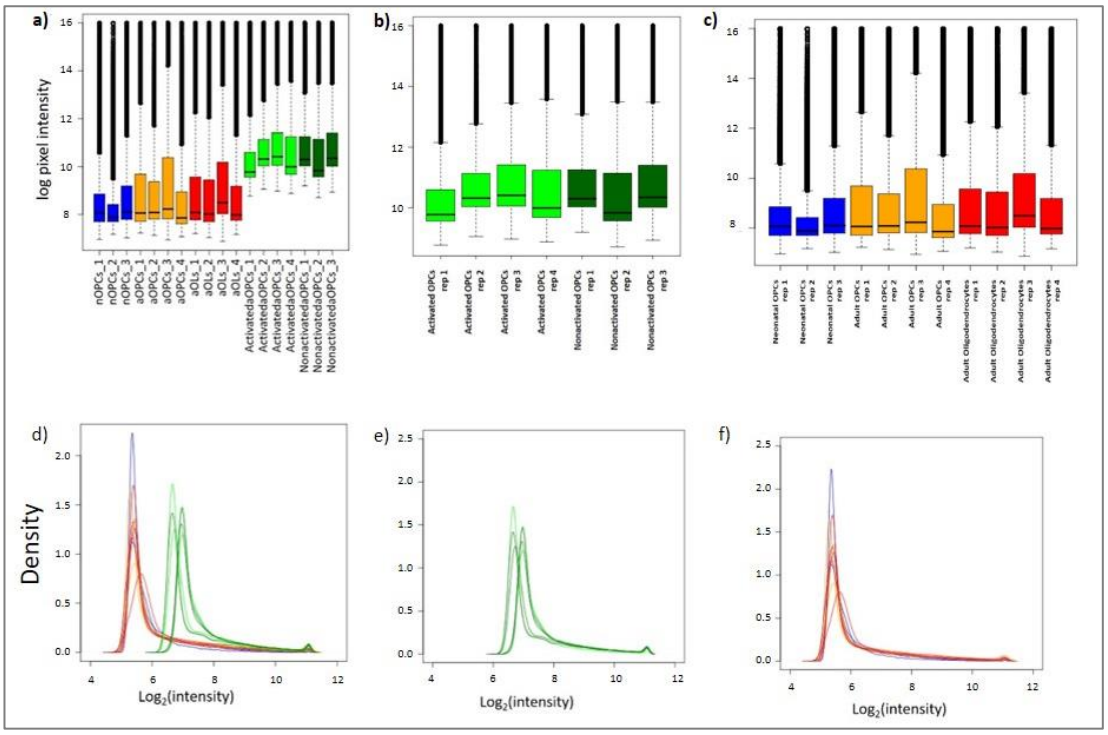


**Figure 3.7 Distribution of pre-normalisation mean pixel intensity values for all arrays representing the different oligodendroglial cell types in the Moyon *et* al., 2015 data set show that the arrays fall into two distinct groups.** For boxplots, the coloured boxes extend from quartile 1 to quartile 3 intersected by the median, which is represented by a line, the minimum to maximum extent of the data is signified by the dashed line and outliers denoted as circles. In all plots arrays of the same cell type are coloured as follows: Neonatal OPCs-Blue, Adult OPCs-Orange, Adult Oligodendrocytes-Red, Activated OPCs-Light Green, Non-activated OPCs-Dark Green. **a)** Pre-normalisation box plot and **d)** pre-normalisation density plots show that the data groups into two separate sets based on the mean and ranges of $\log_2$ intensity for each array and that arrays from the same cell type have broadly similar intensity distribution. **b)** Box plots and **e)** density plots for Intensity Group A, with higher median log pixel intensities of around 10 comprising all the replicates for activated OPCs and non-activated OPCs. **c)** Boxplots and **f)** density plots for Intensity Group B, with lower median log pixel intensities of around 8 comprising all the replicates for neonatal OPCs, adult OPCs and adult oligodendrocytes.

To visualise the distribution of probe intensities across the arrays in more detail, I employed MA plots (**Figure 3.3**). As shown in figure **3.8a)** when an MA plot is generated for the arrays of two replicate samples for the same condition, a widespread distribution in average intensity of probes can be observed along the x-axis, while the log ratio M between the two arrays is around zero for the majority of probes. By fitting a local regression line (red), the variation in the log ratio as average intensity increases can be represented using a smooth curve. As expected, the close proximity of features

represented by spots to M=0 across the increasing values of average intensity indicates significant similarity between the two arrays for the same condition.

In figure **3.8b)** when an MA plot is generated for two samples from different conditions with a reasonably similar expression profile (see **figure 3.7**) M~0 for the majority of probes consistent with a lack of differential expression between the two arrays for these genes. As compared to figure **3.8a)** there is a higher proportion of outlying probes indicative of increased differential expression between the two conditions.

As mentioned earlier and indicated by the boxplots and density plots in **figure 3.7**, the arrays in this experiment can be separated into two distinct groups based on the distribution of their probe intensities as in **figures 3.7 b), e) and c), f)**. In figure **3.8c**) arrays from the two groups have been combined. As compared to the previous examples in **figures 3.8a)** and **3.8b),** M=0 for very few of the probes and the whole data set is skewed with big differences in expression between lowly expressed probes.

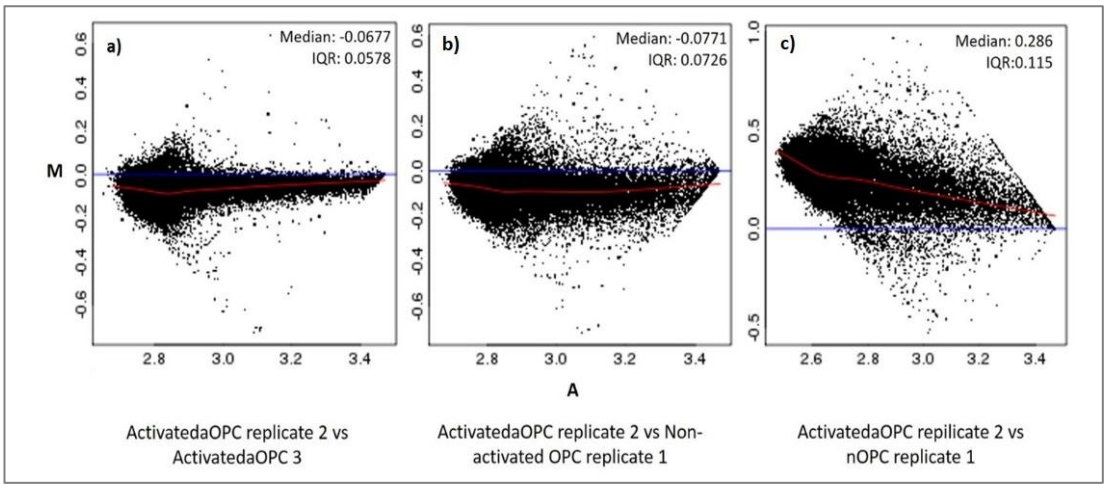


**Figure 3.8. Example MA plots: The log ratio (M) of the pixel intensities for two microarray samples is plotted against the average pixel intensity (A) of each probe pre-normalisation. IQR=Interquartile Range, Local Regression line denoted in red. a)** $M=\log_2$(Activated adult OPC replicate 2) – $\log_2$(Activated adult OPC replicate 3) pre-normalisation, an example of two replicates of the same condition between which little variation should be expected with the vast majority of genes evenly distributed around an M of 0. Deviation of the local regression line from M=0 indicates that normalisation steps will be required for this data **b)** $M=\log_2$(Activated adult OPC replicate 2) – $\log_2$(Non-activated OPC replicate 1), an example of arrays from two different sample conditions with similar raw pixel intensity distributions (both Intesity Group A) pre-normalisation. The vast majority of genes are distributed around M=0, variation in the magnitude of M is as expected for two samples from different conditions. Deviation of the local regression line from M=0 indicates that normalisation steps will be required for this data. **c)** M= $\log_2$(Activated adult OPC replicate 2) – (Neontal OPC replicate 1), an example of replicates from two different samples with extremely divergent raw pixel intensity distributions (from different intensity groups), pre-normalisation. Universally increased expression values on the Activated adult OPC replicate 2 chip as compared to the Neonatal OPC replicate 1 chip results in a skewed plot with the majority of probes > M=0. Robust deviation of the local regression line from M=0 indicates that there may be technical issues with the data.

From the box-plots, density plots and MA plots above, I concluded that the quality of the data had been compromised. A possible explanation for this could be a high background to foreground ratio on the arrays.

### 3.3.3 Background Signal Issue

To find out if high background signal was an issue in this dataset, I looked at the background reading for each array in the data set. On the Agilent array platform, along with the foreground readings representing the biological signal, for each spot on the

array a background signal representing the ambient signal is generated from the average pixel intensity surrounding each probe spot.

As shown in **figure 3.9**, I generated boxplots for the background signal of each array. On comparison of the foreground signal (**figure 3.9a)**) with the background signal (**figure 3.9b)**), it became obvious that the background signal for all the arrays was extremely high, averaging at around 70-90% of the mean foreground signal. As shown in **figure 3.9c)**, due to the high background signal, background correction has a deleterious effect on the data, leaving almost no data for further analysis.

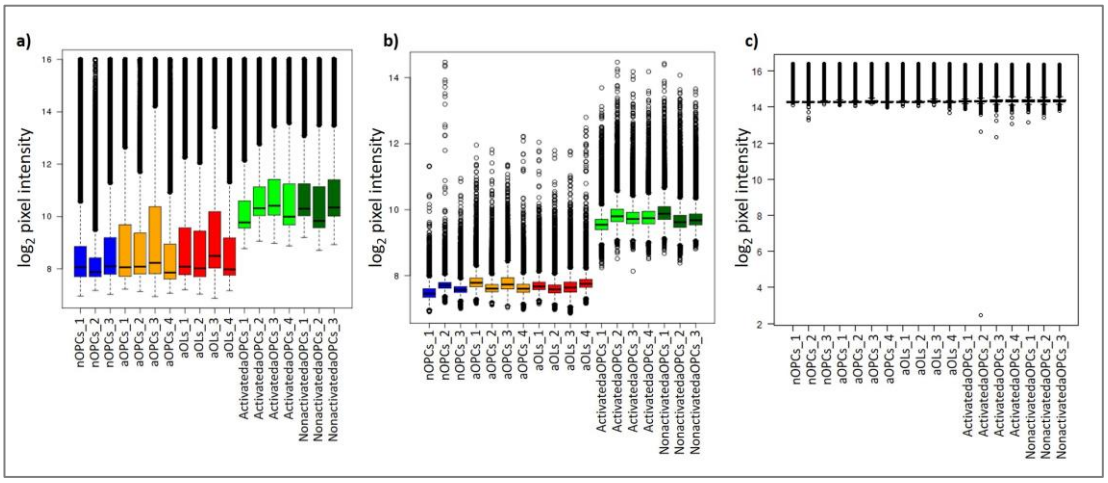


**Figure 3.9 Background correction has a deleterious effect on Moyon et al., 2015 data.** Box plots showing distribution of $log_2$ raw pixel intensity data for all arrays with replicates of the same cell type and condition represented by colour. Arrays of the same cell type are coloured as follows: Neonatal OPCs-Blue, Adult OPCs-Orange, Adult Oligodendrocytes-Red, Activated OPCs-Light Green, Non-activated OPCs-Dark Green. **a)** Foreground measurements **b)** Background measurements reveal that background intensities for Intensity Group A and Intensity Group B have similar median values to their corresponding foreground probes, indicative of high signal:background noise ratio **c)** Foreground measurements after background correction (subtraction of background from foreground, offset with the addition of the biggest difference between foreground and background to keep all background corrected intensities > 0). The background values represent such a large portion of the foreground values that subtraction of the background leaves very little data to be analysed.

Background readings can generally be attributed to experimental error such as optical noise from the scanner or errors in treatment of the microarray chip such as deposits remaining post wash stage or user DNA or RNA contamination (reviewed Ritchie et al., 2007). In principle, subtraction of the background from the foreground should eliminate

non-specific signal, however in this case background correction is too disruptive to be appropriate. For this reason, I skipped any background correction step for this data-set.

Due to the high background signal, small differences in gene expression in this data-set are difficult to detect, because their signal is obscured by the background noise. However, changes in gene expression of higher magnitude will still be detectable, the net effect is that fewer significantly varying genes are likely to be detected.

As a result of the difference in the distribution of both background and foreground intensities between the two groups of samples (Neonatal OPCs, Adult OPCs and Adult Oligodendrocytes vs Activated OPCs and Nonactivated OPCs), without batch correction, direct comparison of gene expression cannot be made between the two groups. Taking this into account, along with the focus of this thesis being the biology of adult OPCs, I decided to eliminate the lower intensity samples (Neonatal OPCs, Adult OPCs and Adult Oligodendrocytes) from further analysis and focus solely on the comparison between Activated OPCs and Nonactivated OPCs.

#### 3.3.4 Normalisation

My next step was to counteract non-biological variation between arrays using a modified version of Robust Multichip Averaging (RMA) normalisation developed by Irizarry et al., 2003. RMA normalisation is usually performed in three stages: background correction, scaling and aggregation of signals pertaining to the same gene.

As detailed in the exploratory analysis above, I determined background correction to be deleterious to this data set. I thus applied only the scaling and aggregation steps. The data was scaled by quantile normalisation between arrays and the signal was aggregated by averaging replicate probes for the same gene.

#### 3.3.5 Hierarchical Clustering and Principal Component Analysis

Having normalised the data, I next wanted to find out how closely the arrays correlated with one another, firstly, to ascertain whether replicate arrays for the same sample were highly correlated, and secondly to investigate the relationship between the different samples.

I used Pearson's correlation coefficient to measure the similarity in overall gene expression between each of the arrays. The Pearson's correlation coefficients for each possible pair of samples in the two groups were then ranked, allowing the hierarchical clustering dendrograms in **figure 3.10** to be constructed.

As shown in the dendrogram in **figure 3.10**, the two sets of replicates for Activated and Non-activated OPCs separate to form the two major branches of the dendrogram with replicates of the same cell type grouping together, this shows that replicate samples for the same cell type are more strongly correlated with one another than with samples for the opposing cell type.

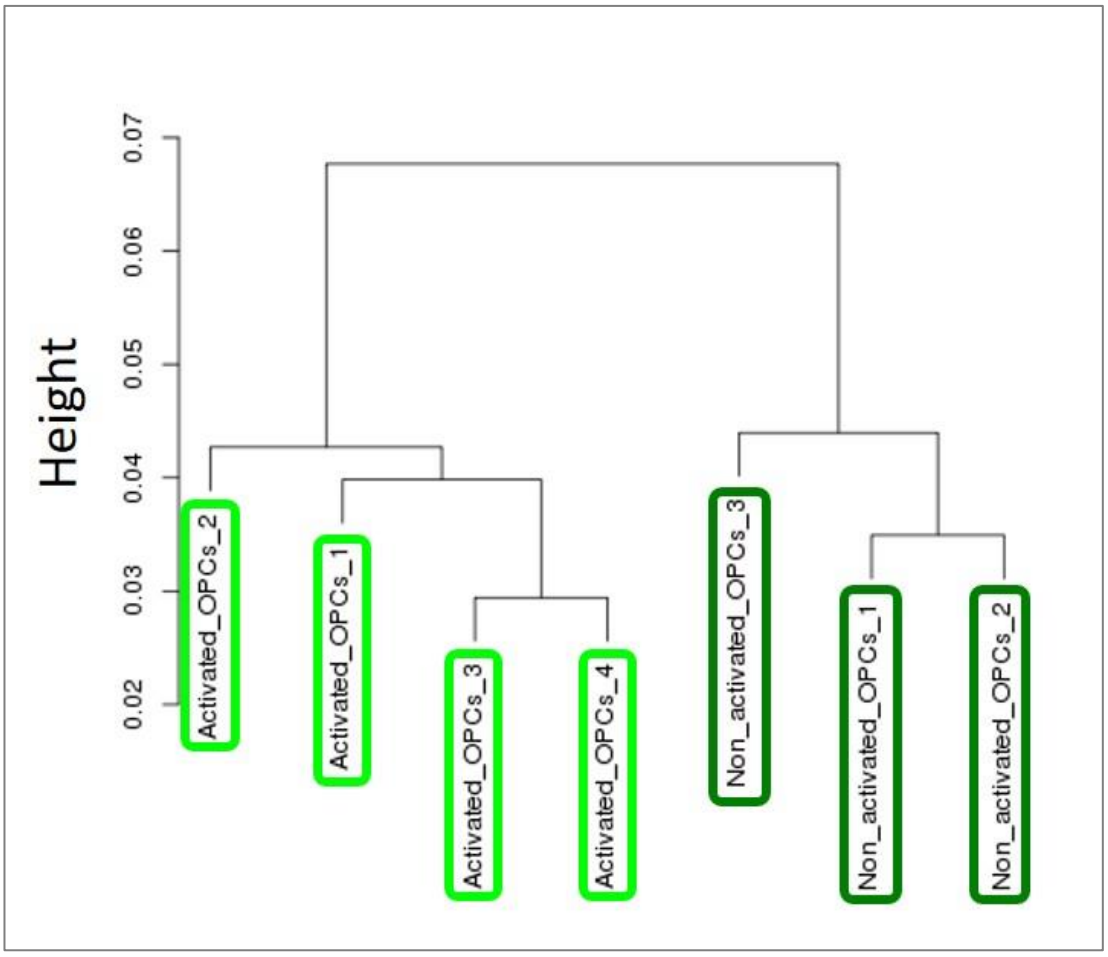


**Figure 3.10 Hierarchical clustering of normalised intensity values using Pearson's correlation coefficient shows degree of correlation between arrays.** Activated OPCs - Light Green, Non-activated OPCs - Dark Green, replicates cluster by cell type. Replicate arrays for Activated OPCs group separately from the replicate arrays for Nonactivated OPCs indicating higher correlation between arrays for the same cell type than for arrays for different cell types.

While hierarchical clustering using Pearson's correlation coefficient may give some indication of the relationships between samples and the averages of pooled samples, it relies heavily on cumulative variance of all the probe-sets on the array and assumes that features and therefore the genes they represent vary independently. Following any change in cellular conditions, the subsequent conformational change in gene transcription is not the sum of independently functioning individual genes, but a complex network of co- and interdependent regulatory elements resulting in the co-expression of interrelated sets of genes.

### 3.3.5 Principal Component Analysis of Normalised Data

As with the Huang, Jarjour et al., 2011 data, a technique better equipped to deal with this phenomenon is principal component analysis, a statistical paradigm used to simplify complex data sets by multidimensional matrix reduction (reviewed, Raychaudhuri et al., 2000).

As shown in **figure 3.11**, PCA of the Moyon et al., 2015 dataset groups the replicates for each time point together, although there is close association between the 14 dpl and 28 dpl time-points with the 5 dpl time-point more distantly correlated. The contributions of the individual principal components can be found in **appendix 1**, along with the genes whose variation is captured most by each principal component.

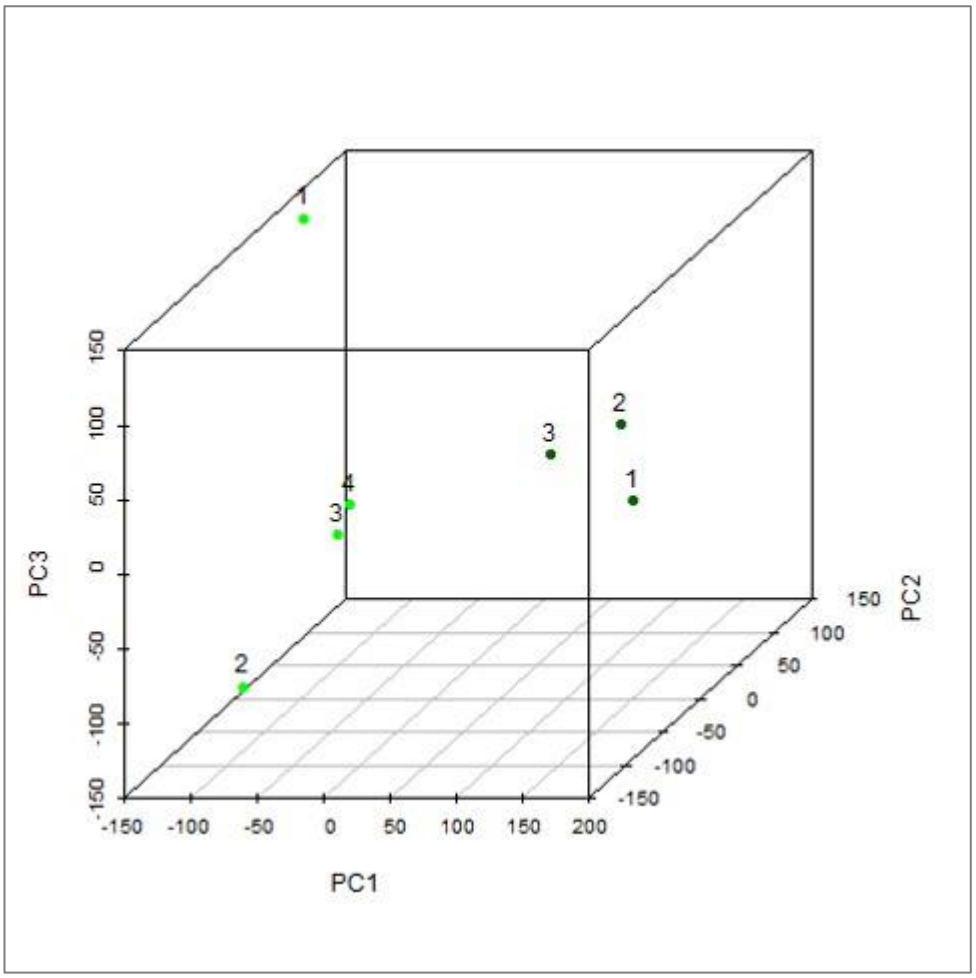


**Figure 3.11 Scatterplot of Principal Component Analysis of Moyon et al., 2015 Data**

Activated OPCs - Light Green spots, Non-activated OPCs - Dark Green spots, spot numbers represent the name of the replicate number. Replicate arrays for Activated OPCs group separately from the replicate arrays for Nonactivated OPCs indicating higher correlation between arrays for the same cell type than for arrays for different cell types

Satisfied that by both hierarchical clustering and PCA, the arrays for Activated and Non-activated OPCs grouped by sample type, I next performed differential expression analysis to determine which gene were more highly expressed in Activated OPCs.

### 3.3.6 Differential Expression Analysis of Moyon et al., 2015 Data

Having produced arrays of quantile normalised expression values for Activated and Non-activated OPCs, the next step in my analysis was to discover which genes were differentially expressed between the two cell types. I performed differential analysis and

the statistical analyses required to accompany it using the limma package available for R.

As before, I applied limma in two stages: firstly, I created a model matrix specifying which arrays represent replicates for the same timepoint and applied it to the data thus allowing mean expression values for every probe for each timepoint to be calculated.

The second phase of the limma analysis was the application of the contrast matrix designating that the means of the replicates for Activated and Non-activated OPCs were to be compared to one another. This contrast was calculated as $\log_2$ fold changes and the statistical tests were carried out to give the outputs listed in **table 3.2**.

To eliminate genes with no significant variance between Activated and Non-activated OPCs, I excluded features without an adjusted p-value of ≤0.05 from further analysis. In this way, from the 45,181 features on the array I found only 2,447 (5.42%) which were differentially expressed between Activated and Non-activated OPCs. The low number of features identified at this stage reflects the high background data issue discussed in **chapter 3.3.3**, expression of low expression features was lost in the background noise, leaving only the highly expressed features. I then selected only those which were more highly expressed in activated OPCs by excluding any gene with a negative $\log_2$ fold change, discovering 1,329 (2.94% of genes on the array) genes upregulated in activated OPCs.

### 3.3.7 Selection of Secreted Factors Using Ensembl Biomart

The aim of analysing this dataset, was to identify cell surface receptors expressed by Activated (migrating) OPCs. For this reason, having identified the significantly differentially expressed genes I utilised the Ensembl Biomart tool (Herrero et al., 2016, Ensembl release 84, http://www.ensembl.org/biomart/martview/84ae73fe2c935c797186934eba30f2e9) to obtain a list of all the genes on the Agilent 026655 Whole Mouse Genome Microarray whose proteins were known to be cell surface bound.

In the Ensembl Biomart web interface, I selected Ensembl Genes 84 database and the Mouse genes (GRCm38.p5) dataset. On the Attributes tab, I selected Gene ID, Transcript ID and Associated Gene Name as outputs from the GENE dropdown list and

Transmembrane domain (tmhmm) from the list of Transmembrane and Signal Domains as an output from the PROTEIN DOMAINS AND FAMILIES dropdown list. This produced a list of all of the mouse genes listed as having a transmembrane domain indicative of cell membrane localisation in their corresponding proteins.

I then matched my differentially upregulated gene list to this transmembrane domain list and identified 266 significantly differentially upregulated genes with a transmembrane domain in their corresponding proteins.

### 3.4 Selection of CX3CR1/CX3CL1 for Further Investigation Based on Data from Both Studies

By filtering by adjusted p-value, protein domain and correlation analysis, I produced a list of 266 putative cell surface receptors from the Moyon *et al*., 2015 activated OPC dataset and a list of 410 correlating secreted factors from the Huang/Jarjour *et al*., 2011 whole lesion site dataset. The next stage was to identify receptor ligand pairs which appeared on both lists.

To achieve this, I used the International Union of Basic and Clinical Pharmacology(IUPHAR)/British Pharmacological Society(BPS) Guide to Pharmacology database (http://www.guidetopharmacology.org/), to annotate the list of cell surface receptors from the Moyon *et al*., 2015 paper with their known ligands. Of the 266 factors, only 35 were found to have known ligand published in the literature. Of these 33 factors, 8 (Grm5, Srebf1, Axl, Darc, Fgfr1, Ltbr, Fzd1 and Ntrk3) were immediately eliminated because they each had five or more known ligands, making them unattractively complex to study using *in vitro* and *in vivo* models.

Having identified these ligands, I then searched the list of secreted factors from the Huang/Jarjour *et al*., 2011 paper to find out if they also appeared there. Of the remaining 25 putative receptors on activated OPCs, only 2 had known ligands which appeared in the list of secreted factors. Receptor Tyrosine Phosphatase Z1 (PTPRZ1) with its ligand Contactin-1 (CNTN1) and CX3C Chemokine Receptor 1 (CX3CR1) and its singular known ligand CX3C Chemokine 1 (CX3CL1), otherwise known as Fractalkine.

Studies in the published literature have found PTPRZ1 to negatively impact OPC differentiation as well as myelination by oligodendrocytes (Kuboyama et al., 2012;

Pendleton et al., 2013), an observation confirmed in a more recent study which showed that inactivation of PTPTZ1 actively promoted OPC differentiation and remyelination (Kuboyama et al., 2015). The focus of this PhD project was to find factors that might improve remyelination through the modulation of OPC biology. Since the published literature suggested PTPRZ1 had exactly the opposite effect, it was not adopted for further investigation.

This left a singular receptor ligand pair: CX3CL1/Fractalkine and CX3CR1. Existing literature had little explored the effect of CX3CL1 on OPC biology making it an attractive candidate. I therefore took the CX3CR1/CX3CL1 receptor ligand pair forward for *in vitro* studies, as described in **Chapter 5**: CX3CL1 is a Master Regulator of OPC Mediated Regeneration.

### 3.5 Development and Implementation of an Interactive Data Display Tool for Microarray Data

On completion of my analysis of the two microarray data sets, I set out to create an interactive database allowing researchers without bioinformatics experience easy access to pre-analysed gene expression data.

#### 3.5.1 Rationale and Functionality of Online Tool

An existing example of such a tool is the brain RNA-seq database developed for mouse and data and published by the Barres group in 2014 (http://www.stanford.edu/group/barres_lab/brain_rnaseq.html, Zhang et al., 2014), now expanded with human datasets (http://web.stanford.edu/group/barres_lab/brainseqMariko/brainseq2.html, Zhang et al., 2016).

The group created online search tools which allow users to view a bar plot graphing the expression levels (in Fragments Per Kilobase of transcript per Million mapped reads (FPKM)) of a single named gene, with the intention of facilitating easier identification of receptor-ligand pairs specific to the individual cell types (Zhang et al., 2014). However, while the Barres database has proved to be an incredibly useful tool, the website design limits the user to viewing only one gene at a time and accesses the existing data sets.
In order to make the data I have analysed accessible, I designed and implemented a web based tool – CatVis, in which users may compare the expression of multiple genes from multiple data sets. Website access is available at https://stembio.github.io/williams

(University of Edinburgh VPN required). As demonstrated in **figure 3.12,** on accessing the tool's landing page, the graphical user interphase (GUI) presents the user with a drop down list of the available data sets. Data sets are selected by clicking the "Add DataSet" button and multiple data sets may be displayed at the same time.

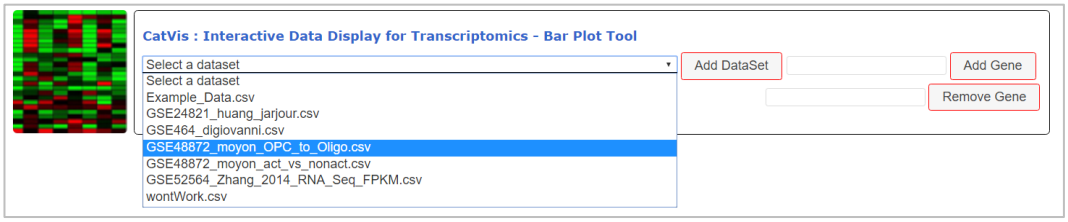


**Figure 3.12 Screenshot illustrating the range of data sets available on CatVis** Graphical User Interface (GUI) for CatVis utilises a drop down menu from which data sets to be visualised can be selected (multiple data sets may be selected at once), the name of a gene to be added to the graph(s) can be typed into the Add Gene field which provides a list of suggestions based on the letters typed and the name of a gene to be removed from the graph(s) can be typed into the Remove Gene field which provides a list of suggestions limited to the genes which are already visible.

Genes of interest are selected by typing the gene symbol into the "Add Gene" field which makes suggestions based on the letters typed and the gene names available in the selected datasets. Genes can also be deselected by typing the gene symbol into the "Remove Gene" field, which also provides suggestions, this time based on the letters typed and the genes plotted on the graph.

As the screenshot in **figure 3.13** shows, the expression patterns of selected genes can be displayed simultaneously, allowing genes to be compared and contrasted.


**Figure 3.13 Screenshot of CatVis in action.** Visualisation of patterns of gene expression across two data sets GSE48872 Moyon et al., 2015 OPC to Oligodendrocyte and GSE24821 Huang, Jarjour et al., 2011. Multiple genes are being compared at once: MBP, PDGFα, CX3CR1 and CXCL12.

### 3.5.2 Development of Online Tool Using Java and JavaScript/jQuery

In the design of this tool, the flexibility to simultaneously access multiple datasets and genes necessitated a different computational approach from that used in the Barres database.

In the development of the Barres database, a single static Portable Network Graphic (PNG) image was generated for the expression pattern of each gene in the RNA-seq data set using an R script. Typing the gene symbol for a gene of interest into the "*Enter Gene*" field results in the return of the static image associated with that gene name which is displayed to the user in the Common Gateway Interface (CGI)/Python/HyperText Markup Language (HTML) coded web page.

While the Barres database design allows for easy access to the expression pattern of an individual gene in a single dataset, the use of pre-made images limits the display options available to the user and lacks the flexibility to display multiple genes or incorporate new datasets. In my tool, in contrast to displaying pre-prepared images, the bar plots displayed to the user are generated after the datasets and first gene have been selected. Bar plots can then be modified with the addition or removal of additional genes.

To achieve this flexibility, I utilised the Stembio visualisation server system developed by Duncan Godwin (PhD student and software developer in the Tomlinson lab), which uses the Java and JavaScript/jQuery programming languages.

### 3.5.3 Gene Expression Data for CatVis is stored in an Online GitHub Repository

As illustrated in **figure 3.14**, the CatVis tool can be broadly split into three components which interact with one another to build its interactive functionality

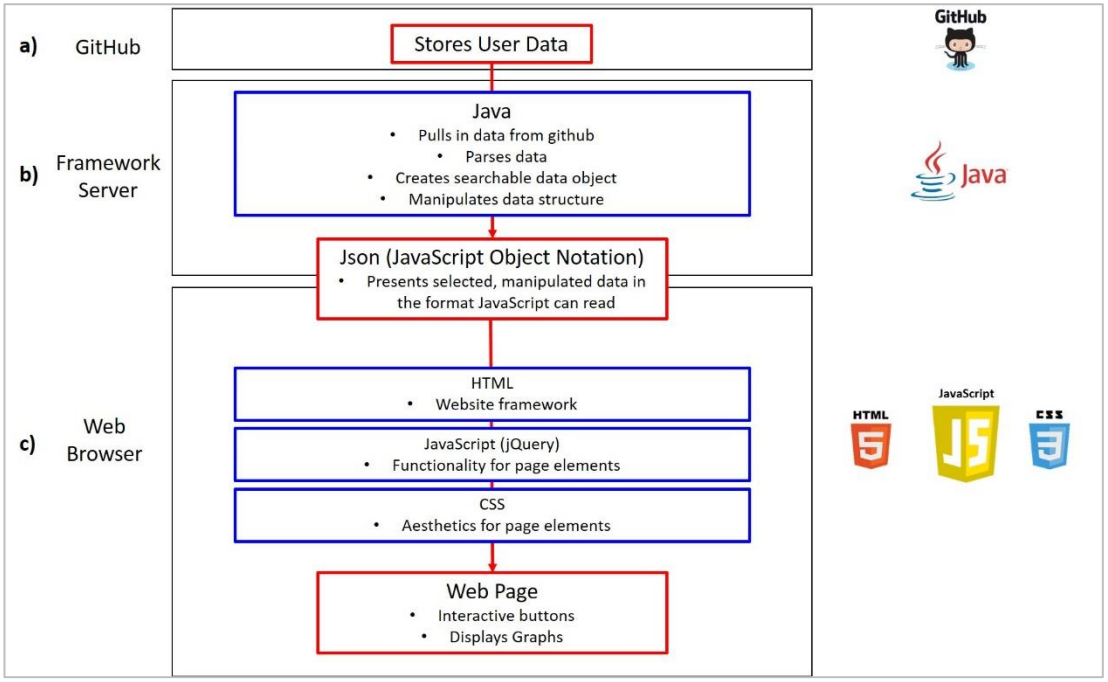


**Figure 3.14 Flow diagram of computational approach used for the development of CatVis. a)** Pre-analysed microarray data in .csv format is stored in an online GitHub repository. **b)** Through the visualisation Framework Server, Java is used to access the GitHub repository in which the data is stored and parse the data into a new searchable data object manipulated into the JSON format necessary for the graph. **c)** Genes selected using the GUI are searched for using JavaScript and selected from the JSON using the gene symbol as a key to access the row of data associated with that gene. d3/jQuery (a JavaScript library) is used to convert the rows of data into a bar plot which is displayed in a web page. The framework for the webpage including the positions of the bar plot and other elements such as buttons and images is defined in HTML and the aesthetic appearance (colour, font etc) of the page elements are defined in the accompanying CSS file. The interactive functionality of page elements such as buttons and drop down menus is implemented using a combination of HTML and jQuery.

As shown in **figure 3.14 a)**, the data for the tool is stored in an online GitHub repository. GitHub is a code hosting platform which allows multiple users to access and edit communal files (https://guides.github.com/activities/hello-world/). In this case, pre-processed microarray data expression tables in the Comma Separated Values (.csv) format with the column header 'Gene' in the top, left cell, were uploaded to a communal GitHub (See **figure 3.15**).

| Gene | d5_mean | d14_mear | d28_mean |
|---|---|---|---|
| Pdxk | 7.058454 | 6.747242 | 6.50066 |
| Kir3dl1 | 5.803803 | 5.854261 | 5.827244 |
| Hexim2 | 6.907621 | 7.009091 | 7.330435 |

**Figure 3.25 Example of .csv data format required for CatVis.** First four rows of the .csv file for the Huang/Jarour et al., 2011 dataset. With the required column header 'Gene' in the top left most cell, the other column headers are the experimental conditions. All other rows begin with a gene symbol which will be used to identify the rows after parsing by Java. The data is the averaged, normalised and intensity values analysed using the methods in **chapters 3.2** and **3.3**.

### 3.5.4 Server Side Java Parses Gene Expression Data from the GitHub Repository into a JSON

The second integral component is the server side Java which prepares the data for bar plot display (see **figure 3.14 b)**) and is hosted on the Stembio visualisation server. The visualisation server framework developed by the Tomlinson lab, provides a system for the development of data visualisation tools which packages up server side Java and web based JavaScript in a format, which can be easily incorporated into an HTML web page. Following dataset selection by the user, commands in the Java parse the data retrieved from the GitHub repository into a new data object in lookup-table format in which each row from the original data can be identified using the gene symbols from the left most column of the .CSV file as keys. This new data object is known as a JavaScript Object Notation (JSON), which can be read using JavaScript.

### 3.5.5 Data for Genes to be Displayed on the Graph is Selected Using jQuery

Once the data has been converted into a JSON, it is ready to be used by the jQuery commands which define the functionality and appearance of the graph. jQuery is a versatile library of JavaScript commands which simplify the development of functional elements for web pages (https://jquery.com/). When a user types gene symbols into the "Add Gene" box, the jQuery searches through the JSON and selects rows with a key matching the symbol entered. The jQuery then reformats the data into the correct tabular format for the graph.

### 3.5.6 Displayed Bar Plots are Built Using d3.js

A useful subset of jQuery is the d3.js library which can be used to allow data to be manipulated via a website interface (https://d3js.org/). The specific bar plot displayed on the CatVis website was based on the open source d3.js code for the Grouped Bar Chart developed by d3.js user Mike Bostock (http://bl.ocks.org/mbostock/3887051), adapted for the microarray data to be displayed.

The d3.js code is hosted along with the Java on the Stembio visualisation server, through which the bar plot can be trialled and populated with data, ready to be embedded in the CatVis webpage. Everything which appears within the graph area in which the bar plot is displayed is built using the d3.js hosted on the Stembio visualisation server and was added to the webpage by adding the lines of code automatically generated by the Stembio visualisation manager to the header of the HTML file.

### 3.5.7 Structure and Function for the CatVis Webpage was Developed in jQuery and HTML with Aesthetics in CSS

As shown in **figure 3.14 c)**, I built the CatVis website using a combination of HTML, Cascading Style Sheets (CSS) and jQuery. The HTML was used to design the framework for the website and defines the elements such as buttons, drop down menus and the graph areas which appear on the webpage. The functionality for the elements on the webpage was coded into the header of the HTML using jQuery and the aesthetic appearance for page elements including colour, font and size was written in CSS in a separate .css file.

While the Java and d3.js components are hosted on the Stembio visualisation server, the .html and .css files are stored in a second GitHub repository. Opening the CatVis webpage at https://stembio.github.io/williams accesses the .html file store on GitHub. Scripts in the header portion of this .html file point to the .css file also in the GitHub repository and the Java and jQuery hosted on the Stembio visualisation server.

### 3.5.8 New Datasets Uploaded to the Linked GitHub Repository are Instantly Available to Users

A major advantage written into CatVis is the easy addition of new datasets. The linked GitHub repository currently includes the data I have analysed from the Moyon *et al*., 2015 and Huang/Jarjour *et al*., 2011 studies along with the data from the Barres database. Any additional datasets uploaded to the GitHub repository in the correct format, will instantly be added to the CatVis website ready to be visualised.

As new datasets are added to GitHub, the available datasets on the web tool are updated in real time, allowing users to instantly access the newly available data sets by refreshing the web page.

This instant access is available because when the webpage initiates, the jQuery and HTML based website communicates with the Java server which sends back the names of all the datasets in the GitHub repository to which it is linked. Dataset names returned from the server are then used to populate the "Add DataSet" dropdown list (see **figures 3.12** and **3.13**) with options for all the datasets, which are present in the GitHub repository.

Together, the GitHub, visualisation server and webpage components combine to build a functional user friendly website which allows non-bioinformaticians easy access to the expression data for multiple genes in multiple studies. This endows users with the ability to simultaneously visualise the expression of related genes (e.g. gene families, receptor-ligand pairs) in diverse models and conditions.

By providing quick and easy access to gene expression data, it is hoped that CatVis will aid researchers in generating the inferences which inform project driving hypotheses, thus contributing to understanding of disease models and biological systems.

### 3.6 Discussion

The aim of this thesis chapter was to identify secreted factors and cell surface receptors by bioinformatic analysis of gene expression array data from published studies. By utilising online data repositories, I selected datasets from two published microarray studies.: the first, on the Illumina rat microarray platform detailing gene expression in whole lesion sites after demyelinating injury (Huang, Jarjour et al., 2011)., the second, on the Agilent mouse microarray platform detailing the gene expression in Activated and Non-activated adult OPCs (Moyon et al., 2015).

It should be noted that the two microarray studies from which the data for this thesis chapter were drawn, were from two different chips, from two different species. Of the total 39,487 genes represented on the Agilent mouse chip used in Moyon et al., 2015, 19,583 (49.59%) also appear on the Illumina rat chip used in Huang, Jarjour et al 2011. In the case of the rat chip used in Huang, Jarjour et al., 2011, of the 22,227 genes represented on the array, 19,617(88.26%) also appeared on the on the Agilent mouse chip used in Moyon et al., 2015. That such a large proportion of the genes on the 2015 mouse array do not appear on the 2011 rat array, can be explained by the later production of the array chip, and by the generally better annotation available for transcripts in the mouse genome compared to transcripts in the rat genome.

Using microarray packages for the statistical analysis software R, I normalised and investigated the data and performed differential gene expression analysis. As illustrated in **figure 3.21**, using a combination of gene ontological information from Ensembl and correlation analysis, I reduced the Moyon *et al*., 2015 data down to 266 putative receptors expressed by activated OPCs and the Huang/Jarjour *et al*., 2011 dataset down to 286 putative secreted factors with an expression pattern correlating with PDGFα and CXCL12.

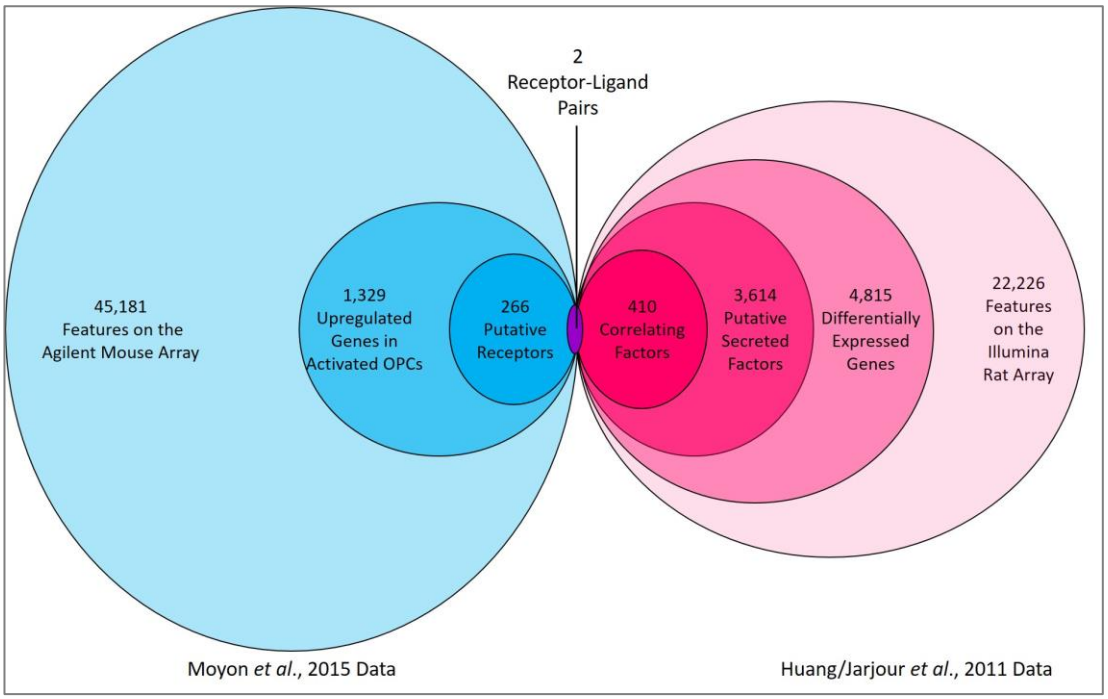


**Figure 3.15 Venn Diagram Illustrating Methods for Target Selection.**

By matching these lists of putative receptors and secreted factors, I identified only two receptor-ligand pairs, one of which was eliminated based on unfavourable reports in the literature.

In this way, gene expression array analysis lead me to a single receptor ligand pair: CX3CR1 which is upregulated in activated OPCs and CX3CL1/Fractalkine which is expressed at the lesion site following demyelinating injury and has an expression pattern correlating with known modulators of OPC biology.

In addition, I have created an online resource CatVis, making the data accessible to other biologists. This online resource includes the written in flexibility to compare multiple genes in multiple datasets and add data from new studies.

In the context of my PhD project, the purpose of investigating the Huang, Jarjour et al., 2011 dataset was to identify extracellular secreted factors which might regulate OPC biology during remyelination. On my first analysis of the data, I hypothesised that mediators of OPC migration might be most highly expressed before and during the period in which OPCs are migrating. However, to this end my analysis was somewhat confounded by the omission of an uninjured control from the Huang, Jarjour et al., 2011

data set. It would be useful to know whether the expression of factors at 5dpl is elevated, reduced or unchanged in comparison to uninjured controls. Had I been able to perform contrasts between the earliest time-point (5dpl, by which time OPC migration would be expected) and an uninjured control I would likely have gleaned a more realistic impression of gene expression in early injury.

The purpose of this PhD project, was to identify regulators of OPC biology active during the regenerative process of remyelination. To this end, it was necessary to analyse data sets from experiments which use models of injured and regenerated tissue, rather than data sets from normal uninjured tissue, such as the Barres Databases (Zhang et al., 2014, 2016) and human OPC data from the Goldman lab (Sim et al., 2006, 2011).

In conclusion, I successfully identified a target by bioinformatic analysis of relevant data and developed a database to make the data accessible. In the following chapters, I will illustrate how I optimised a migration assay system and used it and other cell biology techniques to show that the target I identified in my bioinformatic screen, CXCL1/Fractalkine is a master regulator of OPC biology.

Chapter 4

# Migration Assays

## 4.1 Introduction

In the regenerative biology of the CNS, OPCs are guided toward injury sites by a chemotactic gradient in which the concentration of chemokinetically active factor increases from the location of distally scattered OPCs to the site of demyelinating insult. Having identified candidate regeneratively active modulators of OPC migration in my bioinformatic screen, the next step was to discover if any of these factors had a chemomigratory effect on OPCs *in vitro*.

As previously iterated, the objective of this thesis was to identify and validate genes or proteins which increase OPC migration, thus facilitating OPC led regeneration. To validate any targets identified in my bioinformatics screen, it was therefore of utmost importance that I found a way to quantify OPC migration *in vitro*.

I thus, began this phase of the project by evaluating and testing different *in vitro* cell migration assays.

In the following chapter I will detail the shortcomings which lead me to reject a number of existing migration assays. I will then outline the advantages of the X-celligence Real Time Cell Analysis (RTCA) Cell Invasion and Migration (CIM) system, as well as how I adapted this system to measure proliferation and differentiation, and how I used these adaptions to discover one novel proliferation factor and one novel migration factor for OPCs *in vitro*.

## 4.2 Disadvantages of existing migration assays

### 4.2.1 Live Cell Imaging

One of the most straightforward ways to analyse cell migration, is to simply seed cells into flat bottomed multi-well plates and image them periodically. Cell tracking software can then be used to follow individual cells, computing metrics such as velocity of migration and distance travelled.

While this technique can be effective in capturing some of the migration of OPCs, much useful data can be lost in the imaging and tracking process. Based on cell morphology, software (such as Harmony) identifies only a small fraction of the cells which can be identified by eye due to the complex morphology of actively migrating cells. This difficulty in cell identification applies to all the images making it extremely difficult to follow individual cells over long time periods. As a result, very few cells can be tracked, and only over a brief period of time.

A further limitation is related to the difference between the experimental set-up and the conditions experienced by OPCs migrating in the adult brain. Without modifications, it is only possible to expose OPCs seeded in multi-well plates to a solid concentration of any factors added to their media. In contrast, migrating OPCs in the adult CNS are exposed to gradients of factors, allowing the cell to sense the difference in the amount of ligand-receptor binding between the front and back of the cell. It is this gradient sensing ability which stimulates cells to actively directionally migrate, a process also known as chemotaxis.

#### 4.2.2 Oris cell invasion assay

The Oris cell migration/invasion assay also utilises a flat multi-well plate format, in this case 96 wells. As shown in **figure 4.1**, this format is modified by the addition of a stopper which eliminates cell growth from the centre of the well. Cells are seeded with the stopper in place and after the cells are settled the stopper is removed, leaving a cell free area into which cells may migrate.

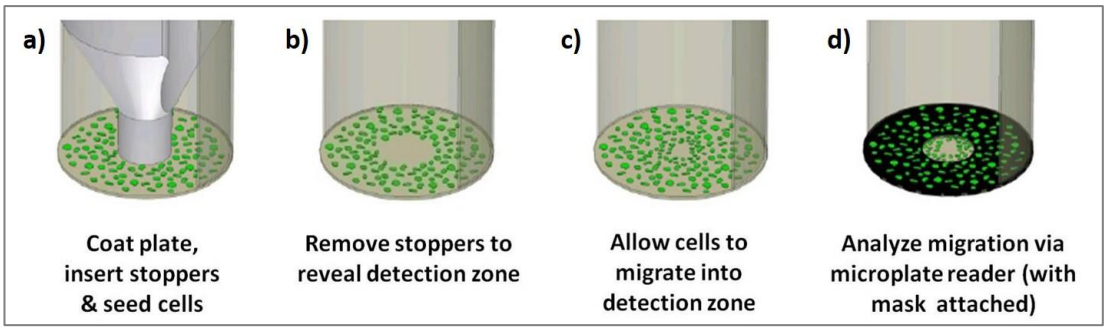


**Figure 4.1 Oris migration and invasion assay a)** Cells are seeded into the Oris assay well with a physical stopper barrier in place **b)** After the cells have settled, the stoppers are removed **c)** The cells migrate into the area left by the stopper **d)** The cells are fixed and imaged with the help of the microplate reader mask, which covers the periphery of the wells, leaving only the central region where the stopper was for imaging (Image from http://www.arunabiomedical.com/index.php?id=52)

To test this assay, I seeded OPCs at a density of 10,000 cells per Oris assay well with the stopper in place, incubated overnight at 37°C and 7.5% $CO_2$ until the cells were well adhered, and removed the stopper. Cells were incubated at 37°C and 7.5% $CO_2$ over a 30 hour period before fixing with 4% paraformaldehyde and staining the cell nuclei with Hoechst. I then imaged the wells by fluorescent microscopy and counted the number of OPCs which had migrated into the centre of the well.

As shown in **figure 4.2**, on analysis of my images, I found a significant increase in the number of cells that had migrated into the stopper region in OPCs exposed to PDGFα, a known OPC chemoattractant and proliferative factor. However, it was impossible to discern whether PDGFα stimulated the directional chemotaxis of OPCs, or simply increased their background motility, or even just increased their proliferation.

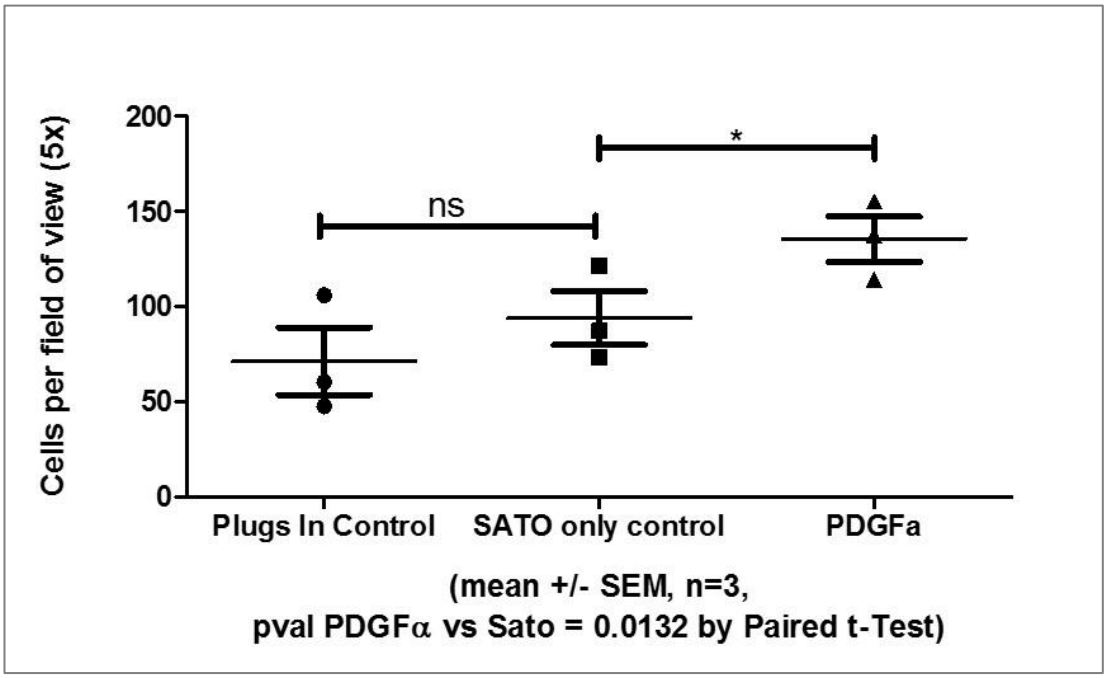


**Figure 4.2 Preliminary results from Oris migration and invasion assay** Post shake-off rat OPCs were seeded at a cell density of 10,000 OPCs per Oris assay well and cultured for a period of 30 hours in either Sato media with the stoppers left in or Sato media or human recombinant PDGFα at a concentration of 10ng per ml Sato media with the stoppers removed. A significant difference between OPCs in PDGFα and the controls could be detected.

OPCs are motile cells, which exhibit random migratory behaviour even in the absence of any stimulating factor. To identify factors for directional OPC migration, or chemotaxis,

it is therefore imperative to include Sato media only controls which account for background motility. Proliferation could also be eliminated by adding an anti-mitotic agent such as mitomycin C.

While the cells in the Oris assay have the ability to create their own local gradient by removing the closest chemokinetic particles by ligand receptor binding (Tweedy et al., 2016), as with live imaging, the assay only really exposes OPCs to a single solid concentration of the factor being tested (in this case PDGFα) and does not recapitulate the gradients of chemokines experienced by chemotaxing OPCs *in vivo*.

Concluding that while the Oris assay might expose some of the OPCs to a local gradient, this experimental set-up was ineffective in recapitulating the extracellular ligand gradient experienced by migrating OPCs in the CNS, I turned my attention to other assays which engineer a ligand gradient.

### 4.2.3 Cline Nanogradient Assay

I also had the opportunity to trial the newly developed Cline Nanogradient Technology as a suitable migration assay for OPCs (http://www.clinescientific.com/?page=162). As shown in **figure 4.3**, the Cline Nanogradient consists of a glass slide onto which gold nanoparticles are affixed. Molecules of ligand are attached to the gold nanoparticles by biotinylation and the gradient is created by the positioning of the ligand coated nanoparticles on the glass slide.

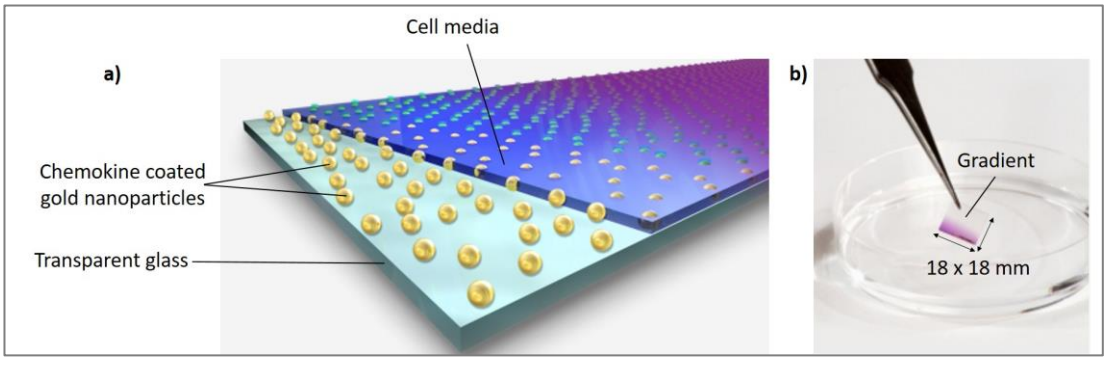


**Figure 4.3 Cline Nanogradient a)** Cline nanogradient showing chemokine coated 10nm gold nanoparticles interspersed to form a gradient on transparent glass covered with cell media **b)** 18x18mm Cline nanogradient with nanoparticle gradient visible (images modified from http://www.clinescientific.com/?page=162)

While the concept of a gradient of chemokine immobilised on a glass slide seems ideal, the Cline Nanogradients proved extremely difficult to use. Cells seeded at the low end of the gradient would be expected to migrate in the direction of the increasing gradient, however, the glass slide tended to move around and it was difficult to monitor the axes of the gradient for analysis of directional migration.

I was also somewhat dubious of how well the fixed flat gradient truly captured the conditions experienced by OPCs in the CNS. While some chemokines are known to be bound to the cell surface, many others are soluble and are secreted into the extracellular milieu forming a liquid gradient (de Castro and Bribián, 2005).

On consideration of the technical difficulties and absence of a liquid gradient with the Cline Nanogradient, I continued my search for a more directional assay.

#### 4.2.4 Boyden Chamber transwell chemotaxis assay

A well established method for the quantification of directional cell migration is the Boyden chamber. As shown in **figure 4.4a),** in this set-up, two media-filled chambers are separated only by a permeable membrane; the lower chamber contains the factor to be tested, and the upper chamber the migratory cells. Pores in the membrane allow the test factor-impregnated media from the lower chamber to diffuse into the media from the upper chamber, resulting in the formation of a gradient of test factor particles within the pores. This more closely approximates the chemokinetic gradient experienced by OPCs *in vivo* because it is an OPC independent liquid gradient.

However, my initial trials of the Boyden chamber assay gave inconsistent results and as shown in the example experiment in **figure 4.4b)**, I was unable to detect statistically significant differences in migration between OPCs exposed to known chemoattractant Semaphorin 3F (Spassky et al., 2002), known chemorepellant Sema3a (Spassky et al., 2002; Sugimoto et al., 2001). While other researchers have produced results with the Boyden chamber, I was unable to replicate their results with the Boyden chamber in my hands.

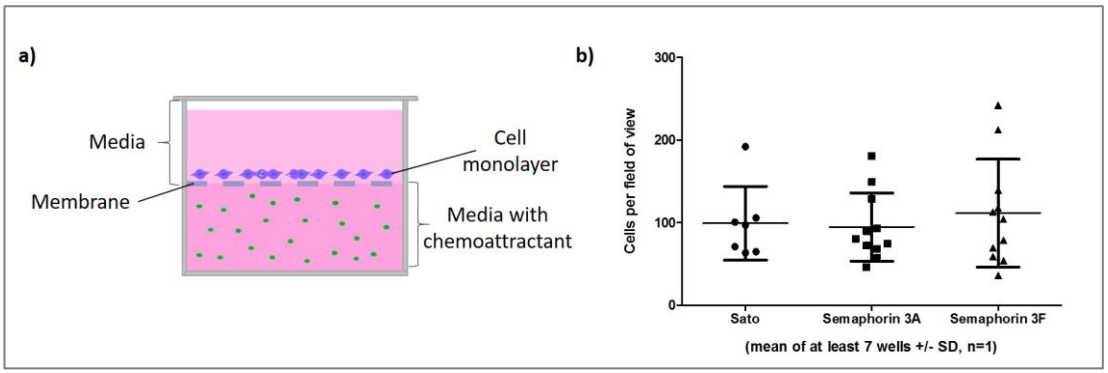


**Figure 4.4 The Boyden chamber directional chemotaxis assay a)** The Boyden chamber is composed of two media filled chambers separated by a polyethylene terephthalate membrane with pores 8µm in diameter, cells are seeded in media in the upper chamber and the lower chamber is filled with media containing a chemoattractant, thus creating a steep gradient of the chemoattractant in the pores. Over time, cells migrate through the pores and adhere to the underside of the membrane. Cells attached to the membrane can then be fixed, imaged by fluorescent microscopy and quantified by manual counting **b)** Result of my initial Boyden chamber experiments; no difference in cell count is apparent between OPCs cultured with Sato media in both chambers, OPCs cultured with the chemorepellant Semaphorin 3A in the lower chamber or OPCs cultured with the chemoattractant Semaphorin 3F in their lower compartment

The inconsistency in results can perhaps be attributed to the inherent limitations of the Boyden chamber assay. Following initial set up, Boyden chamber experiments were run for a period of 16.5 hours after which membranes were fixed in 4% PFA and the cells stained with Hoechst and counted via fluorescent microscopy. For the experiment to work, it is assumed that all OPCs migrate through the permeable membrane and become adhered to its underside, where they can be quantified at the conclusion of the experiment. However, it is possible that some OPCs might migrate through the membrane, adhere to the underside of the membrane and later become detached, possibly by displacement by other OPCs, and thus not be counted upon quantification.

Another issue is that as an end point assay (in this case at 16.5 hours), Boyden chamber results cannot be mined for information regarding fluctuations in chemokinetics over the period of cell migration. This is important because of the possibility that some chemoattractants might affect migration more quickly than others. The gradient may also dissipate at different rates with different chemotactic molecules. In the absence of real-time data, it is difficult to evaluate the effectiveness of one chemokine as compared to another.

## 4.3 Description of the X-celligence RTCA CIM system and its advantages as a migration assay

An assay system which collects real time data, as well as preserving the cell independent gradient system of the Boyden chamber assay, is the X-celligence Real Time Cell Analysis (RTCA) Cell Invasion and Migration (CIM) system developed by ACEA biosciences. The X-celligence RTCA CIM system may be viewed as an improved version of the Boyden chamber. As shown in **figure 4.5**, the X-celligence RTCA CIM system similarly generates its cell independent gradient using two media-filled chambers separated by a porous membrane.

The innovative aspect of the X-celligence RTCA CIM plate is the incorporation of an array of gold microelectrodes covering 70-80% of the underside of the porous membrane. At defined intervals over the course of the experiment, an electronic potential is passed through the electrodes. In the absence of cells, the stream of electrons making up the electrical potential passes between the electrodes via the electrically conductive media. In the presence of cells, the efficiency of the passage of the electrical potential is hindered, a metric which can be measured as electrical impedance.

Electrical impedance readings are taken at three critical points in an X-celligence RTCA CIM plate experiment. A base reading is taken before the cells are added, after both the normal media in the upper chambers and the chemoattractant-impregnated media in the lower chambers have acclimatised in the incubator for 1 hour, allowing the gradient to become established. A second nominal impedance value is taken 30 minutes after the cells are added (30 minutes is required to give the cells time to settle into a monolayer). From this point onward, the X-celligence RTCA system takes electrical impedance readings at intervals defined by the user, throughout the remaining course of the experiment.

As illustrated in **figure 4.5**, electrical impedance readings are instantly transferred to the X-celligence RTCA software, which computes electrical impedance readings into unitless Cell Index values which are calculated using the following equation:

$$\text{Cell Index (CI)} = \frac{\text{Electrical Impedance at time point n} - \text{Electrical Impedance in the absence of cells}}{\text{Nominal Electrical Impedance value 30 minutes after cells are first added}}$$

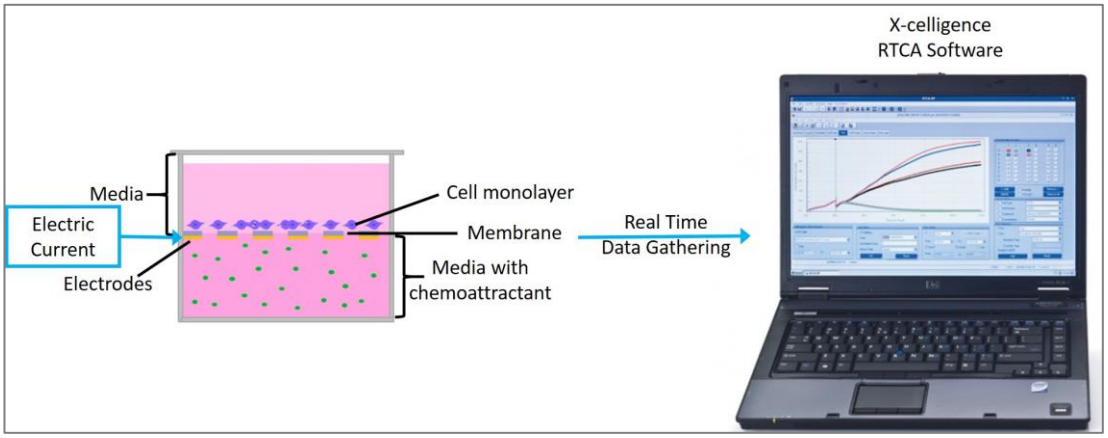


**Figure 4.5 The X-celligence Real Time Cell Analysis Cell Invasion and Migration System** Similar to the Boyden chamber assay, the X-celligence RTCA CIM system creates a gradient of chemoattractant in the 8µm pores of a polyethylene terephthalate membrane separating two media filled chambers, the upper chamber containing the cells and the lower chamber containing media impregnated with the chemoattractant. In an improvement to the Boyden chamber, the X-celligence RTCA CIM system features an array or microelectrodes on the underside of the porous membrane

CI values from throughout the experiment can be visualised as plots on the X-celligence RTCA software. As shown in **figure 4.6**, on the conclusion of the experiment, the CI plot for each X-celligence RTCA CIM well must be adjusted up or down to give all the wells a CI value of zero at the first measured time-point to eliminate technical variation between wells. Thus, the Cell Index is not a raw measure of the cell coverage of the underside of the membrane, but a measure of the change in Cell Index compared the initial reading.

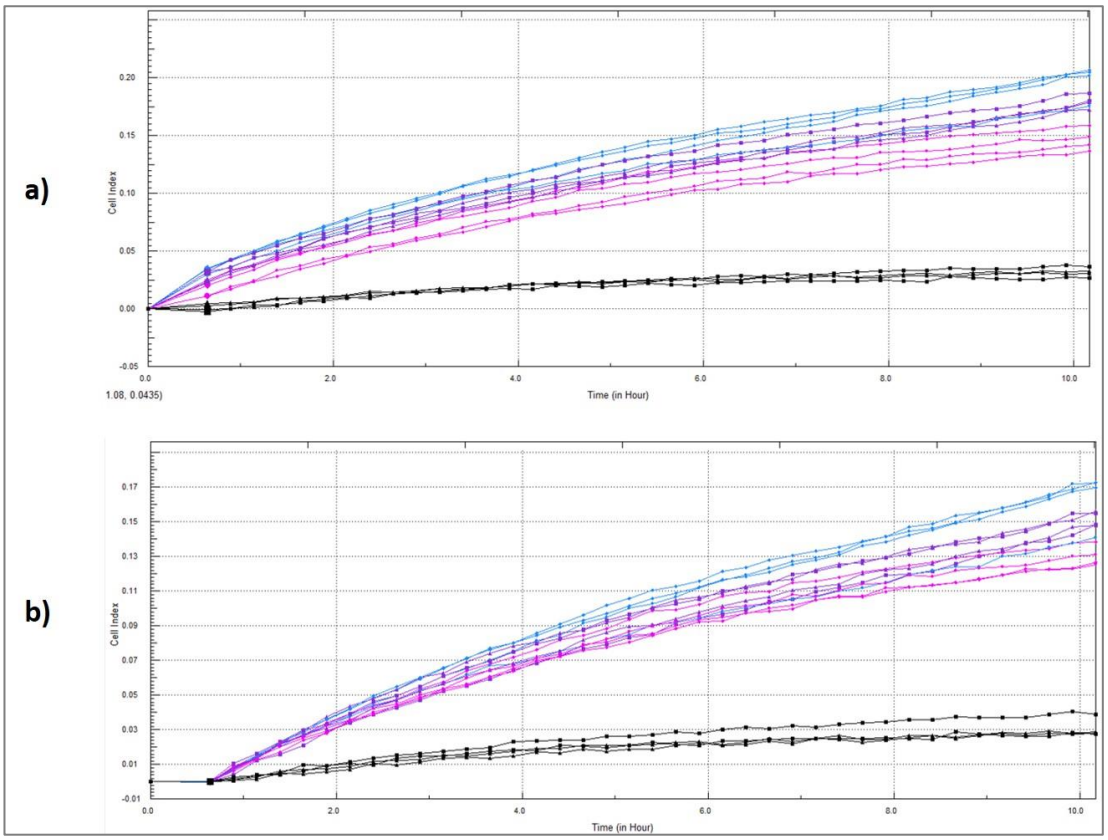


**Figure 4.6 Example X-celligence RTCA Cell Index plots a)** Before curve adjustment **b)** After curve adjustment, reducing all initial readings to zero. Each line represents readings from 1 well.

Using periodic Cell Index(CI) measurements, the X-celligence RTCA CIM system allows real time measurement of the coverage of the underside of the membrane. Satisfied that the X-celligence RTCA CIM system generates real time measurements of the activity of OPCs exposed to a liquid gradient of the factor being tested, I next trouble shot the system for use with OPCs.

## 4.4 Optimisation of the X-celligence RTCA CIM system for OPCs

### 4.4.1 Preliminary experiments generated extremely low Cell Index values

For my preliminary experiments with the X-celligence RTCA CIM system, I compared OPCs cultured with media only in both chambers, with OPCs cultured with media only in the upper chamber and 10ng human recombinant PDGFα per ml of Sato media in the lower chamber. In this way, I was able to control for the non-directional background migration of OPCs and investigate their chemotaxis up a gradient of PDGFα.

Briefly, the lower chambers of X-celligence RTCA CIM plates were filled with Sato media containing recombinant human PDGFα at a concentration of 10ng per ml Sato media and a baseline electrical impedance reading was taken. 50,000 post-shake-off OPCs were then seeded into the upper chambers in a volume of 150ul Sato media and a second electrical impedance reading was taken. OPCs were cultured in the X-celligence RTCA CIM plates for a period of 16.5 hours and further electrical impedance readings were taken every 15 minutes.

As shown in **figure 4.7**, the results obtained from these experiments proved to be variable both between different wells for the same condition and between OPCs from different litters of rat pups. This result was somewhat unexpected given that I had used the cell density from the protocol from ACEA Biosciences provided with the X-celligence RTCA CIM system.

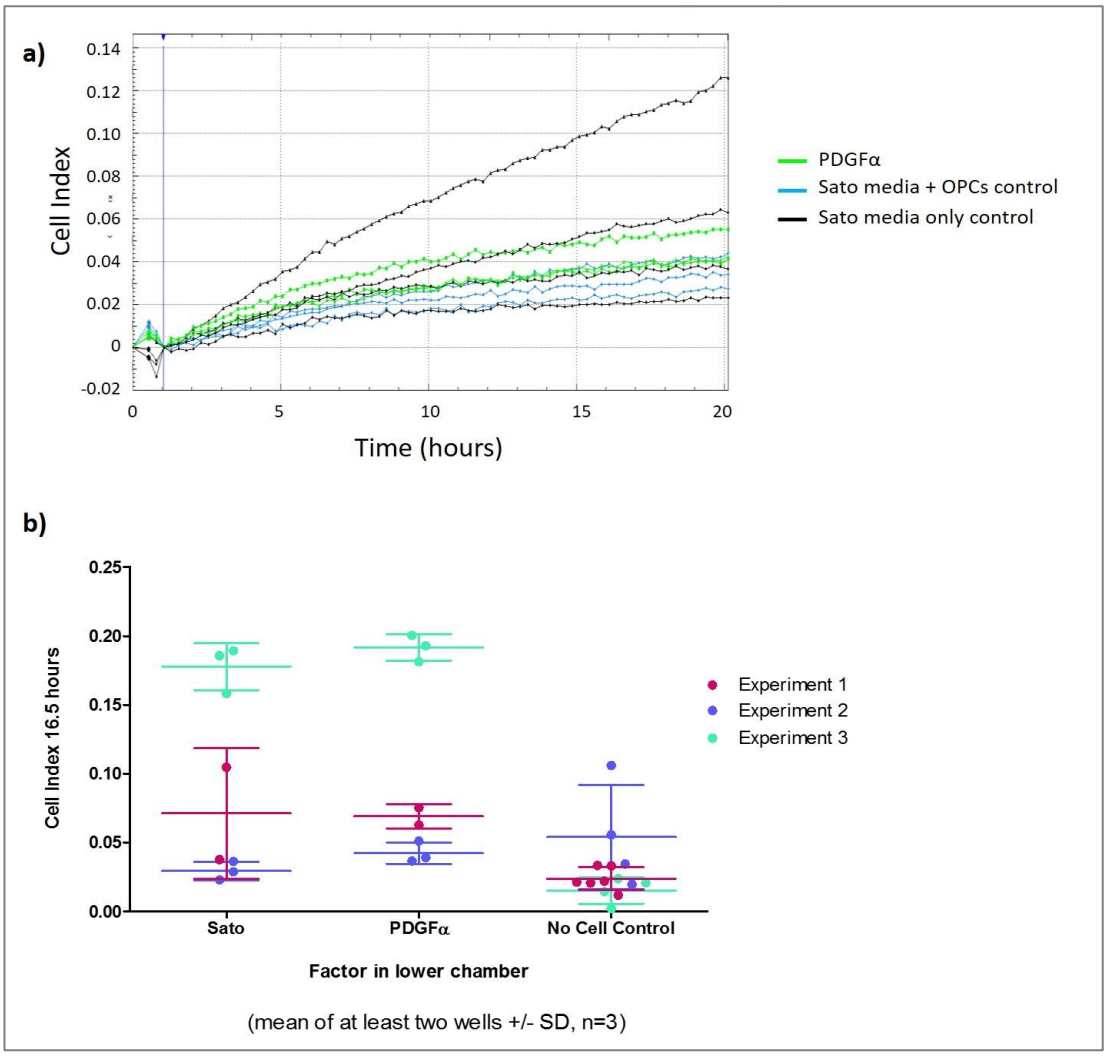


**Figure 4.7 Preliminary X-celligence RCTA CIM experiments** Results of X-celligence experiments with OPCs from 3 litters of rat pups. OPCs were seeded in the upper wells of X-celligence RTCA CIM plates with either standard Sato media or Sato media with 10ng per ml human recombinant PDGFα. **a)** Representative X-celligence machine readout plotting the Cell Index of each well, readings taken every 15 minutes over a 20 hour period **b)** Results from 3 replicate experiments, No significant difference in Cell Index results for wells containing OPCs vs control wells without OPCs was found by paired T-test.

To find out if there was some difference between my experiments and those reported by other researchers, I reviewed the existing literature from studies published using the X-celligence RTCA CIM system.

On my review of the literature, I was immediately struck by difference between the Cell Index ranges in the published studies and my experimental Cell Index range. As shown in **figure 4.8**, my cell index range of 0-0.2 was dwarfed by the reported Cell Index ranges of 0 to as much as 9 (Zieker et al., 2013).

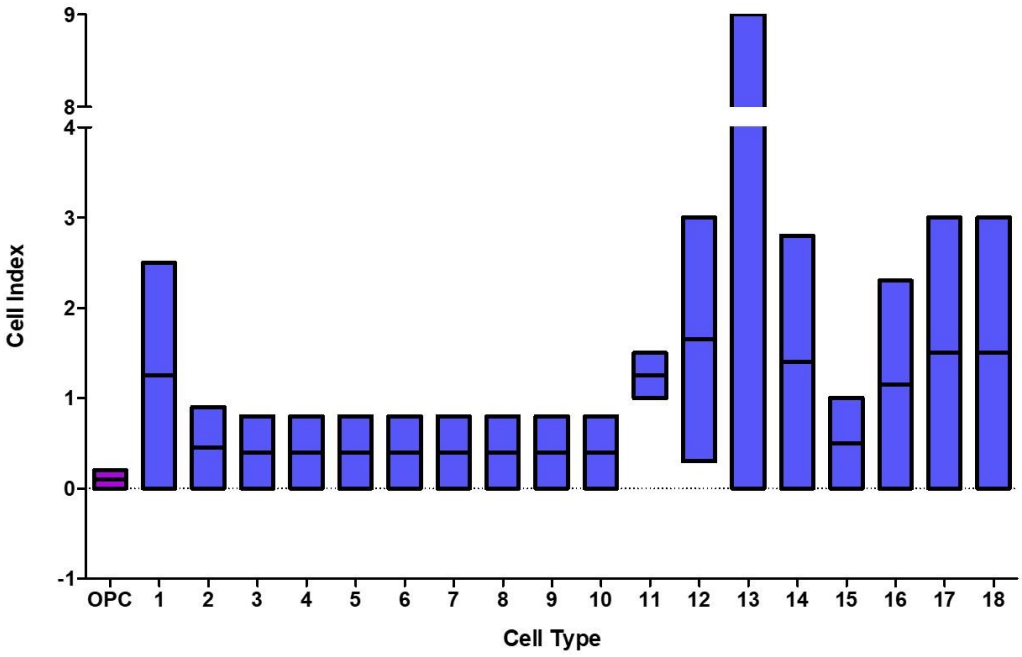


1. Human umbilical vein Endothelial Cells (HUVECs; PromoCell), 500,000 cells per well (Niland et al., 2013)
2. HT1080 human fibrosarcoma cells, 100,000 cells per well (Arlinghaus and Eble, 2013)
3. MDA-MB-231 Established human breast cancer line - Invasive phenotype, 50,000 cells per well (Mandel et al., 2013)
4. MDA-MB-435s Established human breast cancer line - Invasive phenotype, 50,000 cells per well (Mandel et al., 2013)
5. MCF-7 Established human breast cancer line - Non-invasive phenotype, 50,000 cells per well (Mandel et al., 2013)
6. MDA-MB-468 Established human breast cancer line - Non-invasive phenotype, 50,000 cells per well (Mandel et al., 2013)
7. Primary NSCLC (Non-small cell lung cancer) cells (Tu459), 50,000 cells per well (Mandel et al., 2013)
8. Patient-derived primary human breast cancer epithelial cells (HBCEC), 50,000 cells per well (Mandel et al., 2013)
9. Normal human mammary epithelial cells (HMEC), 50,000 cells per well (Mandel et al., 2013)
10. MCF-7 Established human breast cancer line - Non-invasive phenotype, 50,000 cells per well (Mandel et al., 2013)
11. MCF-7 Established human breast cancer line - Non-invasive phenotype, cell count not specified (Döppler et al., 2013)
12. PC-3 Human prostate cancer cell line, 30,000 cells per well (Jevnikar et al., 2013)
13. MKN-45 - Human Gastric Cancer Cell Line, 60,000 cells per well (Zieker et al., 2013)
14. MDA-MB-231 Established human breast cancer line - Invasive phenotype, 40,000 cells per well (Akison et al., 2012)
15. MDA-MB-231 Established human breast cancer line - Invasive phenotype, 30,000 cells per well (Limame et al., 2012)
16. A549 - Human Lung cancer cell line, 30,000 cells per well (Limame et al., 2012)
17. Panc-1 Pancreatic ductal adenocarcinoma, 30,000 cells per well (Bartscht et al., 2012)
18. Colo 357 Pancreatic ductal adenocarcinoma, 60,000 cells per well (Bartscht et al., 2012)

**Figure 4.8 Comparison of initial OPC X-celligence RTCA CIM Cell Index range to Cell Index ranges from the published literature** Boxes extend from the minimum Cell Index value to the minimum cell index value reported over the duration of the X-celligence RTCA CIM run with the mean of the maximum and minimum represented by a line, Purple box - Post-shake-off rat OPCs were seeded into

the upper wells of X-celligence RTCA CIM plates containing either Sato media only, or PDGFα at a concentration of 10ng/ml in Sato media in their lower wells, X-celligence experiments were then run for a period of 16.5 hours, Blue bars - Cell Index ranges from a range of published X-celligence RTCA CIM studies, all published study results show a wider range and higher maximum Cell Index value than with OPCs.

### 4.4.2 Cell Index values are improved by increasing the number of cells seeded

On further review of the literature, I noted that many of the cell types used in other experiments were considerably larger than OPCs. As shown in **figure 4.9**, OPCs are typically only 5-20µm in length, markedly smaller than some of the cells included in the published in the published studies such as HUVECs (Niland et al., 2013) at ~80µm and A549 - Human Lung cancer cell line (Limame et al., 2012) at ~50µm.

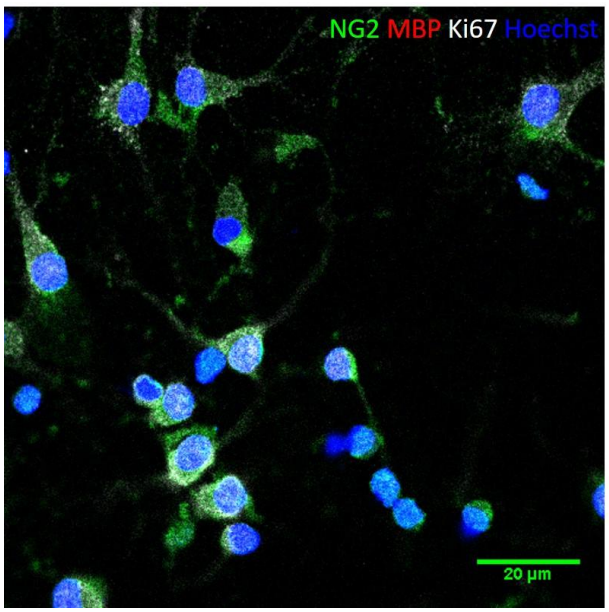


**Figure 4.9 OPCs are small cells at 5-20µm in length** OPCs were cultured on glass coverslips at a cell density of 50,000 OPCs per well of a 24 well plate in Sato media for a period of 16.5 hours. At this pre-differentiation stage OPCs have limited $NG2^{+}$ processes, do not express MBP and also express the proliferative marker Ki67.

I also noticed that although ACEA recommend seeding 50,000 cells per X-celligence RTCA CIM well in their standard protocol, as shown in **figure 4.8**, in some of the publications as many as 100,000 or even 500,000 cells were seeded per X-celligence RTCA CIM well.

Putting together the information that OPCs were a much smaller cell type than had been typically analysed and that many published studies reported higher Cell Index values and a greater number of cells being seeded, I surmised that the published studies reported higher Cell Index values because a greater surface area of the underside of the membrane was being covered, either by larger cells or by an increased number of cells. As a consequence of these observations, I hypothesized that increasing the number of OPCs seeded into each X-celligence RTCA CIM well, might lead to an increase in Cell Index values.

To find out if increasing the OPC cell count increased Cell Index values, I seeded OPCs at densities of 50,000, 100,000, 250,000, 500,000 and 1,000,000 cells per well into the upper chamber of X-celligence RCTA CIM wells, with SATO media only in the lower chamber. I also ran cell-free control wells with SATO media only in both chambers. As shown in **figure 4.10**, when wells containing OPCs are compared to cell-free control wells, a significant difference in Cell Index can only be perceived by the X-celligence RTCA CIM system, at 250,00, 500,000 and 1,000,000 OPCs per well.

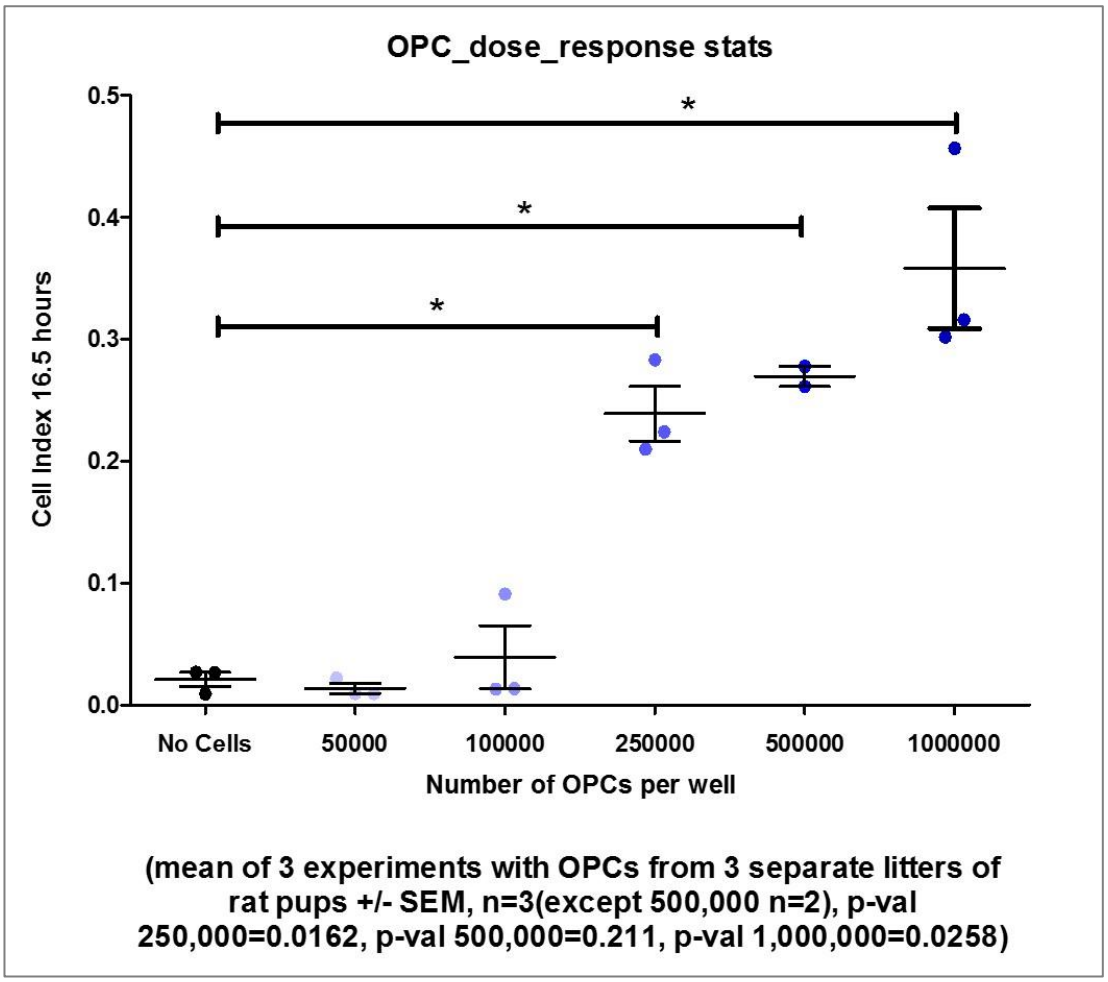


**Figure 4.10 X-celligence RTCA CIM system senses OPC migration when at least 250,000 OPCs are seeded per well** Different cell densities of Post-shake-off rat OPCs were seeded into the upper wells of X-celligence RTCA CIM plates containing Sato media only in both their upper and lower chambers and X-celligence RTCA CIM experiments were run for 16.5 hours. The X-celligence RTCA CIM system only perceives a significant difference between wells containing cells and cell-free control wells at 250,000, 500,000 and 1,000,000 OPCs seeded per well.

Having established that significant results could be generated by seeding 250,000 OPCs per well, I thus altered my standard protocol to reflect this cell count. All further X-celligence RTCA CIM data reported in this thesis are from experiments run using 250,000 OPCs per well (excluding cell-free controls).

### 4.4.3 Fluctuations in environmental conditions can impact Cell Index ranges between experiments

Throughout my X-celligence RTCA CIM system, I noticed that there was considerable variation between the Cell Index ranges for replicate experiments with OPCs from different litters of rat pups. Bearing in mind that I was simultaneously carrying out other experiments with the same cells (immunofluorescent stains, RT-PCR *etc.*) and finding no discernible difference between replicates it seems unlikely that the differences in Cell Index observed was the result of true biological differences between litters of rat pups.

Over the course of my X-celligence experiments I had also noticed that slight differences in the way the RTCA CIM plates were treated could impact the Cell Index values. As iterated earlier, at the 0 hour time point, a Cell Index reading is taken for the X-celligence RTCA CIM wells which contain only the media and migration factors without any cells. After the Cell Index reading has been taken, the RTCA CIM plates are removed from the incubator to allow the cells to be seeded. Once the cells are in the wells they are incubated for 30 minutes to allow the cells to settle. This can either be done by placing the RTCA CIM plates on a shelf in the incubator (then transferring them to the X-celligence machine after the 30 minutes has elapsed) or replacing them in the cradles of the X-celligence machine. As shown in **figure 4.11a)**, when the cell equilibration step is carried out with the plates on a shelf in the incubator a peak in Cell Index can be observed between the 0 and 1 hour timepoints. In contrast, when the equilibration step is carried out with the plates in the X-celligence machine the peak in Cell Index does not occur (**figure 4.11b)**).

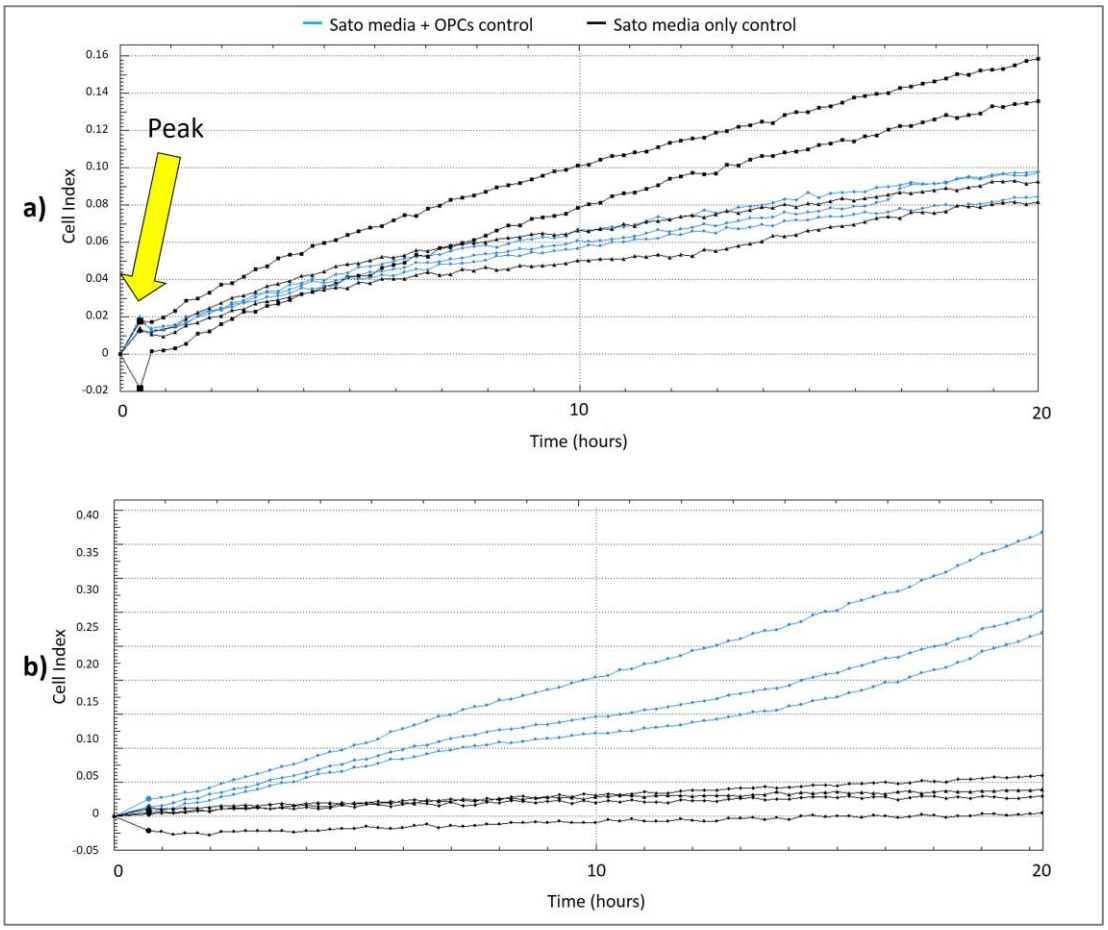


**Figure 4.11 Equilibration of OPCs for the 30 minutes following cell seeding in the cradle of the X-celligence RTCA CIM system eliminates early peak in Cell Index. a)** OPCs were seeded into the upper chambers of X-celligence RTCA CIM wells at a density of 50,000 cells per well and were then equilibrated on a shelf in the incubator for 30 minutes before transfer to the X-celligence machine. **b)** OPCs were seeded into the upper chambers of X-celligence RTCA CIM wells at a density of 250,000 cells per well and were then equilibrated in the cradle of the X-celligence machine. The early peak in Cell index (arrow) represents confounding technical noise which can be eliminated by equilibrating the plates in the X-celligence machine.

The peak in Cell Index observed in **figure 4.11a)**, is likely the result of the fluctuation in temperature or $CO_2$ concentration which occurs as a result of opening the incubator door, or the mechanical disruption of moving the plates from the incubator shelf to the X-celligence machine. This result shows that small changes in temperature, $CO_2$ concentration or plate movement can have a discernible impact on Cell Index values. Consequently, I always equilibrated the cells with the RTCA CIM plates in the X-celligence machine, however the differences in Cell Index range between experiments persisted.

Based on my observations, I suspect that the difference in Cell Index ranges might reflect changes in environment resulting from the hazards of using a communal incubator such as the opening and closing of the incubator door and accidental shaking of shelves caused by the movement of plates and culture dishes. While further experimentation would be required to confirm this suspicion, I found that I could eliminate these batch differences from my data by simply calculating the mean fold change between conditions (e.g. Sato media only vs PDGFα) for each replicate and combining these values to calculate the final experimental results.

#### 4.4.4 Verification of the X-celligence RTCA CIM system as a suitable directional migration assay for OPCs

Having established that 250,000 OPCs per well were required to generate reliable Cell Index values, I next set out to find out whether the system properly functioned as a migration assay at this cell density. To this end, I repeated the experiment detailed in **figure 4.7**, using PDGFα as a chemoattractant for OPCs seeded at a density of 250,000 cells per X-celligence RTCA CIM well.

As shown in **figure 4.12**, with 250,000 OPCs seeded per well, there is a significant increase in Cell Index when OPCs are stimulated with a gradient of PDGFα, as compared to SATO media only controls.

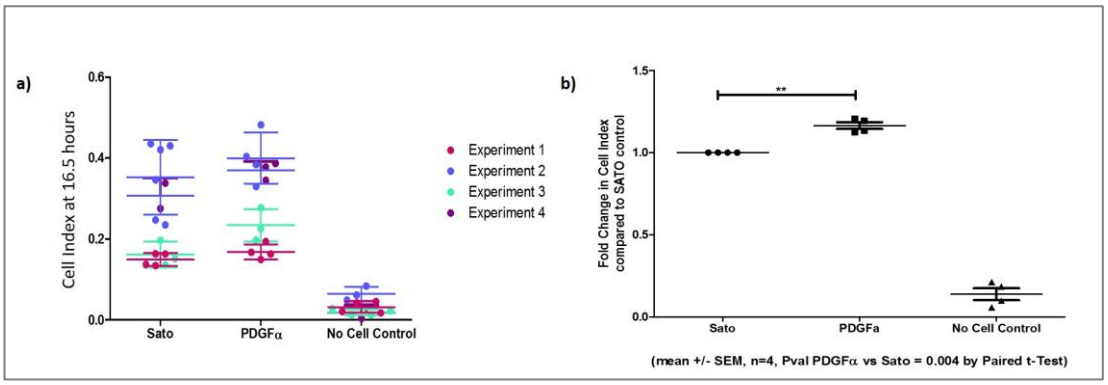


**Figure 4.12 When 250,000 OPCs are seeded per well, an increase in Cell Index between PDGFα and the Sato media only control was detected by the X-celligence RTCA CIM system** OPCs were seeded in the upper chamber of X-celligence CIM plates and a gradient between the upper and lower chambers was established by the addition of 10ng recombinant PDGFα per ml Sato media. After 16.5 hours, there was an increase in Cell Index in PDGFα stimulated OPCs compared to unstimulated OPCs. **a)** The experiment was run 4 times, each dot representing the Cell Index for each well, with an increase in every replicate, although there was considerable variation between replicates. **b)** To ameliorate the variation between replicates, increases were computed as a fold change in electrical impedance, which was highly significant by paired t-Test

According to the manufacturers of the X-celligence RTCA system, an increase in Cell Index such as this one should be interpreted as an increase in directional cell migration. However, changes in electrical impedance across the underside of the membrane quantified as Cell Index may reflect cellular processes other than migration, including proliferation and changes in cell morphology (Limame et al., 2012).

### 4.4.5 The X-celligence RTCA CIM system is ineffective as an assay to study chemorepellants for OPCs

Having established that the X-celligence RTCA system was an effective assay to study chemoattractants for OPCs, I next evaluated the system as an assay to study chemorepellants. As shown in **figure 4.13**, when I exposed OPCs to the known chemorepellant Semaphorin 3A (Sema 3A) (Boyd et al., 2013a; Spassky et al., 2002; Sugimoto et al., 2001) at a concentration of 1µg per ml Sato media, I found no significant difference in Cell Index between Sema 3A stimulated OPCs and OPCs in Sato media only controls.

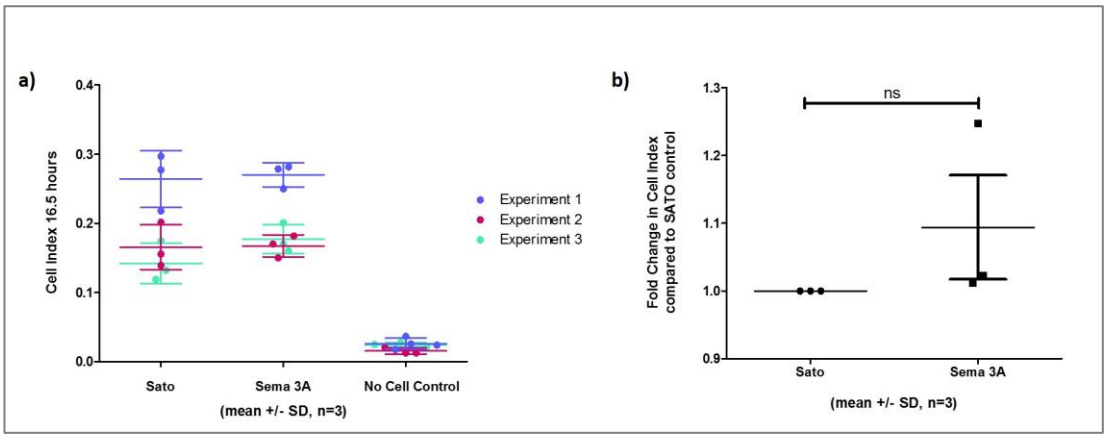


**Figure 4.13 When 250,000 OPCs are seeded per well no significant difference in Cell Index between Sema 3A and the Sato media only control was detected by the X-celligence RTCA CIM system** OPCs were seeded in the upper chamber of X-celligence CIM plates and a gradient between the upper and lower chambers was established by the addition of 1µg recombinant Sema 3A per ml Sato media. After 16.5 hours, there was no difference in electrical impedance (Cell Index) in Sema 3A stimulated OPCs compared to unstimulated OPCs. **a)** The experiment was run 3 times, each dot representing the Cell Index for each well, with no difference between Sema 3A and Sato media only controls, although there was considerable variation between replicates. **b)** To ameliorate the variation between replicates, fold change in electrical impedance in Sema 3A stimulated OPCs compared to Sato media only controls, which was no significant difference between the two conditions was found by paired t-test

I had expected that when exposed to a chemorepellant in the lower X-celligence RTCA CIM chamber, OPCs would migrate away from the chemorepellant and so fewer OPCs would migrate through the membrane resulting in a reduction in Cell Index. In the absence of any Cell Index reducing effect, I wondered if the concentration of the gradient of chemorepellant experienced by the OPCs through the pores between the two chambers might be too weak a signal to induce OPC repulsion. To further investigate the chemorepulsive effect, I redesigned the X-celligence RTCA CIM well set up. As shown in **figure 4.14a)**, I reversed the media filling the two chambers so that OPCs were seeded into the upper chamber which contained the chemorepellant and had the opportunity to 'escape' the chemorepellant through the pores of the X-celligence RTCA CIM chamber. I expected that the presence of a chemorepellant in the upper chamber would induce directional migration of OPCs through the pores, and away from the chemorepellant resulting in an increase in Cell Index.

Conversely, I expected that the presence of a chemoattractant in the upper chamber would result in a decrease in Cell Index as more OPCs would stay in the upper chamber closer to the chemoattractant. I confirmed this reverse chemoattractant effect by seeding OPCs into the upper chambers of X-celligence RTCA CIM wells containing the chemoattractant PDGFα. As **figure 4.14b)**, shows there is a reduction in Cell Index compared to Sato media only controls when PDGFα is in the upper chamber.

To find out if this modification of the system could be used to measure a chemorepellant effect, I seeded OPCs into the upper chambers of X-celligence RTCA CIM wells containing either Sema 3A at a concentration of 1µg per ml Sato media, or another known OPCs chemorepellant Netrin-1 (Jarjour et al., 2003; Tepavčević et al., 2014) at a concentration of 100ng per ml Sato media. As shown in **figure 4.14 c)** and **d)**, I could discern no significant difference in Cell Index between either the Sema 3A or Netrin-1 conditions and the Sato media only controls.

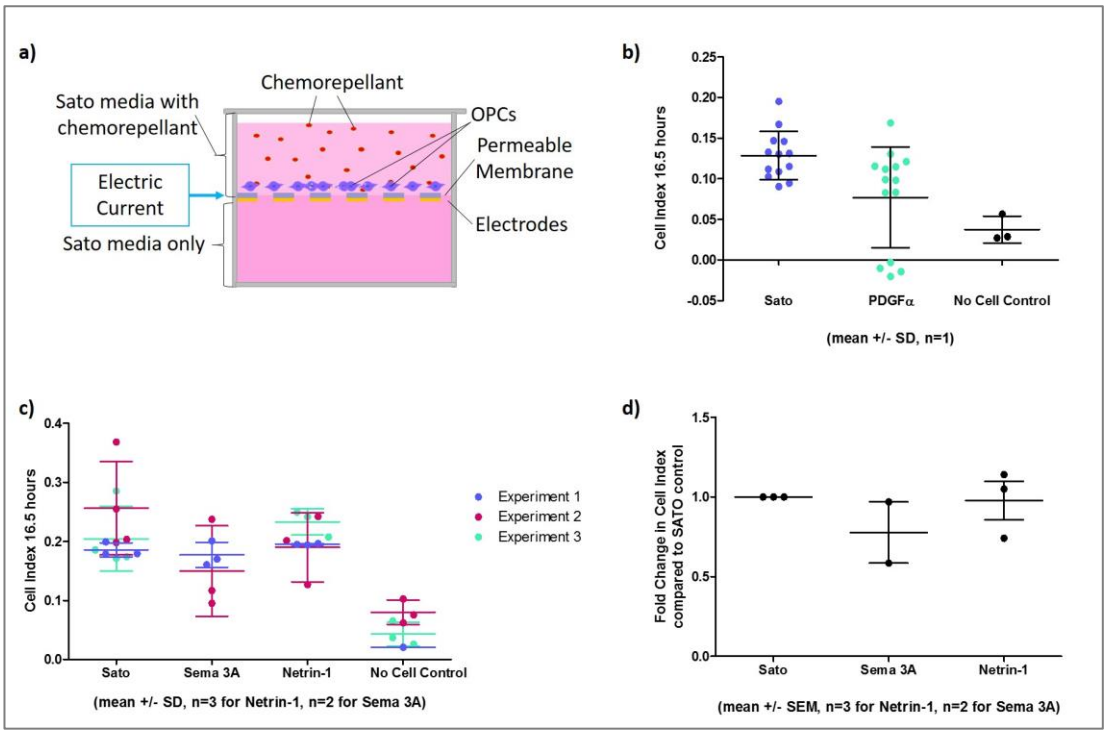


**Figure 4.14 The X-celligence RTCA CIM system is not an effective assay with which to study chemorepellants for OPCs *in vitro* a)** Modification to the X-celligence RTCA CIM set-up for the study of chemorepulsion, OPCs are seeded into the upper chambers of X-celligence RTCA CIM wells which contain a chemorepellant, with Sato media only in the lower chamber **b)** 250,000 Post shake-off rat OPCs were seeded into the upper wells of X-celligence RTCA CIM plates containing the chemoattractant PDGFα, and X-celligence RTCA CIM experiments were run for 16.5 hours. Seeding of OPCs into the upper chambers of X-celligence RTCA CIM wells containing the chemoattractant PDGFα, results in a decrease in Cell Index compared to Sato media only controls **c)** 250,000 Post shake-off rat OPCs were seeded into the upper wells of X-celligence RTCA CIM plates containing one of the chemorepellants Sema 3A or Netrin-1 and X-celligence RTCA CIM experiments were run for 16.5 hours **d)** For each replicate for the same condition, technical variation has been eliminated by calculating the fold change between OPCs exposed to a chemoattractant in their upper X-celligence RTCA CIM well and their corresponding OPCs in Sato media only controls. No significant difference in Cell Index can be observed between chemorepellant stimulated OPCs and OPCs in Sato media only controls.

The result that the X-celligence RTCA CIM system could not be used to identify chemorepellants for OPCs was somewhat disappointing, and brought with it the added implication that a lack of significant difference in Cell Index between X-celligence RTCA CIM wells containing a factor to be tested and Sato media only controls, could mean that either the factor had no impact on OPCs or that it could be a chemorepellant.

I was confident however, that any increase in Cell Index in the presence of a tested factor could not be the result of chemorepulsion. I therefore turned my attention to verifying whether an increase in Cell Index could truly be attributed to directional chemoattraction.

#### 4.4.5 The X-celligence RTCA CIM system is an effective assay to study chemoattractants for OPCs

As illustrated in **figure 4.15**, while the increase in Cell Index observed in the presence of PDGFα (see **figure 4.13**) may be the result of genuine directional migration as in **figure 4.15a)**, it is possible that this result may be the result of PDGFα-independent migration of a small number of OPCs to the underside of the membrane coupled with proliferation of these cells as in **figure 4.15b)**. The teasing apart of these two possibilities in of particular significance given that PDGFα has been shown to increase both the migration and proliferation of OPCs (Baron et al., 2000; Franklin, 2002; Frost et al., 1996, 2003, 2009; Tsai et al., 2002; Woodruff et al., 2004).

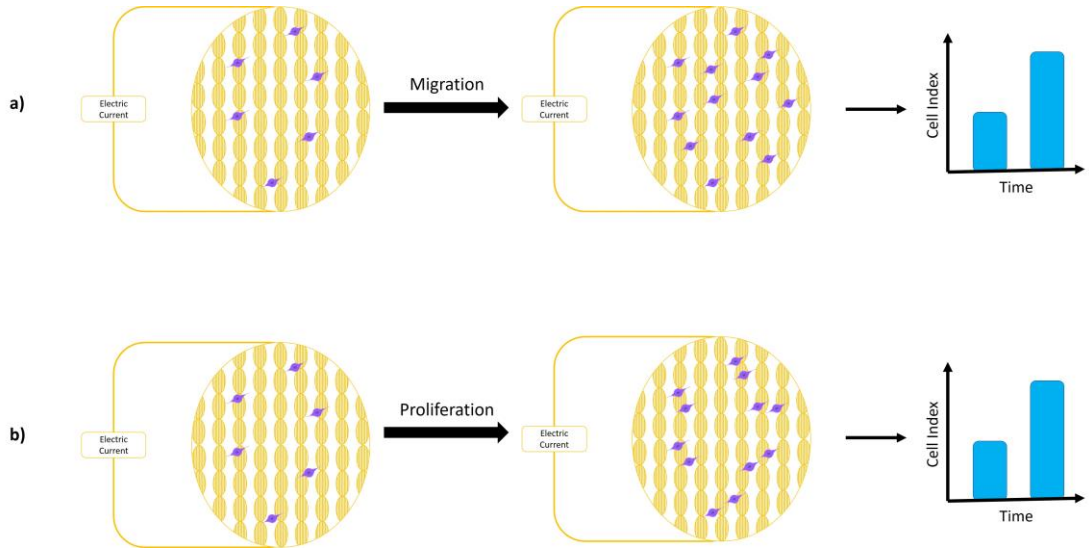


**Figure 4.15 Cell Index values can be increased by proliferation as well as migration** Cell Index is a measure of electrical impedance over the electrodes on the surface of the underside of the membrane, therefore increasing coverage of the underside of the membrane increases electrical impedance. Coverage of the membrane could be increased either by **a)** continual directional migration of OPCs over the course of the experiment or **b)** background cell motility resulting in a few OPCs migrating through the membrane which then proliferate. (Figure modified from Limame et al., 2012)

To eliminate proliferation, I treated OPCs with a range of concentrations of the proliferation inhibitor mitomycin C, a DNA crosslinking agent (Li et al., 2015; Werner et al., 2013). As shown in **figure 4.16a)**, I used a TUNEL assay (Click-iT TUNEL Alexa Fluor 647 Imaging Assay, for microscopy HCS, Thermo Fisher Scientific, Catalogue Number:C10247) to assess OPC cell death in response to mitomycin C and found that it was safe for OPC treatment up to a concentration of 5µg mitomycin C per ml SATO media. The proliferation rate of post shake-off OPCs was also assessed using a Click-It EdU kit (Life Technologies), and was found to be around 5.3% of all cells in post shake-off OPCs cultures grown in culture in the absence of any growth factors (see **figure 4.16b)**). I also used immunoreactivity of antibodies for the proliferation marker Ki67 to determine that mitomycin C abolishes OPC proliferation at a concentration of 5µg per ml Sato media (see **figure 4.16c)**).

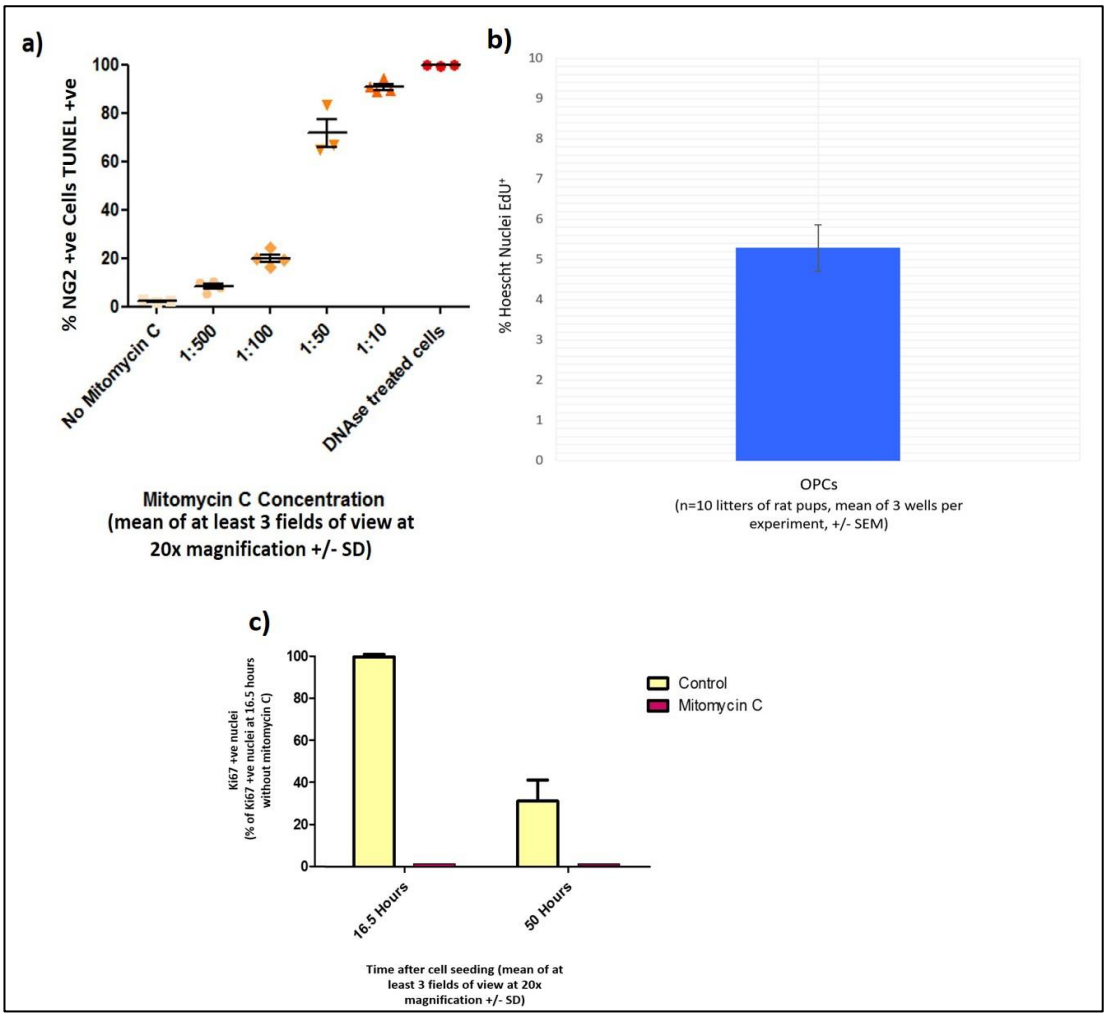


**Figure 4.16 Mitomycin C can be used to safely inhibit proliferation a)** Post shake-off rat OPCs were exposed to various dilutions of the proliferation inhibitor mitomycin C in Sato media, 1:500=1ug/ml, 1:100=5µg/ml, 1:50=10µg, 1:10=50µg/ml for two hours prior to seeding onto glass coverslips at a concentration of 50,000 OPCs per 500µl Sato media and incubated overnight at 37°C and 7.5% $CO_2$, staining and TUNEL assay were performed on fixed cells, OPC survival was quantified as the percentage of NG2 positive cells with TUNEL positive nuclei **b)** Post shake-off rat OPCs were cultured in the absence of any growth factors. OPCs from 10 separate rat pup litters were EdU labelled using a Click-It kit. Edu positivity was quantified as the % of total Hoescht stained nuclei. 5.3% of total nuclei in post-shake-off OPC culture were $Edu^+$ (data courtesy of Gregor Skeldon and Elitsa Peeva) **c)** Post shake-off rat OPCs were exposed to mitomycin C at a concentration of 5µg per ml Sato media for two hours prior to seeding onto glass coverslips at a concentration of 50,000 OPCs per 500µl Sato media and incubated for 16.5 or 50 hours at 37°C and 7.5% $CO_2$, staining was performed on fixed cells, OPC proliferation was quantified as the NG2 positive cells with Ki67 positive nuclei as a %age of NG2 positive cells with Ki67 positive nuclei at 16.5 hours. At both 16.5 and 50 hours 0% of NG2 positive OPCs treated with mitomycin C expressed Ki67.

Having verified the effectiveness of proliferation inhibition in OPCs using mitomycin C, I next ran X-celligence experiments in which OPCs were first treated with 0.5µg mitomycin C per ml Sato media for a period of two hours prior to seeding in the upper chambers of X-celligence RTCA CIM wells with Sato media only in both the upper and lower chambers. As shown in **figure 4.17a)**, both with and without mitomycin C there is considerable variation between replicates for the same condition. To allay this variation, I calculated the fold change between the X-celligence RTCA CIM wells containing OPCs and the control cell free wells included in the same experimental run. As shown in **figure 4.17b)**, using the fold change a significant difference between OPCs with and without mitomycin C treatment has been detected by the X-celligence RTCA CIM system which can be attributed to the loss of proliferation in mitomycin C treated OPCs.

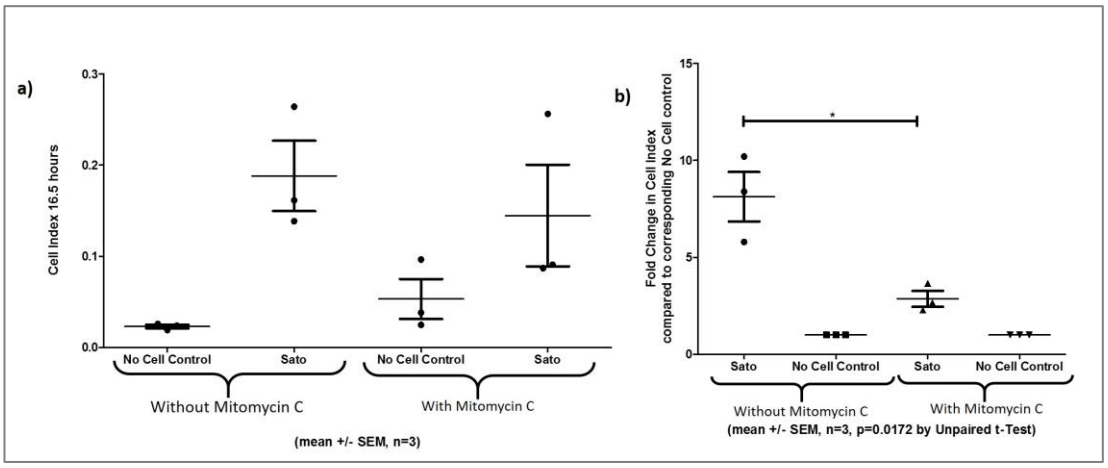


**Figure 4.17 The X-celligence RTCA CIM system can be used to detect OPC proliferation** 250,000 Post shake-off rat OPCs either with or without 2 hours of exposure to the proliferation inhibitor mitomycin C at a concentration of 5µg per ml Sato media, were seeded into the upper wells of X-celligence RTCA CIM plates containing Sato media only in both their upper and lower chambers and X-celligence RTCA CIM experiments were run for 16.5 hours. **a)** The X-celligence RTCA system detects the presence of cells as an increase in Cell Index both with and without mitomycin C treatment although there is considerable variation between replicates **b)** Variation between replicates for the same condition, has been eliminated by calculating the fold change between OPCs with and without mitomycin C treatment and their corresponding cell free controls. A significant difference was found between OPCs with and without mitomycin C treatment, this difference can be attributed to higher OPC proliferation in the absence of mitomycin C.

Having shown that the X-celligence RTCA system can be used to quantify OPC proliferation as well as migration, I repeated my PDGFα X-celligence RTCA CIM experiment, this time treating the OPCs with a concentration of 5µg mitomycin C per ml Sato media for two hours prior to cell seeding. As **figure 4.18a)** reveals, when proliferation is inhibited by mitomycin C treatment, there is still an increase in Cell Index in the presence of PDGFα. As shown in **figure 4.18b)**, the Cell Index values reported in the presence of mitomycin C treatment are lower than in its absence, reflecting the blockage of proliferation in both PDGFα-stimulated OPCs and OPCs in Sato media-only controls.

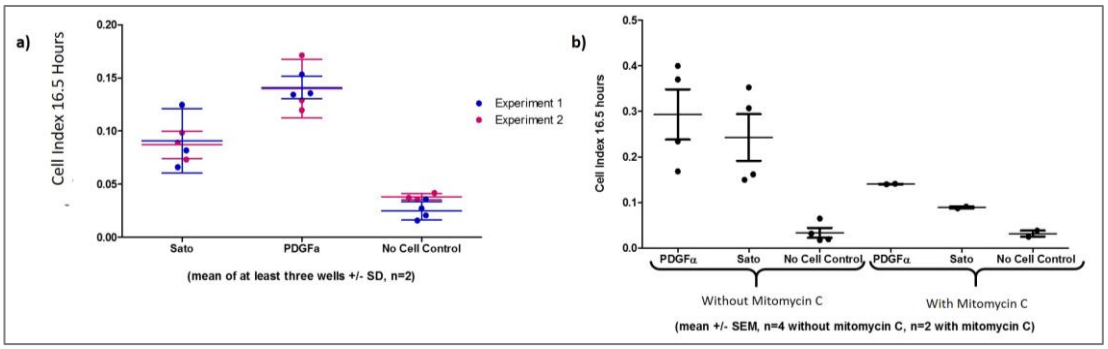


**Figure 4.18 Inhibition of proliferation results in a larger increases Cell Index in X-celligence RTCA CIM wells** 250,000 Post shake-off rat OPCs were exposed to the proliferation inhibitor mitomycin C for 2 hours, were seeded into the upper wells of X-celligence RTCA CIM plates containing recombinant PDGFα at a concentration of 10ng per ml Sato media and X-celligence RTCA CIM experiments were run for 16.5 hours. **a)** The experiment was run twice, each dot representing the mean Cell Index for each well, with an increase between mitomycin C treated OPCs with Sato media in both chambers and mitomycin C treated OPCs exposed to PDGFα in the lower chamber, although there was considerable variation between replicates. **b)** Compared to the Sato media only control, Cell Index is increased for OPCs exposed to PDGFα in the lower chambers, both for OPCs without mitomycin C treatment, and for OPCs with mitomycin C treatment, although there is more variation between experiments for proliferating OPCs

These experiments showed that increased Cell Index as the result of migration or proliferation can be separated using the experimental protocol I had developed. Using my system, for each new factor tested for its effect on OPCs using the X-celligence RTCA system, experiments need to be run both with and without proliferation inhibition using

mitomycin C. If the Cell Index is higher when proliferation occurs, then this shows that the factor induces proliferation in OPCs. If, in contrast, the Cell Index is the same both with and without proliferation then proliferation can be eliminated showing that the factor is a chemoattractant for OPCs.

Thus, running experiments both with and without a proliferation inhibitor, the X-celligence RTCA CIM system can be used to separately quantify both the proliferative and migratory effects of factors on OPCs.

#### 4.4.6 The X-celligence RTCA CIM system can be used to study OPC differentiation as well as migration

Another possible source of increased Cell Index, is the differentiation of OPCs into mature oligodendrocytes. As shown in **figure 4.19**, oligodendrocytes (**figure 4.19a)**) produce extensive MBP positive processes giving the cells a much larger surface area than OPCs (**figure 4.19b)**).

As **figure 4.19c)** illustrates, differentiation of a few compact OPCs into bulky mature oligodendrocytes could increase the surface area covered by the cells, thus increasing electrical impedance and consequently Cell Index.

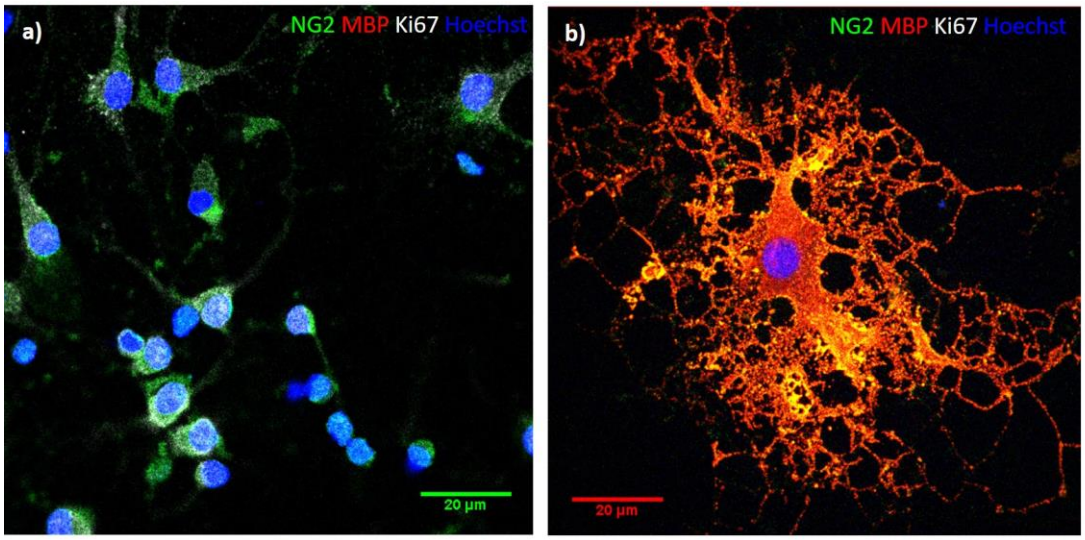


OPCs after 16.5 hours in culture

Early oligodendrocyte after 50 hours in culture

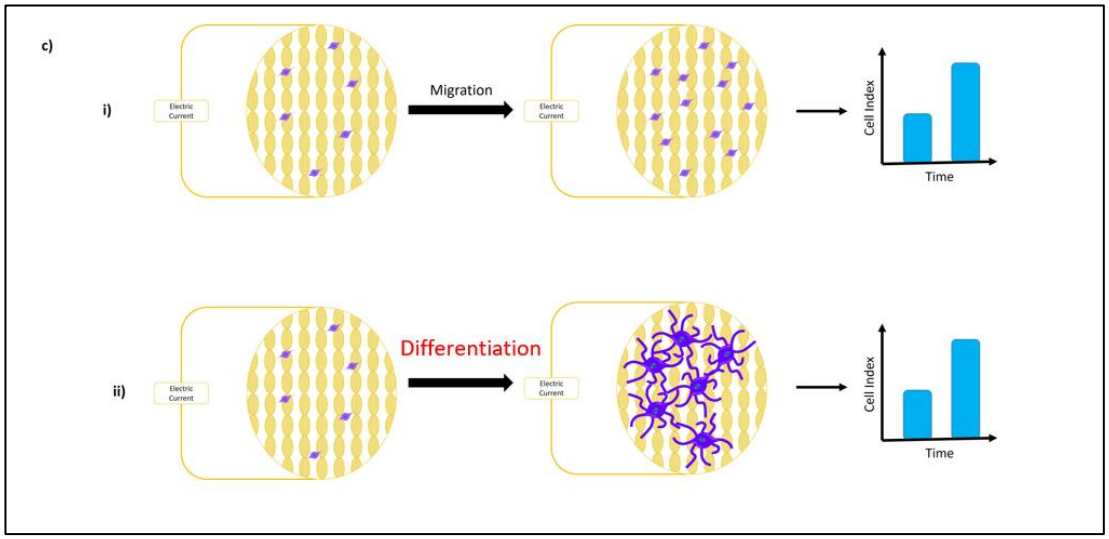


**Figure 4.19 Mature oligodendrocytes cover a larger surface area than immature OPCS a)** Post-shake-off rat OPCs were seeded at a cell density of 50,000 OPCs per 500µl Sato media on glass coverslips, cultured for 16.5 hours in Sato media at 37°C and 7.5% $CO_2$ before fixing and staining with antibodies for NG2 (OPC marker), Ki67 (proliferation marker) and MBP (mature oligodendrocyte marker). After 16.5 hours in culture OPCs are small cells at around 5-10µm in diameter and express NG2 and Ki67 but not MBP **b)** Post-shake-off rat OPCs were cultured as before but the culture period was extended to 50 hours by which point they were differentiating into oligodendrocytes. After 50 hours oligodendrocytes express the mature oligodendrocyte marker MBP as well as OPC marker NG2 but not proliferation marker Ki67, oligodendrocytes are much larger than OPCs with networks of bulky MBP positive processes **c)** In X-celligence RTCA CIM experiments, Cell Index can be thought of as a measure of coverage of the underside of the X-celligence RTCA CIM well membrane. **i)** The continual directional migration of OPCs through and adherence to the underside of the membrane could give

similar Cell Index readings as **ii)** migration of a few OPCs through and adherence to the underside of the membrane, followed by differentiation of OPCs into large oligodendrocytes with extensive processes which increase the surface area covered by the cells, giving a similar Cell Index reading. (Figure modified from Limame et al., 2012)

To find out if OPC maturation was reflected in an increase in Cell Index, I developed methods which would allow staining of the underside of the X-celligence RTCA CIM plates. As shown in **figure 4.20a)** and **4.20b)**, X-celligence RTCA CIM plates are composed of two separate pieces which can be clipped together, the upper part incorporating the upper chambers and the permeable membranes and electrodes, and the lower part incorporating only the lower chambers.

To access the cells on the permeable membranes, I fixed the cells by filling both the upper and lower chambers with 4% PFA and clipping the two parts of the plate back together for 10 minutes, before separating and washing with PBS. Cells were also immunofluorescently stained using antibodies for markers of OPCs and mature oligodendrocytes by flooding both the upper and lower chambers with antibodies and clipping the plate back together. In order to excise the electrodes and membrane from the underside of the lower chambers, I then ran a scalpel around the edge of the plastic sheet with the electrodes and membranes on it and then carefully peeled the plastic away taking the membranes and electrodes with it (see **figure 4.20c)**). With the fixed membranes/electrodes extracted, I then mounted them on glass slides with Fluoromount and glass coverslips (see **figures 4.20b)** and **4.20c)**).

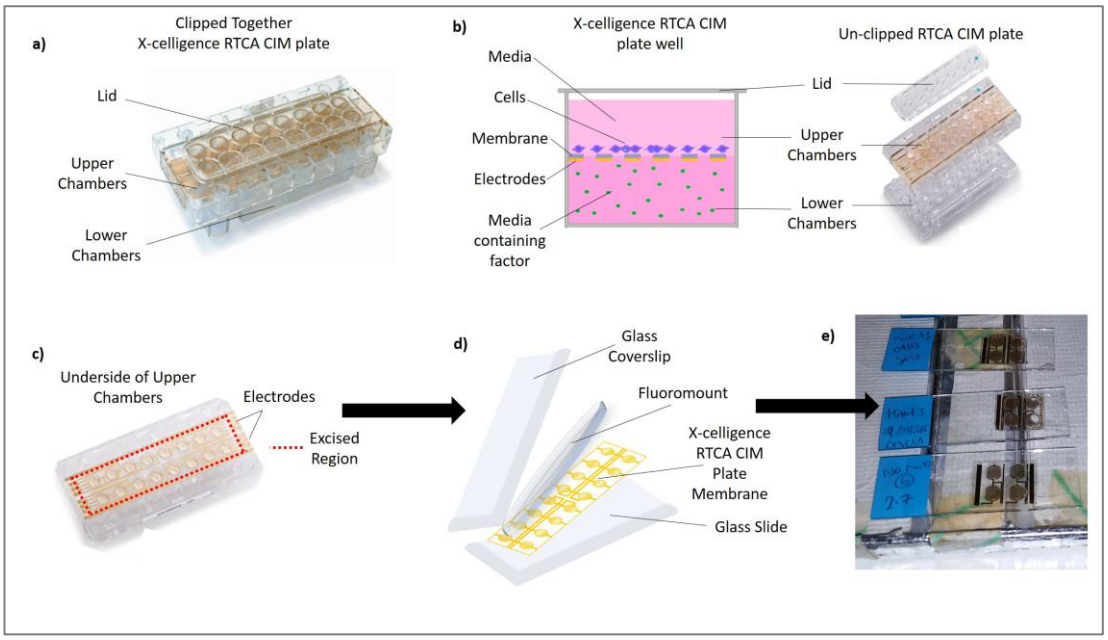


**Figure 4.20 Development of methods to excise OPC bound X-celligence RTCA CIM plate membranes and electrodes for imaging a)** X-celligence RTCA CIM plates are made up of three parts, the upper and lower chambers and lid which must be clipped together during culture to bring the electrode covered membranes into contact with the media in the lower chambers **b)** Schematic of a single X-celligence RTCA CIM well and its correspondence to the structure of the X-celligence RTCA CIM plate **c)** At the end of an X-celligence RTCA CIM experiment, the membrane and electrodes can be accessed by unclipping, aspirating the fluid from the plate, and flipping the upper chamber section over. Excision can be achieved by running a scalpel around the underside of the membrane and electrodes and carefully peeling them away in a single piece **d)** and **e)** Membranes can then be mounted on glass slides using Fluoromount and imaged by conventional fluorescent microscopy.

Having accessed, immunofluorescently stained and mounted the membranes, the cells were then imaged by confocal microscopy (Leica SP8). **Figure 4.21**, shows the result of an experiment in which OPCs were seeded into the upper chambers of X-celligence RTCA CIM wells with Sato media only in both the upper and lower chambers. In this experiment, OPCs were cultured in the X-celligence RTCA CIM plates for a period of either 16.5 hours (**figure 4.21a)**) or 3 days by which point they would be expected to be maturing into oligodendrocytes (**figure 4.21b)**).

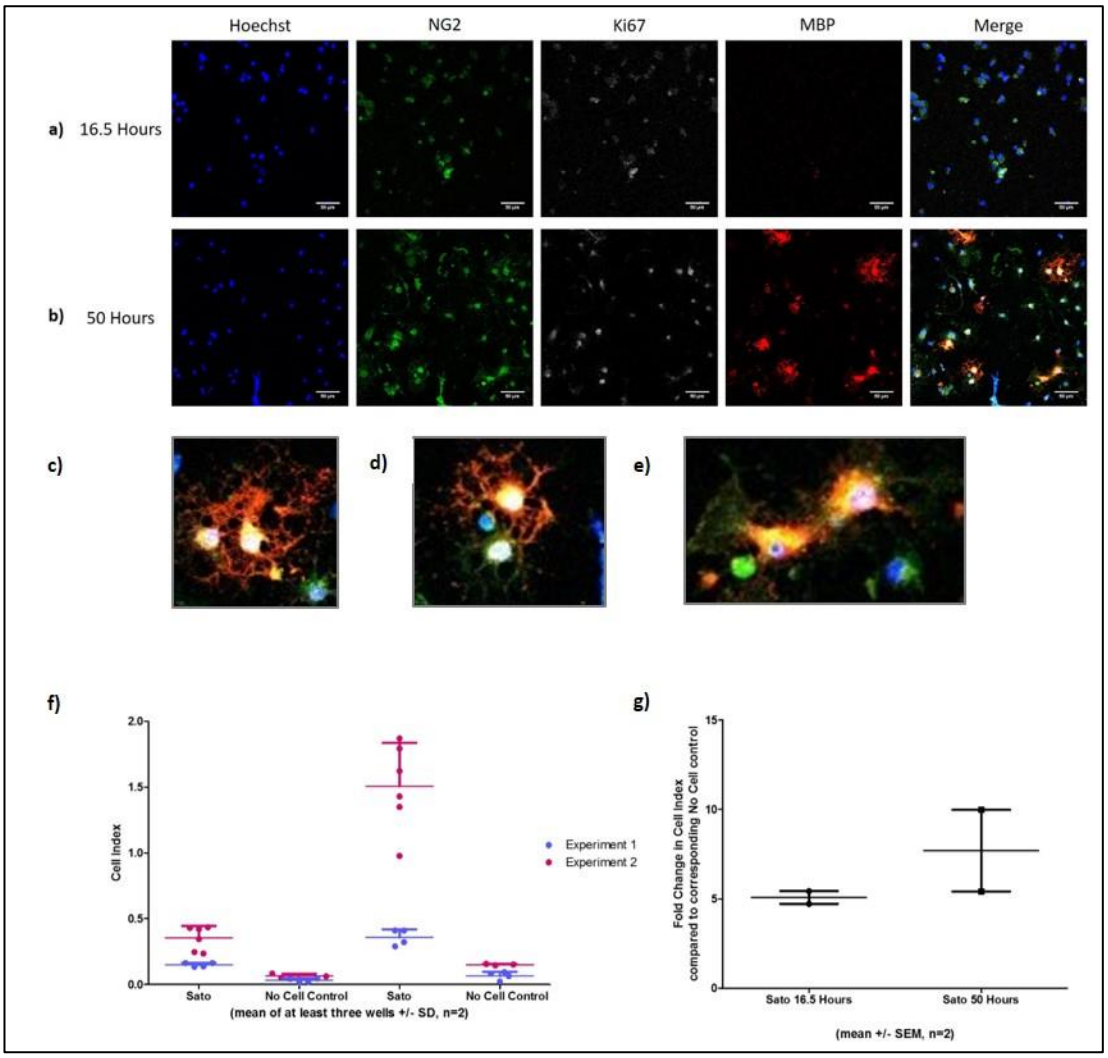


**Figure 4.22 Differentiation of OPCs on X-celligence RTCA CIM plates can be detected as an increase in Cell Index** 250,000 Post shake-off rat OPCs were seeded into the upper wells of X-celligence RTCA CIM plates containing Sato media only in both their upper and lower chambers and X-celligence RTCA CIM experiments were run for 16.5 or 50 hours. **a)** After 16.5 hours, X-celligence experiment was stopped and the membranes, electrodes and cells were fixed, stained and imaged by fluorescent confocal microscopy, OPCs are small and round in morphology and express NG2 and Ki67 but not MBP **b)** After 50 hours, X-celligence experiment was stopped and the membranes, electrodes and cells were fixed, stained and imaged by fluorescent confocal microscopy, OPCs have begun to differentiate into oligodendrocytes with extensive MBP positive processes **c) – e)** Inserts from **b)** showing colocalization between NG2 (green) and MBP (red) **f)** Results of corresponding X-celligence experiments, show an increase in Cell Index between 16.5 hours and 50 hours **g)** Variation between replicates for X-celligence experiments was eliminated by calculation of the fold change between X-celligence RTCA CIM wells containing OPCs/oligodendrocytes and corresponding cell free control wells, matched to the same time point.

As **figure 4.22b) – e)** shows, large MBP positive oligodendrocytes can be observed after 50 hours which results in higher coverage of the membrane/electrodes than by the NG2 positive OPCs at 16.5 hours (see **figure 4.22f)**, **g)**). This shows that in the absence of any stimulant some OPCs still migrate through the membrane before adhering to the underside and differentiating into mature oligodendrocytes. Bearing in mind the possibility that a pro differentiation factor might accelerate OPC differentiation resulting in mature oligodendrocytes within 16.5 hours increasing the Cell Index value, this technique can be used to determine whether an increase in Cell Index at 16.5 hours is the result of migration or accelerated differentiation.

### 4.5 Lipocalin-2 is a proliferation factor for OPCs *in vitro*

Having verified the X-celligence RTCA CIM system as an effective assay for directional OPC migration and developed methods to use the system to assay both proliferation and differentiation, I then used the system to study the effects of candidate factors on OPC biology.

Lipocalin-2(LCN2) is a small intracellular protein which has been reported to be highly expressed in astrocytes and the cerebral spinal fluid in EAE mouse models of MS (Marques et al., 2012; Nam et al., 2014) and in demyelinating human optic neuritis (Chun et al., 2015). While it has been shown that injured neurons secrete LCN2 as a way of signalling to astrocytes and microglia which express its receptor 24p3r (Xing et al., 2014), the effect of these signals on OPCs has never previously been characterised.

Hypothesizing that the LCN2 neuronal distress signal might also elicit a response in OPCs, I first determined whether or not the LCN2 receptor 24p3r was also expressed by OPCs.

As shown in **figure 4.23**, I referred to the gene expression array dataset from Moyon et al., 2015 (see **Chapter 3**) and found that there was a small but significant decrease in 24p3r in Activated OPCs as compared to Non-activated OPCs.

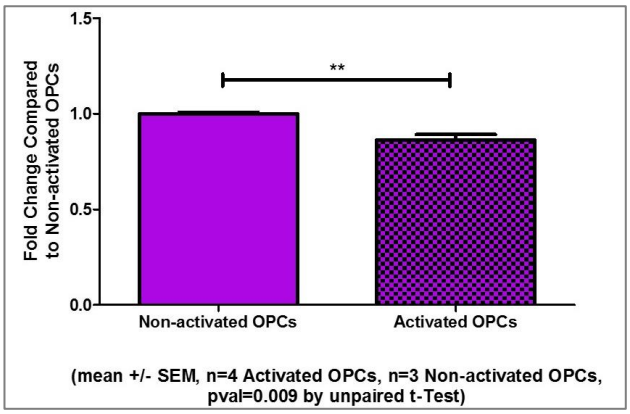


**Figure 4.23 Expression of the LCN2 receptor 24p3r in the cuprizone injury data set from Moyon et al., 2015** There is a small but significant decrease in the expression of 24p3r in Activated OPCs as compared to Non-activated OPCs

As shown in **figure 4.24a)**, I looked at the expression of LCN2 in the Huang, Jarjour et al., 2011 dataset (see **Chapter 3)**, and found that expression of LCN2 was apparently highest at 28 days post lesion when remyelination should be well underway, although there was high variation between the three replicates. This small difference might suggest a role for LCN2 in remyelination, however the result is not statistically robust due to the variation and consequently high SEM between the replicates for the 28dpl time point. This variation could be due to genuine biological variation in gene expression between the replicates, but this is not reflected in the expression patterns of other genes in the data set. It is also possible that the variation may be due to some technical disparity such as RNA degradation during storage or inexpert manual handling of the microarray during processing resulting in damage to the reactive surface. In any case further experiments analysing the expression of LCN2 in *in vivo* LPC induced demyelination would be necessary to verify this result.

Interestingly, as shown in **figure 4.24b)**, when I analysed the expression of 24p3r in this data set, I found a significant increase in expression, both between 14 days post lesion and 5 days post lesion and between 28 days post lesion and 5 days post lesion. Even more interestingly, I found that the expression pattern of 24p3r had a Pearson's correlation with PDGFα of 0.93.

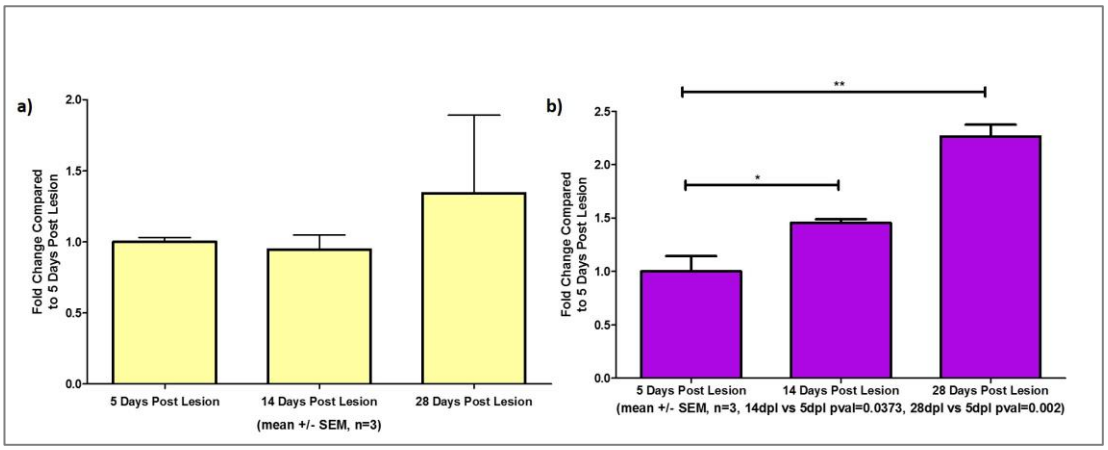


**Figure 4.24 Expression of LCN2 and 24p3r in the focal demyelination injury set from Huang, Jarjour et al., 2011 a)** LCN2 appears to be most highly expressed at 28 days post lesion, but there is high variation between the replicates **b)** Expression of 24p3r significantly increases between 14 and 5 days post lesion and 28 and 5 days post lesion, in a similar expression pattern to PDGFα.

In addition, I also looked at the expression of 24p3r in my processed data from the developmental series in Moyon et al., 2015. Interestingly, as shown in **figure 4.25** below, 24p3r is significantly more highly expressed in neonatal OPCs than in either adult OPCs or adult oligondedrocytes. While this result suggests that the expression of 24p3r may be linked to less developed, and therefore more proliferative OPCs, further experiments would be necessary to verify this result *in vitro* or *in vivo*.

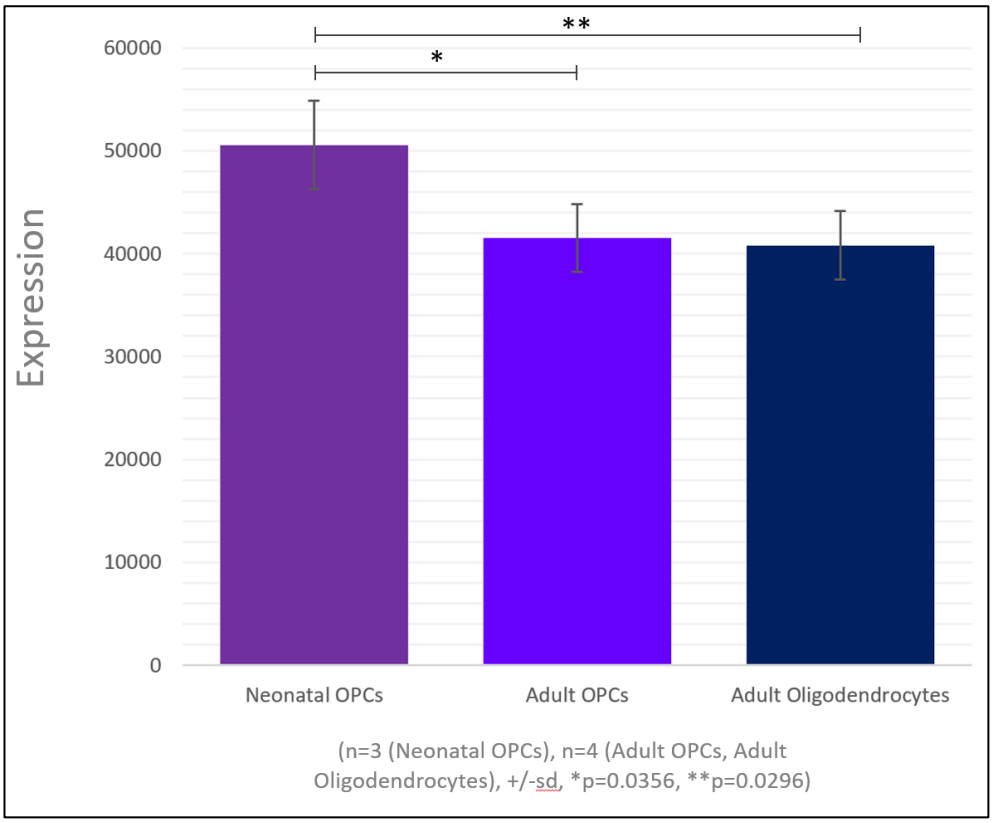


**Figure 4.25 Expression of 24p3r in the OPC development set from Moyon et al., 2015** 24p3r appears to be most highly expressed in Neonatal OPCs, and is significantly more highly expressed in Neonatal OPCs than in either Adult OPCs or Adult Oligodendrocytes.

To find out if 24p3r was expressed by post shake-off rat OPCs, as shown in **figure 4.26**, I used immunofluorescent staining of OPCs cultured overnight on glass coverslips at a cell density of 50,000 OPCs per 500µl Sato media to show, for the first time, that 24p3r is expressed by OPCs *in vitro*.

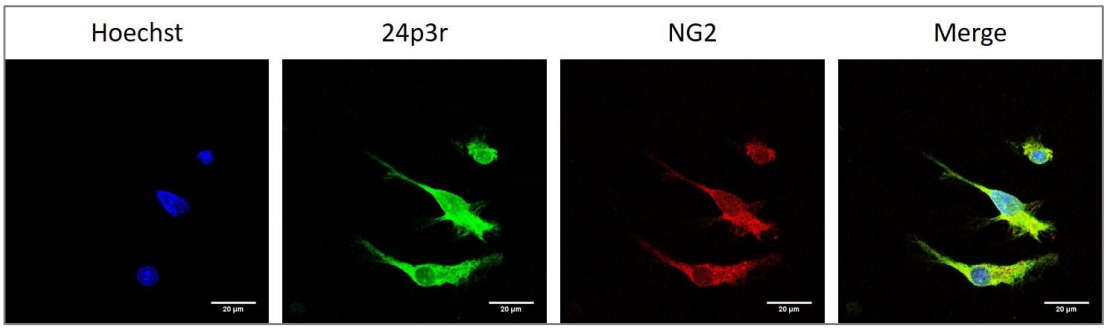


**Figure 4.26 OPCs express 24p3r the receptor for LCN2 *in vitro*** Post shake-off OPCs were seeded onto glass coverslips at a cell density of 50,000 OPCs per ml Sato media and cultured overnight in Sato media at 37ºC and 7.5% $CO_2$. OPCs on glass coverslips were then fixed and stained before imaging by immunofluorescent confocal microscopy. NG2 positive OPCs also express 24p3r.

Having shown for the first time that OPCs also expressed the receptor for LCN2 I next performed X-celligence RTCA CIM experiments to determine the effect of LCN2 administration to OPCs. As shown in **figure 4.27a)** and **b)**, when OPCs seeded in the upper chambers of X-celligence RTCA CIM wells are exposed to rat recombinant LCN2 (Recombinant Rat Lipocalin-2/NGAL, CF, R&D Systems, catalogue number: 3508-LC-050) at a concentration of 0.5µg per ml Sato media in the lower chambers, a highly significant increase in Cell Index value can be observed as compared to Sato media only controls.

To find out if this result could be attributed to proliferation, I repeated the experiment, this time inhibiting proliferation by treatment of the OPCs with mitomycin C. As shown in **figure 4.27c)** and **d)**, the increase in Cell Index when OPCs are exposed to LCN2 as compared to SATO media only, is completely abolished when proliferation is inhibited.

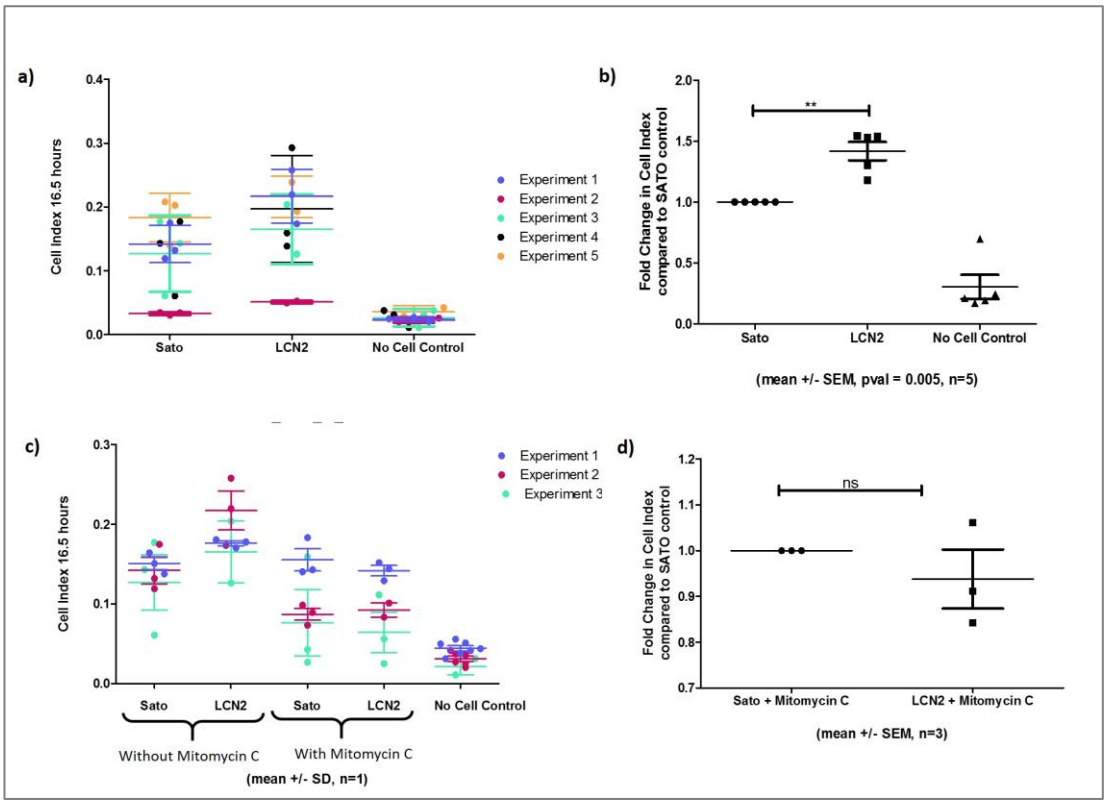


**Figure 4.27 LCN2 is a proliferation factor for OPCs *in vitro* a)** 250,000 Post shake-off rat OPCs were seeded into the upper wells of X-celligence RTCA CIM plates containing recombinant rat LCN2 at a concentration of 25µg per ml Sato media only in their lower chambers or Sato media only in both their upper and lower chambers and X-celligence RTCA CIM experiments were run for 16.5 hours **b)** Variation between replicates for the same condition, has been eliminated by calculating the fold change between OPCs exposed to LCN2 and OPCs in Sato media only controls. There is a highly significant increase in OPCs exposed to LCN2 as compared to Sato media only controls **c)** 250,000 Post shake-off rat OPCs, either with or without proliferation inhibition using mitomycin C, were seeded into the upper wells of X-celligence RTCA CIM plates containing recombinant rat LCN2 at a concentration of 25µg per ml Sato media only in their lower chambers or Sato media only in both their upper and lower chambers and X-celligence RTCA CIM experiments were run for 16.5 hours **d)** Variation between replicates for the same condition, has been eliminated by calculating the fold change between OPCs exposed to LCN2 with proliferation inhibited using mitomycin C and proliferation inhibited OPCs in Sato media only controls, no significant difference was found.

To make sure that the observed increase in cell index in the presence of LCN2 was not the result of the differentiation of OPCs into oligodendrocytes, I visualised the OPCs on the underside of the membrane using the methods described in **chapter 4.4.6**. As shown

in **figure 4.28a)**, OPCs populate the underside of the X-celligence RTCA CIM membrane by both proliferation and migration. In the presence of LCN2, more proliferating OPCs colonise the underside of the membrane by background migration and increased proliferation (see **figure 4.28b)**) and there is no evidence of increased differentiation. These results revealed that the increase in Cell Index in response to LCN2 could not be the result of differentiation confirming the result that LCN2 is a proliferation factor for OPCs *in vitro*.

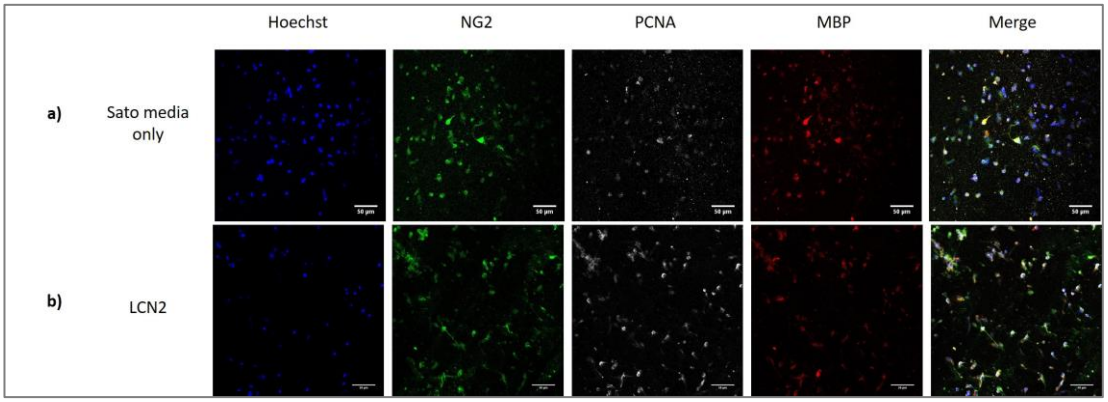


**Figure 4.28 Increased X-celligence Cell Index when OPCs are exposed to LCN2 is not the result of OPC differentiation** 250,000 Post shake-off rat OPCs either with or without proliferation inhibited using mitomycin C were seeded into the upper wells of X-celligence RTCA CIM plates containing either LCN2 at a concentration of 25µg per ml of Sato media in their lower chambers or Sato media only in both their upper and lower chambers. X-celligence RTCA CIM experiments were run for 16.5. After 16.5 hours, X-celligence RTCA CIM experiment was stopped and the membranes, electrodes and cells were fixed, stained and imaged by fluorescent confocal microscopy **a)** OPCs exposed to Sato media only, populate the underside of the X-celligence RTCA CIM membrane by background migration and proliferation and express NG2 and the proliferation marker PCNA with some expressing MBP **b)** Proliferating OPCs exposed to LCN2, populate the underside of the X-celligence RTCA membrane by increased proliferation and express NG2, PCNA and very limited MBP.

Taken together, these results show for the first time, that the LCN2 receptor 24p3r is expressed by OPCs and that the LCN2 is a proliferation factor for OPCs *in vitro*.

### 4.6.7 CXCl12 is a chemoattractant for OPCs *in vitro*

Another factor for which I found interesting results using the X-celligence system was C-X-C motif chemokine 12 (CXCL12). CXCL12 (also known as stromal-cell derived factor 1 (SDF-1)), has been documented as both a proliferation and differentiation factor for

OPCs during remyelination (Patel et al., 2012; Williams et al., 2014) and has been found to promote developmental OPC migration (Dziembowska et al., 2005).

As shown in **Appendix 2**, in my bioinformatic analysis of the data in Huang, Jarjour et al., 2011, of the 410 secreted factors correlating with PDGFα expression I identified in **Chapter 3**, I identified only two which belonged to the chemokine family: CX3CL1 (which will be discussed at length in **Chapter 5**), and CXCL12. As shown in **figure 4.29**, CXCL12 expression rises over the course of LPC induced demyelinating injury and is most highly expressed at 28 days post lesion when remyelination should be well under way.

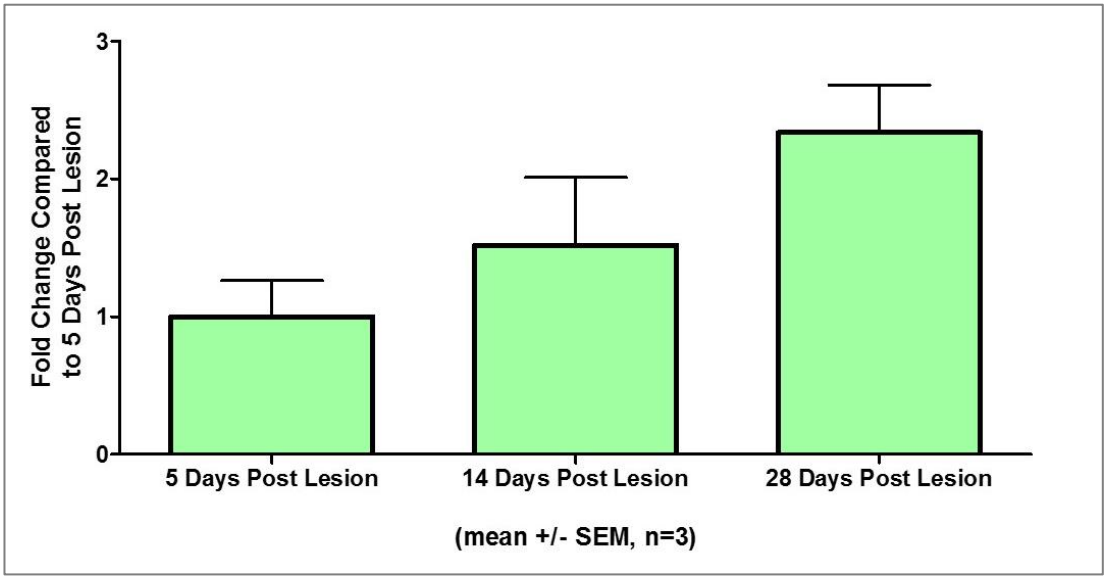


**Figure 4.29 Expression of CXCL12 rises over the course of LPC induced demyelinating injury from Huang, Jarjour et al., 2011, peaking when remyelination should be well under way**

I also checked the expression of the two receptors for CXCL12, CXCR4 and CXCR7, in the data I analysed from Moyon et al., 2015, but as shown in **figure 4.30**, there was very little difference in the expression of either receptor between Activated and Non-activated OPCs. However, I hypothesized that this could reflect high receptor expression in both Activated and Non-activated OPCs.

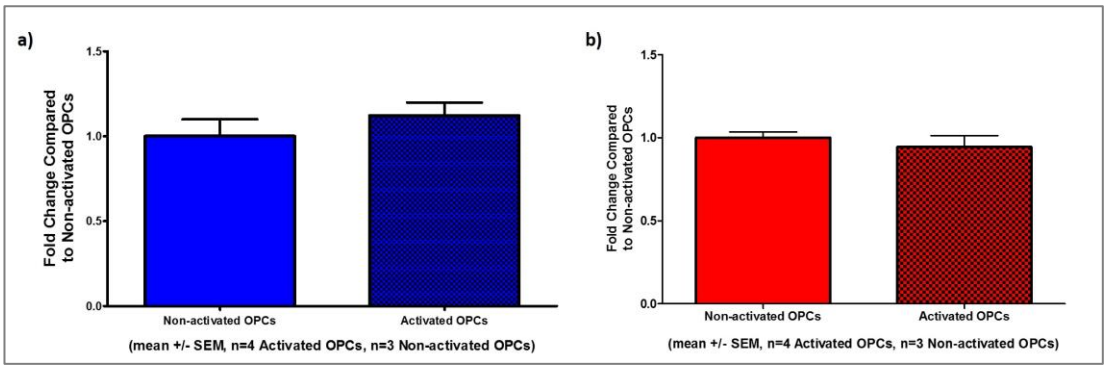


**Figure 4.30 Expression of a) CXCR4 and b) CXCR7, the receptors for CXCL12 in the Cuprizone injury data from Moyon et al., 2015**

To find out if the receptors for CXCL12 were strongly expressed on post shake-off rat OPCs, I performed immunofluorescent antibody staining on OPCs cultured overnight at 37°C and 7.5% $CO_2$. As shown in **figure 4.31**, NG2 positive OPCs also expressed both receptors for CXCL12, CXCR4 (see **figure 4.31 a)**) and CXCR7 (see **figure 4.31 b)**).

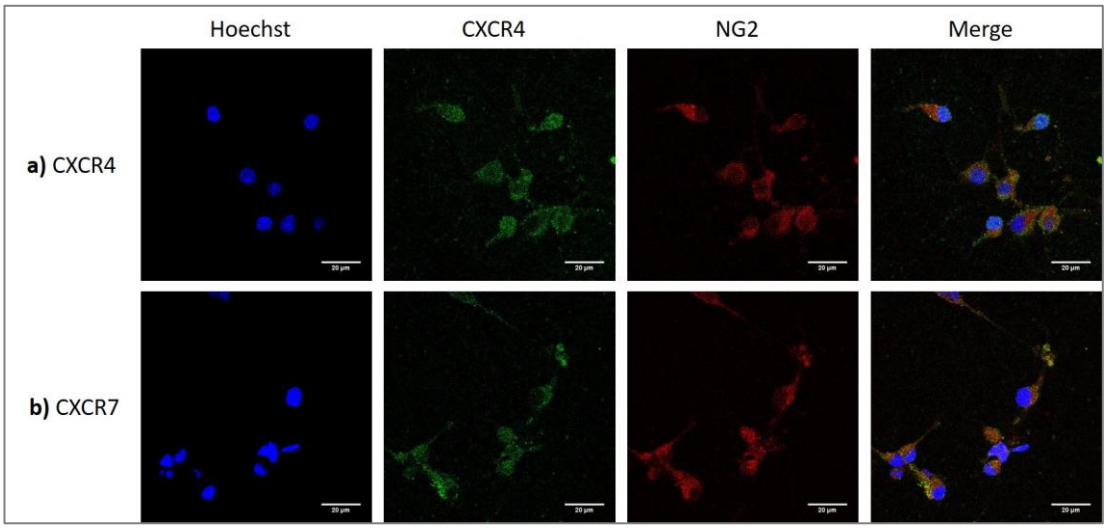


**Figure 4.31 OPCs express CXCR4 and CXCR7 the receptors for CXCL12 *in vitro*** Post shake-off OPCs were seeded onto glass coverslips at a cell density of 50,000 OPCs per 500µl Sato media and cultured overnight in Sato media at 37°C and 7.5% $CO_2$. OPCs on glass coverslips were then fixed and stained before imaging by immunofluorescent confocal microscopy. NG2 positive OPCs also express **a)** CXCR4 and **b)** CXCR7.

To find out if recombinant CXCL12 acts as a chemoattractant for OPCs *in vitro*, I ran X-celligence RTCA CIM experiments in which OPCs were seeded in the upper chambers and exposed to recombinant rat CXCL12 at a concentration of 1µg per ml Sato media in the lower chambers. As shown in **figure 4.32 a)** and **b)**, there was a significant increase in Cell Index when OPCs were exposed to CXCL12.

To eliminate proliferation as the source of increased Cell Index in the presence of CXCL12, I repeated the experiments with OPCs which had first been treated with mitomycin C to inhibit proliferation. As shown in **figure 4.32 c)** and **d)**, the increase in Cell Index observed in CXCL12 stimulated OPCs was reduced by not entirely abolished in the absence of proliferation. These results show that while a proliferative effect of CXCL12 cannot be ruled out, proliferation alone is not responsible for the increase in Cell Index; at least some of this increase can be attributed to either directional migration or differentiation.

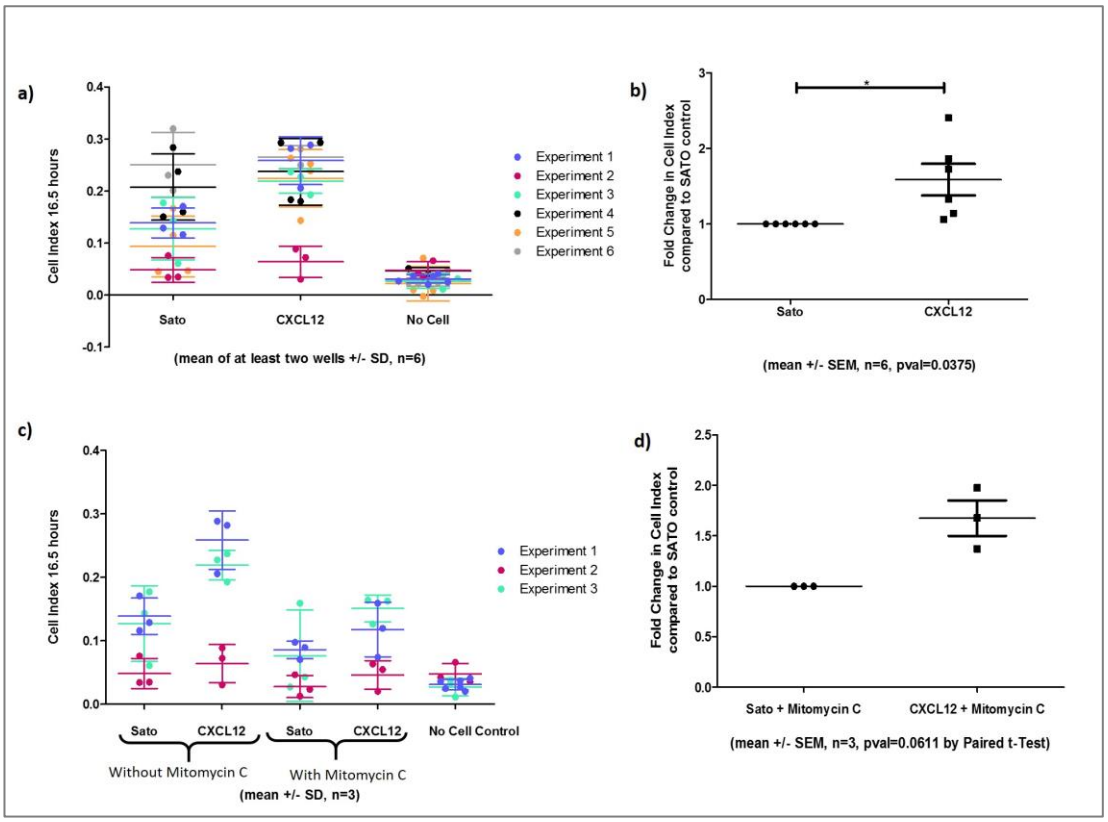


**Figure 4.32 CXCL12 is a chemoattractant for OPCs *in vitro* a)** 250,000 Post shake-off rat OPCs were seeded into the upper wells of X-celligence RTCA CIM plates containing recombinant rat CXCL12 at a concentration of 1µg per ml Sato media only in their lower chambers or Sato media only in both their upper and lower chambers and X-celligence RTCA CIM experiments were run for 16.5 hours **b)** Variation between replicates for the same condition, has been eliminated by calculating the fold change between OPCs exposed to CXCL12 and OPCs in Sato media only controls. There is a significant increase in OPCs exposed to LCN2 as compared to Sato media only controls **c)** 250,000 Post shake-off rat OPCs, either with or without proliferation inhibition using mitomycin C, were seeded into the upper wells of X-celligence RTCA CIM plates containing recombinant rat CXCL12 at a concentration of 1µg per ml Sato media only in their lower chambers or Sato media only in both their upper and lower chambers and X-celligence RTCA CIM experiments were run for 16.5 hours **d)** Variation between replicates for the same condition, has been eliminated by calculating the fold change between OPCs exposed to CXCL12 with proliferation inhibited using mitomycin C and proliferation inhibited OPCs in Sato media only controls, there was an increase in Cell Index when proliferation is inhibited.

The increase in CXCL12 exposed OPCs compared to OPCs in Sato media only controls is not lost when proliferation is inhibited using mitomycin C.

To establish whether the increases in Cell Index observed could be the result of OPC differentiation, I imaged the underside of the X-celligence plates and as shown in **figure 4.33**, no discernible difference in MBP expression or process formation could be seen between OPCs exposed to CXCL12(**figure 4.33 b**)) and OPC in Sato media only controls either with (**figure 4.33 a)**).

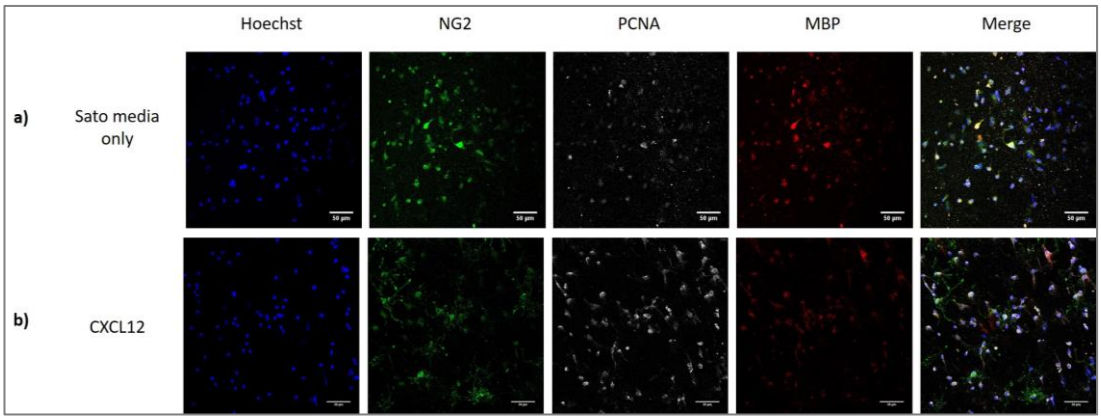


**Figure 4.33 Increased X-celligence Cell Index when OPCs are exposed to CXCL12 is not the result of OPC differentiation** 250,000 Post shake-off rat OPCs either with or without proliferation inhibited using mitomycin C were seeded into the upper wells of X-celligence RTCA CIM plates containing either CXCL12 at a concentration of 1µg per ml of Sato media in their lower chambers or Sato media only in both their upper and lower chambers. X-celligence RTCA CIM experiments were run for 16.5. After 16.5 hours, X-celligence RTCA CIM experiment was stopped and the membranes, electrodes and cells were fixed, stained and imaged by fluorescent confocal microscopy **a)** OPCs exposed to Sato media only, populate the underside of the X-celligence RTCA CIM membrane by background migration and proliferation and express NG2 and the proliferation marker PCNA with and some MBP **b)** OPCs exposed to CXCL12, populate the underside of the X-celligence RTCA membrane by directional chemotaxis toward CXCL12 and express NG2, PCNA and very limited MBP

Thus, results for my experiments with CXCL12 show that in addition to proliferation, CXCL12 is also a chemoattractant for post shake-off rat OPCs *in vitro*.

## 4.7 Discussion

### 4.7.1 Results Summary

At the outset of this phase of the project, I set out to identify and optimise a suitable assay with which to study the chemotaxis of OPCs in response to novel factors *in vitro*. On review of current commercially available assays designed for this purpose, I identified both the formation of a liquid gradient and analysis of cell migration in real time as essential components for a suitable chemotaxis assay.

The X-celligence RTCA CIM system developed by ACEA Biosciences, incorporates both these features in its design. The system consists of two media filled chambers separated by a porous membrane, the upper chamber containing the cells and the lower chamber containing the factor to be tested. A gradient of the factor tested forms in the pores of the membrane, and cells migrate through the pores in response to this gradient, before adhering to the underside of the membrane. Cell Index values reflecting the change electrical impedance across the underside of the membrane are measured by microelectrodes, arrayed on the underside of the membrane.

My preliminary experiments indicated that optimisation of the system for the specific requirements of OPCs was necessary. Firstly, I increased the number of cells seeded into each well to 250,000 OPCs per well. Next I used the proliferation inhibitor mitomycin C to control for proliferation, allowing the system to be used to monitor proliferation in addition to migration. I then developed a system to extract membranes from the X-celligence RTCA CIM plates at the conclusion of the experiment, and stain them to reveal the differentiation stage of the cells bound to its underside. In this way, differentiation could both, be eliminated as a cause of increased Cell Index in response to migration, and also studied using the X-celligence RTCA CIM system.

Having optimised the X-celligence RTCA CIM system for the analysis of the directional migration, proliferation and differentiation of OPCs *in vitro*, I then used the system to make novel inferences regarding the effect of the factors LCN2 and CXCL12 on OPC biology.

The addition of LCN2 to OPCs in X-celligence RTCA CIM experiments, resulting in a statistically significant increase in Cell Index, but only when proliferation was not inhibited. I found no evidence of increased OPC differentiation in response to LCN2. In this way, my results show, for the first time, both that OPCs express the LCN2 receptor 24p3r, and that LCN2 is a proliferation factor for OPCs *in vitro*.

Conversely, the addition of CXCL12 to OPCs in X-celligence RTCA CIM experiments, resulted in an increase in Cell Index which remained robust in the absence of proliferation. Staining of the underside of X-celligence RTCA CIM membranes revealed no increase in OPC differentiation in response to CXCL12. These results show, for the first time, that CXCL12 is a chemoattractant for OPCs *in vitro*.

#### 4.7.2. Evidence from LCN2 suggests OPC proliferation may occur late during focal demyelinating injury

As iterated above, this thesis includes the novel finding that 24p3r is expressed by post shake-off OPCs and LCN2 functions as a proliferation factor for OPCs *in vitro*. The results from the Moyon et al., 2015 cuprizone data set, that 24p3r is more highly expressed in Non-activated than Activated OPCs, and the results from the Huang, Jarjour et al., 2011 dataset show increasing expression of 24p3r over the course of demyelinating injury, similar to the expression pattern of PDGFα. Taken together, these results may indicate that the proliferation of OPCs occurs late in demyelinating injury, after OPC migration. Further experimentation classifying the expression of 24p3r and LCN2 in both human MS lesions and throughout LPC induced demyelination in mice.

#### 4.7.3 CXCL12 as a migration, proliferation and differentiation factor for OPCs

In their 2012 study, Patel et al., showed that CXCL12 functions as both a proliferation and differentiation factor for OPCs in cuprizone induced global demyelination. In a further study they also showed that CNS remyelination could be improved by antagonism of CXCR7 (Williams et al., 2014) (CXCR7 sequesters CXCL12 for degradation, reducing the number of CXCL12 molecules available to bond CXCR4, thus muting the cellular response to CXCL12 stimulation (Boldajipour et al., 2008; Cruz-Orengo et al., 2011; Naumann et al., 2010)). No migratory effect on OPCs was reported in either study.

In contrast to the published data, using the X-celligence RTCA CIM system, I have shown that CXCL12 functions as a chemoattractant for OPCs *in vitro*. This was not a hugely surprising result, given that CXCL12 has been found to augment migration in a wide variety of cell types (reviewed in Puchert and Engele, 2014).

Cuprizone is a model of global demyelination, because of this, it is possible that the lack of OPC migration reported could be explained by the lack of formation of a directional gradient of CXCL12 in this model. It would therefore be interesting to study the effect of CXCL12 in LPC induced focal demyelinating injury. As my results from the gene

expression array data from Huang, Jarjour et al., 2011 shows, the concentration of CXCL12 at the lesion site rises over the course of LPC induced focal demyelination. This rising expression pattern which correlates with PDGFα, could represent the accumulation of CXCL12 at the lesion site, which forms a gradient up which OPCs migrate.

Chapter 5

# CX3CL1 is a Regulator of Oligodendrocyte Precursor Cell Biology *in vitro*

## 5.1 Introduction

### 5.1.1 Selection of the CX3CR1/CX3CL1 Receptor Ligand Pair for *in vitro* Analysis

On my review of the existing literature pertaining to the biology of Oligodendrocyte Precursor Cells (OPCs) at the beginning of my project, I was struck by the lack of high throughput data analysis applied to understanding the role of OPCs in CNS regeneration. Many previous studies investigating OPC migration had used a candidate gene approach, selecting a single target based on existing literature concerning OPCs in CNS development, or other known migration pathways such as axon guidance. With my particular interest in bioinformatics, I reasoned that a less biased genome wide approach might reveal new previously unconsidered targets with important roles in regeneration.

As detailed in **Chapter** 3, having discovered relevant data sets, I took a two pronged approach mining gene expression array data from isolated OPCs (Moyon et al., 2015) for cell surface receptors as well as gene expression array data from whole demyelinating lesion sites (Huang et al., 2011) for extracellularly secreted factors. On my combined analysis of the two data sets, I discovered that of all the cell surface receptors identified as being upregulated in activated OPCs (fold change of at least 2 as compared to non-activated OPCs), only two had known ligands which were significantly differentially expressed in at least one post-injury time-point and expressed in a pattern correlating with both PDGFα and CXCL12 (Pearson's correlation coefficient of >0.85).

As explained in **Chapter 3.5**, of the two ligand-receptor pairs identified, one, PTPRZ1, could be eliminated as a candidate for further experimentation because previously published studies had found it to be a negative regulator of OPC differentiation and remyelination (Kuboyama et al., 2012, 2015; Pendleton et al., 2013). This left only the CX3CR1/CX3CL1 receptor ligand pair.

### 5.1.2 Structure and Activity of CX3CL1 and CX3CR1

CX3CR1 is a G-protein coupled receptor which features 7 hydrophobic transmembrane domains within its 355 amino acid polypeptide sequence. It was first reported under the name V28, as an orphan receptor identified in human DNA because of its sequence similarity to known chemokine receptors (Raport et al., 1995). CX3CR1 was later shown to be a high affinity receptor for CX3CL1, binding of which induced calcium flux and

migration in leukocytes (Imai et al., 1997). CX3CR1 is as yet the only documented receptor for CX3CL1 (Liu et al., 2016; Poniatowski et al., 2016).

Like other chemokines, CX3CL1 derives its name from the number of amino acids between the first two cysteine residues of its amino acid sequence. Thus, in CX3C the two cysteine residues (C) are separated by 3 other non-conserved amino acids (X3) (Luster, 1998). In contrast with the other main families of human chemokines, C, CC and CXC, all of which include multiple ligands, CX3CL1 is the only known member of the CX3C family.

CX3CL1 (fractalkine) is composed of 373 amino acids and is expressed in a range of organs including the lung, heart, kidney, small intestine and brain. As illustrated in **figure 5.1a)**, the amino acid sequence of the CX3CL1 protein can be divided into 5 regions. The first is a 25 amino acid N-terminal signal peptide sequence, indicative of the secretory or membrane associated character of the newly synthesized polypeptide. This is followed by a 76 amino acid chemokine domain, a 241 amino acid mucin-like stalk region, a 19 amino acid transmembrane domain and terminates with a 37 amino acid intracellular domain(Bazan et al., 1997).

CX3CL1 is unique amongst chemokines, in that is it has both a membrane bound form and a soluble form which can be secreted from the cell surface following proteolysis (Bazan et al., 1997; Imai et al., 1997). The unusual structure of CX3CL1 in which the chemokine domain is anchored to the transmembrane and intracellular domains by a mucin like stalk (see **figure 5.1b)**), facilitates two modes of interaction with CX3CR1.

Firstly, the chemokine domain can be released into the extracellular milieu by cleavage of the stalk (see **figure 5.1c)**). The untethered chemokine domain may then travel through the CNS parenchyma and activate distal CX3CR1 expressing cells, triggering downstream intracellular signalling cascades resulting in the expression of migration associated genes (see **figure 5.1d)**). In contrast, CX3CL1 acting as a single membrane tethered protein, has the ability to adhere CX3CL1 and CX3CR1 expressing cells through the interaction of the chemokine domain and CX3CR1 (see **figure 5.1e)**).

#### 5.1.3 The Role of CX3CR1/CX3CL1 in Microglia in the CNS

While the CX3CR1/CX3CL1 has been found to play a role in a variety of human diseases (reviewed in Liu et al., 2016), it is of particular importance in CNS pathology. CX3CL1 is highly expressed in the brain, particularly in neuron rich regions, while CX3CR1 is

expressed by microglia, for which the chemokine domain of CX3CL1 acts as a chemoattractant (Harrison et al., 1998).

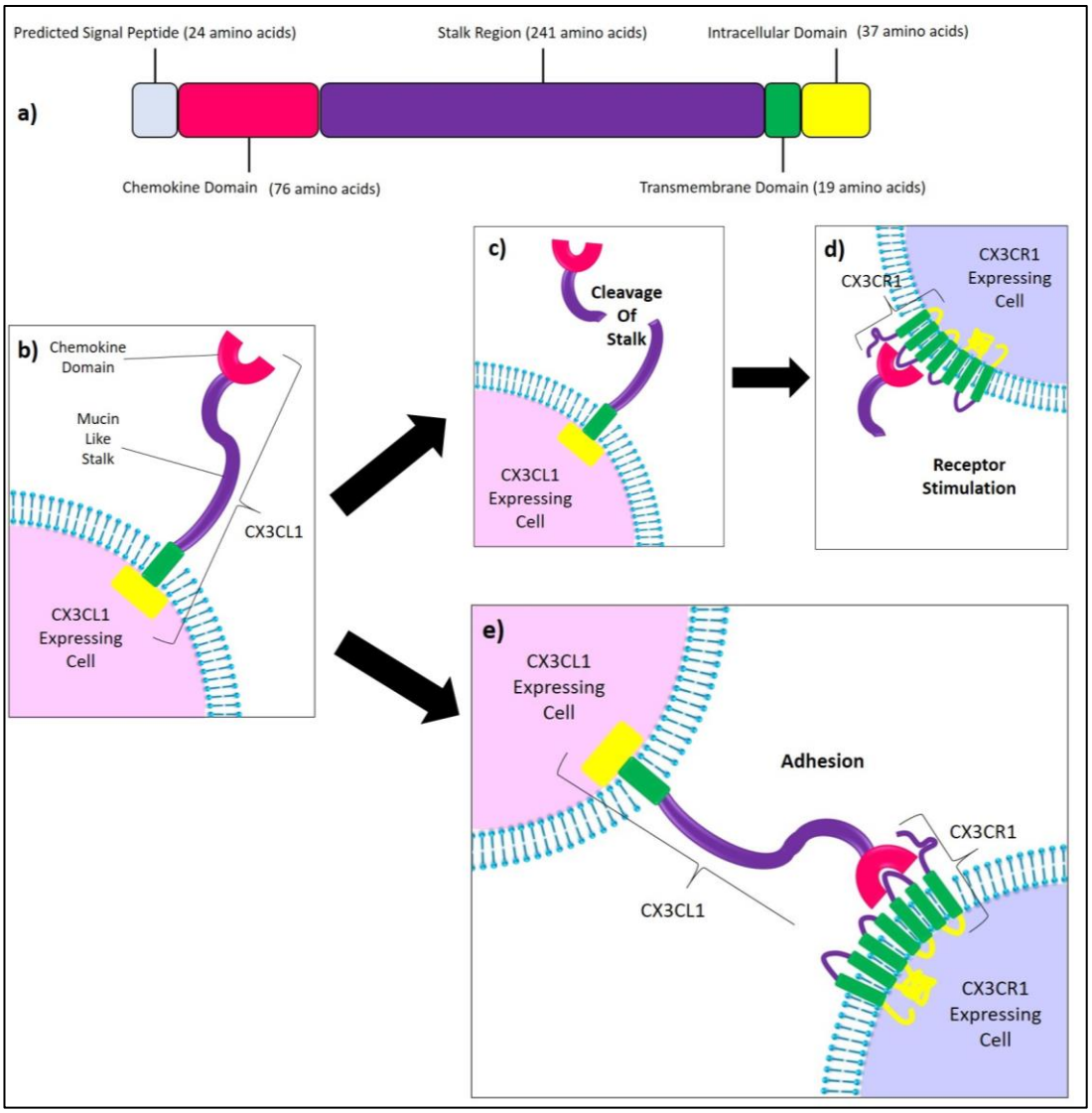


**Figure 5.1 Structure and Function of CX3CL1 Protein. a)** Schematic representation of the CX3CL1 protein, scaled by number of amino acids and coloured by protein region function **b) – e)** Functional activity of CX3CL1 through interaction with CX3CR1 **b)** On the surface of CX3CL1 expressing cells, the chemokine domain of CX3CL1 is attached to its transmembrane and intracellular domains by an extended mucin like stalk **c)** Cleavage of the stalk results in the release of the chemokine domain into the extracellular environment **d)** The free floating chemokine domain of CX3CL1 binds to CX3CR1 triggering an intracellular signalling cascade in the CX3CR1 expressing cell **e)** Alternatively, CX3CL1 as a single, un-cleaved molecule binds to the CX3CR1 receptor of a neighbouring cell, forming a cell to cell adhesion.

In the CNS, the process of inflammation is chiefly modulated by the microglia. Microglia are the resident macrophages of the CNS and make up 5-12% of the overall cell population (Lawson et al., 1990; Miron and Franklin, 2014). In the very earliest stages of CNS injury, microglia become activated, before performing neuroregenerative functions including phagocytosis of debris, orchestration of monocyte derived macrophages and the secretion of pro-regenerative factors (Kreutzberg, 1996; Miron and Franklin, 2014; Miron et al., 2013).

However, other factors secreted by microglia have been found to negatively impact CNS biology, a process which is implicated in the inappropriate inflammatory response in pathologies such as MS (Miron and Franklin, 2014).

The CX3CR1/CX3CL1 axis however, is reported to positively impact neuroregeneration. Administration of CX3CL1 has been found to increase microglial survival by blocking apoptosis *in vitro* (Boehme et al., 2000), while the loss of the CX3CR1/CX3CL1 axis through the knock-out or antagonism of CX3CR1 has been shown to disrupt regenerative microglial activities and increase neurotoxicity in a variety of CNS injury models (Bellavance et al., 2015; Cardona et al., 2006; Harrison et al., 1998; Lampron et al., 2015; Rivest, 2015).

In summary, the view of CX3CR1/CX3CL1 CNS function established in the literature is that CX3CL1 is primarily secreted by neurons as a way of signalling to microglia, the only CNS cells to express CX3CR1.

#### 5.1.4 Polymorphisms in CX3CR1 are Associated With MS

It has been postulated that polymorphisms modulating the binding affinity of CX3CL1 for its receptor CX3CR1 may be implicated in the rapidity of MS disease course. In MS patients, heterozygosity for the V249I polymorphism, located in the transmembrane region of CX3CR1, has been associated with protracted initial relapsing and remitting (RR) phase and slower transition into the secondary progressive (SP) phase(Arli et al., 2013; Stojković et al., 2012). CX3CR1 expressing cells with this polymorphism have been shown to bind CX3CL1 more slowly, resulting in deficient calcium flux and ultimately reduced migration in response to a CX3CL1 gradient (McDermott et al., 2003).

In their 2012 study, Broux and colleagues investigated the expression of CX3CL1 and CX3CR1 in the brains of MS patients. A cytokine antibody array found upregulation of CX3CL1 in the cerebrospinal fluid of MS patients at their first clinical manifestation of the disease, and immunofluorescent staining revealed increased expression of CX3CL1 in inflammatory MS lesions compared to non-lesioned tissue. Immunofluorescent staining was also used to reveal CX3CR1 expression in the NAWM of MS patients, as well as in the perivascular cuff of active MS lesions. In addition, the same study documented the migration of pro-inflammatory CX3CR1 expressing CD4(+) CD28(-) T-cells up an increasing gradient of CX3CL1 *in vitro*. Taken together, these data suggest that the CX3CL1/CX3CR1 interaction orchestrates the recruitment of CD4(+) CD28(-) T-cells to inflammatory MS lesions.

Interestingly, the same study also found expression of CX3CR1 in CD4(+) T-cells, microglia and oligodendrocytes in MS lesions, indicative of a broader role for the CX3CL1/CX3CR1 interaction in demyelinating injury.

#### 5.1.5 CX3CR1 Expression in the CNS May Not be Limited to Microglia

The pervasive notion that CX3CR1 is exclusively expressed by microglia in the CNS appears to stem from Harrison *et al*., 1998. However, while this study clearly documents the expression of CX3CR1 on microglia, it does not record the analysis of other brain cell types for the expression of CX3CR1.

In addition, it has been reported that in the brain lesions of EAE rats, while the majority of CX3CR1 expressing cells can be identified as phagocytic macrophages or microglia, a subset of CX3CR1 expressing cells lacking immunoreactivity for antibodies for macrophages, microglia, astrocytes or neurons can also be detected (Sunnemark et al., 2005).

Having found the expression of CX3CR1 in activated OPCs in my microarray screen, I wondered if the unidentified CX3CR1 expressing cells might be OPCs and accordingly, searched the literature for any known effects of the CX3CR1/CX3CL1 axis on OPCs.

#### 5.1.5 Migration of OPCs in Response to Demyelination is Impaired in CX3CR1 Knock-out Mice

I discovered almost no pre-existing data on the effect of the CX3CL1 ligand on OPC biology although a recent paper predominantly investigating the effects of CX3CR1 knock out on the functionality of microglia in cuprizone induced demyelination in the

mouse CNS (Lampron et al., 2015) found that CX3CR1 knock-out impeded the regenerative process. The authors attributed this obstruction of remyelination purely to inefficient clearance of myelin debris by microglia, however, they also included a single figure showing a reduction in the presence of PDGFRα+ OPCs in the demyelinated corpus callosum. This failure of OPC recruitment may be secondary to failure of microglia entry and clearance of debris, but may also be a primary failure of OPC recruitment.

#### 5.1.6 Expression of CX3CR1 and CX3CL1 in Uninjured Brain Tissue

To garner more information about the CX3CR1/CX3CL1 interaction I referred to the Barres Brain RNA-seq Database for isolated CNS cell types from uninjured tissue in mice (Zhang et al., 2014) and in humans (Zhang et al., 2016). I began by looking at the mouse data and found that while CX3CL1 had some low expression in astrocytes, newly formed oligodendrocytes, myelinating oligodendrocytes, microglia and endothelial cells, CX3CL1 is by far most highly expressed by neurons, but is also significantly expressed by OPCs (see **Figure 5.2a)**).

The mouse data for CX3CR1 showed that in uninjured brain tissue CX3CR1 is predominantly expressed in microglia while there is some expression in OPCs, although the authors include a caveat that the OPC isolate was contaminated with around 5% microglia (see **Figure 5.2b)**).

In humans, the data from the Barres Brain RNA-seq Database shows that CX3CL1 is expressed by foetal astrocytes, mature astrocytes and neurons, but more significantly by endothelial cells (see **figure 5.2d)**). Similar to the mouse data, CX3CR1 is highly expressed by microglia/macrophages, but also by oligodendrocytes (**figure 5.2e)**).,

Interestingly, while OPCs are not included in the human dataset, the cell surface receptor PDGFRα which is highly expressed by mouse OPCs (**figure 5.2c)**), is also expressed by human oligodendrocytes (**figure 5.2f)**), suggesting that other cell surface receptors expressed by mouse OPCs might be detected in this human oligodendrocyte isolate, either from contaminating OPCs or a biological similarity between OPCs and oligodendrocytes in humans. This might explain why CX3CR1 expression could be detected in the human (**figure 5.2e)**) but not the mouse (**figure 5.2b)**) oligodendrocyte isolates.

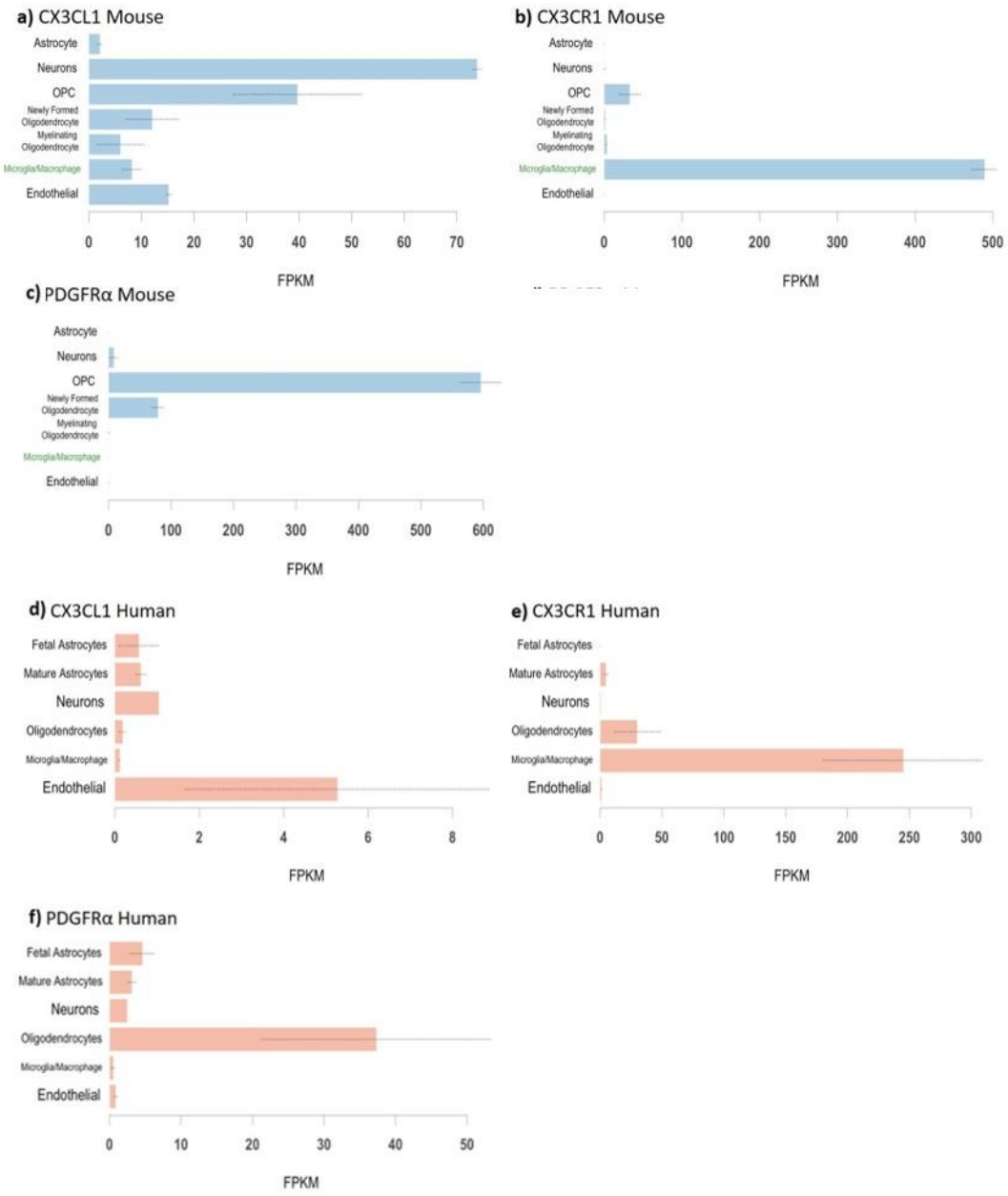


**Figure 5.2 Expression of CX3CL1, CX3CR1 and CD68 in uninjured brain tissue according to the Barres Brain RNA-seq.** Data from RNA-seq for isolated CNS cell types from uninjured tissue, noting that the OPC isolate has 5% microglial contamination (Zhang et al., 2014). Expression for each cell type calculated as Fragments Per Kilobase of exon per Million fragments mapped (FPKM). **a)-c)** Mouse**, d)-f)** Human. In mice, CX3CL1 **a)** is expressed by all cell types but is most highly expressed in neurons and OPCs. In agreement with previously published literature, CX3CR1 **b)** is very highly expressed by microglia but also has some expression in OPCs. (Although there is 5% contamination of the OPC isolate by microglia) **c)** PDGFRα is included as an example of a cell surface receptor which is highly expressed on OPCs. In humans, **d)** While CX3CL1 is expressed by neurons, it is also highly expressed by endothelial cells. **e)** CX3CR1 is expressed by microglia and oligodendrocytes. While OPCs are not

included separately in the human data, **f)** PDGFRα, an OPC marker, is expressed by oligodendrocytes, suggesting that “Oligodendrocytes” might also include OPCs.

These observations suggested to me a strong case for further investigation of whether or not CX3CR1 was expressed in OPCs as well as microglia.

In this chapter, I will describe how I indisputably show that CX3CR1 is expressed by OPCs *in vitro*, before going on to describe the dynamic effects of different concentrations of CX3CL1 on the migration, proliferation and maturation of OPCs and how control of these processes defines CX3CL1 as a master regulator of OPC mediated CNS regeneration.

## 5.2 CX3CR1 is Expressed by Oligodendrocyte Precursor Cells

### 5.2.1 CX3CR1 is expressed in 'activated' OPCs in gene array expression analysis data

As discussed earlier, the first of the bioinformatics data sets I analysed was run on an Agilent microarray platform and I used it to compare gene expression between OPCs activated in response to cuprizone induced demyelination and non-activated OPCs from uninjured tissue (Moyon et al., 2015). As shown in **figure 5.3,** the result from my analysis of this comparison was that the G-protein coupled receptor CX3CR1 was differentially expressed 3-fold higher in activated OPCs as compared to non-activated OPCs (Linear fold change=2.99915894372415, Log2 fold change=1.61064724969289).

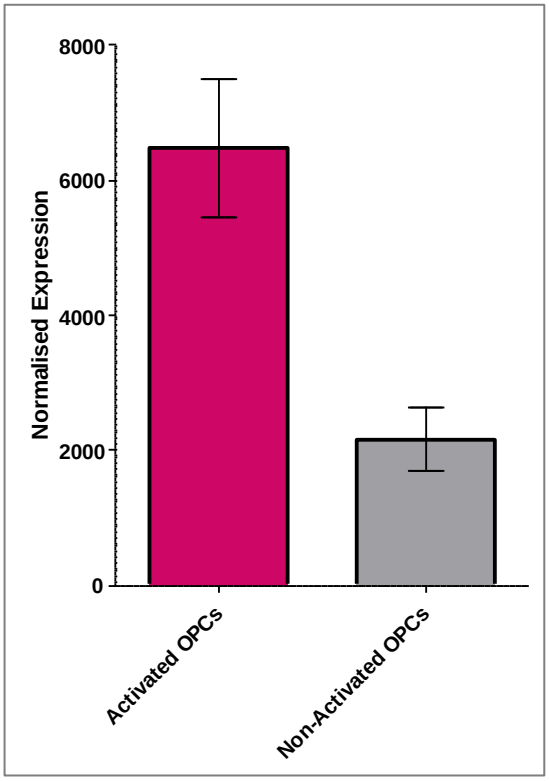


**Figure 5.3 Expression of CX3CR1 expression triples between Non-Activated and Activated OPCs.** Results of gene expression array analysis of the data from Moyon et al., 2015. Normalised expression is 3 times higher in Activated OPCs from cuprizone injured brain tissue than in Non-Activated OPCs from uninjured brain tissue (mean of 4 replicates for Activated OPCs and 3 replicates for Non-Activated OPCs +/- SEM, p=0.02077755 by differential expression analysis using Limma).

As explained in **Chapter 3**, the expression levels for all the features in the Moyon et al., 2015 dataset were elevated by significant background noise, such that fold changes between the two conditions are reduced from what would be expected without high

background. Thus, the 3-fold increase between non-activated and activated OPCs is likely to reflect an even larger increase in expression than could be detected in this dataset.

I thus began my *in vitro* experiments with the verification of the result from the bioinformatics data, that CX3CR1 protein is expressed on OPCs.

#### 5.2.2 CX3CR1 expression can be detected in OPC cultures by western Blot

To achieve this aim, with the assistance of visiting PhD student Misuzu Hashimoto, expression of CX3CR1 in OPCs was confirmed by western blot (see methods **chapter 2.2.6.3**). As the bioinformatics data showed upregulated expression of CX3CR1 in "activated" OPCs, lysates were prepared from rat OPCs cultured either normally (unstimulated) or in the presence of 0.03µg/ml recombinant rat CX3CL1 for 16 hours (stimulated) and probed for the expression of CX3CR1, using GAPDH as a loading control. A single band at ~50kDa for CX3CR1 was detected in both CX3CL1 stimulated and non-stimulated OPCs again suggesting the presence of the CX3CR1 protein in OPCs (see **Figure 5.4**).

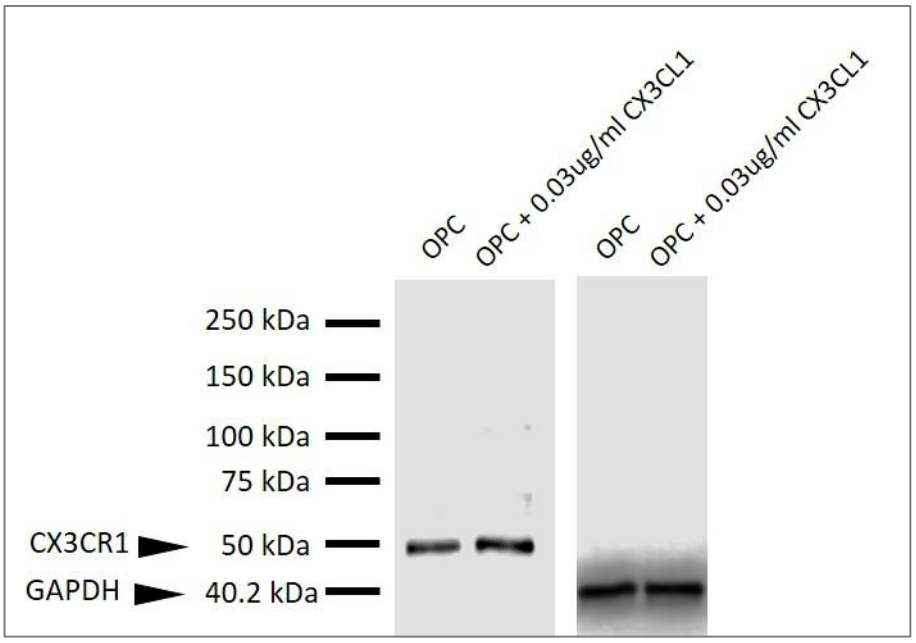


**Figure 5.4 Confirmation of CX3CR1 expression in OPCs by western blot.** Specific bands for CX3CR1 are detected with the polyclonal antibody at ~50kDa in post-shake-off rat OPCs both normally (unstimulated) or in the presence of 0.03µg/ml recombinant rat CX3CL1 for 16 hours (stimulated), using the housekeeping gene GAPDH as a loading control.

However, when rat OPCs are prepared using the shake-off method(see McCarthy and de Vellis, 1980 and methods **chapter 2.2.3**), microglia are only removed from the culture by virtue of their weaker adhesion, and there is a risk that the final cultures are contaminated by residual microglia that are inefficiently removed in this manner. With the overwhelming evidence in the literature that CX3CR1 is expressed by microglia (Bellavance et al., 2015; Broux et al., 2012; Cardona et al., 2006; Harrison et al., 1998; Lampron et al., 2015; Paolicelli et al., 2014; Rivest, 2015), and no literature suggesting it is expressed in OPCs, it was imperative to eliminate the possibility that the immunoreactivity of CX3CR1 seen by western blot was due to the presence of CX3CR1 expression in contaminating microglia rather than in OPCs.

### 5.2.3 CX3CR1 is expressed by Olig2$^{+}$/MBP$^{-}$ OPCs

Verification of the purity of post shake-off OPCs, was carried out by Hui Zhang, a previous student in the Williams lab. As shown in **figure 5.5** below, rat OPC cultures were immunostained for lineage specific markers for the oligodendroglial lineage(Olig2), astrocytes (GFAP) and microglia (CD68). Around 85% of the cultures were found to be expressing Olig2, while around 14% of the cell were found to be contaminating astrocytes. Although there is some evidence of microglial contamination, CD68 expressing microglia made up less than 1% of the total cells.

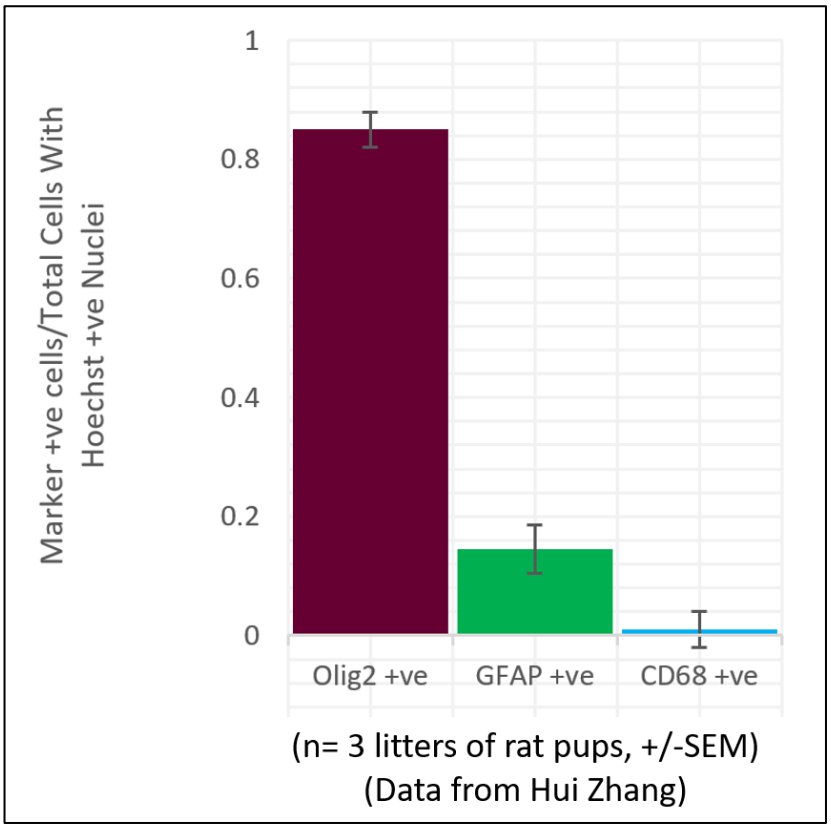


**Figure 5.5 Purity of Post Shake-Off Rat OPC Culture** Cultures from 3 separate litters of rat pups prepared according to methods section **2.2.3 Preparation of primary rat OPCs from neonatal brain tissue**. Following shake-off, mixed glial cultures were immuostained for markers of glial cell types. 0.85 Marker +ve cells/Total Cells With Hoechst +ve Nuclei were found to express the Olig2 marker of oligodendroglia, 0.145 Marker +ve cells/Total Cells With Hoechst +ve Nuclei were found to express the GFAP marker of astrocytes, and 0.00995 Marker +ve cells/Total Cells With Hoechst +ve Nuclei were found to express the CD68 marker of microglia, verifiying that microglia make up only a very small fraction of the post shake-off OPC culture.

To establish the expression of CX3CR1 specifically in OPCs, I immunostained rat OPC cultures using antibodies for oligodendroglial-specific markers and CX3CR1 (see **chapter 2.2.9.2** for full antibody list). Post shake-off rat OPCs were either normally cultured or stimulated with recombinant rat CX3CL1 at increasing concentrations: 0.01µg/ml, 0.03µg/ml, 0.1µg/ml, 0.3µg/ml, 0.9µg/ml, 2.7µg/ml overnight.

Visual examination of images generated by confocal microscopy revealed expression of CX3CR1 in $Olig2^{+}/MBP^{-}$ OPCs (**Figure 5.6 a)-g)**) in all conditions as well as increased

abundance of Olig2+/MBP- oligodendrocyte at the highest concentrations of CX3CL1 stimulation (**Figure 5.6 f)** and **g)**).

To verify this result, I repeated the same experimental set-up using the Operetta high content fluorescent microscopy system (PerkinElmer) and quantified CX3CR1 expression in $Olig2^{+}/MBP^{-}$ OPCs in these images using Columbus analysis software. As shown in **Figure 5.6.h),** without CX3CL1 stimulation, on average 93.98% of Olig2+/MBP- cells are also CX3CR1 positive. When cells were stimulated with CX3CL1, CX3CR1 expression can be detected in over 90% of $Olig2^{+}/MBP^{-}$ cells across all concentrations (0.01μg/ml = 95.41%, 0.03μg/ml = 93.95%, 0.1μg/ml = 92.78%, 0.3μg/ml = 95.27%, 0.9μg/ml = 95.86%, 2.7μg/ml = 95.88% (means plus s.e.m. plotted in figure)).
As $Olig2^{+}/MBP^{-}$ cells are by definition immature oligodendroglial lineage cells or OPCs, this result eliminates the possibility that detection of CX3CR1 immunoreactivity is the product of microglial contamination and verifies that CX3CR1 is expressed by OPCs.

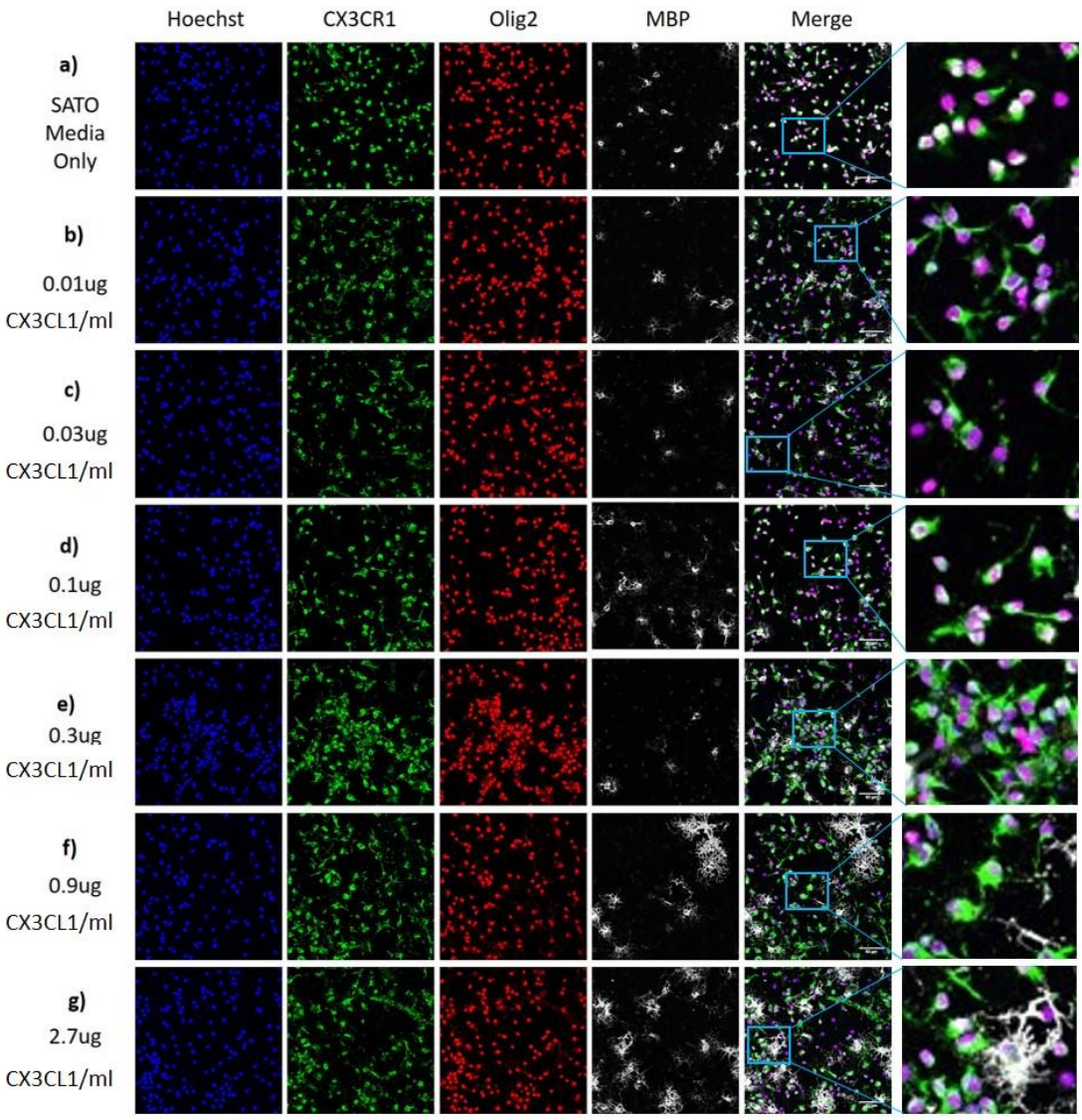
Hoechst
CX3CR1
Olig2
MBP
Merge
a)
SATO
Media
Only
b)
0.01ug
CX3CL1/ml
c)
0.03ug
CX3CL1/ml
d)
0.1ug
CX3CL1/ml
e)
0.3ug
CX3CL1/ml
f)
0.9ug
CX3CL1/ml
g)
2.7ug
CX3CL1/ml

**h)**

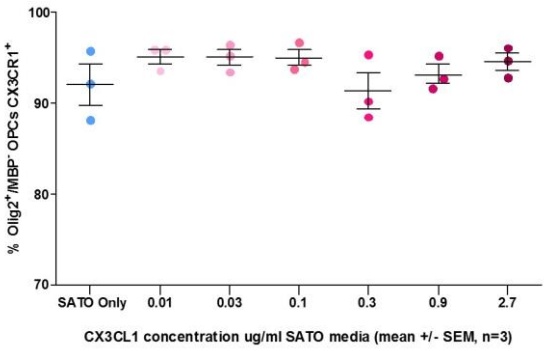
% Olig2+/MBP- OPCs CX3CR1+
100
90
80
70
SATO Only
0.01
0.03
0.1
0.3
0.9
2.7
CX3CL1 concentration ug/ml SATO media (mean +/- SEM, n=3)

**Figure 5.6 Verification of CX3CR1 expression in Olig2$^{+}$/MBP$^{-}$ OPCs by immunofluorescence. a)-g)** CX3CR1 is expressed in Olig2$^{+}$/MBP$^{-}$ OPCs cultured overnight either normally or stimulated with increasing concentrations of recombinant CX3CL1. In addition, abundance of Olig2$^{+}$/MBP$^{+}$ oligodendrocytes is increased at higher CX3CL1 concentrations.

**h)** Quantification of CX3CR1 expression in Olig2$^{+}$/MBP$^{-}$ OPCs.

## 5.3 CX3CL1 modulates OPC biology *in vitro*

### 5.3.1 CX3CL1 expression increases over the course of CNS regeneration

With the expression of CX3CR1 in OPCs initially identified by gene expression array analysis confirmed by my *in vitro* immunofluorescence experiments I then leveraged the data from the Huang, Jarjour et al., 2011 dataset to investigate the expression pattern of CX3CL1, the ligand for CX3CR1, in CNS demyelination.

In their 2011 paper, Huang, Jarjour *et al*., induced demyelination in the caudal cerebral peduncle of rats by injection of the detergent lysophosphatidylcholine and extracted RNA from the regenerating whole lesion site at 5, 14 and 28 days after demyelination. The expression levels of CX3CL1 rose steadily over this time course, (see **Figure 5.7)**) with a 1.3-fold increase between day 5 and day 14 and a further 1.38-fold increase between day 14 and day 28.

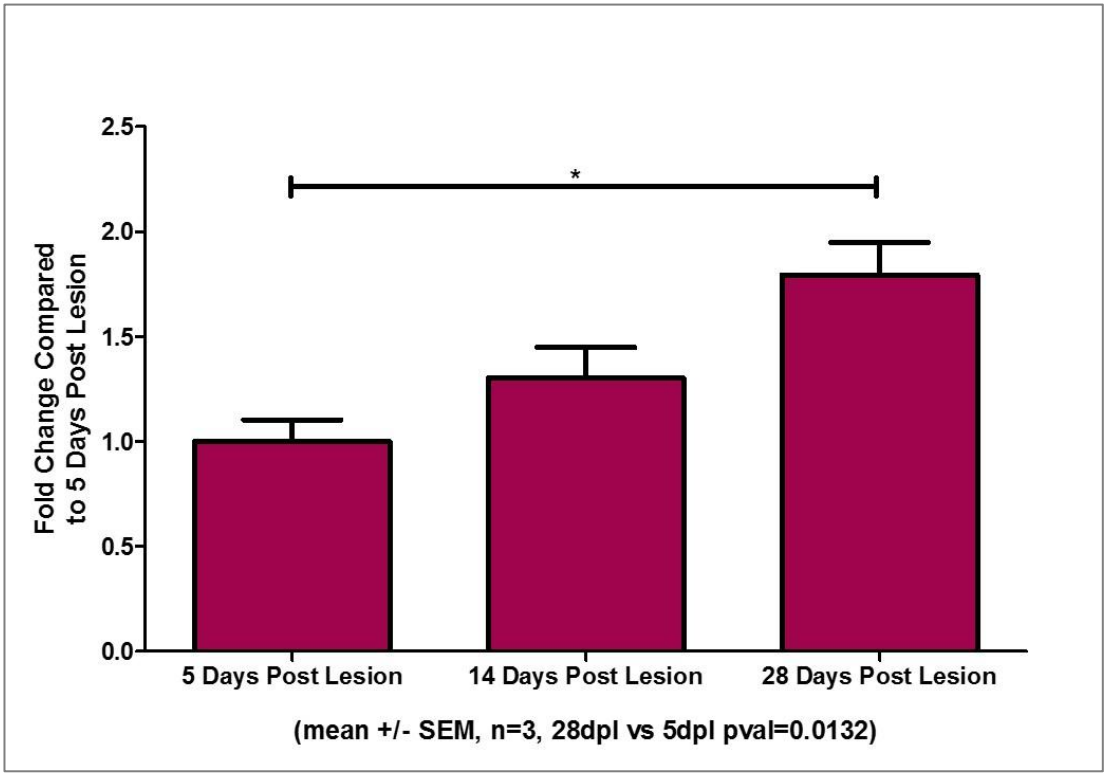


**Figure 5.7 Expression of CX3CL1 in gene expression array data from whole regenerating lesion sites.** In lysophosphatidylcholine induced demyelinated lesions (data reanalysed from Huang et al., 2011), CX3CL1 expression increases steadily from 5 to 28 days post lesion (mean of 3 replicates for each condition +/- SEM). There is a significant increase in expression between 5 days post lesion and 28 days post lesion.

While this result suggests that CX3CL1 might be an important pro-regenerative factor, there is no data prior to 5 days post lesion, by which point OPC migration is well underway. Therefore, we cannot yet speculate whether CX3CL1 is involved in early regenerative processes such as the activation or directional migration of OPCs.

### 5.3.2 OPCs migrate in response to stimulation by a low concentration gradient of CX3CL1

Having established that CX3CR1 is expressed by OPCs as well as microglia *in vitro* and that CX3CL1 increases in expression at the RNA level over the course of remyelination in both spinal cord injury and lysophosphatidylcholine induced demyelination, I then set out to discover if CX3CL1 has migratory effects on OPCs. To achieve this aim (with the assistance of Misuzu Hashimoto), I utilised the X-celligence migration plate system, previously described in **chapter 4**.

OPCs, seeded in the upper X-celligence chamber, were exposed to a gradient of recombinant CX3CL1 from a concentration of 0.1µg/ml Sato media in the lower X-celligence chamber. As shown in **figure 5.8**, after a period of 16.5 hours a significant increase in Cell Index was detected. As discussed earlier, although the X-celligence CIM system is designed to detect migration, an increase in impedance (cell index) may also be secondary to an increase in either cell proliferation or maturation into a bulkier adult cell type.

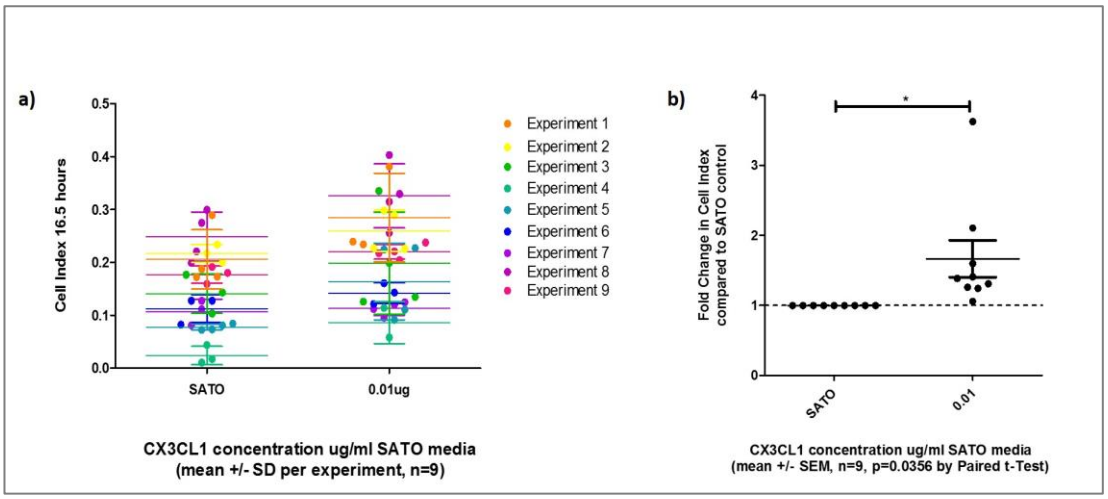


**Figure 5.8 Administration of a low concentration of CX3CL1 (0.01µg/ml) to OPCs increases Cell Index on X-celligence migration plates.** OPCs were seeded in the upper chamber of X-celligence CIM plates and a gradient between the upper and lower chambers was established by the addition of 0.01µg recombinant CX3CL1 per ml Sato media. After 16.5 hours there was a significant increase in Cell Index in CX3CL1 stimulated OPCs compared to unstimulated OPCs. **a)** The experiment was run 9 times, each dot representing the mean Cell Index for each well, with an increase in every replicate, although there was considerable variation between replicates. **b)** To ameliorate the variation between replicates, increases were computed as a fold change between OPCs exposed to 0.01µg CX3CL1 per ml Sato media and OPCs in Sato media only controls for each experiment, there was a significant increase between the two conditions by paired t-Test

To eliminate OPC proliferation as the cause of the increased Cell Index in my X-celligence results, I repeated the experiment, this time treating the OPCs with proliferation inhibitor mitomycin-C for two hours prior to the initiation of the X-celligence experiment. As illustrated in **figure 5.8**, the observed increase in Cell Index remains robust when proliferation is inhibited.

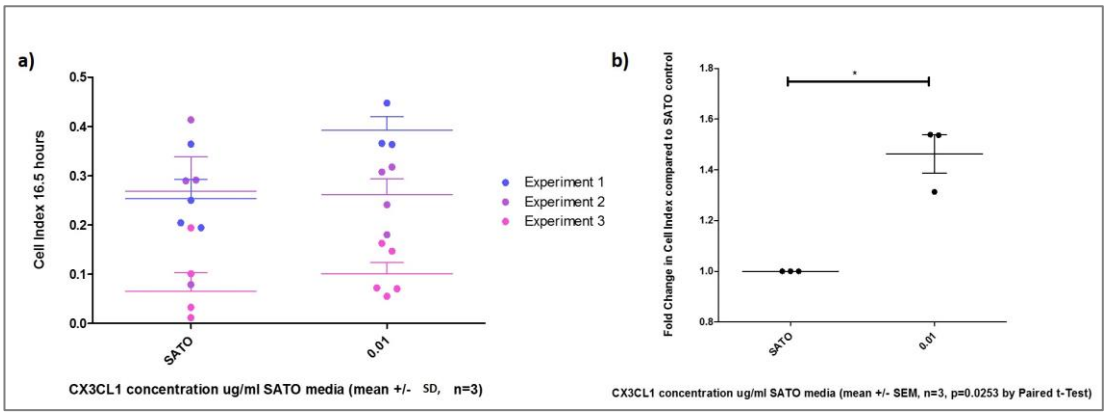


**Figure 5.9 Increased Cell Index on X-celligence migration plates in response to administration of 0.01ng/ml CX3CL1 to OPCs is robust in the absence of proliferation.** OPCs were treated with the proliferation inhibitor mitomycin-C and seeded in the upper chamber of X-celligence CIM plates. A gradient between the upper and lower chambers was established by the addition of 0.01µg recombinant CX3CL1 per ml SATO media. After 16 hours, there was a significant increase in Cell Index in CX3CL1 stimulated OPCs compared to unstimulated OPCs. **a)** The experiment was run 3 times, with an increase in every replicate, although there was considerable variation between replicates. **b)** To ameliorate the variation between replicates, increases were computed as a fold change between proliferation inhibited OPCs exposed to 0.01µg CX3CL1 per ml Sato media and proliferation inhibited OPCs in Sato media only controls for each experiment, there was a significant increase between the two conditions by paired t-Test

To eliminate maturation of OPCs as being responsible for the increased Cell Index, I imaged the underside of the membrane of the X-celligence plates (as described in **chapter 4.4.6)** from the proliferating OPC s. As shown in **figure 5.10**, in the Sato media only controls (**figure 5.10a)**), many NG2/Ki67 positive OPCs have migrated through the pores and adhered to the underside of the membrane. NG2/Ki67 OPCs exposed to 0.01 µg CX3CL1 per ml Sato media appear to have colonised the underside of the membrane in greater numbers, however there is no evidence of the increased NG2 positive process formation or MBP expression which would be associated with OPC differentiation.

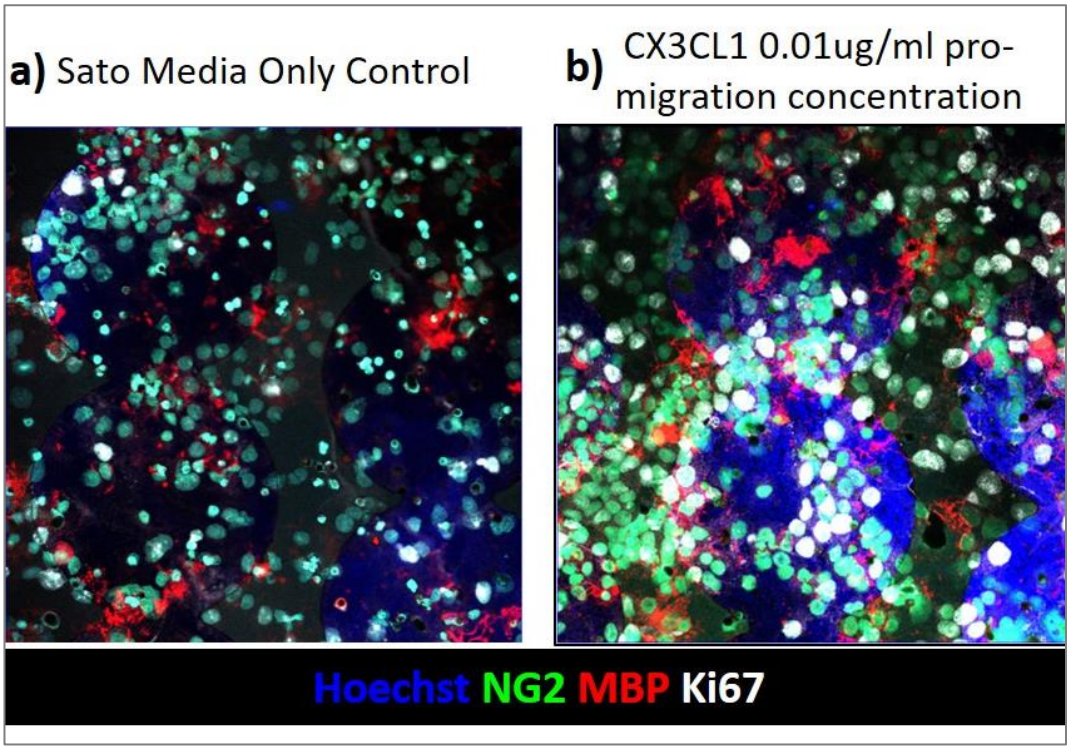


**Figure 5.10 Increased Cell Index at 0.01µg CX3CL1 per ml Sato media as compared to Sato media controls is not the result of OPCs maturation** The underside of the membranes of X-celligence RTCA CIM plates were extracted, stained and imaged by fluorescent microscopy a) OPCs in Sato media only controls have migrated through the membrane by background motility, the express NG2, Ki67 and limited MBP **b)** OPCs exposed to 0.01µg recombinant CX3CL1 per ml Sato media in the lower chambers of X-celligence RTCA CIM wells appear to have migrated through the membrane in greater numbers than in the Sato only controls, they express NG2, Ki67 and limited MBP. No increase in the formation of NG2 positive processes or MBP expression is immediately obvious as compared to Sato only controls

To confirm this result, I grew OPCs overnight in SATO media impregnated with recombinant CX3CL1 at the same concentration as in the X-celligence experiment (0.01µg/ml SATO media). As **figure 5.11**, demonstrates, no significant difference in the number of MBP positive mature oligodendrocytes could be discerned between CX3CL1 stimulated and unstimulated OPCs.

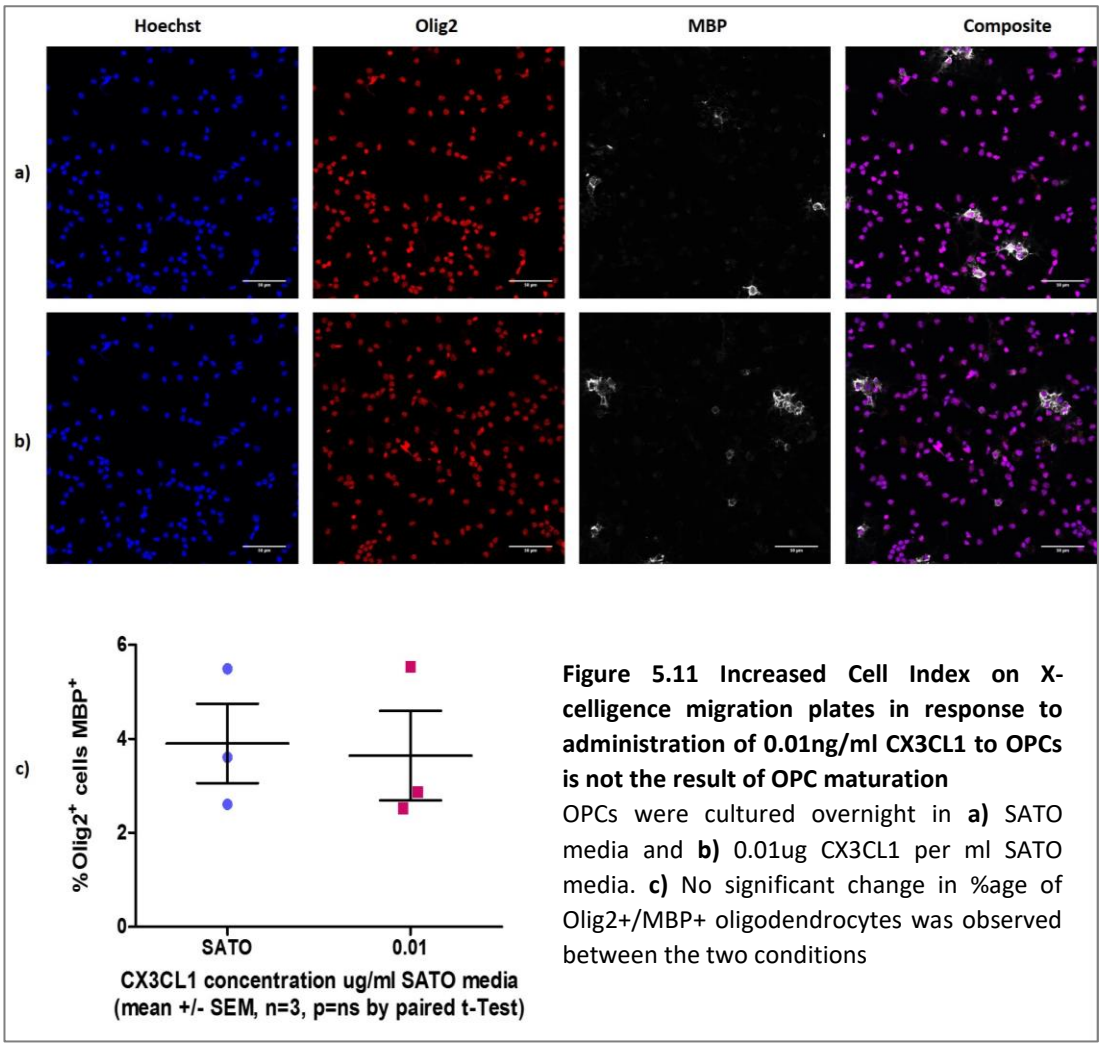


**Figure 5.11 Increased Cell Index on X-celligence migration plates in response to administration of 0.01ng/ml CX3CL1 to OPCs is not the result of OPC maturation**
OPCs were cultured overnight in **a)** SATO media and **b)** 0.01ug CX3CL1 per ml SATO media. **c)** No significant change in %age of Olig2+/MBP+ oligodendrocytes was observed between the two conditions

With the elimination of both proliferation and maturation, it can be assumed that CX3CL1 stimulates OPC migration along a low concentration gradient peaking at a concentration of 0.01µg/ml.

5.3.3 OPC maturation is accelerated in the presence of a high concentration of CX3CL1

In addition to the low CX3CL1 concentration, I also ran X-celligence experiments exposing OPCs to a gradient of CX3CL1 peaking with the much higher concentration of 2.7µg CX3CL1 per ml SATO media. As shown in **figure 5.12**, I found a small increase in Cell Index in all three replicates of the experiment, although this was not statistically significant by paired t-Test.

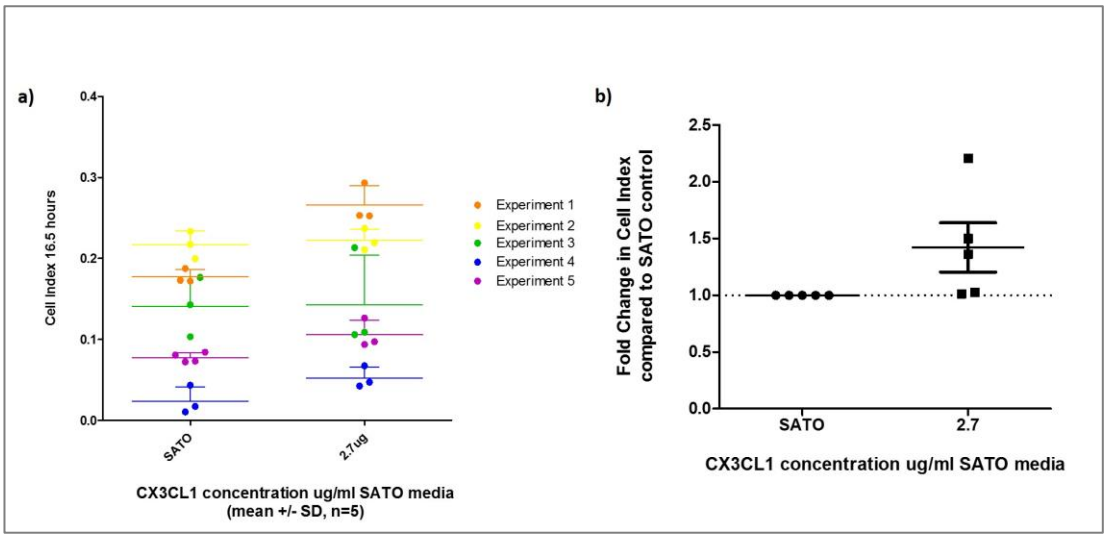


**Figure 5.12 Administration of a high concentration of CX3CL1 (2.7µg/ml) to OPCs slightly increases Cell Index on X-celligence migration plates.** OPCs were seeded in the upper chamber of X-celligence CIM plates and a gradient between the upper and lower chambers was established by the addition of 2.7µg recombinant CX3CL1 per ml SATO media. After 16 hours, there was a slight increase in Cell Index in CX3CL1 stimulated OPCs compared to unstimulated OPCs. **a)** The experiment was run 5 times, with an increase in every replicate, although there was considerable variation between replicates. **b)** To ameliorate the variation between replicates, increases were computed as a fold change between OPCs exposed to 2.7µg CX3CL1 per ml Sato media and OPCs in Sato media only controls for each experiment, there was a significant increase between the two conditions by paired t-Test

To establish whether this small increase could be attributed to OPC proliferation, as before, I ran the X-celligence experiments again, this time treating the OPCs with the proliferation inhibitor mitomycin-C prior to seeding. As **figure 5.13** demonstrates, inhibition of proliferation results in the abolition of the increase in Cell Index and appears to reduce Cell Index.

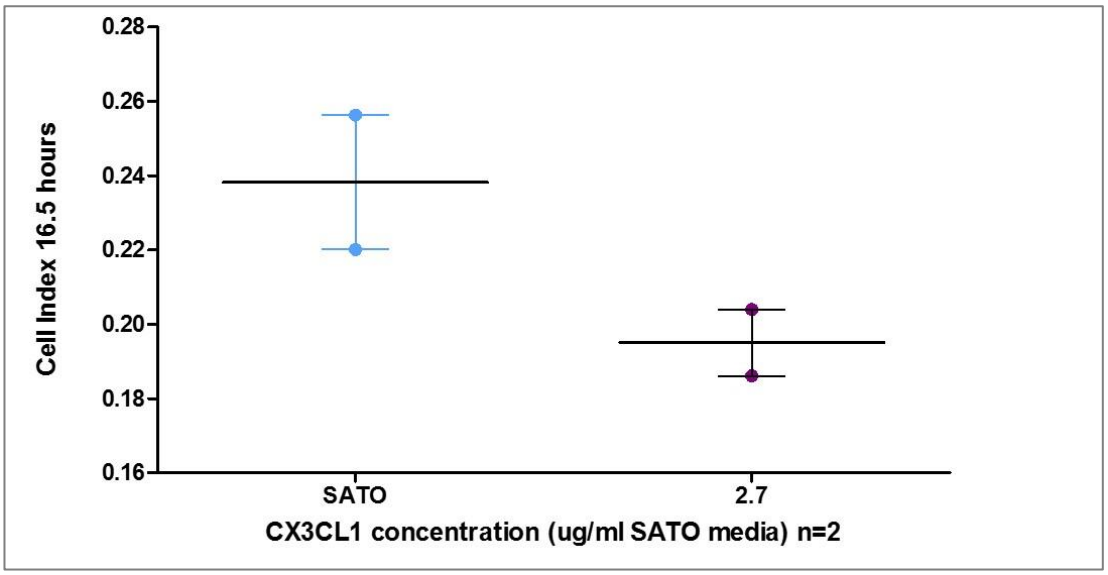


**Figure 5.13 The small increase in Cell Index on X-celligence migration plates in response to administration of 2.7ng/ml CX3CL1 to OPCs is reversed in the absence of proliferation.** OPCs were treated with the proliferation inhibitor mitomycin-C and seeded in the upper chamber of X-celligence CIM plates. A gradient between the upper and lower chambers was established by the addition of 2.7µg recombinant CX3CL1 per ml SATO media. After 16 hours, there was a decrease in Cell Index in CX3CL1 stimulated OPCs compared to unstimulated OPCs.

While this result suggested that the increase in Cell Index at 2.7µg CX3CL1 per ml Sato media might be due to proliferation, I also stained the underside of the X-celligence plates to find out if maturation of OPCs might also contribute to the increased Cell index. As shown in **figure 5.14**, after 16.5 hours, OPCs exposed to 2.7µg CX3CL1 per ml Sato in the lower chamber of the X-celligence RTCA CIM wells produce extensive MBP positive processes, covering a large proportion of the underside of the X-celligence RTCA CIM plate membrane.

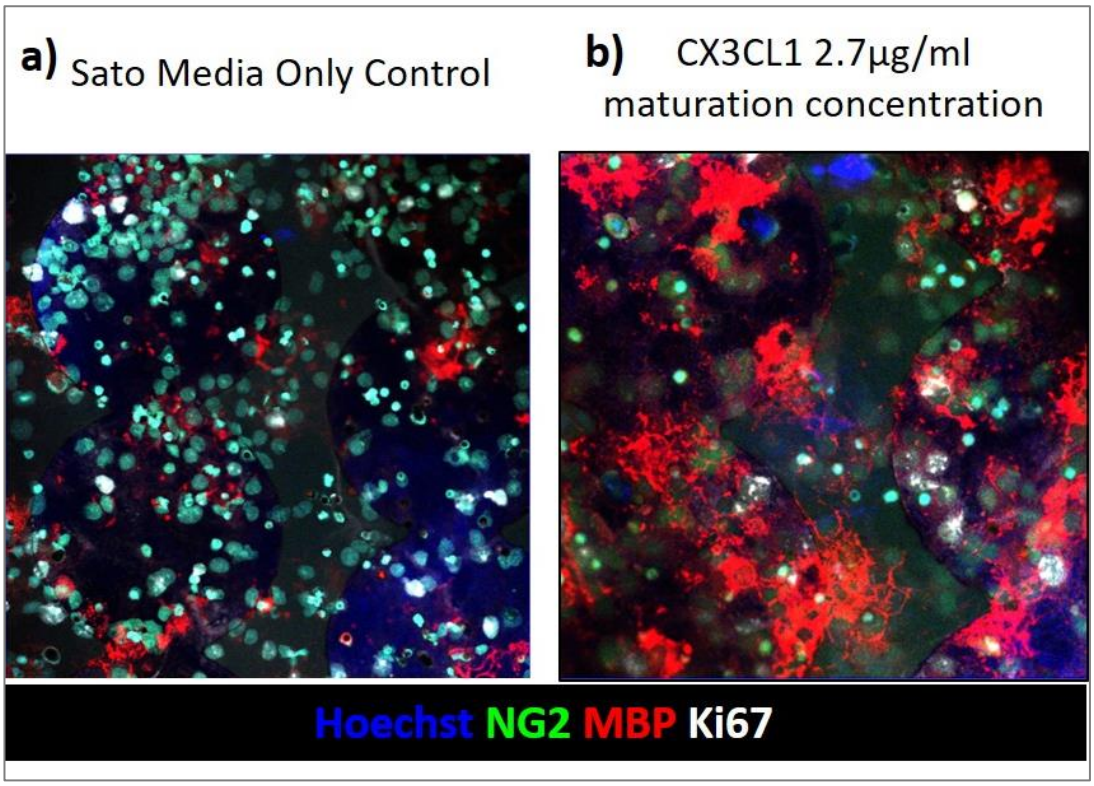


**Figure 5.14 Exposure to 2.7µg CX3CL1 per ml Sato media through the X-celligence RTCA CIM plate membrane induces OPCs to differentiate into mature oligodendrocytes a)** Post-shake-off rat OPCs were cultured in X-celligence RTCA CIM wells containing Sato media only in both their upper and lower chambers for a period of 16.5 hours. Membranes were excised, stained and imaged revealing that many OPCs have migrated through the membrane, OPCs express the OPC marker NG2 and proliferative marker Ki67 with limited expression of the mature oligodendrocyte marker MBP **b)** Post-shake-off rat OPCs were cultured in X-celligence RTCA CIM wells containing 2.7µg recombinant CX3CL1 per ml Sato media in their lower chambers for a period of 16.5 hours. Membranes were excised, stained and imaged revealing that the majority of OPCs on the underside of the membrane have differentiated into oligodendrocytes with large MBP positive processes and limited expression of NG2 and Ki67.

To find out if this increased maturation effect held true in the absence of a gradient, I used standard OPC cultures. OPCs were cultured overnight in 2.7µg recombinant CX3CL1 per ml SATO media. As **figure 5.15** reveals**,** exposure to this higher concentration resulted in a significant increase in the percentage of Olig2 positive cells expressing MBP, a marker of mature oligodendrocytes.

As exemplified in **figure 5.15b)**, it can also be observed that in high CX3CL1 concentration cultures, the maturing oligodendroglia produce lots of complex MBP positive processes within only 18 hours, a process which normally takes as much as 2-3 days in unstimulated cultures.

Together, these results suggest low concentrations of 0.01µg/ml CX3CL1 induces increased migration, while at 2.7µg/ml CX3CL1 there is increased OPC maturation into mature oligodendrocytes.

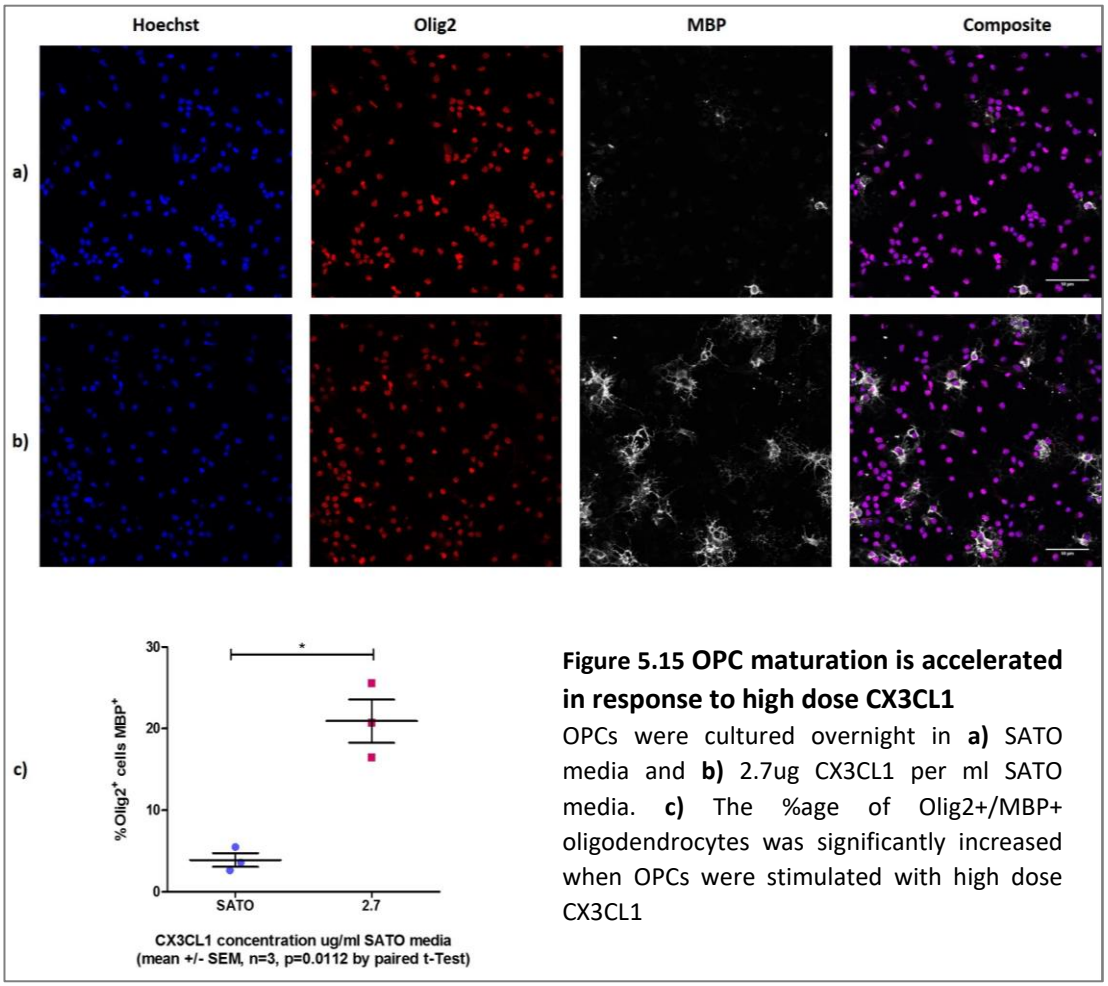


**Figure 5.15 OPC maturation is accelerated in response to high dose CX3CL1**
OPCs were cultured overnight in **a)** SATO media and **b)** 2.7ug CX3CL1 per ml SATO media. **c)** The %age of Olig2+/MBP+ oligodendrocytes was significantly increased when OPCs were stimulated with high dose CX3CL1

## 5.4 Discussion

### 5.4.1 Results summary

As iterated above, the bioinformatic screen identified CX3CR1 as a cell surface receptor expressed significantly more by activated OPCs in demyelinated tissue than non-activated OPCs in healthy tissue. This result was matched with the discovery of CX3CL1 as a secreted factor with rising expressing over the course of focal demyelinating injury. In this chapter, I verified the expression of CX3CR1 on the surface of OPCs. I then used a combination of the protocols I developed for the X-celligence CIM plate system to show that a gradient of CX3CL1 peaking at a low concentration induces directional OPC migration and that exposure to high dose CX3CL1 accelerates OPC maturation.

While these data are *in vitro* only, these results show for the first time, both that CX3CR1 is expressed by OPCs and that CX3CL1 modulates OPC biology. Based on my results and information in the literature, it is possible to envisage a model in which CX3CL1 is the master regulator of remyelination, which I discuss further below.

### 5.4.2 Model for the mode of action of CX3CL1 in regeneration after demyelinating injury

CX3CR1 has long been known to be expressed by microglia(Bellavance et al., 2015; Boehme et al., 2000; Cardona et al., 2006; Harrison et al., 1998), and CX3CR1 knock-out has been shown to impact remyelination trough inefficient clearance of myelin debris by microglia (Lampron et al., 2015), which is a necessary part of early stage infiltration of microglia into demyelinating injuries (Miron and Franklin, 2014).

While no difference has been found in the expression of the CX3CL1 gene between uninjured and globally demyelinated brains (Lampron et al., 2015), there is evidence that cleavage of the fractalkine chemokine domain is increased during (Chapman et al., 2000). In contrast, in the Huang, Jarjour et al., 2011 data set from focal demyelinating injury, I found steady rising expression of CX3CL1 over the entire injury time course (see **figure 5.6**).

The crosstalk between neurons and microglia via the CX3CR1/CX3CL1 axis reported in the published data, combined with my OPC results, leads me to hypothesize a model where differing concentrations of CX3CL1 emanating from a demyelinating lesion, control the regenerative response of OPCs (and microglia) to this lesion.

CX3CL1 secreted by neurons, diffuses outward from the site of demyelination, leading to ever-decreasing concentrations contacting distal OPCs distant to the lesion. The neuron-derived CX3CL1 chemokine domain may bind to distal CX3CR1 expressed by OPCs, perhaps releasing OPCs hitherto adhered to neighbouring cells via CX3CR1/CX3CL1 cell-to-cell interactions. OPCs then may migrate up the gradient of CX3CL1 towards the lesion site.

On arrival at the lesion site, the CX3CL1 concentration is higher, stimulating OPC differentiation. It may be that all the CX3CR1 receptors on the OPCs become saturated with CX3CL1, rendering OPCs unable to sense the chemokinetic gradient. This halts OPC migration, allowing differentiation into myelinating oligodendrocytes. These mature oligodendrocytes then are able to remyelinate the injured axons, regenerating the lesion site.

This model suggests that increased expression of CX3CL1 dissipating from the lesion site might improve the entire process of regeneration, from microglial debris clearance to OPC recruitment and remyelination.

#### 5.4.3 Additional experiments to test this model

The response of microglia to CX3CL1 after demyelinating injury (Lampron et al., 2015) and my *in vitro* OPC results suggest that CX3CL1 expression by neurons/axons might be expected to increase following injury. My bioinformatic result showing increased expression of CX3CL1 throughout focal demyelinating injury (see **figure 5.6**) supports this view. However, Lampron et al., 2015 found no increase in CX3CL1 mRNA expression between globally demyelinated and healthy brain tissue. The extraordinary structure of CX3CL1, with its membrane bound and freely released forms could explain this result. It is possible that while mRNA expression of CX3CL1 does not increase initially, release of CX3CL1 by neurons occurs at the protein level by cleavage of the mucin stalk freeing the chemokine domain.

To test whether release of the CX3CL1 chemokine domain is increased at sites of focal demyelination, tissue from our focally demyelinated model (demyelination of the mouse corpus callosum by injection of lysophosphatidylcholine), could be stained for immunoreactivity with antibodies for the CX3CL1 chemokine domain. Tissue sections

could be generated for a wide range of time-points throughout the process of focal demyelination and remyelination and could be co-stained with markers of myelin to visualise the location of CX3CL1 within the geography of the lesion site and surrounding white matter.

Sections of tissue from both the lesion epicentre and corresponding tissue from uninjured controls, could also be excised, the RNA extracted and then run as a qPCR to determine whether the lack of increased CX3CL1 mRNA observed in a model of global demyelination (cuprizone-induced) also holds true for focal demyelination (LPC-induced).

Staining of focally demyelinated mouse tissue could also be used to confirm the expression of CX3CR1 on the surface of OPCs, by co-staining with OPC markers such as PDGFRα, NG2 or Olig2.

To find out whether remyelination in focally demyelinated lesions is impaired in the absence of CX3CR1, focal demyelinating lesions could be induced in the corpus callosum of both WT and CX3CR1 knock-out mice. Tissue sections could be taken at a range of time-points throughout regeneration and immunostaining for OPCs and adult oligodendrocyte markers used to confirm that both OPC infiltration into the lesion site and remyelination are impaired in CX3CR1 knock-out mice.

To discover whether the predicted impairment of OPC-led regeneration in CX3CR1 knock-out mice can be rescued by the presence of CX3CR1 positive OPCs, CX3CR1 positive OPCs from WT mice could then be injected adjacent to the lesion site in the CX3CR1 knock-out mice. Tissue sections could again be taken at a range of time-points throughout regeneration and immunostaining for OPC and oligodendrocyte markers used to determine if OPC infiltration and remyelination is restored.

A caveat with the previous experiment is that addition of OPCs will not improve inefficient clearance of myelin debris by microglia which could still impact remyelination. To find out if stimulation of both microglia and OPCs by CX3CL1 is necessary for improved remyelination, a further *in vivo* experiment could be carried out. In WT mice, lesion induction could be followed by the addition of recombinant CX3CL1 chemokine domain into the lesion epicentre at a time-point prior to the expected induction of OPC migration. Immunofluorescence of microglia and myelin debris markers should be used in tissue sections from within hours of lesion induction to find

out whether phagocytosis of myelin debris is improved. Sections could also be taken 3-5 days after lesion induction and stained for OPC markers to determine if the abundance of OPCs within the lesion site has increased. Finally, tissue sections taken prior to and during the expected time-course of remyelination could be stained for mature oligodendrocyte markers, to determine whether the abundance of mature oligodendrocytes and myelin is either increased at earlier time points or increased overall.

In addition to the data shown here, I have also carried out preliminary experiments which suggest that at a medium concentration of 0.1μg CX3CL1 per ml SATO media may induce OPC proliferation. Repetition of X-celligence experiments testing this CX3CL1 concentration both with and without inhibition of proliferation using mitomycin-C, with the addition of testing OPCs cultured overnight in media at this CX3CL1 concentration for markers of proliferation (e.g. Ki67, PCNA), are necessary experiments to confirm this result. Proliferation of OPCs at this medium concentration, could also fit with the hypothesis. It can be postulated that following migration, OPCs meeting this CX3CL1 concentration when they first infiltrate the lesion site, first proliferate before the accumulation of CX3CL1 resulting from increasing mRNA expression (see **figure 5.6**) induces OPC differentiation.

Testing of this proliferation hypothesis could be easily added to the above in vivo experiments, by staining tissue sections from for proliferative markers and looking for co-localisation with OPC markers.

#### 5.4.4 Conclusion

In this chapter, I used *in vitro* methods to verify the expression of CX3CR1 in cultured OPCs and used the X-celligence system and antibody immunoreactivity for markers of OPCs and adult oligodendrocytes to show that OPCs migrate up a low concentration gradient of CX3CL1 and accelerate maturation into adult oligodendrocytes when stimulated by a high concentration of CX3CL1.

Taken in the context of existing literature and the model I have proposed, and with the addition of the *in vivo* experiments outlined above, this research represent a significant contribution to our knowledge of OPC led regeneration in the CNS.

In the following discussion chapter, I will discuss the impact of these results in the wider context of MS research.

Chapter 6

# Discussion

There are thought to be 2.5 million MS patients worldwide (Pugliatti et al., 2002), with some populations affected more than others. A single cause for the onset of MS pathology has never been identified, MS may therefore be considered as a multifactorial disorder, the result of a combination environmental and genetic factors.

**Geography**

The incidence and prevalence of MS are not equal across all global populations. Rather, there is a strong association to geography in which generally, in which MS cases increase in frequency with increasing distance from the equator (Compston and Coles, 2008; Kurtzke, 1975, 1993). However, while this geographical rule can be used to generalise the world population, there are exceptions which appear to be linked to the geographical origins of the populations involved.

In general, MS is more pervasive in populations of northern European origin, however, there is evidence that the geographical region in which individuals reside during early life also contributes to their MS risk (Compston and Coles, 2008; Goodin, 2016b). Studies of immigration to regions of varying MS prevalence including the UK (Elian et al., 1990), South Africa (Dean and Kurtzke, 1971), Hawaii (Detels et al., 1977), Israel (Alter et al., 1962), and Australia (Hammond et al., 2000) have found the geographical region of an individual's formative years (up to the age of around 15 (Hammond et al., 2000)), to be a stronger predictor of MS risk than the geographical region to which an individual migrates as an adult.

**Viral Infection**

It has been postulated that the initiation of the biological dysregulation which leads to MS pathology may be the result of viral infiltration. There is evidence that this correlation may be exacerbated by a lack of microbial and/or viral infection during early life. The 'hygiene hypothesis' proposes that individuals raised in a fastidiously clean environment, thus less exposed to minor infections in early life, are more likely to contract autoimmune disorders including MS (Compston and Coles, 2008). A range of infections regularly contracted in early childhood including the Epstein-Barr virus and measles, mumps and rubella have been reported to be first contracted later in MS patients than in HLA-DR2 matched controls (Martyn et al., 1993).

A molecular basis for the association between MS and these early life infections has been found in the case of the Epstein-Barr virus. A 2003 study demonstrated that the T-cell

receptor (TCR) of an MS patient, recognized both myelin basic protein (MBP) and an Epstein-Barr virus peptide (Lang et al., 2002). On Epstein-Barr infection, T-cells reacting to the presence of viral particles may potentially attack MBP within the myelin sheath, resulting in demyelination.

Further evidence of the role of Epstein-Barr infection in the triggering of MS has also been found in a 2007 study of post mortem tissue samples from secondary progressive MS patients (Serafini et al., 2007). In 95% of cases studied, a high proportion of brain infiltrating B cells were found to be enriched with Epstein-Barr Virus encoded small nuclear mRNAs. In addition, metanalyses found that patients with a history of infectious mononucleosis, a common complication of Epstein-Barr virus infection, had an increased risk of developing MS (Handel et al., 2010; Sundqvist et al., 2012).

Nearly 100% of MS patients have been found to test positive for Epstein-Barr virus infection (Burnard et al., 2017), with one study reporting 100% seroconversion prior to MS diagnosis (Levin et al., 2010). However, no study has as yet established whether Epstein-Barr infection directly causes MS, or if Epstein-Barr susceptibility is simply a side effect of the alterations in the immune system which ultimately lead to MS (Burnard et al., 2017).

A major caveat of the association of Epstein-Barr infection with MS, is that as many as 90% of the human population are infected with the virus (Gao et al., 2006), but only a very small proportion develop MS. It has been suggested that the random integration of viral genetic material into the host cell genome (Santpere et al., 2014; Takakuwa et al., 2004), could result in the disruption of protein coding genes, or epigenetic alterations to MS associated loci which are yet to be identified, although this hypothesis has not yet been tested (Burnard et al., 2017).

Other pathogenic infections implicated in triggering MS pathology include typhoid, smallpox, herpes virus(HHP)-6, chickenpox and *chlamydia.* Although no single infecting agent solely responsible for MS has been identified thus far (Compston and Coles, 2008). Regardless of the pathogen implicated, not all infected individuals go on to develop MS, suggesting any pathogenic trigger must be coupled with additional enivironmental and/or genetic factors.

**Genetic**

As previously mentioned, the genetic relatives of MS patients, have a greater risk of developing the disorder than the general population. With brothers or sisters of MS probands with a 20-30 fold increase in risk and more than a 200 fold increase for monozygotic twins (Goodin, 2016b). In addition, the association of MS with populations of northern European origin (as iterated above), suggests that genetic factors may also be involved.

In recent years, advances in high throughput sequencing and bioinformatics have facilitated the identification of MS associated loci through genome-wide association studies. In this way a strong link between the MS susceptibility and polymorphisms in the Major Histocompatibility Complex gene set in addition to 103 other MS associated loci, however, identified genetic risk factors contribute only around 30% of total MS risk (Burnard et al., 2017; Hollenbach and Oksenberg, 2015).

**Environmental**

While genetic risk factors are likely to contribute to the increased risk of development in MS for related individuals, effects relating to the external environment to which individuals are exposed have also been postulated as a possible cause of MS, this is thought to contribute to the geographical pattern mentioned earlier (Goodin, 2016b). One proposed explanation is the, 'month of birth' effect, which postulates that individuals gestated during the winter months, have a greater likelihood of developing MS. A phenomenon reported in Denmark (Templer et al., 1992), Norway (Torkildsen et al., 2014), Northern Europe, Canada (Sadovnick et al., 2007; Willer et al., 2005) and Australia (Staples et al., 2010). A proposed reason for this, is reduced maternal exposure to light, resulting in decreased vitamin D availability *in utero* (Chaudhuri, 2005; Goodin, 2016b; Willer et al., 2005).

Further evidence for the vitamin D hypothesis is the correlation between increased dietary vitamin D and low MS incidence in isolated populations within geographical regions of otherwise high MS incidence. Dietary sources of vitamin D in high enough quantities to make an impact are restricted to a limited number of animal species including reindeer and oily fishes (Gillie, 2006). One of these low risk populations is the Inuit of North America and Faroe islanders of northern Europe (Sinclair, 1977), whose diets include large quantities of vitamin D rich oily fish, and the other is the Sami or Lapps of northern Scandinavia whose diet is largely dependent on vitamin D rich reindeer (Gillie, 2006; Grønlie et al., 2000; Koch-Henriksen, 1995).

An extensive study of sun exposure in Tasmanian MS patients found a strong correlation between MS susceptibility and sun exposure between the ages 6 and 15 (no data was generated from birth to 5 years old) (van der Mei et al., 2003). In addition, other longitudinal studies have found vitamin D intake (whether from exposure to sunlight, dietary supplements or a combination of the two) to be inversely correlated with MS diagnosis (Munger et al., 2004, 2006).

In summary, while a number of factors have been discussed as the cause of MS, no single factor has yet emerged as the sole origin. With evidence pertaining to so many possibilities, a complex epidemiology comprised of multiple contributing factors appears more likely. In the absence of an identified pathological root, the development of treatment based on the molecular pathology of the already advancing disease course is of even greater importance.

At present no regenerative therapies have been developed for the demyelinating disorder Multiple Sclerosis (MS). While anti-inflammatory treatments are available for the relapsing and remitting form of the disease, these treatments are not effective in preventing disease progression toward the degenerative phase of the disease in the long term.

The Williams lab have previously demonstrated the absence of OPCs in some MS lesions, particularly chronic active lesions in which the OPC chemorepellent Sema3A is highly expressed (Boyd et al., 2013a). Using our mouse model of focal demyelination in the corpus callosum (CC), it was also discovered that recruitment of OPCs to demyelinating lesions can be improved by the administration of OPC chemoattractant Sema3F or reduced by the addition of OPC chemorepellent Sema3A. These results illustrated a clear role for modulators of OPC migration in the regeneration of demyelinated lesions.

The purpose of this thesis was to improve understanding of the role of OPC migration in regeneration by identifying novel modulators of OPC biology in demyelinating injury. By bioinformatic analysis of previously published gene expression array data from models of demyelination, I successfully identified factors secreted at the injury site, and cell surface receptors expressed by OPCs following demyelination. I also optimised the X-celligence RTCA CIM system as an assay for the simultaneous study of the migration, proliferation and differentiation of OPCs *in vitro*. I then brought these two aspects of the project together, to study the effects of factors secreted after demyelinating injury on the biology of OPCs *in vitro*. In this way, I identified and verified the OPC proliferation factor

LCN2, the OPC migration factor CXCL12 and finally CX3CL1(fractalkine) which functions as chemoattractant for OPCs at a low concentration and differentiation factor for OPCs at high concentrations.

## 6.1 CX3CL1 – A Single Molecule Modulates Both the Inflammatory Microglial Response and the Reparative OPC Response After Demyelination

While a number of modulators of OPC migration and differentiation have been previously described, in this thesis, a single factor with effects on both migration and differentiation is documented. As iterated in chapter 5, in vivo studies of these effects are required to fully validate these results, however a model of the activity of OPCs in response to CX3CL1 can be hypothesised based on the in vitro results alone.

In their 2015 study, Lampron and colleagues used the cuprizone demyelination model to clearly show that the loss of the CX3CR1/CX3CL1 interaction impaired the clearance of myelin debris by microglia (Lampron et al., 2015). Taken with my results, these findings paint a picture of a single molecule with the ability to orchestrate the migration of both OPCs and microglia.

As shown in **figure 6.1**, the model of action I propose for CX3CL1 in focal demyelinating injury incorporates both the clearance of debris by microglia and the repair of damaged myelin by differentiating OPCs. In the uninjured CNS, the myelin sheath is maintained by existing oligodendrocytes which facilitate saltatory conduction and provide trophic support to the axons, while OPCs and microglia appear quiescent (see **figure 6.1a)**). As shown in **figure 6.1b)**, following a demyelinating insult, myelin debris is present at the lesion site, and the denuded axon, and perhaps activated astrocytes, upregulate the release of CX3CL1, both by increased gene expression and by cleavage of the CX3CL1 chemokine domain. CX3CL1, released from the lesion site, diffuses through the CNS and stimulates both OPCs and microglia by binding to CX3CR1 (see **figure 6.1c)**). Both OPCs and microglia sense the gradient of CX3CL1 and migrate up the gradient towards the lesion site. On arrival, the solid, high concentration of CX3CL1 induces both cell types to cease migration, OPCs then begin to differentiate while the microglia clear myelin debris by phagocytosis (see **figure 6.1d)**). In this way, the OPCs differentiate into mature oligodendrocytes, which can access the denuded axon in the absence of any myelin debris and reform the myelin sheath, thus protecting the axon from degeneration (see **figure 6.1e)**).

**Figure 6.1f)** illustrates the mechanism of gradient sensing (reviewed in Jin, 2013); an OPC exposed to a gradient of CX3CL1 at a low concentration senses the occupancy of CX3CR1 at only one end of the cell, and migrates in that direction. In the presence of a solid high concentration of CX3CL1, the CX3CR1 receptors over the whole cell surface

are occupied, and in the absence of any directional cue, the OPC stops migrating and differentiates.

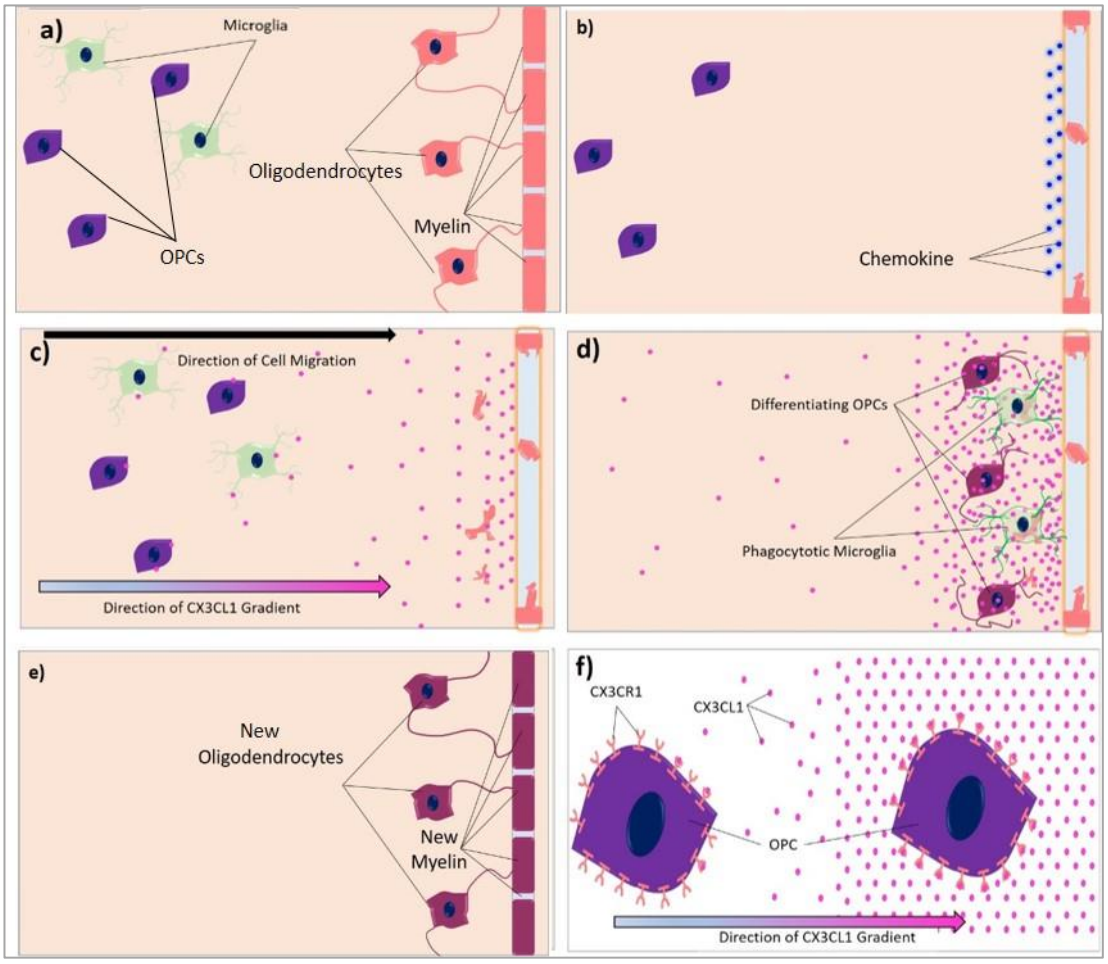


**Figure 6.1 Proposed Mechanism of Action of CX3CL1 in CNS Regeneration a)** In the healthy CNS an axon is wrapped by the myelin sheath formed by an oligodendrocyte. OPCs and microglia are quiescent. **b)** In demyelinating injury, the oligodendrocyte and myelin are destroyed, leaving myelin debris. In response, the axon upregulates the release of CX3CL1. **c)** Continual release of CX3CL1 from the axon establishes a CX3CL1 gradient emanating from the injury site. CX3CL1 binds CX3CR1 on the leading edge of OPCs and microglia, inducing chemotaxis towards the injury site. **d)** On arrival at the site of demyelination, the high CX3CL1 concentration induces the cessation of cell migration, microglia phagocytose myelin debris and OPCs begin to differentiate into adult OPCs. **e)** Differentiation of OPCs into new oligodendrocytes, which reform the myelin sheath, is completed. **f)** In a low concentration gradient of CX3CL1, only CX3CR1 at the front of the OPCs become occupied by CX3CL1, the OPC senses the gradient and begins to migrate. At a high solid concentration of CX3CL1, all CX3CR1 on the surface of OPCs becomes occupied by CX3CL1. Complete receptor occupation induces OPC to stop migrating before differentiating into an oligodendrocyte.

OPCs are widely known as a motile cell type, however the question of how a quiescent OPC is induced to become migratory persists. The 3-fold increase in CX3CR1 expression in Activated as opposed to Non-activated OPCs that I reported in **chapter 5** (as a result of my bioinformatic screen in **chapter 3**), suggests that response to CX3CR1 stimulation is a feature of Activated rather than Non-activated or quiescent OPCs. It is therefore likely that CX3CR1 expression on OPCs is increased in response to a damage or distress signal, released at the earliest stages of demyelination.

## Impact of the Expression of Both CX3CR1 and CX3CL1 on OPCs

The results in this thesis, show that, at least *in vitro*, OPCs migrate in response to the presence of a chemotactic gradient of CX3CL1. In addition, as shown in **figure 6.2 a)** below, in my analysed results from the Moyon et al., 2015 data set, CX3CL1 is significantly more highly expressed in Activated OPCs, than in Non-Activated OPCs (fold change = 1.24, p-val = 0.0459 by unpaired t-Test). Expression of CX3CL1 in OPCs from non-injured tissue is also fairly high, as shown in **figure 6.2b)**.

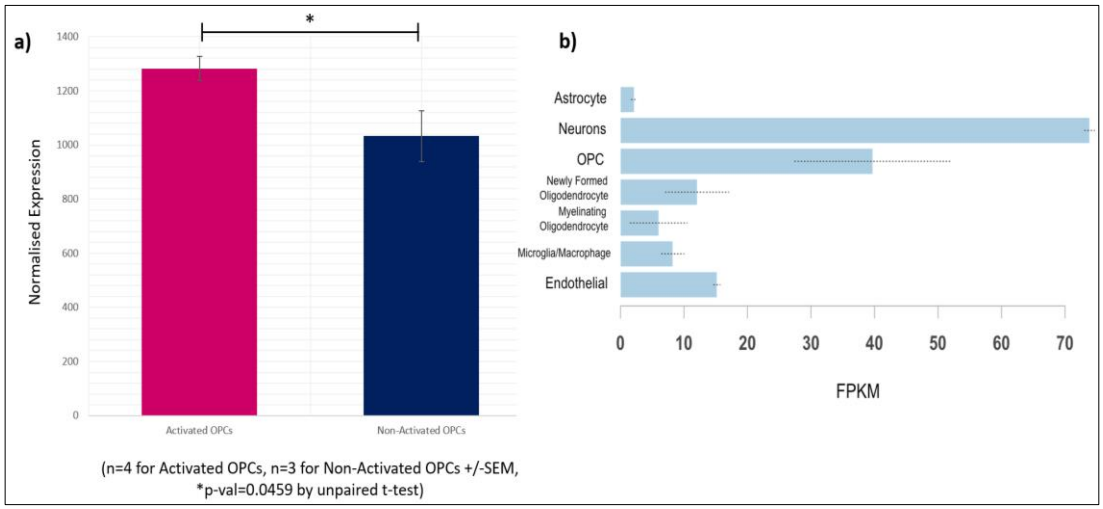


**Figure 6.2 CX3CL1 is expressed by OPCs a)** Results of gene expression array analysis of the data from Moyon et al., 2015. Normalised expression is 1.24 times higher in Activated OPCs from cuprizone injured brain tissue than in Non-Activated OPCs from uninjured brain tissue (mean of 4 replicates for Activated OPCs and 3 replicates for Non-Activated OPCs +/- SEM, p=0.0459 by differential expression analysis using Limma). **b)** Data from RNA-seq for isolated CNS cell types from uninjured tissue, noting that the OPC isolate has 5% microglial contamination (Zhang et al., 2014). Expression for each cell type calculated as Fragments Per Kilobase of exon per Million fragments mapped (FPKM). In mice, CX3CL1 is expressed by all cell types but is most highly expressed in neurons and OPCs.

There is evidence in the published literature, that migrating cells have the ability to direct their own migration, by altering the concentration of chemokinetic particles in their immediate environment (Tweedy et al., 2016). In addition to the generation of the bioinformatics data, in their 2015 study, Moyon et al., found that the chemokine CCL2 stimulated chemotaxis of OPCs, and that this acceleration was increased when CCL2 was over expressed by the OPCs themselves (Moyon et al., 2015). With the preliminary evidence that CX3CL1 is expressed by OPCs, it is possible that these cells may be using the secretion of the chemokine to regulate their own migration. If self-secretion of CX3CL1 by OPCs follows a similar pattern to that observed for CCL2, it is possible that migrating OPCs might secrete CX3CL1 in order to accelerate their migration. However, the results in this thesis show that high abundance of CX3CL1 induces the accelerated differentiation of OPCs into oligodendrocytes. It could therefore be extrapolated that expression of CX3CL1 by OPCs arriving at the demyelinated lesion site, might function as a mechanism to drive their differentiation. Thus, accelerating the repair of the lesion, though facilitating remyelination. Investigation of such a phenomenon, is certainly dependent on the confirmation of expression of CX3CL1 on actively migrating OPCs in the vicinity of a demyelinated lesion *in vivo*. Confirmation of CX3CL1 expression, could be achieved by immunostaining of tissue sections from LPC lesioned tissue, for co-expression of CX3CL1 with OPC markers such as PDGFα or NG2.

**Neonatal vs Adult OPCs**

A caveat with the experimental design in this thesis, is that the bioinformatics data analysed in **chapter 3** is from studies in adult tissue, while the OPC cells used for the *in vitro* experiments in **chapter 4** and **chapter 5**, is from neonatal OPCs. As described in **chapter 2**, in this thesis, relatively pure cultures of OPCs were produced using the shake-off method first described by McCarthy and de Vellis in 1980, and refined by Milner and ffrench-Constant in 1994. In the 1994 study, the authors found that by extended culture, the 10% oligodendrocyte 90% OPC culture at 4 hours post shake-off, had differentiated into a 95% oligodendrocyte culture by day 10. While this capacity to readily differentiate into adult OPCs, makes post shake-off OPCs well suited to the study of factors thought to improve OPC maturation, it must be considered that this cultured cell population may not accurately reflect the behaviour of OPCs *in vivo*. However, transplanted OPCs produced using the shake-off method, have been shown to effectively myelinate myelin deficient *ex-vivo* cortice tissue (Bin et al., 2012).

It is likely that there is some difference in gene expression between the *in vivo* derived OPCs in the Moyon et al., 2015 data set and the post shake-off OPCs used in the *in vitro* experiments in this thesis. However, one of the major findings from Moyon et al., 2015, was that the gene expression profile of activated OPCs (derived from globally demyelinated, injured tissue) was more similar to the gene expression profile of neonatal OPCs, than to OPCs from uninjured tissue (Moyon et al., 2015). This suggests, that although post shake-off OPCs are derived from neonatal tissue, the cells may closely resemble OPCs active in the repair of adult demyelinated tissue. Regardless of the similarity of post shake-off OPCs to OPCs actively repairing adult tissue, the *in vitro* results described herein will need to verified with *in vivo* experiments investigating the expression of CX3CR1 and response to CX3CL1, of *in situ* OPCs in injured tissue.

As mentioned in **chapter 3**, the Huang, Jarjour et al., 2011 data set could be improved by expansion into earlier time-points than 5 days post lesion, and with the addition of an uninjured control, perhaps with the use of RNA-seq to detect more nuanced gene expression changes. In an approach, similar to the one I developed in **chapter 3**, secreted factors highly expressed at the earliest post-lesion time-points, as compared to uninjured controls, could be matched with cell surface receptor genes, this time more highly expressed in Non-activated as opposed to Activated OPCs. Candidate secreted factors could then be added to Non-activated OPCs *in vitro*, and tested for alterations in gene expression (perhaps with a panel of the most differentially expressed genes between activated and Non-activated OPCs) by qPCR, microarray or RNA-seq, to find out if administration of the secreted factor triggered modification of OPCs to an activated phenotype.

It is also possible that CX3CR1 expression in Non-activated OPCs might be increased in response to stimulation by CX3CL1 in a positive regulation loop. In my experiments with post shake-off OPCs, I found no evidence of increase CX3CR1 expression in response to the addition of CX3CL1(see **figure 5.5**). However, given their background motility and ease of differentiation *in vitro*, it is likely that post shake-off OPCs represent a somewhat activated population in which the expression of CX3CR1 is already high. It has been shown that the CX3CR1/CX3CL1 interaction can be used in cell-to-cell adhesion, through CX3CL1 in its membrane bound form. CX3CR1/CX3CL1 mediated adhesions are preferentially released on the addition of the secreted chemokine domain of CX3CL1 (Imai et al., 1997). It is therefore possible that quiescent/Non-activated OPCs in the CNS parenchyma might use CX3CR1/CX3CL1 interactions to adhere to neighbouring cells,

preferentially breaking these adhesions in response to the secreted chemokine domain of CX3CL1, thus priming OPCs for migration. This would make CX3CL1 an inducer of not only OPC migration and differentiation, but also activation. Such an effect could be tested *in vitro*, by the addition of CX3CL1 to Non-activated OPCs and analysis to look for substantial changes of gene expression by qPCR, microarray or RNA-seq.

In addition to the question of how OPCs are induced to migrate, until now it has also been unclear what signals, internal or external, might induce OPCs to stop migrating when they get to sites of injury. My i*n vitro* results show that OPC differentiation is accelerated in response to a high solid concentration of CX3CL1 (see **chapter 5.3.3**). As illustrated in **figure 6.1f)**, eukaryotic cells sense a 'spatial gradient' of chemokine through the occupancy of receptors along their length (reviewed in Jin, 2013). In the case of OPCs, directional chemotaxis in response to a gradient of chemokine e.g. CX3CL1 is induced by occupancy of more receptors (e.g. CX3CR1) at the front of the cell than at the back. However, in a high concentration of CX3CL1, complete receptor occupancy essentially eliminates the gradient element, and the OPC ceases chemotaxis in the absence of any directional cue. This may be able to be tested using a fluorescent-tagged version of a chemokine ligand such as CX3CL1, and high resolution live imaging, to visualise receptor occupancy and then cellular movement.

It is of particular interest that the addition of a high concentration of CX3CL1 to X-celligence RTCA CIM plates resulted in accelerated differentiation of OPCs. Due to the loss of gradient sensing, it might have been predicted that addition of such a high concentration of chemoattractant would result in the arrest of migration only. In contrast, my results show OPC differentiation in the presence of high concentration CX3CL1 earlier than expected in culture at only 16.5-18 hours (see **figures 5.13b)**, **5.14b)**), more akin to the level of OPC differentiation at 50 hours in primary culture with Sato media only (see **figures 4.19a)** and **4.22b)**). This raises an interesting question as to whether the OPC interprets the high CX3CL1 concentration as a direct signal to differentiate (which reduces migration), or as a direct signal to cease migration (followed by differentiation). In the latter case, this may suggest that cessation of migration is in itself a signal to differentiate, indicating that the 'default setting' for activated OPCs without a directional cue is to differentiate. However, the fact that OPCs cultured in Sato media only (and so in the absence of a chemotactic gradient) are highly motile and do not exhibit accelerated differentiation suggests that full receptor occupancy of CX3CR1 by CX3CL1 specifically may be the direct driver of differentiation. This could be tested

further by adding other chemokines that are known to be chemorepellents for OPCs, such as Netrin-1, and determining whether high concentrations of this only prevent migration of OPCs, or whether this also promotes differentiation.

**Investigation of the CX3CR1/CX3CL1 axis using the Cre-Lox System**

As previously mentioned, as well as on OPCs, the CX3CR1 receptor is also expressed by microglia in the CNS. In their 2015 study, Lampron et al., found that in CX3CR1 knock-out mice, the clearance of myelin debris by microglia from sites of cuprizone induced demyelination, was impaired (Lampron et al., 2015). However, this study also noted that CX3CR1 knock-out impaired the recruitment of OPCs to sites of demyelination, and thus did not determine whether the deleterious impact on remyelination could truly be attributed to loss of CX3CR1 on microglia, OPCs or a combination of the loss of functional CX3CR1 on both cell types. Further studies into the role of the CX3CR1/CX3CL1 axis is remyelination must therefore investigate the effect of CX3CR1 knock-out on microglia and OPCs in isolation.

One way of studying the role of CX3CR1 *in vivo*, would be to use the Cre-Lox system to create conditional knock-out mice. Conditional gene targeting by this method, employs the insertion of the gene for tamoxifen inducible site-specific recombinase CreER (*c*yclization *re*combination) under the control of a cell specific marker gene promotor sequence, coupled with floxing of an essential exon of the gene to be knocked out (reviewed in Feil et al., 2009).

In the case of targeted CX3CR1 knock-out, mouse lines with tamoxifen inducible CreER could be placed under the control of the gene for either PDGFrα in the case of OPCs or CD68 in the case of microglia. These inducible Cre mouse lines could then be crossed with a CX3CR1 floxed line. In the resulting progeny, on the administration of tamoxifen CreER PDGFrα/floxed CX3CR1 mice could be induced to knock out CX3CR1 specifically in OPCs on, while CreER CD68/floxed CX3CR1 mice could be induced to knock out CX3CR1 specifically in microglia. *In vivo*, concurrent tamoxifen administration with the induction of a demyelinated lesion using LPC in the CreER PDGFrα/floxed CX3CR1 and CreER CD68/floxed CX3CR1 mice, could then be used to investigate the behaviour of CX3CR1 deficient OPCs or microglia in isolation. Fluorescent microscopy using PDGFrα and CD68 antibodies in conjunction with CX3CR1 antibodies, could be used to study the activity of OPCs and microglia in demyelinating lesions in the absence of CX3CR1.

From this experimental design, it would be interesting to establish whether CX3CR1+ve OPCs effectively migrate into LPC induced lesion sites and differentiate upon arrival, in the absence of CX3CR1+ve microglia. Conversely, it would be interesting to determine whether effective myelin clearance by CX3CR1+ve microglia in the absence of CX3CR1+ve OPCs, is enough to restore efficient remyelination. Bearing in mind the data from Lampron et al., 2015 showing that loss of CX3CR1 results in insufficient clearance of myelin debris by microglia and impaired recruitment of OPCs following demyelination, it can be hypothesized that active CX3CR1 is required on both microglia and OPCs for efficient myelination.

## 6.2 Similarity of the effects of CX3CL1 and CXCL12 on OPCs

In previously published literature, a number of other factors have been found to improve the migration or differentiation of OPCs in models of CNS demyelination. Foremost amongst these are CCL2 and IL1β, both of which improve the migration, but not differentiation of OPCs (Moyon et al., 2015). As previously highlighted in **chapter 1.4.3**, other factors shown to be chemoattractants for OPCs include FGF-2 (Clemente et al., 2011), PDGFα (Redwine and Armstrong, 1998; Zhang et al., 2004), prostacyclin (Takahashi et al., 2013) and Semaphorin-3F (Piaton et al., 2011; Williams et al., 2007), while OPC chemorepellents include Anosmin-1 (Clemente et al., 2011; Murcia-Belmonte et al., 2016), Netrin-1 (Jarjour et al., 2003) and Semaphorin-3F (Piaton et al., 2011; Williams et al., 2007). However, none of these factors have been shown to improve the differentiation of OPCs in the regeneration of demyelinating injury.

In contrast, factors modulating the differentiation of OPCs into oligodendrocytes have also been identified, LINGO-1 for example, has been shown to inhibit the differentiation of OPCs in the spinal cords of EAE mice (Mi et al., 2005), with antagonism of this factor improving both OPC differentiation and remyelination following injury (Mi et al., 2009). On the other hand, factors which improve OPC differentiation into adult oligodendrocytes, thus improving remyelination following demyelination. As previously mentioned, the major finding from the Huang, Jarjour etl., 2011 paper from which the transcriptomic data analysed in **chapter 3.2**, was that RXR-γ was expressed by OPCs during remyelination, and that Knockdown of RXR-γ by RNA interference or RXR-specific antagonists resulted in markedly impaired differentiation of OPCs and consequently, myelination.

As noted in **chapter 4.6.7**, the secreted factor CXCL12, has been found to improve the proliferation and differentiation of OPCs during remyelination, and act as a chemoattractant for OPCs during development (Dziembowska et al., 2005; Patel et al., 2012; Williams et al., 2014).

However, while the secreted factors stated above have all been found to modulate the behaviour of OPCs, no single factor has yet been identified which promotes both the migration and differentiation of OPCs following demyelinating injury. There is strong evidence that both the differentiation and migration of OPCs are impaired in MS lesions (Boyd et al., 2013b; Kuhlmann et al., 2008; Shen et al., 2008; Sim et al., 2002; Wolswijk, 1998; Woodruff et al., 2004). The data in this thesis documents both the expression of CX3CL1 during remyelination, and its ability to improve both the migration and differentiation of OPCs *in vitro*. This ability to improve both regeneratively essential processes makes CX3CL1 an attractive candidate for further studies and as a putative possibility for future regenerative therapy. Targeting of the CX3CL1/CX3CR1 axis, has the scope to improve both processes simultaneously, delivering both increased numbers of OPCs to the lesion site, and effectively stimulating their differentiation on arrival.

As described earlier, another factor that I investigated was CXCL12 or SDF-1. In LPC-induced focal brain demyelination, from the Huang, Jarjour et al., 2011 dataset, CXCl12 has an extremely similar expression pattern to CX3CL1 (see **figures 4.28**, and **5.6**). Also, in the Moyon et al., 2015 cuprizone demyelination data set, CXCR4, (the receptor

principally responsible for the activation of downstream signalling in response to CXCL12) is more highly expressed in activated OPCs as compared to non-activated OPCs, similarly to CX3CR1, although with a much smaller fold-change (see **figures 4.29** and **3.5**). CXCL12 has previously been demonstrated to be a proliferation and differentiation factor for OPCs (Patel et al., 2012) and my X-celligence RTCA CIM results show that CXCl12 is also a chemoattractant for OPCs (see **figure 4.31**).

The similarities in my results for these two factors suggests that they are similarly important in the regulation of OPC directed regeneration. Indeed, it has been previously shown that increased binding of CXCL12 to CXCR4 results in an increase in mature oligodendrocytes in demyelinated lesions (Williams et al., 2014). However, a major complication with the CXCL12 system is the activity of a second cell surface receptor CXCR7. Unlike CXCR4, CXCR7 does not actively trigger any downstream signalling cascades, and so the binding of CXCL12 to CXCR7 does not induce dynamic cellular processes in OPCs such as cell migration, proliferation or maturation. CXCR7 sequesters and internalises CXCL12, indirectly controlling the activation of dynamic cell processes by limiting the availability of CXCL12 for CXCR4 binding. This dual receptor system naturally complicates the development of any potential treatment involving CXCL12 since effective augmentation of CXCL12 mediated regeneration would require the simultaneous agonism of CXCR4 and antagonism of CXCR7 (Williams et al., 2014).

In addition, according to the Barres database (Zhang *et al*., 2014) CXCL12, CXCR4 and CXCR7 are all highly expressed in endothelial cells suggesting that intervention into this system might impact endothelial cell biology, which may not be beneficial. Taking these limitations into account, it is clear that CX3CL1/CXC3CR1 makes a much more attractive drug target, requiring only the agonism of a single receptor, without the complication of endothelial disruption. It is possible that there may be some redundancy in the function of CX3CL1 and CXCL12 and it would be interesting to know if administration of the two factors together, or the knock-out of both CX3CR1 and CXCR4, would seriously impact remyelination.

### 6.3 Targeting the CX3CR1/CX3CL1 Axis as a Treatment for MS

As mentioned above, current treatments for MS are focussed on treating the inflammatory attacks associated with the relapsing and remitting phase of the disease course. Although no regenerative therapy is currently commercially available, clinical trials in human patients are underway.

As previously mentioned, abundance of the protein LINGO-1 has been shown to reduce OPC differentiation in the spinal cord (Mi et al., 2005), and antagonism of LINGO-1 has been found to increase OPC differentiation and remyelination following LPC induced demyelination (Mi et al., 2009). In phase 2 clinical trials, treatment of relapsing and remitting and/or secondary progressive MS patients with intravenous infusions of an anti-LINGO-1 antibody had mixed results. A SYNERGY trial found no improvement in physical or cognitive function in patients. In contrast, a RENEW trial focussing exclusively on patients with a single episode of acute optic neuritis, found improvement in optic nerve signalling in patients after 6 intravenous treatments of anti-LINGO-1 antibody (https://www.mssociety.org.uk/node/690821, ClinicalTrials.gov Identifier: NCT01721161).

Another potential therapy is the antihistamine Clesmastine which is being tested as a potential remyelinating factor in patients with relapsing and remitting MS (https://www.mssociety.org.uk/ms-research/treatments-in-the-pipeline/clemastine). Results from a stage 2 clinical trial, showed some improvement in optic nerve signalling, suggestive of improved myelin damage repair as a result of suppression of the immune response (ClinicalTrials.gov Identifier: NCT02040298).

While clinical trials of regenerative therapies for MS are still ongoing, further research into the improvement of remyelination is needed to identify and implement optimal treatment for progressive neurodegeneration.

An ideal MS treatment to avoid progressive neurodegeneration in MS, might consist of augmenting phagocytosis of microglia while controlling inflammation, coupled with factors targeting oligodendrocytes (Rivest, 2015).

My data suggests that modulation of the CX3CR1/CX3CL1 axis would target OPCs as well as microglia. A potential treatment in the form of an agonist for CX3CR1, might therefore serve the dual purpose of increasing the migration and phagocytosis of debris by microglia, and increasing the recruitment and differentiation of OPCs.

As mentioned in **chapter 5.1**, a polymorphism in CX3CR1 which reduces its binding affinity for CX3CL1 is associated with accelerated progression from relapsing and remitting to secondary progressive MS (Arli et al., 2013; Broux et al., 2012; Stojković et al., 2012). For treatment of MS where neurodegeneration is prominent, optimal MS

treatment might combine an agonist for CX3CR1 to encourage regeneration, coupled with existing immunomodulators (to combat adaptive immune-driven pathology).

Given that my results show that the formation of chemotactic gradients is fundamentally important for the directional migration of OPCs, a more measured approach might be to identify and target the upstream regulators of CX3CL1 expression in neurons or astrocytes, or to increase the cleavage of the chemokine domain of CX3CL1 at the lesion site. Both of these approaches would result in an increase in local CX3CL1 expression at the lesion site, which could then diffuse outward to recruit OPCs and microglia.

However, some negative effects of the CX3CL1/CX3CR1 axis in MS associated biology have also been reported. Increased CX3CL1 has been found in the CSF of MS patients, and is thought to be involved in the recruitment of inflammatory T-cells. Administration of CX3CL1 to T-cells derived from relapsing and remitting MS patients, has also been shown to increase the expression of inflammatory cytokines IFN-γ and TNFα in (Blauth et al., 2015). CX3CR1+ T-cells have also been shown to follow a gradient of CX3CL1 into sites of inflammation and may even kill oligodendrocytes in active MS lesions (Broux et al., 2012). A 2014 study also found that subcutaneous injection of a CX3CR1 inhibitor, reduced disease pathology in EAE rats(Ridderstad Wollberg et al., 2014). However, very little of the CX3CR1 inhibitor crossed the blood brain barrier, and the EAE ameliorating effect was thought to be the result of blocking the invasion of circulating leukocytes.

To circumvent these issues, any direct or indirect pharmaceutical modulation of the CX3CR1/CX3CL1 axis would require nuanced targeting of OPCs or injured neurons, crossing the blood brain barrier. In a previous study, the Williams group used nanoparticles with NG2 surface antibodies to target delivery of LIF to OPCs and improved remyelination by increasing OPC differentiation *in vivo* (Rittchen et al., 2015). It is therefore possible to envisage a treatment either targeting a CX3CR1 agonist to OPCs or targeting distressed neurons with an upstream inducer of CX3CL1 expression. This delivery system has both the advantages of targeting specific cells and being small enough to cross the blood brain barrier.

Treatments targeting the CX3CR1/CX3CL1 axis could also be used in the treatment of other pathologies. Another injury type which features demyelination is contusion spinal cord injury and there is evidence that the transplantation of myelinating cells into spinal cord injuries may improve regeneration (reviewed in Myers et al., 2016). In contrast to the difficulties in the delivery of pharmaceuticals to MS lesions due to multiple lesions

occurring over a considerable timespan, treatments utilising an agonist of CX3CR1 could be administered directly into the heart of the spinal cord traumatic lesion site.

However, it must be noted that, regardless of the mode of delivery, direct injection of CX3CL1 or CX3CR1 agonists into the CNS carries considerable risk of off-target effects. A more nuanced option, might be to upregulate endogenous expression of CX3CL1 and/or CX3CR1 by intralesional injection of lentiviral vectors. Such experiments could be carried out in a similar fashion to the overexpression of Semaphorin 3A and Semaphorin 3F (Piaton et al., 2011), and Netrin-1 (Tepavčević et al., 2014). Loss of function experiments knocking down CX3CL1 or CX3CR1 using siRNAs (short interfering ribonucleic acids), could also be used to confirm the importance of the CX3CR1/CX3CL1 axis during remyelination.

## 6.4 Conclusion

In this thesis, I combined bioinformatic data analysis and *in vitro* laboratory techniques to identify and verify novel mediators of OPC biology. Using these methods, I have created a data resource to make the data accessible to other researchers and identified a single factor which modulates both the migration and maturation of OPCs *in vitro*.

In conclusion, this thesis represents a body of work which extends current knowledge of OPC biology *in vitro*, and while these results require further verification in *in vivo* models of demyelination, the CX3CR1/CX3CL1 interaction presents a novel possible opportunity for the development of regenerative therapies for MS.

# References


Akison, L.K., Alvino, E.R., Dunning, K.R., Robker, R.L., and Russell, D.L. (2012). Transient invasive migration in mouse cumulus oocyte complexes induced at ovulation by luteinizing hormone. Biol. Reprod. *86*, 125.

Alter, M., Halpern, L., Kurland, L.T., Bornstein, B., Leibowitz, U., and Silberstein, J. (1962). Multiple sclerosis in Israel. Prevalence among immigrants and native inhabitants. Arch. Neurol. *7*, 253–263.

Alvarez-Buylla, A., García-Verdugo, J.M., and Tramontin, A.D. (2001). A unified hypothesis on the lineage of neural stem cells. Nat. Rev. Neurosci. *2*, 287–293.

Arli, B., Irkec, C., Menevse, S., Yilmaz, A., and Alp, E. (2013). Fractalkine gene receptor polymorphism in patients with multiple sclerosis. Int. J. Neurosci. *123*, 31–37.

Arlinghaus, F.T., and Eble, J.A. (2013). The Collagen-binding Integrin α2β1 Is a Novel Interaction Partner of the Trimeresurus flavoviridis Venom Protein Flavocetin-A. J. Biol. Chem. *288*, 947–955.

Armstrong, R., Friedrich, V.L., Holmes, K.V., and Dubois-Dalcq, M. (1990a). In vitro analysis of the oligodendrocyte lineage in mice during demyelination and remyelination. J. Cell Biol. *111*, 1183–1195.

Armstrong, R.C., Harvath, L., and Dubois-Dalcq, M.E. (1990b). Type 1 astrocytes and oligodendrocyte-type 2 astrocyte glial progenitors migrate toward distinct molecules. J. Neurosci. Res. *27*, 400–407.

Bankston, A.N., Mandler, M.D., and Feng, Y. (2013). Oligodendroglia and neurotrophic factors in neurodegeneration. Neurosci. Bull. *29*, 216–228.

Bansal, R., Kumar, M., Murray, K., Morrison, R.S., and Pfeiffer, S.E. (1996). Regulation of FGF receptors in the oligodendrocyte lineage. Mol. Cell. Neurosci. *7*, 263–275.

Baron, W., Metz, B., Bansal, R., Hoekstra, D., and de Vries, H. (2000). PDGF and FGF-2 signaling in oligodendrocyte progenitor cells: regulation of proliferation and differentiation by multiple intracellular signaling pathways. Mol. Cell. Neurosci. *15*, 314–329.

Bartscht, T., Lehnert, H., Gieseler, F., and Ungefroren, H. (2012). The Src family kinase inhibitors PP2 and PP1 effectively block TGF-beta1-induced cell migration and invasion in both established and primary carcinoma cells. Cancer Chemother. Pharmacol. *70*, 221–230.

Baumann, N., and Pham-Dinh, D. (2001). Biology of oligodendrocyte and myelin in the mammalian central nervous system. Physiol. Rev. *81*, 871–927.

Bazan, J.F., Bacon, K.B., Hardiman, G., Wang, W., Soo, K., Rossi, D., Greaves, D.R., Zlotnik, A., and Schall, T.J. (1997). A new class of membrane-bound chemokine with a CX3C motif. Nature *385*, 640–644.

Bellavance, M.-A., Gosselin, D., Yong, V.W., Stys, P.K., and Rivest, S. (2015). Patrolling monocytes play a critical role in CX3CR1-mediated neuroprotection during excitotoxicity. Brain Struct. Funct. *220*, 1759–1776.

Benjamini, Y., and Hochberg, Y. (1995). Controlling the False Discovery Rate: A Practical and Powerful Approach to Multiple Testing. J. R. Stat. Soc. Ser. B Methodol. *57*, 289–300.

Bergles, D.E., Roberts, J.D.B., Somogyi, P., and Jahr, C.E. (2000). Glutamatergic synapses on oligodendrocyte precursor cells in the hippocampus. Nature *405*, 187–191.

Bin, J.M., Rajasekharan, S., Kuhlmann, T., Hanes, I., Marcal, N., Han, D., Rodrigues, S.P., Leong, S.Y., Newcombe, J., Antel, J.P., et al. (2013). Full-length and fragmented netrin-1 in multiple sclerosis plaques are inhibitors of oligodendrocyte precursor cell migration. Am. J. Pathol. *183*, 673–680.

Blakemore, W.F., and Franklin, R.J.M. (2008). Remyelination in experimental models of toxin-induced demyelination. Curr. Top. Microbiol. Immunol. *318*, 193–212.

Blakemore, W.F., and Patterson, R.C. (1978). Suppression of remyelination in the CNS by X-irradiation. Acta Neuropathol. (Berl.) *42*, 105–113.

Blauth, K., Zhang, X., Chopra, M., Rogan, S., and Markovic-Plese, S. (2015). The role of fractalkine (CX3CL1) in regulation of CD4(+) cell migration to the central nervous system in patients with relapsing-remitting multiple sclerosis. Clin. Immunol. Orlando Fla *157*, 121–132.

Boehme, S.A., Lio, F.M., Maciejewski-Lenoir, D., Bacon, K.B., and Conlon, P.J. (2000). The chemokine fractalkine inhibits Fas-mediated cell death of brain microglia. J. Immunol. Baltim. Md 1950 *165*, 397–403.

Boldajipour, B., Mahabaleshwar, H., Kardash, E., Reichman-Fried, M., Blaser, H., Minina, S., Wilson, D., Xu, Q., and Raz, E. (2008). Control of chemokine-guided cell migration by ligand sequestration. Cell *132*, 463–473.

Boulanger, J.J., and Messier, C. (2014). From precursors to myelinating oligodendrocytes: contribution of intrinsic and extrinsic factors to white matter plasticity in the adult brain. Neuroscience *269*, 343–366.

Boullerne, A.I. (2016). The history of myelin. Exp. Neurol. *283*, *Part B*, 431–445.

Boyd, A., Zhang, H., and Williams, A. (2013a). Insufficient OPC migration into demyelinated lesions is a cause of poor remyelination in MS and mouse models. Acta Neuropathol. (Berl.) *125*, 841–859.

Boyd, A., Zhang, H., and Williams, A. (2013b). Insufficient OPC migration into demyelinated lesions is a cause of poor remyelination in MS and mouse models. Acta Neuropathol. (Berl.) *125*, 841–859.

Bribián, A., Barallobre, M.J., Soussi-Yanicostas, N., and de Castro, F. (2006). Anosmin-1 modulates the FGF-2-dependent migration of oligodendrocyte precursors in the developing optic nerve. Mol. Cell. Neurosci. *33*, 2–14.

Bribián, A., Esteban, P.F., Clemente, D., Soussi-Yanicostas, N., Thomas, J.-L., Zalc, B., and de Castro, F. (2008). A novel role for anosmin-1 in the adhesion and migration of oligodendrocyte precursors. Dev. Neurobiol. *68*, 1503–1516.

Broux, B., Pannemans, K., Zhang, X., Markovic-Plese, S., Broekmans, T., Eijnde, B.O., Van Wijmeersch, B., Somers, V., Geusens, P., van der Pol, S., et al. (2012). CX(3)CR1 drives cytotoxic CD4(+)CD28(-) T cells into the brain of multiple sclerosis patients. J. Autoimmun. *38*, 10–19.

Browne, P., Chandraratna, D., Angood, C., Tremlett, H., Baker, C., Taylor, B.V., and Thompson, A.J. (2014). Atlas of Multiple Sclerosis 2013: A growing global problem with widespread inequity. Neurology *83*, 1022–1024.

Bulfone, A., Puelles, L., Porteus, M.H., Frohman, M.A., Martin, G.R., and Rubenstein, J.L. (1993). Spatially restricted expression of Dlx-1, Dlx-2 (Tes-1), Gbx-2, and Wnt-3 in the embryonic day 12.5 mouse forebrain defines potential transverse and longitudinal segmental boundaries. J. Neurosci. Off. J. Soc. Neurosci. *13*, 3155–3172.

Burnard, S., Lechner-Scott, J., and Scott, R.J. (2017). EBV and MS: Major cause, minor contribution or red-herring? Mult. Scler. Relat. Disord. *16*, 24–30.

Cai, J., Qi, Y., Hu, X., Tan, M., Liu, Z., Zhang, J., Li, Q., Sander, M., and Qiu, M. (2005). Generation of oligodendrocyte precursor cells from mouse dorsal spinal cord independent of Nkx6 regulation and Shh signaling. Neuron *45*, 41–53.

Canoll, P.D., Musacchio, J.M., Hardy, R., Reynolds, R., Marchionni, M.A., and Salzer, J.L. (1996). GGF/neuregulin is a neuronal signal that promotes the proliferation and survival and inhibits the differentiation of oligodendrocyte progenitors. Neuron *17*, 229–243.

Cardona, A.E., Pioro, E.P., Sasse, M.E., Kostenko, V., Cardona, S.M., Dijkstra, I.M., Huang, D., Kidd, G., Dombrowski, S., Dutta, R., et al. (2006). Control of microglial neurotoxicity by the fractalkine receptor. Nat. Neurosci. *9*, 917–924.

de Castro, F., and Bribián, A. (2005). The molecular orchestra of the migration of oligodendrocyte precursors during development. Brain Res. Brain Res. Rev. *49*, 227–241.

de Castro, F., Bribián, A., and Ortega, M.C. (2013). Regulation of oligodendrocyte precursor migration during development, in adulthood and in pathology. Cell. Mol. Life Sci. CMLS *70*, 4355–4368.

Cayre, M., Courtès, S., Martineau, F., Giordano, M., Arnaud, K., Zamaron, A., and Durbec, P. (2013). Netrin 1 contributes to vascular remodeling in the subventricular zone and promotes progenitor emigration after demyelination. Dev. Camb. Engl. *140*, 3107–3117.

Chang, A., Tourtellotte, W.W., Rudick, R., and Trapp, B.D. (2002). Premyelinating oligodendrocytes in chronic lesions of multiple sclerosis. N. Engl. J. Med. *346*, 165–173.

Chapman, G.A., Moores, K., Harrison, D., Campbell, C.A., Stewart, B.R., and Strijbos, P.J. (2000). Fractalkine cleavage from neuronal membranes represents an acute event in the inflammatory response to excitotoxic brain damage. J. Neurosci. Off. J. Soc. Neurosci. *20*, RC87.

Chaudhuri, A. (2005). Why we should offer routine vitamin D supplementation in pregnancy and childhood to prevent multiple sclerosis. Med. Hypotheses *64*, 608–618.

Chiang, C., Litingtung, Y., Lee, E., Young, K.E., Corden, J.L., Westphal, H., and Beachy, P.A. (1996). Cyclopia and defective axial patterning in mice lacking Sonic hedgehog gene function. Nature *383*, 407–413.

Chizhikov, V.V., and Millen, K.J. (2005). Roof plate-dependent patterning of the vertebrate dorsal central nervous system. Dev. Biol. *277*, 287–295.

Chun, B.Y., Kim, J.-H., Nam, Y., Huh, M.-I., Han, S., and Suk, K. (2015). Pathological Involvement of Astrocyte-Derived Lipocalin-2 in the Demyelinating Optic Neuritis. Invest. Ophthalmol. Vis. Sci. *56*, 3691–3698.

Clanet, M. (2008). Jean-Martin Charcot. 1825 to 1893. Int. MS J. *15*, 59–61.

Clemente, D., Ortega, M.C., Arenzana, F.J., and de Castro, F. (2011). FGF-2 and Anosmin-1 are selectively expressed in different types of multiple sclerosis lesions. J. Neurosci. Off. J. Soc. Neurosci. *31*, 14899–14909.

Cohen, R.I., Rottkamp, D.M., Maric, D., Barker, J.L., and Hudson, L.D. (2003). A role for semaphorins and neuropilins in oligodendrocyte guidance. J. Neurochem. *85*, 1262–1278.

Compston, A., and Coles, A. (2008). Multiple sclerosis. The Lancet *372*, 1502–1517.

Compston, A., McDonald, I., Noseworthy, J., Lassmann, H., Miller, D., Smith, K., Werkerle, H., and Confavreux, C. (2005). McAlpine's multiple sclerosis (Philadelphia: Churchill Livingstone Elsevier).

Crawford, A.H., Stockley, J.H., Tripathi, R.B., Richardson, W.D., and Franklin, R.J.M. (2014). Oligodendrocyte progenitors: adult stem cells of the central nervous system? Exp. Neurol. *260*, 50–55.

Crawford, A.H., Tripathi, R.B., Foerster, S., McKenzie, I., Kougioumtzidou, E., Grist, M., Richardson, W.D., and Franklin, R.J.M. (2016). Pre-Existing Mature Oligodendrocytes Do Not Contribute to Remyelination following Toxin-Induced Spinal Cord Demyelination. Am. J. Pathol. *186*, 511–516.

Cruz-Martinez, P., Martinez-Ferre, A., Jaramillo-Merchán, J., Estirado, A., Martinez, S., and Jones, J. (2014). FGF8 activates proliferation and migration in mouse post-natal oligodendrocyte progenitor cells. PloS One *9*, e108241.

Cruz-Orengo, L., Holman, D.W., Dorsey, D., Zhou, L., Zhang, P., Wright, M., McCandless, E.E., Patel, J.R., Luker, G.D., Littman, D.R., et al. (2011). CXCR7 influences leukocyte entry into the CNS parenchyma by controlling abluminal CXCL12 abundance during autoimmunity. J. Exp. Med. *208*, 327–339.

Dawson, M.R.L., Polito, A., Levine, J.M., and Reynolds, R. (2003). NG2-expressing glial progenitor cells: an abundant and widespread population of cycling cells in the adult rat CNS. Mol. Cell. Neurosci. *24*, 476–488.

Dean, G., and Kurtzke, J.F. (1971). On the risk of multiple sclerosis according to age at immigration to South Africa. Br. Med. J. *3*, 725–729.

Decker, L., Avellana-Adalid, V., Nait-Oumesmar, B., Durbec, P., and Baron-Van Evercooren, A. (2000). Oligodendrocyte precursor migration and differentiation: combined effects of PSA residues, growth factors, and substrates. Mol. Cell. Neurosci. *16*, 422–439.

Dessaud, E., McMahon, A.P., and Briscoe, J. (2008). Pattern formation in the vertebrate neural tube: a sonic hedgehog morphogen-regulated transcriptional network. Dev. Camb. Engl. *135*, 2489–2503.

Detels, R., Visscher, B.R., Malmgren, R.M., Coulson, A.H., Lucia, M.V., and Dudley, J.P. (1977). Evidence for lower susceptibility to multiple sclerosis in Japanese-Americans. Am. J. Epidemiol. *105*, 303–310.

Döppler, H., Bastea, L.I., Eiseler, T., and Storz, P. (2013). Neuregulin Mediates F-actin-driven Cell Migration through Inhibition of Protein Kinase D1 via Rac1 Protein. J. Biol. Chem. *288*, 455–465.

Dubois-Dalcq, M., and Murray, K. (2000). Why are growth factors important in oligodendrocyte physiology? Pathol. Biol. *48*, 80–86.

Dunning, M.J., Smith, M.L., Ritchie, M.E., and Tavaré, S. (2007). beadarray: R classes and methods for Illumina bead-based data. Bioinforma. Oxf. Engl. *23*, 2183–2184.

Dziembowska, M., Tham, T.N., Lau, P., Vitry, S., Lazarini, F., and Dubois-Dalcq, M. (2005). A role for CXCR4 signaling in survival and migration of neural and oligodendrocyte precursors. Glia *50*, 258–269.

Ebers, G.C., Sadovnick, A.D., and Risch, N.J. (1995). A genetic basis for familial aggregation in multiple sclerosis. Canadian Collaborative Study Group. Nature *377*, 150–151.

Echelard, Y., Epstein, D.J., St-Jacques, B., Shen, L., Mohler, J., McMahon, J.A., and McMahon, A.P. (1993). Sonic hedgehog, a member of a family of putative signaling molecules, is implicated in the regulation of CNS polarity. Cell *75*, 1417–1430.

Elian, M., Nightingale, S., and Dean, G. (1990). Multiple sclerosis among United Kingdom-born children of immigrants from the Indian subcontinent, Africa and the West Indies. J. Neurol. Neurosurg. Psychiatry *53*, 906–911.

Fodor, S.P., Read, J.L., Pirrung, M.C., Stryer, L., Lu, A.T., and Solas, D. (1991). Light-directed, spatially addressable parallel chemical synthesis. Science *251*, 767–773.

Fogarty, M., Richardson, W.D., and Kessaris, N. (2005). A subset of oligodendrocytes generated from radial glia in the dorsal spinal cord. Dev. Camb. Engl. *132*, 1951–1959.

Franklin, R.J.M. (2002). Why does remyelination fail in multiple sclerosis? Nat. Rev. Neurosci. *3*, 705–714.

Franklin, R.J.M., and ffrench-Constant, C. (2008). Remyelination in the CNS: from biology to therapy. Nat. Rev. Neurosci. *9*, 839–855.

French Research Group on Multiple Sclerosis (1992). Multiple sclerosis in 54 twinships: concordance rate is independent of zygosity. French Research Group on Multiple Sclerosis. Ann. Neurol. *32*, 724–727.

Fricker-Gates, R.A., Winkler, C., Kirik, D., Rosenblad, C., Carpenter, M.K., and Björklund, A. (2000). EGF infusion stimulates the proliferation and migration of embryonic progenitor cells transplanted in the adult rat striatum. Exp. Neurol. *165*, 237–247.

Frohman, E.M., Racke, M.K., and Raine, C.S. (2006). Multiple sclerosis--the plaque and its pathogenesis. N. Engl. J. Med. *354*, 942–955.

Frost, E., Kiernan, B.W., Faissner, A., and ffrench-Constant, C. (1996). Regulation of oligodendrocyte precursor migration by extracellular matrix: evidence for substrate-specific inhibition of migration by tenascin-C. Dev. Neurosci. *18*, 266–273.

Frost, E.E., Nielsen, J.A., Le, T.Q., and Armstrong, R.C. (2003). PDGF and FGF2 regulate oligodendrocyte progenitor responses to demyelination. J. Neurobiol. *54*, 457–472.

Frost, E.E., Zhou, Z., Krasnesky, K., and Armstrong, R.C. (2009). Initiation of oligodendrocyte progenitor cell migration by a PDGF-A activated extracellular regulated kinase (ERK) signaling pathway. Neurochem. Res. *34*, 169–181.

Fruttiger, M., Karlsson, L., Hall, A.C., Abramsson, A., Calver, A.R., Boström, H., Willetts, K., Bertold, C.-H., Heath, J.K., Betsholtz, C., et al. (1999). Defective oligodendrocyte development and severe hypomyelination in PDGF-A knockout mice. Development *126*, 457–467.

Fuccillo, M., Rallu, M., McMahon, A.P., and Fishell, G. (2004). Temporal requirement for hedgehog signaling in ventral telencephalic patterning. Dev. Camb. Engl. *131*, 5031–5040.

Gage, F.H. (2000). Mammalian neural stem cells. Science *287*, 1433–1438.

Gao, L., and Miller, R.H. (2006). Specification of optic nerve oligodendrocyte precursors by retinal ganglion cell axons. J. Neurosci. *26*, 7619–7628.

Gao, J., Luo, X., Tang, K., Li, X., and Li, G. (2006). Epstein-Barr virus integrates frequently into chromosome 4q, 2q, 1q and 7q of Burkitt's lymphoma cell line (Raji). J. Virol. Methods *136*, 193–199.

Garcion, E., Faissner, A., and ffrench-Constant, C. (2001). Knockout mice reveal a contribution of the extracellular matrix molecule tenascin-C to neural precursor proliferation and migration. Dev. Camb. Engl. *128*, 2485–2496.

Gautier, L., Cope, L., Bolstad, B.M., and Irizarry, R.A. (2004). affy—analysis of Affymetrix GeneChip data at the probe level. Bioinformatics *20*, 307–315.

Gentleman, R.C., Carey, V.J., Bates, D.M., Bolstad, B., Dettling, M., Dudoit, S., Ellis, B., Gautier, L., Ge, Y., Gentry, J., et al. (2004). Bioconductor: open software development for computational biology and bioinformatics. Genome Biol. *5*, R80.

Geren, B.B., and Schmitt, F.O. (1954). THE STRUCTURE OF THE SCHWANN CELL AND ITS RELATION TO THE AXON IN CERTAIN INVERTEBRATE NERVE FIBERS*. Proc. Natl. Acad. Sci. U. S. A. *40*, 863–870.

Gillie, O. (2006). A new government policy is needed for sunlight and vitamin D. Br. J. Dermatol. *154*, 1052–1061.

Goodin, D.S. (2016a). Chapter 11 - The epidemiology of multiple sclerosis: insights to a causal cascade†. In Handbook of Clinical Neurology, F.B. and D.F.S. Michael J. Aminoff, ed. (Elsevier), pp. 173–206.

Goodin, D.S. (2016b). The epidemiology of multiple sclerosis. Handb. Clin. Neurol. *138*, 173–206.

Grabel, L. (2012). Developmental origin of neural stem cells: the glial cell that could. Stem Cell Rev. *8*, 577–585.

Grønlie, S.A., Myrvoll, E., Hansen, G., Grønning, M., and Mellgren, S.I. (2000). Multiple sclerosis in North Norway, and first appearance in an indigenous population. J. Neurol. *247*, 129–133.

Gunderson, K.L., Kruglyak, S., Graige, M.S., Garcia, F., Kermani, B.G., Zhao, C., Che, D., Dickinson, T., Wickham, E., Bierle, J., et al. (2004). Decoding Randomly Ordered DNA Arrays. Genome Res. *14*, 870–877.

Hamilton, N.B., Clarke, L.E., Arancibia-Carcamo, I.L., Kougioumtzidou, E., Matthey, M., Káradóttir, R., Whiteley, L., Bergersen, L.H., Richardson, W.D., and Attwell, D. (2017). Endogenous GABA controls oligodendrocyte lineage cell number, myelination, and CNS internode length. Glia *65*, 309–321.

Hammond, S.R., English, D.R., and McLeod, J.G. (2000). The age-range of risk of developing multiple sclerosis: evidence from a migrant population in Australia. Brain J. Neurol. *123 ( Pt 5)*, 968–974.

Handel, A.E., Williamson, A.J., Disanto, G., Handunnetthi, L., Giovannoni, G., and Ramagopalan, S.V. (2010). An updated meta-analysis of risk of multiple sclerosis following infectious mononucleosis. PloS One *5*.

Harrison, J.K., Jiang, Y., Chen, S., Xia, Y., Maciejewski, D., McNamara, R.K., Streit, W.J., Salafranca, M.N., Adhikari, S., Thompson, D.A., et al. (1998). Role for neuronally derived fractalkine in mediating interactions between neurons and CX3CR1-expressing microglia. Proc. Natl. Acad. Sci. U. S. A. *95*, 10896–10901.

He, L., and Lu, Q.R. (2013). Coordinated control of oligodendrocyte development by extrinsic and intrinsic signaling cues. Neurosci. Bull. *29*, 129–143.

Herrero, J., Muffato, M., Beal, K., Fitzgerald, S., Gordon, L., Pignatelli, M., Vilella, A.J., Searle, S.M.J., Amode, R., Brent, S., et al. (2016). Ensembl comparative genomics resources. Database J. Biol. Databases Curation *2016*.

Hitoshi, S., Tropepe, V., Ekker, M., and van der Kooy, D. (2002). Neural stem cell lineages are regionally specified, but not committed, within distinct compartments of the developing brain. Dev. Camb. Engl. *129*, 233–244.

Hollenbach, J.A., and Oksenberg, J.R. (2015). The immunogenetics of multiple sclerosis: A comprehensive review. J. Autoimmun. *64*, 13–25.

Holloway, A.J., van Laar, R.K., Tothill, R.W., and Bowtell, D.D.L. (2002). Options available—from start to finish—for obtaining data from DNA microarrays II. Nat. Genet. *32*, 481–489.

Huang, J.K., Jarjour, A.A., Oumesmar, B.N., Kerninon, C., Williams, A., Krezel, W., Kagechika, H., Bauer, J., Zhao, C., Evercooren, A.B.-V., et al. (2011). Retinoid X receptor gamma signaling accelerates CNS remyelination. Nat Neurosci *14*, 45–53.

Hughes, E.G., Kang, S.H., Fukaya, M., and Bergles, D.E. (2013). Oligodendrocyte progenitors balance growth with self-repulsion to achieve homeostasis in the adult brain. Nat. Neurosci. *16*, 668–676.

Huxley, A.F., and Stämpfli, R. (1949). Evidence for saltatory conduction in peripheral myelinated nerve fibres. J. Physiol. *108*, 315–339.

Imai, T., Hieshima, K., Haskell, C., Baba, M., Nagira, M., Nishimura, M., Kakizaki, M., Takagi, S., Nomiyama, H., Schall, T.J., et al. (1997). Identification and molecular characterization of fractalkine receptor CX3CR1, which mediates both leukocyte migration and adhesion. Cell *91*, 521–530.

Irizarry, R.A., Hobbs, B., Collin, F., Beazer-Barclay, Y.D., Antonellis, K.J., Scherf, U., and Speed, T.P. (2003). Exploration, normalization, and summaries of high density oligonucleotide array probe level data. Biostatistics *4*, 249–264.

Islam, T., Gauderman, W.J., Cozen, W., Hamilton, A.S., Burnett, M.E., and Mack, T.M. (2006). Differential twin concordance for multiple sclerosis by latitude of birthplace. Ann. Neurol. *60*, 56–64.

Jarjour, A.A., Manitt, C., Moore, S.W., Thompson, K.M., Yuh, S.-J., and Kennedy, T.E. (2003). Netrin-1 is a chemorepellent for oligodendrocyte precursor cells in the embryonic spinal cord. J. Neurosci. *23*, 3735–3744.

Jessell, T.M. (2000). Neuronal specification in the spinal cord: inductive signals and transcriptional codes. Nat. Rev. Genet. *1*, 20–29.

Jessen, K.R., and Mirsky, R. (2016). The repair Schwann cell and its function in regenerating nerves. J. Physiol. *594*, 3521–3531.

Jevnikar, Z., Rojnik, M., Jamnik, P., Doljak, B., Fonovic, U.P., and Kos, J. (2013). Cathepsin H mediates the processing of talin and regulates migration of prostate cancer cells. J. Biol. Chem. *288*, 2201–2209.

Jin, T. (2013). Gradient sensing during chemotaxis. Curr. Opin. Cell Biol. *25*, 532–537.

Kessaris, N., Pringle, N., and Richardson, W.D. (2001). Ventral neurogenesis and the neuron-glial switch. Neuron *31*, 677–680.

Kessaris, N., Fogarty, M., Iannarelli, P., Grist, M., Wegner, M., and Richardson, W.D. (2006). Competing waves of oligodendrocytes in the forebrain and postnatal elimination of an embryonic lineage. Nat. Neurosci. *9*, 173–179.

Kiernan, B.W., Götz, B., Faissner, A., and ffrench-Constant, C. (1996). Tenascin-C inhibits oligodendrocyte precursor cell migration by both adhesion-dependent and adhesion-independent mechanisms. Mol. Cell. Neurosci. *7*, 322–335.

Kiernan, B.W., Garcion, E., Ferguson, J., Frost, E.E., Torres, E.M., Dunnett, S.B., Saga, Y., Aizawa, S., Faissner, A., Kaur, R., et al. (1999). Myelination and behaviour of tenascin-C null transgenic mice. Eur. J. Neurosci. *11*, 3082–3092.

Kingwell, E., Marriott, J.J., Jetté, N., Pringsheim, T., Makhani, N., Morrow, S.A., Fisk, J.D., Evans, C., Béland, S.G., Kulaga, S., et al. (2013). Incidence and prevalence of multiple sclerosis in Europe: a systematic review. BMC Neurol. *13*, 128.

Klinghoffer, R.A., Hamilton, T.G., Hoch, R., and Soriano, P. (2002). An Allelic Series at the PDGFαR Locus Indicates Unequal Contributions of Distinct Signaling Pathways During Development. Dev. Cell *2*, 103–113.

Koch-Henriksen, N. (1995). Multiple sclerosis in Scandinavia and Finland. Acta Neurol. Scand. Suppl. *161*, 55–59.

Kreutzberg, G.W. (1996). Microglia: a sensor for pathological events in the CNS. Trends Neurosci. *19*, 312–318.

Kuboyama, K., Fujikawa, A., Masumura, M., Suzuki, R., Matsumoto, M., and Noda, M. (2012). Protein tyrosine phosphatase receptor type z negatively regulates oligodendrocyte differentiation and myelination. PloS One *7*, e48797.

Kuboyama, K., Fujikawa, A., Suzuki, R., and Noda, M. (2015). Inactivation of Protein Tyrosine Phosphatase Receptor Type Z by Pleiotrophin Promotes Remyelination through Activation of Differentiation of Oligodendrocyte Precursor Cells. J. Neurosci. Off. J. Soc. Neurosci. *35*, 12162–12171.

Kuhlmann, T., Miron, V., Cui, Q., Cuo, Q., Wegner, C., Antel, J., and Brück, W. (2008). Differentiation block of oligodendroglial progenitor cells as a cause for remyelination failure in chronic multiple sclerosis. Brain J. Neurol. *131*, 1749–1758.

Kurtzke, J.F. (1975). A reassessment of the distribution of multiple sclerosis. Part one. Acta Neurol. Scand. *51*, 110–136.

Kurtzke, J.F. (1993). Epidemiologic evidence for multiple sclerosis as an infection. Clin. Microbiol. Rev. *6*, 382–427.

Kurtzke, J.F. (2000). Multiple sclerosis in time and space--geographic clues to cause. J. Neurovirol. *6 Suppl 2*, S134-140.

Lampron, A., Larochelle, A., Laflamme, N., Préfontaine, P., Plante, M.-M., Sánchez, M.G., Yong, V.W., Stys, P.K., Tremblay, M.-È., and Rivest, S. (2015). Inefficient clearance of myelin debris by microglia impairs remyelinating processes. J. Exp. Med. *212*, 481–495.

Lang, H.L.E., Jacobsen, H., Ikemizu, S., Andersson, C., Harlos, K., Madsen, L., Hjorth, P., Sondergaard, L., Svejgaard, A., Wucherpfennig, K., et al. (2002). A functional and structural basis for TCR cross-reactivity in multiple sclerosis. Nat. Immunol. *3*, 940–943.

Laursen, L.S., Chan, C.W., and ffrench-Constant, C. (2009). An integrin-contactin complex regulates CNS myelination by differential Fyn phosphorylation. J. Neurosci. Off. J. Soc. Neurosci. *29*, 9174–9185.

Lawson, L.J., Perry, V.H., Dri, P., and Gordon, S. (1990). Heterogeneity in the distribution and morphology of microglia in the normal adult mouse brain. Neuroscience *39*, 151–170.

Levin, L.I., Munger, K.L., O'Reilly, E.J., Falk, K.I., and Ascherio, A. (2010). Primary infection with the Epstein-Barr virus and risk of multiple sclerosis. Ann. Neurol. *67*, 824–830.

Li, C., Liang, S., Zhang, C., Liu, Y., Yang, M., Zhang, J., Zhi, X., Pan, F., and Cui, D. (2015). Allogenic dendritic cell and tumor cell fused vaccine for targeted imaging and enhanced immunotherapeutic efficacy of gastric cancer. Biomaterials *54*, 177–187.

Li, H., de Faria, J.P., Andrew, P., Nitarska, J., and Richardson, W.D. (2011). Phosphorylation regulates OLIG2 cofactor choice and the motor neuron-oligodendrocyte fate switch. Neuron *69*, 918–929.

Liem, K.F., Tremml, G., and Jessell, T.M. (1997). A role for the roof plate and its resident TGFbeta-related proteins in neuronal patterning in the dorsal spinal cord. Cell *91*, 127–138.

Limame, R., Wouters, A., Pauwels, B., Fransen, E., Peeters, M., Lardon, F., Wever, O.D., and Pauwels, P. (2012). Comparative Analysis of Dynamic Cell Viability, Migration and Invasion Assessments by Novel Real-Time Technology and Classic Endpoint Assays. PLOS ONE *7*, e46536.

Liu, W., Jiang, L., Bian, C., Liang, Y., Xing, R., Yishakea, M., and Dong, J. (2016). Role of CX3CL1 in Diseases. Arch. Immunol. Ther. Exp. (Warsz.) *64*, 371–383.

Lu, Q.R., Yuk, D., Alberta, J.A., Zhu, Z., Pawlitzky, I., Chan, J., McMahon, A.P., Stiles, C.D., and Rowitch, D.H. (2000). Sonic hedgehog--regulated oligodendrocyte lineage genes encoding bHLH proteins in the mammalian central nervous system. Neuron *25*, 317–329.

Lu, Q.R., Sun, T., Zhu, Z., Ma, N., Garcia, M., Stiles, C.D., and Rowitch, D.H. (2002). Common developmental requirement for Olig function indicates a motor neuron/oligodendrocyte connection. Cell *109*, 75–86.

Lucchinetti, C., Brück, W., Parisi, J., Scheithauer, B., Rodriguez, M., and Lassmann, H. (1999). A quantitative analysis of oligodendrocytes in multiple sclerosis lesions. A study of 113 cases. Brain J. Neurol. *122 ( Pt 12)*, 2279–2295.

Ludwin, S.K. (1978). Central nervous system demyelination and remyelination in the mouse: an ultrastructural study of cuprizone toxicity. Lab. Investig. J. Tech. Methods Pathol. *39*, 597–612.

Luster, A.D. (1998). Chemokines--chemotactic cytokines that mediate inflammation. N. Engl. J. Med. *338*, 436–445.

Mandel, K., Seidl, D., Rades, D., Lehnert, H., Gieseler, F., Hass, R., and Ungefroren, H. (2013). Characterization of Spontaneous and TGF-β-Induced Cell Motility of Primary Human Normal and Neoplastic Mammary Cells In Vitro Using Novel Real-Time Technology. PLOS ONE *8*, e56591.

Marques, F., Mesquita, S.D., Sousa, J.C., Coppola, G., Gao, F., Geschwind, D.H., Columba-Cabezas, S., Aloisi, F., Degn, M., Cerqueira, J.J., et al. (2012). Lipocalin 2 is present in the EAE brain and is modulated by natalizumab. Front. Cell. Neurosci. *6*, 33.

Martyn, C.N., Cruddas, M., and Compston, D.A. (1993). Symptomatic Epstein-Barr virus infection and multiple sclerosis. J. Neurol. Neurosurg. Psychiatry *56*, 167–168.

McCarthy, K.D., and de Vellis, J. (1980). Preparation of separate astroglial and oligodendroglial cell cultures from rat cerebral tissue. J. Cell Biol. *85*, 890–902.

McDermott, D.H., Fong, A.M., Yang, Q., Sechler, J.M., Cupples, L.A., Merrell, M.N., Wilson, P.W.F., D'Agostino, R.B., O'Donnell, C.J., Patel, D.D., et al. (2003). Chemokine receptor mutant CX3CR1-M280 has impaired adhesive function and correlates with protection from cardiovascular disease in humans. J. Clin. Invest. *111*, 1241–1250.

McKay, R. (1997). Stem cells in the central nervous system. Science *276*, 66–71.

McKinnon, R.D., Smith, C., Behar, T., Smith, T., and Dubois-Dalcq, M. (1993). Distinct effects of bFGF and PDGF on oligodendrocyte progenitor cells. Glia *7*, 245–254.

Mehler, M.F. (2002). Mechanisms regulating lineage diversity during mammalian cerebral cortical neurogenesis and gliogenesis. Results Probl. Cell Differ. *39*, 27–52.

van der Mei, I. a. F., Ponsonby, A.-L., Dwyer, T., Blizzard, L., Simmons, R., Taylor, B.V., Butzkueven, H., and Kilpatrick, T. (2003). Past exposure to sun, skin phenotype, and risk of multiple sclerosis: case-control study. BMJ *327*, 316.

Merchán, P., Bribián, A., Sánchez-Camacho, C., Lezameta, M., Bovolenta, P., and de Castro, F. (2007). Sonic hedgehog promotes the migration and proliferation of optic nerve oligodendrocyte precursors. Mol. Cell. Neurosci. *36*, 355–368.

Mi, S., Miller, R.H., Lee, X., Scott, M.L., Shulag-Morskaya, S., Shao, Z., Chang, J., Thill, G., Levesque, M., Zhang, M., et al. (2005). LINGO-1 negatively regulates myelination by oligodendrocytes. Nat. Neurosci. *8*, 745–751.

Mi, S., Miller, R.H., Tang, W., Lee, X., Hu, B., Wu, W., Zhang, Y., Shields, C.B., Zhang, Y., Miklasz, S., et al. (2009). Promotion of central nervous system remyelination by induced differentiation of oligodendrocyte precursor cells. Ann. Neurol. *65*, 304–315.

Michael, K.L., Taylor, L.C., Schultz, S.L., and Walt, D.R. (1998). Randomly ordered addressable high-density optical sensor arrays. Anal. Chem. *70*, 1242–1248.

Miller, D.J., Duka, T., Stimpson, C.D., Schapiro, S.J., Baze, W.B., McArthur, M.J., Fobbs, A.J., Sousa, A.M.M., Sestan, N., Wildman, D.E., et al. (2012). Prolonged myelination in human neocortical evolution. Proc. Natl. Acad. Sci. U. S. A. *109*, 16480–16485.

Milner, R., and Ffrench-Constant, C. (1994). A developmental analysis of oligodendroglial integrins in primary cells: changes in alpha v-associated beta subunits during differentiation. Dev. Camb. Engl. *120*, 3497–3506.

Milner, R., Edwards, G., Streuli, C., and Ffrench-Constant, C. (1996). A role in migration for the αvβ1 integrin expressed on oligodendrocyte precursors. J. Neurosci. *16*, 7240–7252.

Milner, R., Anderson, H.J., Rippon, R.F., McKay, J.S., Franklin, R.J., Marchionni, M.A., Reynolds, R., and Ffrench-Constant, C. (1997). Contrasting effects of mitogenic growth factors on oligodendrocyte precursor cell migration. Glia *19*, 85–90.

Miron, V.E., and Franklin, R.J.M. (2014). Macrophages and CNS remyelination. J. Neurochem. *130*, 165–171.

Miron, V.E., Boyd, A., Zhao, J.-W., Yuen, T.J., Ruckh, J.M., Shadrach, J.L., van Wijngaarden, P., Wagers, A.J., Williams, A., Franklin, R.J.M., et al. (2013). M2 microglia and macrophages drive oligodendrocyte differentiation during CNS remyelination. Nat. Neurosci. *16*, 1211–1218.

Moyon, S., Dubessy, A.L., Aigrot, M.S., Trotter, M., Huang, J.K., Dauphinot, L., Potier, M.C., Kerninon, C., Melik Parsadaniantz, S., Franklin, R.J.M., et al. (2015). Demyelination Causes Adult CNS Progenitors to Revert to an Immature State and Express Immune Cues That Support Their Migration. J. Neurosci. *35*, 4–20.

Mumford, C.J., Wood, N.W., Kellar-Wood, H., Thorpe, J.W., Miller, D.H., and Compston, D.A. (1994). The British Isles survey of multiple sclerosis in twins. Neurology *44*, 11–15.

Munger, K.L., Zhang, S.M., O'Reilly, E., Hernán, M.A., Olek, M.J., Willett, W.C., and Ascherio, A. (2004). Vitamin D intake and incidence of multiple sclerosis. Neurology *62*, 60–65.

Munger, K.L., Levin, L.I., Hollis, B.W., Howard, N.S., and Ascherio, A. (2006). Serum 25-hydroxyvitamin D levels and risk of multiple sclerosis. JAMA *296*, 2832–2838.

Murcia-Belmonte, V., Esteban, P.F., Martínez-Hernández, J., Gruart, A., Luján, R., Delgado-García, J.M., and de Castro, F. (2016). Anosmin-1 over-expression regulates oligodendrocyte precursor cell proliferation, migration and myelin sheath thickness. Brain Struct. Funct. *221*, 1365–1385.

Muroyama, Y., Fujihara, M., Ikeya, M., Kondoh, H., and Takada, S. (2002). Wnt signaling plays an essential role in neuronal specification of the dorsal spinal cord. Genes Dev. *16*, 548–553.

Myers, S.A., Bankston, A.N., Burke, D.A., Ohri, S.S., and Whittemore, S.R. (2016). Does the preclinical evidence for functional remyelination following myelinating cell engraftment

into the injured spinal cord support progression to clinical trials? Exp. Neurol. *283*, 560–572.

Nakahira, E., Kagawa, T., Shimizu, T., Goulding, M.D., and Ikenaka, K. (2006). Direct evidence that ventral forebrain cells migrate to the cortex and contribute to the generation of cortical myelinating oligodendrocytes. Dev. Biol. *291*, 123–131.

Nam, Y., Kim, J.-H., Seo, M., Kim, J.-H., Jin, M., Jeon, S., Seo, J., Lee, W.-H., Bing, S.J., Jee, Y., et al. (2014). Lipocalin-2 protein deficiency ameliorates experimental autoimmune encephalomyelitis: the pathogenic role of lipocalin-2 in the central nervous system and peripheral lymphoid tissues. J. Biol. Chem. *289*, 16773–16789.

Naruse, M., Ishizaki, Y., Ikenaka, K., Tanaka, A., and Hitoshi, S. (2016a). Origin of oligodendrocytes in mammalian forebrains: a revised perspective. J. Physiol. Sci. JPS.

Naruse, M., Ishino, Y., Kumar, A., Ono, K., Takebayashi, H., Yamaguchi, M., Ishizaki, Y., Ikenaka, K., and Hitoshi, S. (2016b). The Dorsoventral Boundary of the Germinal Zone is a Specialized Niche for the Generation of Cortical Oligodendrocytes during a Restricted Temporal Window. Cereb. Cortex N. Y. N 1991 *26*, 2800–2810.

Naumann, U., Cameroni, E., Pruenster, M., Mahabaleshwar, H., Raz, E., Zerwes, H.-G., Rot, A., and Thelen, M. (2010). CXCR7 functions as a scavenger for CXCL12 and CXCL11. PloS One *5*, e9175.

Niehaus, A., Stegmüller, J., Diers-Fenger, M., and Trotter, J. (1999). Cell-surface glycoprotein of oligodendrocyte progenitors involved in migration. J. Neurosci. Off. J. Soc. Neurosci. *19*, 4948–4961.

Niland, S., Ditkowski, B., Parrandier, D., Roth, L., Augustin, H., and Eble, J.A. (2013). Rhodocetin-αβ-induced neuropilin-1-cMet association triggers restructuring of matrix contacts in endothelial cells. Arterioscler. Thromb. Vasc. Biol. *33*, 544–554.

Noseworthy, J.H., Lucchinetti, C., Rodriguez, M., and Weinshenker, B.G. (2000). Multiple sclerosis. N. Engl. J. Med. *343*, 938–952.

Okano, H., and Temple, S. (2009). Cell types to order: temporal specification of CNS stem cells. Curr. Opin. Neurobiol. *19*, 112–119.

Olivier, C., Cobos, I., Perez Villegas, E.M., Spassky, N., Zalc, B., Martinez, S., and Thomas, J.L. (2001). Monofocal origin of telencephalic oligodendrocytes in the anterior entopeduncular area of the chick embryo. Dev. Camb. Engl. *128*, 1757–1769.

Ono, K., Yasui, Y., Rutishauser, U., and Miller, R.H. (1997). Focal ventricular origin and migration of oligodendrocyte precursors into the chick optic nerve. Neuron *19*, 283–292.

Orduz, D., Maldonado, P.P., Balia, M., Vélez-Fort, M., de Sars, V., Yanagawa, Y., Emiliani, V., and Angulo, M.C. (2015). Interneurons and oligodendrocyte progenitors form a structured synaptic network in the developing neocortex. eLife *4*.

O'Rourke, M., Gasperini, R., and Young, K.M. (2014). Adult myelination: wrapping up neuronal plasticity. Neural Regen. Res. *9*, 1261–1264.

Osterhout, D.J., Ebner, S., Xu, J., Ornitz, D.M., Zazanis, G.A., and McKinnon, R.D. (1997). Transplanted oligodendrocyte progenitor cells expressing a dominant- negative FGF receptor transgene fail to migrate in vivo. J. Neurosci. *17*, 9122–9132.

Pachner, A.R. (2011). Experimental models of multiple sclerosis. Curr. Opin. Neurol. *24*, 291–299.

Paolicelli, R.C., Bisht, K., and Tremblay, M.-È. (2014). Fractalkine regulation of microglial physiology and consequences on the brain and behavior. Front. Cell. Neurosci. *8*, 129.

Patel, J.R., Williams, J.L., Muccigrosso, M.M., Liu, L., Sun, T., Rubin, J.B., and Klein, R.S. (2012). Astrocyte TNFR2 is required for CXCL12-mediated regulation of oligodendrocyte progenitor proliferation and differentiation within the adult CNS. Acta Neuropathol. (Berl.) *124*, 847–860.

Payne, H.R., Hemperly, J.J., and Lemmon, V. (1996). N-cadherin expression and function in cultured oligodendrocytes. Brain Res. Dev. Brain Res. *97*, 9–15.

Pendleton, J.C., Shamblott, M.J., Gary, D.S., Belegu, V., Hurtado, A., Malone, M.L., and McDonald, J.W. (2013). Chondroitin sulfate proteoglycans inhibit oligodendrocyte myelination through PTPσ. Exp. Neurol. *247*, 113–121.

Piaton, G., Aigrot, M.-S., Williams, A., Moyon, S., Tepavcevic, V., Moutkine, I., Gras, J., Matho, K.S., Schmitt, A., Soellner, H., et al. (2011). Class 3 semaphorins influence oligodendrocyte precursor recruitment and remyelination in adult central nervous system. Brain *134*, 1156–1167.

Pierani, A., Brenner-Morton, S., Chiang, C., and Jessell, T.M. (1999). A sonic hedgehog-independent, retinoid-activated pathway of neurogenesis in the ventral spinal cord. Cell *97*, 903–915.

Poniatowski, Ł.A., Wojdasiewicz, P., Krawczyk, M., Szukiewicz, D., Gasik, R., Kubaszewski, Ł., and Kurkowska-Jastrzębska, I. (2016). Analysis of the Role of CX3CL1 (Fractalkine) and Its Receptor CX3CR1 in Traumatic Brain and Spinal Cord Injury: Insight into Recent Advances in Actions of Neurochemokine Agents. Mol. Neurobiol. 1–22.

Prestoz, L., Chatzopoulou, E., Lemkine, G., Spassky, N., Lebras, B., Kagawa, T., Ikenaka, K., Zalc, B., and Thomas, J.L. (2004). Control of axonophilic migration of oligodendrocyte precursor cells by Eph-ephrin interaction. Neuron Glia Biol *1*, 73–83.

Puchert, M., and Engele, J. (2014). The peculiarities of the SDF-1/CXCL12 system: in some cells, CXCR4 and CXCR7 sing solos, in others, they sing duets. Cell Tissue Res. *355*, 239–253.

Pugliatti, M., Sotgiu, S., and Rosati, G. (2002). The worldwide prevalence of multiple sclerosis. Clin. Neurol. Neurosurg. *104*, 182–191.

R Core Team (2016). R: A language and environment for statistical computing. Vienna: R Foundation for Statistical Computing; 2014.

Raff, M.C., Durand, B., and Gao, F.B. (1998). Cell number control and timing in animal development: the oligodendrocyte cell lineage. Int. J. Dev. Biol. *42*, 263–267.

Rao, M.S. (1999). Multipotent and restricted precursors in the central nervous system. Anat. Rec. *257*, 137–148.

Rao, M.S., Noble, M., and Mayer-Pröschel, M. (1998). A tripotential glial precursor cell is present in the developing spinal cord. Proc. Natl. Acad. Sci. U. S. A. *95*, 3996–4001.

Raport, C.J., Schweickart, V.L., Eddy, J., Shows, T.B., and Gray, P.W. (1995). The orphan G-protein-coupled receptor-encoding gene V28 is closely related to genes for chemokine receptors and is expressed in lymphoid and neural tissues. Gene *163*, 295–299.

Raychaudhuri, S., Stuart, J.M., and Altman, R.B. (2000). Principal components analysis to summarize microarray experiments: application to sporulation time series. Pac. Symp. Biocomput. Pac. Symp. Biocomput. 455–466.

Readhead, C., and Hood, L. (1990). The dysmyelinating mouse mutations shiverer (shi) and myelin deficient (shimld). Behav. Genet. *20*, 213–234.

Redwine, J.M., and Armstrong, R.C. (1998). In vivo proliferation of oligodendrocyte progenitors expressing PDGFalphaR during early remyelination. J. Neurobiol. *37*, 413–428.

Ricard, D., Rogemond, V., Charrier, E., Aguera, M., Bagnard, D., Belin, M.-F., Thomasset, N., and Honnorat, J. (2001). Isolation and expression pattern of human Unc-33-like phosphoprotein 6/collapsin response mediator protein 5 (Ulip6/CRMP5): Coexistence with Ulip2/CRMP2 in Sema3A-sensitive oligodendrocytes. J. Neurosci. *21*, 7203–7214.

Richardson, W.D., Smith, H.K., Sun, T., Pringle, N.P., Hall, A., and Woodruff, R. (2000). Oligodendrocyte lineage and the motor neuron connection. Glia *29*, 136–142.

Richardson, W.D., Kessaris, N., and Pringle, N. (2006). Oligodendrocyte wars. Nat. Rev. Neurosci. *7*, 11–18.

Ridderstad Wollberg, A., Ericsson-Dahlstrand, A., Juréus, A., Ekerot, P., Simon, S., Nilsson, M., Wiklund, S.-J., Berg, A.-L., Ferm, M., Sunnemark, D., et al. (2014). Pharmacological inhibition of the chemokine receptor CX3CR1 attenuates disease in a chronic-relapsing rat model for multiple sclerosis. Proc. Natl. Acad. Sci. U. S. A. *111*, 5409–5414.

Ristori, G., Cannoni, S., Stazi, M.A., Vanacore, N., Cotichini, R., Alfò, M., Pugliatti, M., Sotgiu, S., Solaro, C., Bomprezzi, R., et al. (2006). Multiple sclerosis in twins from continental Italy and Sardinia: a nationwide study. Ann. Neurol. *59*, 27–34.

Ritchie, M.E., Silver, J., Oshlack, A., Holmes, M., Diyagama, D., Holloway, A., and Smyth, G.K. (2007). A comparison of background correction methods for two-colour microarrays. Bioinformatics *23*, 2700–2707.

Ritchie, M.E., Phipson, B., Wu, D., Hu, Y., Law, C.W., Shi, W., and Smyth, G.K. (2015). limma powers differential expression analyses for RNA-sequencing and microarray studies. Nucleic Acids Res. *43*, e47.

Rittchen, S., Boyd, A., Burns, A., Park, J., Fahmy, T.M., Metcalfe, S., and Williams, A. (2015). Myelin repair in vivo is increased by targeting oligodendrocyte precursor cells with nanoparticles encapsulating leukaemia inhibitory factor (LIF). Biomaterials *56*, 78–85.

Rivest, S. (2015). CX3CR1 in multiple sclerosis. Oncotarget *6*, 19946–19947.

Sadovnick, A.D., Duquette, P., Herrera, B., Yee, I.M.L., and Ebers, G.C. (2007). A timing-of-birth effect on multiple sclerosis clinical phenotype. Neurology *69*, 60–62.

Saga, Y., Yagi, T., Ikawa, Y., Sakakura, T., and Aizawa, S. (1992). Mice develop normally without tenascin. Genes Dev. *6*, 1821–1831.

Santpere, G., Darre, F., Blanco, S., Alcami, A., Villoslada, P., Mar Albà, M., and Navarro, A. (2014). Genome-wide analysis of wild-type Epstein-Barr virus genomes derived from healthy individuals of the 1,000 Genomes Project. Genome Biol. Evol. *6*, 846–860.

Schena, M., Shalon, D., Davis, R.W., and Brown, P.O. (1995). Quantitative Monitoring of Gene Expression Patterns with a Complementary DNA Microarray. Science *270*, 467–470.

Serafini, B., Rosicarelli, B., Franciotta, D., Magliozzi, R., Reynolds, R., Cinque, P., Andreoni, L., Trivedi, P., Salvetti, M., Faggioni, A., et al. (2007). Dysregulated Epstein-Barr virus infection in the multiple sclerosis brain. J. Exp. Med. *204*, 2899–2912.

Shen, S., Sandoval, J., Swiss, V.A., Li, J., Dupree, J., Franklin, R.J.M., and Casaccia-Bonnefil, P. (2008). Age-dependent epigenetic control of differentiation inhibitors is critical for remyelination efficiency. Nat. Neurosci. *11*, 1024–1034.

Shimogori, T., Banuchi, V., Ng, H.Y., Strauss, J.B., and Grove, E.A. (2004). Embryonic signaling centers expressing BMP, WNT and FGF proteins interact to pattern the cerebral cortex. Dev. Camb. Engl. *131*, 5639–5647.

Sim, F.J., Zhao, C., Penderis, J., and Franklin, R.J.M. (2002). The age-related decrease in CNS remyelination efficiency is attributable to an impairment of both oligodendrocyte progenitor recruitment and differentiation. J. Neurosci. Off. J. Soc. Neurosci. *22*, 2451–2459.

Sim, F.J., Lang, J.K., Waldau, B., Roy, N.S., Schwartz, T.E., Pilcher, W.H., Chandross, K.J., Natesan, S., Merrill, J.E., Goldman, S.A., et al. (2006). Complementary patterns of gene expression by human oligodendrocyte progenitors and their environment predict determinants of progenitor maintenance and differentiation. Ann. Neurol. *59*, 763–779.

Sim, F.J., McClain, C.R., Schanz, S.J., Protack, T.L., Windrem, M.S., and Goldman, S.A. (2011). CD140a identifies a population of highly myelinogenic, migration-competent and efficiently engrafting human oligodendrocyte progenitor cells. Nat. Biotechnol. *29*, 934–941.

Simpson, P.B., and Armstrong, R.C. (1999). Intracellular signals and cytoskeletal elements involved in oligodendrocyte progenitor migration. GLIA *26*, 22–35.

Sinclair, H. (1977). Polyunsaturated fatty acids in multiple sclerosis. Br. Med. J. *2*, 1217.

Smyth, G.K. (2004). Linear models and empirical bayes methods for assessing differential expression in microarray experiments. Stat. Appl. Genet. Mol. Biol. *3*, Article3.

Sousa, V.H., and Fishell, G. (2010). Sonic hedgehog functions through dynamic changes in temporal competence in the developing forebrain. Curr. Opin. Genet. Dev. *20*, 391–399.

Spassky, N., Olivier, C., Cobos, I., LeBras, B., Goujet-Zalc, C., Martínez, S., Zalc, B., and Thomas, J.-L. (2001). The Early Steps of Oligodendrogenesis: Insights from the Study of the plp Lineage in the Brain of Chicks and Rodents. Dev. Neurosci. *23*, 318–326.

Spassky, N., de Castro, F., Le Bras, B., Heydon, K., Quéraud-LeSaux, F., Bloch-Gallego, E., Chédotal, A., Zalc, B., and Thomas, J.-L. (2002). Directional guidance of oligodendroglial migration by class 3 semaphorins and netrin-1. J. Neurosci. Off. J. Soc. Neurosci. *22*, 5992–6004.

Sriram, S. (2011). Role of glial cells in innate immunity and their role in CNS demyelination. J. Neuroimmunol. *239*, 13–20.

Staples, J., Ponsonby, A.-L., and Lim, L. (2010). Low maternal exposure to ultraviolet radiation in pregnancy, month of birth, and risk of multiple sclerosis in offspring: longitudinal analysis. BMJ *340*, c1640.

Stojković, L., Djurić, T., Stanković, A., Dinčić, E., Stančić, O., Veljković, N., Alavantić, D., and Živković, M. (2012). The association of V249I and T280M fractalkine receptor haplotypes with disease course of multiple sclerosis. J. Neuroimmunol. *245*, 87–92.

Stys, P.K., Zamponi, G.W., van Minnen, J., and Geurts, J.J.G. (2012). Will the real multiple sclerosis please stand up? Nat. Rev. Neurosci. *13*, 507–514.

Sugimoto, Y., Taniguchi, M., Yagi, T., Akagi, Y., Nojyo, Y., and Tamamaki, N. (2001). Guidance of glial precursor cell migration by secreted cues in the developing optic nerve. Dev. Camb. Engl. *128*, 3321–3330.

Sundqvist, E., Sundström, P., Lindén, M., Hedström, A.K., Aloisi, F., Hillert, J., Kockum, I., Alfredsson, L., and Olsson, T. (2012). Epstein-Barr virus and multiple sclerosis: interaction with HLA. Genes Immun. *13*, 14–20.

Sunnemark, D., Eltayeb, S., Nilsson, M., Wallström, E., Lassmann, H., Olsson, T., Berg, A.-L., and Ericsson-Dahlstrand, A. (2005). CX3CL1 (fractalkine) and CX3CR1 expression in myelin oligodendrocyte glycoprotein-induced experimental autoimmune encephalomyelitis: kinetics and cellular origin. J. Neuroinflammation *2*, 17.

Sussman, C.R., Dyer, K.L., Marchionni, M., and Miller, R.H. (2000). Local control of oligodendrocyte development in isolated dorsal mouse spinal cord. J. Neurosci. Res. *59*, 413–420.

Takahashi, C., Muramatsu, R., Fujimura, H., Mochizuki, H., and Yamashita, T. (2013). Prostacyclin promotes oligodendrocyte precursor recruitment and remyelination after spinal cord demyelination. Cell Death Dis. *4*, e795.

Takakuwa, T., Luo, W.-J., Ham, M.F., Sakane-Ishikawa, F., Wada, N., and Aozasa, K. (2004). Integration of Epstein-Barr virus into chromosome 6q15 of Burkitt lymphoma cell line (Raji) induces loss of BACH2 expression. Am. J. Pathol. *164*, 967–974.

Takebayashi, H., Yoshida, S., Sugimori, M., Kosako, H., Kominami, R., Nakafuku, M., and Nabeshima, Y. (2000). Dynamic expression of basic helix-loop-helix Olig family members:

implication of Olig2 in neuron and oligodendrocyte differentiation and identification of a new member, Olig3. Mech. Dev. *99*, 143–148.

Takebayashi, H., Nabeshima, Y., Yoshida, S., Chisaka, O., Ikenaka, K., and Nabeshima, Y. (2002). The Basic Helix-Loop-Helix Factor Olig2 Is Essential for the Development of Motoneuron and Oligodendrocyte Lineages. Curr. Biol. *12*, 1157–1163.

Tasaki, I. (1939). The electro-saltatory transmission of the nerve impulse and the effect of narcosis upton the nerve fiber. Am. J. Physiol. *127*, 211–227.

Tekki-Kessaris, N., Woodruff, R., Hall, A.C., Gaffield, W., Kimura, S., Stiles, C.D., Rowitch, D.H., and Richardson, W.D. (2001). Hedgehog-dependent oligodendrocyte lineage specification in the telencephalon. Dev. Camb. Engl. *128*, 2545–2554.

Templer, D.I., Trent, N.H., Spencer, D.A., Trent, A., Corgiat, M.D., Mortensen, P.B., and Gorton, M. (1992). Season of birth in multiple sclerosis. Acta Neurol. Scand. *85*, 107–109.

Tepavčević, V., Kerninon, C., Aigrot, M.S., Meppiel, E., Mozafari, S., Arnould-Laurent, R., Ravassard, P., Kennedy, T.E., Nait-Oumesmar, B., and Lubetzki, C. (2014). Early netrin-1 expression impairs central nervous system remyelination. Ann. Neurol. *76*, 252–268.

Tiwari-Woodruff, S.K., Buznikov, A.G., Vu, T.Q., Micevych, P.E., Chen, K., Kornblum, H.I., and Bronstein, J.M. (2001). OSP/claudin-11 forms a complex with a novel member of the tetraspanin super family and β1 integrin and regulates proliferation and migration of oligodendrocytes. J. Cell Biol. *153*, 295–305.

Torkildsen, O., Aarseth, J., Benjaminsen, E., Celius, E., Holmøy, T., Kampman, M.T., Løken-Amsrud, K., Midgard, R., Myhr, K.-M., Riise, T., et al. (2014). Month of birth and risk of multiple sclerosis: confounding and adjustments. Ann. Clin. Transl. Neurol. *1*, 141–144.

Tripathi, R.B., Rivers, L.E., Young, K.M., Jamen, F., and Richardson, W.D. (2010). NG2 glia generate new oligodendrocytes but few astrocytes in a murine experimental autoimmune encephalomyelitis model of demyelinating disease. J. Neurosci. Off. J. Soc. Neurosci. *30*, 16383–16390.

Tripathi, R.B., Clarke, L.E., Burzomato, V., Kessaris, N., Anderson, P.N., Attwell, D., and Richardson, W.D. (2011). Dorsally and ventrally derived oligodendrocytes have similar electrical properties but myelinate preferred tracts. J. Neurosci. Off. J. Soc. Neurosci. *31*, 6809–6819.

Tsai, H.-H., Frost, E., To, V., Robinson, S., Ffrench-Constant, C., Geertman, R., Ransohoff, R.M., and Miller, R.H. (2002). The chemokine receptor CXCR2 controls positioning of oligodendrocyte precursors in developing spinal cord by arresting their migration. Cell *110*, 373–383.

Tsai, H.-H., Tessier-Lavigne, M., and Miller, R.H. (2003). Netrin 1 mediates spinal cord oligodendrocyte precursor dispersal. Development *130*, 2095–2105.

Tweedy, L., Susanto, O., and Insall, R.H. (2016). Self-generated chemotactic gradients — cells steering themselves. Curr. Opin. Cell Biol. *42*, 46–51.

Vallstedt, A., Muhr, J., Pattyn, A., Pierani, A., Mendelsohn, M., Sander, M., Jessell, T.M., and Ericson, J. (2001). Different levels of repressor activity assign redundant and specific roles to Nkx6 genes in motor neuron and interneuron specification. Neuron *31*, 743–755.

Vallstedt, A., Klos, J.M., and Ericson, J. (2005). Multiple dorsoventral origins of oligodendrocyte generation in the spinal cord and hindbrain. Neuron *45*, 55–67.

Virchow, R. (1854). Über das ausgebreitete Vorkommen einer dem Nervenmark analogen Substanz in den tierischen Geweben. Virchows Arch Pathol Anat 562–572.

Werner, D., Atmaca, A., Pauligk, C., Pustowka, A., Jäger, E., and Al-Batran, S.-E. (2013). Phase I study of everolimus and mitomycin C for patients with metastatic esophagogastric adenocarcinoma. Cancer Med. *2*, 325–333.

Wickham, H. (2009). ggplot2: Elegant Graphics for Data Analysis (Springer-Verlag New York).

Willer, C.J., Dyment, D.A., Risch, N.J., Sadovnick, A.D., Ebers, G.C., and Canadian Collaborative Study Group (2003). Twin concordance and sibling recurrence rates in multiple sclerosis. Proc. Natl. Acad. Sci. U. S. A. *100*, 12877–12882.

Willer, C.J., Dyment, D.A., Sadovnick, A.D., Rothwell, P.M., Murray, T.J., Ebers, G.C., and Canadian Collaborative Study Group (2005). Timing of birth and risk of multiple sclerosis: population based study. BMJ *330*, 120.

Williams, A., Piaton, G., Aigrot, M.-S., Belhadi, A., Théaudin, M., Petermann, F., Thomas, J.-L., Zalc, B., and Lubetzki, C. (2007). Semaphorin 3A and 3F: key players in myelin repair in multiple sclerosis? Brain J. Neurol. *130*, 2554–2565.

Williams, J.L., Patel, J.R., Daniels, B.P., and Klein, R.S. (2014). Targeting CXCR7/ACKR3 as a therapeutic strategy to promote remyelination in the adult central nervous system. J. Exp. Med. *211*, 791–799.

Wolswijk, G. (1998). Chronic stage multiple sclerosis lesions contain a relatively quiescent population of oligodendrocyte precursor cells. J. Neurosci. Off. J. Soc. Neurosci. *18*, 601–609.

Woodruff, R.H., and Franklin, R.J.M. (1999). Demyelination and remyelination of the caudal cerebellar peduncle of adult rats following stereotaxic injections of lysolecithin, ethidium bromide, and complement/anti-galactocerebroside: A comparative study. Glia *25*, 216–228.

Woodruff, R.H., Tekki-Kessaris, N., Stiles, C.D., Rowitch, D.H., and Richardson, W.D. (2001). Oligodendrocyte development in the spinal cord and telencephalon: common themes and new perspectives. Int. J. Dev. Neurosci. Off. J. Int. Soc. Dev. Neurosci. *19*, 379–385.

Woodruff, R.H., Fruttiger, M., Richardson, W.D., and Franklin, R.J.M. (2004). Platelet-derived growth factor regulates oligodendrocyte progenitor numbers in adult CNS and their response following CNS demyelination. Mol. Cell. Neurosci. *25*, 252–262.

Wu, G.F., and Alvarez, E. (2011). The immunopathophysiology of multiple sclerosis. Neurol. Clin. *29*, 257–278.

Wynn, D.R., Rodriguez, M., O'Fallon, W.M., and Kurland, L.T. (1990). A reappraisal of the epidemiology of multiple sclerosis in Olmsted County, Minnesota. Neurology *40*, 780–786.

Xing, C., Wang, X., Cheng, C., Montaner, J., Mandeville, E., Leung, W., van Leyen, K., Lok, J., Wang, X., and Lo, E.H. (2014). Neuronal production of lipocalin-2 as a help-me signal for glial activation. Stroke J. Cereb. Circ. *45*, 2085–2092.

Yamaguchi, M., Seki, T., Imayoshi, I., Tamamaki, N., Hayashi, Y., Tatebayashi, Y., and Hitoshi, S. (2016). Neural stem cells and neuro/gliogenesis in the central nervous system: understanding the structural and functional plasticity of the developing, mature, and diseased brain. J. Physiol. Sci. *66*, 197–206.

Yan, H., and Rivkees, S.A. (2002). Hepatocyte growth factor stimulates the proliferation and migration of oligodendrocyte precursor cells. J. Neurosci. Res. *69*, 597–606.

Young, K.M., Psachoulia, K., Tripathi, R.B., Dunn, S.-J., Cossell, L., Attwell, D., Tohyama, K., and Richardson, W.D. (2013). Oligodendrocyte dynamics in the healthy adult CNS: evidence for myelin remodeling. Neuron *77*, 873–885.

Yu, K., McGlynn, S., and Matise, M.P. (2013). Floor plate-derived sonic hedgehog regulates glial and ependymal cell fates in the developing spinal cord. Dev. Camb. Engl. *140*, 1594–1604.

Zappone, M.V., Galli, R., Catena, R., Meani, N., De Biasi, S., Mattei, E., Tiveron, C., Vescovi, A.L., Lovell-Badge, R., Ottolenghi, S., et al. (2000). Sox2 regulatory sequences direct expression of a (beta)-geo transgene to telencephalic neural stem cells and precursors of the mouse embryo, revealing regionalization of gene expression in CNS stem cells. Dev. Camb. Engl. *127*, 2367–2382.

Zawadzka, M., Rivers, L.E., Fancy, S.P.J., Zhao, C., Tripathi, R., Jamen, F., Young, K., Goncharevich, A., Pohl, H., Rizzi, M., et al. (2010). CNS-resident glial progenitor/stem cells produce Schwann cells as well as oligodendrocytes during repair of CNS demyelination. Cell Stem Cell *6*, 578–590.

Zhang, H., Vutskits, L., Pepper, M.S., and Kiss, J.Z. (2003). VEGF is a chemoattractant for FGF-2-stimulated neural progenitors. J. Cell Biol. *163*, 1375–1384.

Zhang, H., Vutskits, L., Calaora, V., Durbec, P., and Kiss, J.Z. (2004). A role for the polysialic acid-neural cell adhesion molecule in PDGF-induced chemotaxis of oligodendrocyte precursor cells. J. Cell Sci. *117*, 93–103.

Zhang, Y., Chen, K., Sloan, S.A., Bennett, M.L., Scholze, A.R., O'Keeffe, S., Phatnani, H.P., Guarnieri, P., Caneda, C., Ruderisch, N., et al. (2014). An RNA-sequencing transcriptome and splicing database of glia, neurons, and vascular cells of the cerebral cortex. J. Neurosci. Off. J. Soc. Neurosci. *34*, 11929–11947.

Zhang, Y., Sloan, S.A., Clarke, L.E., Caneda, C., Plaza, C.A., Blumenthal, P.D., Vogel, H., Steinberg, G.K., Edwards, M.S.B., Li, G., et al. (2016). Purification and Characterization of Progenitor and Mature Human Astrocytes Reveals Transcriptional and Functional Differences with Mouse. Neuron *89*, 37–53.

Zhou, Q., Wang, S., and Anderson, D.J. (2000). Identification of a novel family of oligodendrocyte lineage-specific basic helix-loop-helix transcription factors. Neuron *25*, 331–343.

Zieker, D., Bühler, S., Ustündag, Z., Königsrainer, I., Manncke, S., Bajaeifer, K., Vollmer, J., Fend, F., Northoff, H., Königsrainer, A., et al. (2013). Induction of tumor stem cell differentiation--novel strategy to overcome therapy resistance in gastric cancer. Langenbecks Arch. Surg. *398*, 603–608.

http://www.genomics.agilent.com/article.jsp?crumbAction=push&pageId=1520 (2015). http://www.genomics.agilent.com/article.jsp?crumbAction=push&pageId=1520.

# Abbreviations

| Abbreviation | Definition |
|---|---|
| WT | Wild Type |
| VPN | Virtual Private Network |
| VEGF | Vascular Endothelial Growth Factor |
| TUNEL | Terminal deoxynucleotidyl transferase dUTP nick end labelling |
| TNFα | Tumour Necrosis Factor Alpha |
| TBST | Tris Buffered Saline |
| SVZ | Sub-ventricular Zone |
| strep | Streptomycin |
| Srebf1 | Sterol Regulatory Element Binding Transcription Factor 1 |
| SRA | Sequence Read Archive |
| SP | Secondary Progressive |
| Sox10 | SRY-Box 10 |
| Shh | Sonic Hedgehog |
| Sema | Semaphorin |
| SEM | Standard Error of Mean |
| SDS | Sodium Dodecyl Sulphate |
| RXR-γ | Retinoic acid receptor gamma |
| RT-PCR | Reverse Transcription Polymerase Chain Reaction |
| RTCA | Real-Time Cell Analysis |
| RT | Room Temperature |
| RR | Relapsing and Remitting |
| RPM | Revolutions Per Minute |
| RNA-seq | Ribonucleic Acid Sequencing |
| RNA | Ribonucleic Acid |
| RIPA | Radioimmunoprecipitation Assay |
| qPCR | Quantitative Polymerase Chain Reaction |
| PVDF | Polyvinylidene Fluoride |
| PTPRZ1 | Protein Tyrosine Phosphatase, Receptor Type Z1 |
| PTPRZ1 | Receptor Tyrosine Phosphatase Z1 |
| PNS | Peripheral Nervous System |
| PNG | Portable Network Graphic |
| PLP | Proteolipid Protein |
| PI | Protease Inhibitor |
| PGI2 | Prostacyclin/prostaglandin-I2 |
| PFA | Paraformaldehyde |
| pen | Penicillin |
| PDL | poly-D-lysine |
| PDGFα | Platelet Derived Growth Factor Alpha |
| PDGFRα | Platelet Derived Growth Factor Receptor Alpha |
| PCNA | Proliferating Cell Nuclear Antigen |
| PCA | Principal Component Analysis |
| PC | Principal Component |
| PBST | PBS + 0.05% tween |
| PBS | Phosphate-Buffered Saline |

| | |
|---|---|
| Pax7 | paired box protein 7 |
| OPC | Oligodendrocyte Precursor Cell |
| Olig2 | Oligodendrocyte Lineage Transcription Factor 2 |
| $^{o}$C | Degrees Centigrade |
| Ntrk3 | Neurotrophic Receptor Tyrosine Kinase 3 |
| NSCs | Neural Stem Cells |
| NG2 | Neuron-Glial Antigen 2 |
| NAWM | Normal-appearing White Matter |
| Msx3 | murine msh homeobox 3 |
| MS | Multiple Sclerosis |
| mRNA | Messenger Ribonucleic Acid |
| MRI | Magnetic Resonance Imaging |
| MOG | myelin oligodendrocyte glycoprotein |
| ml | Millilitre |
| MHCII | Major Histocompatibility Class II |
| MGE | Medial Ganglionic Eminence |
| mg | Milligram |
| MEM | Minimum Essential Medium |
| MBP | Myelin Basic Protein |
| MAG | myelin associated glycoprotein |
| Ltbr | Lymphotoxin beta receptor |
| LPC | Lysophosphatidylcholine |
| LINGO-1 | Leucine rich repeat and Immunoglobin-like domain-containing protein 1 |
| LIF | Leukaemia Inhibitory Factor |
| LCN2 | Lipocalin-2 |
| kg | Kilogram |
| kDa | Kilodalton |
| JSON | JavaScript Object Notation |
| js | JavaScript |
| IUPHAR | International Union of Basic and Clinical Pharmacology |
| ITS | Insulin-transferrin-sodium selenite media supplement |
| IP Receptor | Prostacyclin receptor |
| IL1β | Interleukin-1β |
| IFNγ | Interferon Gamma |
| ICC | Immunocytochemistry |
| HUVECS | Human Umbilical Vein Endothelial Cells |
| HTML | HyperText Markup Language |
| HIHS | Heat Inactivated Horse Serum |
| HGF | Hepatocyte Growth Factor |
| HEPES | 4-(2-hydroxyethyl)-1-piperazineethanesulfonic acid |
| GUI | Graphical User Interface |
| Gsh2 | genetic screened homeobox protein 2 |
| Grm5 | Glutamate Metabotropic Receptor 5 |
| GFP | Green Fluorescent Protein |
| GFAP | Glial fibrillary acidic protein |
| GEO | Gene Expression Omnibus |
| GAPDH | Glyceraldehyde 3-phosphate dehydrogenase |
| Fzd1 | Frizzled Class Receptor 1 |

| | |
|---|---|
| FPKM | Fragments Per Kilobase of exon per Million fragments mapped |
| FIJI | Fiji Is Just ImageJ |
| Fgfr1 | Fibroblast Growth Factor Receptor 1 |
| FGF8 | Fibroblast growth factor 8 |
| FGF2 | Fibroblast Growth Factor 2 |
| FBS | Foetal Bovine Serum |
| Emx1 | Empty Spiracles Homeobox 1 protein |
| EGF | Epidermal Growth Factor |
| ECM | Extracellular matrix |
| ECL | Enhanced Chemoluminescence |
| EAE | Experimental Autoimmune Encephalitis |
| EAE | Experimental Autoimmune Encephalomyelitis |
| dpl | Days Post lesion |
| DNA | Deoxyribonucleic Acid |
| DMEM | Dulbecco's modified Eagle medium |
| DCC | Deleted in Colorectal Cancer |
| DBX1 | developing brain homeobox 1 |
| Darc | Duffy antigen receptor for chemokines |
| CXCR7 | C-X-C chemokine receptor type 7 |
| CXCR4 | C-X-C chemokine receptor type 4 |
| CXCL12 | C-X-C motif chemokine 12 |
| CX3CR1 | CX3C chemokine receptor 1 |
| CSV | Comma-separated Variables |
| CSS | Cascading Style Sheets |
| CSF | Cerebrospinal Fluid |
| $CO_2$ | Carbon Dioxide |
| CNTN1 | Contactin-1 |
| CNS | Central Nervous System |
| CNP | 2',3'-Cyclic nucleotide 3'-phosphodiesterase |
| cm | Centimetre |
| CIM | Cell Invasion Migration |
| CI | Cell Index |
| CGI | Common Gateway Interface |
| CD68 | Cluster of Differentiation 68 |
| CD4 | Cluster of Differentiation 4 |
| CD28 | Cluster of Differentiation 28 |
| CCP | Caudal Cerebellar Peduncle |
| CCL2 | Chemokine (C-C motif) ligand 2 |
| CC | Corpus Callosum |
| BSA | Bovine Serum Albumin |
| BPS | British Pharmacological Society |
| BCA | Bicinchoninic Acid Assay |
| BBB | Blood Brain Barrier |
| Axl | AXL Receptor Tyrosine Kinase |
| Amps | Amperes |
| µl | Microlitre |
| µg | Microgram |

# Appendices

**Huang, Jarjour et al., 2011 Data**

The following tables detail the 10 genes which contribute most to each of the principal components identified for this data set (see **Chapter 3.2.3**).

A ninth principal component was also identified, but this has been omitted here because with a standard deviation of 1.673e-13, its contribution to overall variance is negligible (see **appendix figure 1**).

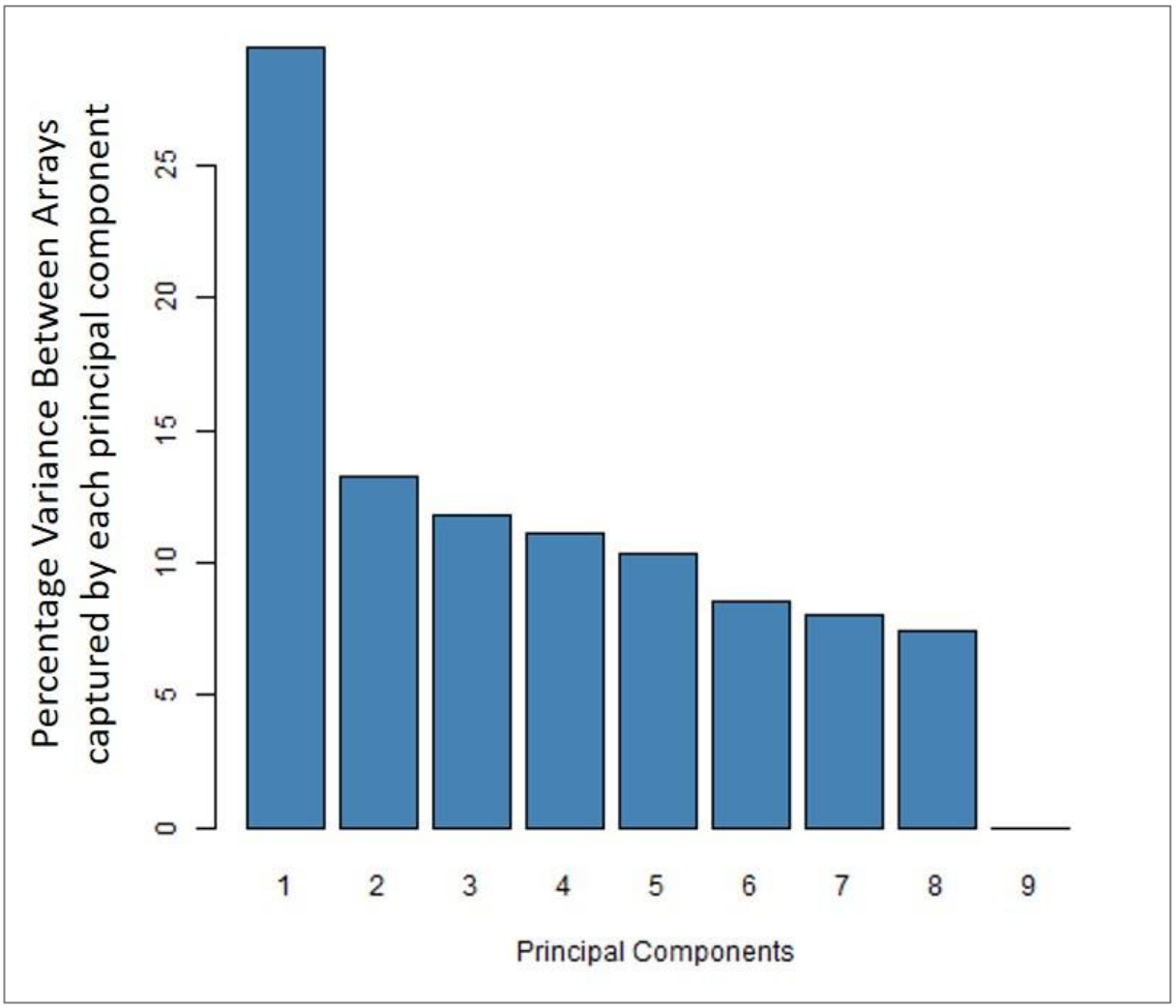


**Appendix figure 1. Percentage of variance between arrays in Huang, Jarjour et al., 2011 data captured by each principal component** PC1captures most of the variation and PC2-PC8 each capture a smaller portion of the variation, PC9 captures almost no variation.

Gene Names and Gene Descriptions are taken from the annotation file for the Illumina ratRef-12 v1.5.0.34 expression bead chip (GEO Accession: GPL8031). Blank cells indicate features which were not fully annotated for this chip release.

**Principal Component 1 -** Accounting for 29.51 % of variance between arrays

| Gene Name | Gene Description | Contribution to Variation (scale -1 to 1) |
|---|---|---|
| Vps36 | vacuolar protein sorting 36 homolog (S. cerevisiae) | 0.012282536 |
| Ier3 | immediate early response 3 | 0.012243057 |
| Sh3bgrl3 | SH3 domain binding glutamate-rich protein like 3 | 0.012222004 |
| | | 0.012221 |
| Mthfs | 5,10-methenyltetrahydrofolate synthetase (5-formyltetrahydrofolate cyclo-ligase) | 0.012220175 |
| Nipsnap3b | nipsnap homolog 3B (C. elegans) | 0.012218185 |
| Naaa | N-acylethanolamine acid amidase | 0.012201257 |
| Iqgap3 | IQ motif containing GTPase activating protein 3 | 0.012193254 |
| Ddx3x | DEAD (Asp-Glu-Ala-Asp) box helicase 3, X-linked | 0.012184154 |
| Emg1 | EMG1 N1-specific pseudouridine methyltransferase | 0.012182846 |

**Principal Component 2 -** Accounting for 13.24 % of variance between arrays

| Gene Name | Gene Description | Contribution to Variation |
|---|---|---|

| | | |
|---|---|---|
| | | (scale -1 to 1) |
| Aig1 | androgen-induced 1 | 0.017414378 |
| Ubac1 | UBA domain containing 1 | 0.017391747 |
| Lbx1 | ladybird homeobox 1 | 0.017339586 |
| Plekhm2 | pleckstrin homology domain containing, family M (with RUN domain) member 2 | 0.017248307 |
| Gripap1 | GRIP1 associated protein 1 | 0.016966322 |
| | | 0.01678169 |
| Olr237 | olfactory receptor 237 | 0.016649064 |
| Tmem106c | transmembrane protein 106C | 0.016648837 |
| Nmrk1 | nicotinamide riboside kinase 1 | 0.016646606 |
| | | 0.016604328 |

**Principal Component 3 -** Accounting for 11.81 % of variance between arrays

| Gene Name | Gene Description | Contribution to Variation (scale -1 to 1) |
|---|---|---|
| Vom2r28 | vomeronasal 2 receptor, 28 | 0.018141498 |
| Cdr2l | cerebellar degeneration-related protein 2-like | 0.018016473 |
| Tmem129 | transmembrane protein 129 | 0.017878401 |
| Sp6 | Sp6 transcription factor | 0.017874195 |

| | | |
|---|---|---|
| | | 0.01779482 |
| Ltbp1 | latent transforming growth factor beta binding protein 1 | 0.017647227 |
| Kdm4c | lysine (K)-specific demethylase 4C | 0.017526853 |
| Nupl1 | nucleoporin like 1 | 0.017512411 |
| | | 0.01750277 |
| Olr299 | olfactory receptor 299 | 0.017495608 |

**Principal Component 4 -** Accounting for 11.11 % of variance between arrays

| Gene Name | Gene Description | Contribution to Variation (scale -1 to 1) |
|---|---|---|
| | | 0.019421642 |
| | | 0.019176375 |
| | | 0.019122428 |
| Sema3d | sema domain, immunoglobulin domain (Ig), short basic domain, secreted, (semaphorin) 3D | 0.01905317 |
| Ttl | tubulin tyrosine ligase | 0.01898213 |
| Wfdc6b | WAP four-disulphide core domain 6B | 0.018889488 |
| | | 0.018717846 |
| Parvb | parvin, beta | 0.018458778 |
| Apc2 | adenomatosis polyposis coli 2 | 0.018369191 |
| | | 0.018286988 |

**Principal Component 5 -** Accounting for 10.32 % of variance between arrays

| Gene Name | Gene Description | Contribution to Variation (scale -1 to 1) |
|---|---|---|
| | | 0.020107182 |
| | | 0.019876087 |
| Olr36 | olfactory receptor 36 | 0.019757322 |
| Olr1695 | olfactory receptor 1695 | 0.019254803 |
| | | 0.019119066 |
| | | 0.01883328 |
| | | 0.018638754 |
| | | 0.01854207 |
| Zfp108 | zinc finger protein 108 | 0.018462245 |
| Slc13a1 | solute carrier family 13 (sodium/sulphate symporter), member 1 | 0.018420846 |

**Principal Component 6 -** Accounting for 8.56% of variance between arrays

| Gene Name | Gene Description | Contribution to Variation (scale -1 to 1) |
|---|---|---|
| | | 0.021155288 |
| | | 0.02100968 |

| | | |
|---|---|---|
| | | 0.020966817 |
| | | 0.020843463 |
| | | 0.020267658 |
| Mrpl50 | mitochondrial ribosomal protein L50 | 0.020227086 |
| | | 0.02021823 |
| Lefty1 | left right determination factor 1 | 0.02018212 |
| Foxn1 | forkhead box N1 | 0.020111267 |
| Olr1600 | olfactory receptor 1600 | 0.020107981 |

**Principal Component 7 -** Accounting for 8.05% of variance between arrays

| Gene Name | Gene Description | Contribution to Variation (scale -1 to 1) |
|---|---|---|
| | | 0.021941456 |
| Ak4 | adenylate kinase 4 | 0.021903287 |
| | | 0.0213217 |
| | | 0.021142214 |
| | | 0.020869042 |
| | | 0.020637065 |
| Crocc | ciliary rootlet coiled-coil, rootletin | 0.020283244 |
| Olr103 | olfactory receptor 103 | 0.020131155 |
| | | 0.020039737 |

| | | |
|---|---|---|
| | | 0.019939651 |

**Principal Component 8 -** Accounting for 7.4% of variance between arrays

| Gene Name | Gene Description | Contribution to Variation (scale -1 to 1) |
|---|---|---|
| Bag4 | BCL2-associated athanogene 4 | 0.022817024 |
| | | 0.022597445 |
| Trim24 | tripartite motif-containing 24 | 0.022294023 |
| | | 0.022198888 |
| | | 0.022051752 |
| Prl3d4 | prolactin family 3, subfamily d, member 4 | 0.021947555 |
| | | 0.021883504 |
| | | 0.021870964 |
| Olr92 | olfactory receptor 92 | 0.021487183 |
| | | 0.021455886 |

**Moyon et al., 2015 Data**

The following tables detail the 10 genes which contribute most to each of the principal components identified for this data set (see **Chapter 3.3.5**).

A seventh principal component was also identified, but this has been omitted here because with a standard deviation of 8.668e-12, its contribution to overall variance is negligible (see **appendix figure 2B)**.

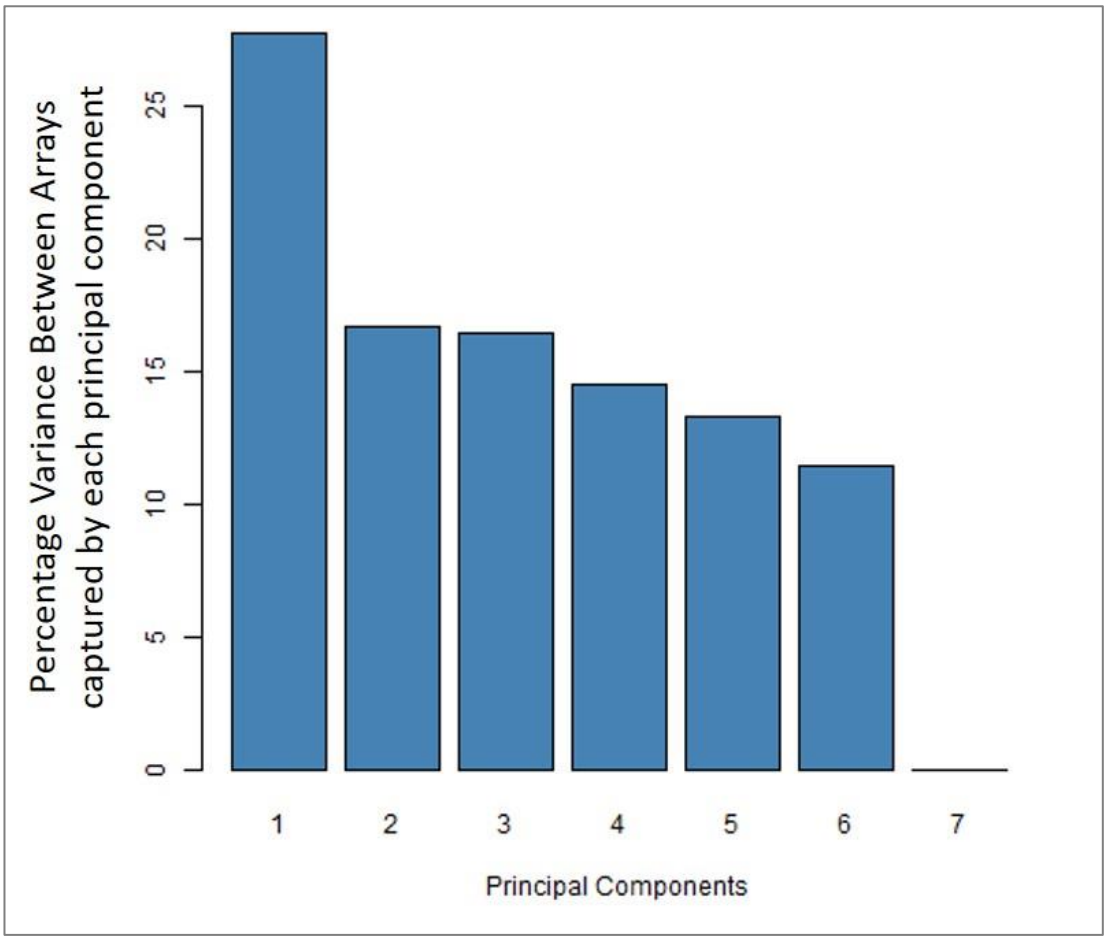


**Appendix figure 2 Percentage of variance between arrays in Moyon et al., 2015 data captured by each principal component** Principal Component Analysis identified six Principal Components which contributed to the variations in the data, Principal Component 1 contributing 17.73%, Principal Component 2 contributing 16.69%, Principal Component 3 contributing 16.39%, Principal Component 4 contributing 14.52%, Principal Component 5 contributing 13.26% and Principal Component 6 contributing 11.41%

Gene Names and Gene Descriptions are taken from the raw data file provided for this data set, GSE48872 on GEO). Blank cells indicate features which were not fully annotated for this chip release.

**Principal Component 1 -** Accounting for 27.74 % of variance between arrays

| Gene Name | Gene Description | Contribution to Variation (scale -1 to 1) |
|---|---|---|
| | Putative uncharacterized protein [Source:UniProtKB/TrEMBL;Acc:Q3UMU7] [ENSMUST00000099292] | 0.008922 |
| Gramd1b | Mus musculus GRAM domain containing 1B (Gramd1b), mRNA [NM_172768] | 0.008905 |
| Defa-rs10 | Mus musculus defensin, alpha, related sequence 10 (Defa-rs10), mRNA [NM_007845] | 0.008888 |
| Synj2 | Mus musculus synaptojanin 2 (Synj2), transcript variant 1, mRNA [NM_001113353] | 0.008866 |
| Krtcap3 | Mus musculus keratinocyte associated protein 3 (Krtcap3), mRNA [NM_027221] | 0.008852 |
| Ypel2 | Mus musculus yippee-like 2 (Drosophila) (Ypel2), mRNA [NM_001005341] | 0.00885 |
| Mast4 | Mus musculus microtubule associated serine/threonine kinase family member 4 (Mast4), mRNA [NM_175171] | 0.008843 |
| Setd7 | Mus musculus SET domain containing (lysine methyltransferase) 7 (Setd7), mRNA [NM_080793] | 0.008842 |
| Trim13 | Mus musculus tripartite motif-containing 13 (Trim13), transcript variant 1, mRNA [NM_001164220] | 0.008839 |
| Fgfr2 | Mus musculus fibroblast growth factor receptor 2 (Fgfr2), | 0.008839 |

| | | |
|---|---|---|
| | transcript variant 1, mRNA [NM_010207] | |

**Principal Component 2 -** Accounting for 16.68 % of variance between arrays

| Gene Name | Gene Description | Contribution to Variation (scale -1 to 1) |
|---|---|---|
| Timm8a1 | Mus musculus translocase of inner mitochondrial membrane 8 homolog a1 (yeast) (Timm8a1), nuclear gene encoding mitochondrial protein, mRNA [NM_013898] | 0.011406 |
| Park7 | Mus musculus Parkinson disease (autosomal recessive, early onset) 7 (Park7), mRNA [NM_020569] | 0.011357 |
| Ndufa7 | Mus musculus NADH dehydrogenase (ubiquinone) 1 alpha subcomplex, 7 (B14.5a) (Ndufa7), mRNA [NM_023202] | 0.011295 |
| Olfr16 | Mus musculus olfactory receptor 16 (Olfr16), mRNA [NM_008763] | 0.011255 |
| BC031181 | Mus musculus cDNA sequence BC031181 (BC031181), mRNA [NM_001001181] | 0.01125 |
| Serpinf1 | Mus musculus serine (or cysteine) peptidase inhibitor, clade F, member 1 (Serpinf1), mRNA [NM_011340] | 0.011247 |
| Spcs2 | Mus musculus signal peptidase complex subunit 2 homolog (S. cerevisiae) (Spcs2), mRNA [NM_025668] | 0.011223 |
| Tpm1 | Mus musculus tropomyosin 1, alpha (Tpm1), transcript variant 1, mRNA [NM_001164248] | 0.011178 |
| | Putative uncharacterized proteinMCG13105, isoform Crab ; [Source:UniProtKB/TrEMBL;Acc:Q9D5E6] [ENSMUST00000094228] | 0.011172 |

| | | |
|---|---|---|
| | Gene name and description as yet uncharacterised | 0.011171 |

**Principal Component 3 -** Accounting for 16.39 % of variance between arrays

| Gene Name | Gene Description | Contribution to Variation (scale -1 to 1) |
|---|---|---|
| St3gal6 | Mus musculus ST3 beta-galactoside alpha-2,3-sialyltransferase 6 (St3gal6), mRNA [NM_018784] | 0.011374 |
| Ccr8 | Mus musculus chemokine (C-C motif) receptor 8 (Ccr8), mRNA [NM_007720] | 0.011347 |
| Pppde1 | Mus musculus PPPDE peptidase domain containing 1 (Pppde1), mRNA [NM_024282] | 0.011342 |
| Kcnj11 | Mus musculus potassium inwardly rectifying channel, subfamily J, member 11 (Kcnj11), mRNA [NM_010602] | 0.011341 |
| LOC100047052 | PREDICTED: Mus musculus similar to Aptx protein (LOC100047052), mRNA [XM_001477288] | 0.011307 |
| Scgb3a1 | Mus musculus secretoglobin, family 3A, member 1 (Scgb3a1), transcript variant B, mRNA [NM_170727] | 0.011271 |
| Calb1 | Calbindin (Vitamin D-dependent calcium-binding protein, avian-type)(Calbindin D28)(D-28K)(Spot 35 protein)(PCD-29) [Source:UniProtKB/Swiss-Prot;Acc:P12658] [ENSMUST00000029876] | 0.011262 |
| Gm10505 | PREDICTED: Mus musculus predicted gene, ENSMUSG00000073430 (ENSMUSG00000073430), mRNA [XM_001472841] | 0.011199 |
| Adam34 | Mus musculus a disintegrin and metallopeptidase domain 34 (Adam34), mRNA [NM_145745] | 0.011193 |
| Klf16 | Mus musculus Kruppel-like factor 16 (Klf16), mRNA [NM_078477] | 0.011174 |

**Principal Component 4 -** Accounting for 14.52 % of variance between arrays

| Gene Name | Gene Description | Contribution to Variation (scale -1 to 1) |
|---|---|---|
| (+)E1A_r60_a107 | | 0.011876 |
| | Ethanolamine-phosphate cytidylyltransferase (EC 2.7.7.14)(Phosphorylethanolamine transferase)(CTP:phosphoethanolamine cytidylyltransferase) [Source:UniProtKB/Swiss-Prot;Acc:Q922E4] [ENSMUST00000106187] | 0.011826 |
| | Putative uncharacterized protein [Source:UniProtKB/TrEMBL;Acc:Q3U0E6] [ENSMUST00000093527] | 0.011749 |
| Lyst | Mus musculus lysosomal trafficking regulator (Lyst), mRNA [NM_010748] | 0.011668 |
| Ankfy1 | Mus musculus ankyrin repeat and FYVE domain containing 1 (Ankfy1), mRNA [NM_009671] | 0.011651 |
| Ttn | Mus musculus titin (Ttn), transcript variant N2-A, mRNA [NM_011652] | 0.011627 |

| | | |
|---|---|---|
| Catsper4 | Mus musculus cation channel, sperm associated 4 (Catsper4), transcript variant 1, mRNA [NM_177866] | 0.011593 |
| Klra5 | Mus musculus killer cell lectin-like receptor, subfamily A, member 5 (Klra5), mRNA [NM_008463] | 0.011561 |
| Ocln | Mus musculus occludin (Ocln), mRNA [NM_008756] | 0.01155 |
| Edem3 | Mus musculus ER degradation enhancer, mannosidase alpha-like 3 (Edem3), mRNA [NM_001039644] | 0.01153 |

**Principal Component 5 -** Accounting for 13.26 % of variance between arrays

| Gene Name | Gene Description | Contribution to Variation (scale -1 to 1) |
|---|---|---|
| Olfr262 | Mus musculus olfactory receptor 262 (Olfr262), mRNA [NM_146688] | 0.012524 |
| Pira3 | Mus musculus paired-Ig-like receptor A3 (Pira3), transcript variant 1, mRNA [NM_011090] | 0.012509 |
| Olfr1504 | Mus musculus olfactory receptor 1504 (Olfr1504), mRNA [NM_146634] | 0.012463 |

| | | |
|---|---|---|
| Olfr860 | Mus musculus olfactory receptor 860 (Olfr860), mRNA [NM_146528] | 0.012449 |
| Icam2 | Mus musculus intercellular adhesion molecule 2 (Icam2), mRNA [NM_010494] | 0.012445 |
| Lep | Mus musculus leptin (Lep), mRNA [NM_008493] | 0.012444 |
| | UPF0249 protein ydjC homolog [Source:UniProtKB/Swiss-Prot;Acc:Q14BV6] [ENSMUST00000115706] | 0.012376 |
| Lin28b | Mus musculus lin-28 homolog B (C. elegans) (Lin28b), mRNA [NM_001031772] | 0.012342 |
| AW413774 | UI-M-AQ0-cix-n-17-0-UI.s1 NIH_BMAP_MHI Mus musculus cDNA clone UI-M-AQ0-cix-n-17-0-UI 3', mRNA sequence [CD775100] | 0.01234 |
| Prrt4 | Mus musculus proline-rich transmembrane protein 4 (Prrt4), mRNA [NM_001101443] | 0.012524 |

**Principal Component 6 -** Accounting for 11.41 % of variance between arrays

| Gene Name | Gene Description | Contribution to Variation (scale -1 to 1) |
|---|---|---|
| Ppfia4 | Mus musculus protein tyrosine phosphatase, receptor type, f polypeptide (PTPRF), interacting protein (liprin), alpha 4 (Ppfia4), mRNA [NM_001144855] | 0.013687 |
| | cadherin 8 isoform 1 [Source:RefSeq peptide;Acc:NP_001034243] [ENSMUST00000109458] | 0.01355 |
| Gm10436 | Mus musculus predicted gene 10436 (Gm10436), mRNA [NM_001105254] | 0.013453 |
| Vwce | Mus musculus von Willebrand factor C and EGF domains (Vwce), mRNA [NM_027913] | 0.01344 |
| 9130023H24Rik | Mus musculus RIKEN cDNA 9130023H24 gene (9130023H24Rik), mRNA [NM_177001] | 0.013416 |
| Gm7157 | PREDICTED: Mus musculus hypothetical LOC635396 (LOC635396), mRNA [XM_001473639] | 0.013369 |
| Rps6ka3 | Mus musculus ribosomal protein S6 kinase polypeptide 3 (Rps6ka3), mRNA [NM_148945] | 0.013323 |
| | Putative uncharacterized protein [Source:UniProtKB/TrEMBL;Acc:Q3U0W5] [ENSMUST00000115260] | 0.013264 |
| | Mus musculus 6E6 monoclonal antibody heavy chain variable region, (IgH) mRNA, partial cds. [AF045501] | 0.013258 |
| Gm7102 | PREDICTED: Mus musculus predicted gene, EG633057 (EG633057), mRNA [XM_907392] | 0.013195 |

## Appendix 2 Secreted Factors Correlating with PDGFα

| Illumina ID | Gene Symbol | Log2 Fold Change | | | | | | Correlation with PDGFα |
|---|---|---|---|---|---|---|---|---|
| | | d28.vs.d5 | d28.vs.d14 | d14.vs.d5 | d14.vs.d28 | d5.vs.d14 | d5.vs.d28 | |
| ILMN_56728 | Pdgfα | 0.757308 | -0.30322 | -0.21195 | 0.303217 | 0.211945 | -0.75731 | 1 |
| ILMN_68952 | Serinc1 | 0.575799 | -0.23147 | -0.15857 | 0.231474 | 0.158565 | -0.5758 | 0.999991 |
| ILMN_52954 | Ift80 | 1.140213 | -0.47344 | -0.31325 | 0.473439 | 0.313254 | -1.14021 | 0.999908 |
| ILMN_53418 | Ldhb | 1.285169 | -0.53626 | -0.38314 | 0.536258 | 0.383139 | -1.28517 | 0.9998 |
| ILMN_56273 | Bnip3 | 0.844723 | -0.32017 | -0.24568 | 0.320166 | 0.245678 | -0.84472 | 0.999775 |
| ILMN_59511 | S100b | 3.381442 | -1.25936 | -0.80733 | 1.259356 | 0.807334 | -3.38144 | 0.99914 |
| ILMN_65990 | Ppp1r14c | 1.376483 | -0.59288 | -0.32966 | 0.592876 | 0.329661 | -1.37648 | 0.998974 |
| ILMN_50866 | Calm3 | 0.676841 | -0.27367 | -0.23161 | 0.273669 | 0.231606 | -0.67684 | 0.998591 |
| ILMN_58575 | Smox | 0.483747 | -0.17176 | -0.15454 | 0.17176 | 0.154541 | -0.48375 | 0.99854 |
| ILMN_53798 | Fbxo2 | 1.171829 | -0.39801 | -0.34353 | 0.398013 | 0.343527 | -1.17183 | 0.998533 |
| ILMN_69508 | Etv1 | 0.754431 | -0.27392 | -0.25858 | 0.273916 | 0.258579 | -0.75443 | 0.99786 |
| ILMN_59598 | Dstyk | 1.045431 | -0.48887 | -0.34881 | 0.488867 | 0.348805 | -1.04543 | 0.997745 |
| ILMN_57362 | Gstm1 | 0.434823 | -0.17493 | -0.15778 | 0.174927 | 0.157781 | -0.43482 | 0.997513 |
| ILMN_63000 | H3f3b | 0.542029 | -0.19941 | -0.19352 | 0.199408 | 0.19352 | -0.54203 | 0.997244 |
| ILMN_60723 | Msl1 | 0.682511 | -0.31422 | -0.24517 | 0.314216 | 0.245169 | -0.68251 | 0.996949 |
| ILMN_49101 | Kank1 | 0.633886 | -0.24818 | -0.23654 | 0.248184 | 0.236537 | -0.63389 | 0.996757 |
| ILMN_69711 | Efcab2 | 0.613548 | -0.23405 | -0.22782 | 0.234053 | 0.227824 | -0.61355 | 0.996699 |
| ILMN_49826 | Rras2 | 0.624546 | -0.18956 | -0.17563 | 0.189561 | 0.175634 | -0.62455 | 0.996495 |
| ILMN_61688 | Olfml2a | 0.803662 | -0.29253 | -0.29851 | 0.292528 | 0.298512 | -0.80366 | 0.99621 |
| ILMN_56986 | Scg3 | 2.068466 | -0.63785 | -0.65832 | 0.637849 | 0.658316 | -2.06847 | 0.996067 |
| ILMN_63650 | Ankrd46 | 0.573237 | -0.22943 | -0.22255 | 0.229428 | 0.222547 | -0.57324 | 0.995794 |
| ILMN_59532 | Hmces | 0.513831 | -0.2252 | -0.19944 | 0.225199 | 0.199441 | -0.51383 | 0.995712 |
| ILMN_70002 | Cdh1 | 2.295962 | -0.68206 | -0.55832 | 0.68206 | 0.558315 | -2.29596 | 0.99569 |
| ILMN_55045 | Add3 | 1.234028 | -0.36878 | -0.38181 | 0.368779 | 0.381809 | -1.23403 | 0.995629 |

| | | | | | | | | |
|---|---|---|---|---|---|---|---|---|
| ILMN_161762 | Fsd1 | 0.647391 | -0.21926 | -0.23633 | 0.219257 | 0.236334 | -0.64739 | 0.995557 |
| ILMN_60221 | Sphk1 | 0.512689 | -0.20696 | -0.20107 | 0.206961 | 0.201074 | -0.51269 | 0.995524 |
| ILMN_58987 | Nqo1 | 1.080322 | -0.35383 | -0.38572 | 0.353833 | 0.385722 | -1.08032 | 0.995447 |
| ILMN_65766 | Lrrn1 | 0.674218 | -0.19843 | -0.20805 | 0.198426 | 0.208046 | -0.67422 | 0.995284 |
| ILMN_50277 | Lppr3 | 0.850471 | -0.33202 | -0.33687 | 0.332021 | 0.336872 | -0.85047 | 0.995041 |
| ILMN_55981 | Zfp191 | 0.822636 | -0.35745 | -0.32886 | 0.357454 | 0.328859 | -0.82264 | 0.994893 |
| ILMN_69655 | Fmo1 | 0.97179 | -0.51131 | -0.31443 | 0.511305 | 0.31443 | -0.97179 | 0.994716 |
| ILMN_57630 | Msmo1 | 1.500514 | -0.43011 | -0.4619 | 0.430105 | 0.461901 | -1.50051 | 0.994645 |
| ILMN_57744 | Fbln5 | 1.851357 | -0.53364 | -0.599 | 0.533641 | 0.598996 | -1.85136 | 0.994249 |
| ILMN_52545 | Fam135a | 0.890648 | -0.46395 | -0.31566 | 0.463949 | 0.315661 | -0.89065 | 0.994175 |
| ILMN_50962 | Fkbp1a | 0.56632 | -0.16136 | -0.18003 | 0.161362 | 0.180034 | -0.56632 | 0.994166 |
| ILMN_60627 | Wfikkn1 | 0.976336 | -0.36007 | -0.39141 | 0.360066 | 0.391411 | -0.97634 | 0.99409 |
| ILMN_67767 | Tars | 0.488348 | -0.14929 | -0.17352 | 0.149295 | 0.173519 | -0.48835 | 0.994068 |
| ILMN_54050 | Pmp22 | 3.369227 | -1.00929 | -1.17943 | 1.009286 | 1.179434 | -3.36923 | 0.993899 |
| ILMN_67298 | Thra | 1.208452 | -0.46691 | -0.49464 | 0.46691 | 0.494644 | -1.20845 | 0.993831 |
| ILMN_161522 | Tmem98 | 1.085483 | -0.29697 | -0.31774 | 0.296972 | 0.317745 | -1.08548 | 0.993756 |
| ILMN_57296 | Mpp6 | 1.82437 | -0.76711 | -0.76189 | 0.767107 | 0.761891 | -1.82437 | 0.993456 |
| ILMN_52052 | Auh | 0.915476 | -0.46603 | -0.35285 | 0.466031 | 0.352846 | -0.91548 | 0.993356 |
| ILMN_52636 | Nedd4 | 0.755968 | -0.20529 | -0.1817 | 0.205293 | 0.181701 | -0.75597 | 0.993354 |
| ILMN_67988 | Lcat | 2.511385 | -0.68233 | -0.58614 | 0.68233 | 0.586138 | -2.51139 | 0.99317 |
| ILMN_60826 | Gltp | 0.510633 | -0.16901 | -0.20151 | 0.169008 | 0.201514 | -0.51063 | 0.992872 |
| ILMN_51725 | Vom2r79 | 1.573979 | -0.58636 | -0.22726 | 0.586358 | 0.227257 | -1.57398 | 0.992562 |
| ILMN_66590 | Tspan33 | 1.095421 | -0.29775 | -0.35825 | 0.297754 | 0.358246 | -1.09542 | 0.992531 |
| ILMN_51890 | Msx1 | 0.647466 | -0.18867 | -0.23519 | 0.188674 | 0.23519 | -0.64747 | 0.992371 |
| ILMN_60514 | Flrt3 | 1.494126 | -0.42382 | -0.28705 | 0.423824 | 0.287049 | -1.49413 | 0.992264 |
| ILMN_63775 | Slc9a6 | 0.901287 | -0.24548 | -0.18729 | 0.245477 | 0.187293 | -0.90129 | 0.992154 |
| ILMN_48364 | Olfml3 | 0.833438 | -0.21509 | -0.24861 | 0.215086 | 0.248612 | -0.83344 | 0.991996 |
| ILMN_52414 | Zfp111 | 0.586089 | -0.15743 | -0.19474 | 0.157434 | 0.194743 | -0.58609 | 0.99196 |

| | | | | | | | | |
|---|---|---|---|---|---|---|---|---|
| ILMN_51350 | RGD1564482 | 1.019166 | -0.32499 | -0.40418 | 0.324995 | 0.404177 | -1.01917 | 0.991919 |
| ILMN_60172 | Eif1b | 0.657883 | -0.22696 | -0.27215 | 0.226962 | 0.272153 | -0.65788 | 0.991911 |
| ILMN_50331 | Rab38 | 0.567792 | -0.14382 | -0.16794 | 0.143815 | 0.167945 | -0.56779 | 0.991498 |
| ILMN_50029 | St3gal2 | 0.579875 | -0.25424 | -0.25468 | 0.254244 | 0.254677 | -0.57988 | 0.991319 |
| ILMN_48088 | Ifitm3 | 1.065912 | -0.27003 | -0.32543 | 0.270025 | 0.325427 | -1.06591 | 0.991274 |
| ILMN_53129 | Mfap5 | 1.01008 | -0.26078 | -0.22183 | 0.260785 | 0.221831 | -1.01008 | 0.991236 |
| ILMN_61532 | Slc16a11 | 0.638946 | -0.20292 | -0.25866 | 0.202915 | 0.258656 | -0.63895 | 0.991078 |
| ILMN_60143 | Katnal1 | 0.548705 | -0.21125 | -0.24043 | 0.211252 | 0.240431 | -0.5487 | 0.990959 |
| ILMN_57534 | Mdga2 | 0.801211 | -0.38174 | -0.35062 | 0.38174 | 0.350617 | -0.80121 | 0.990731 |
| ILMN_55662 | Ispd | 1.483797 | -0.44926 | -0.58896 | 0.449263 | 0.588957 | -1.4838 | 0.990671 |
| ILMN_68729 | Sgcg | 0.631881 | -0.31049 | -0.27434 | 0.310494 | 0.274345 | -0.63188 | 0.990524 |
| ILMN_67593 | Ephb1 | 1.225692 | -0.42207 | -0.52385 | 0.422067 | 0.523845 | -1.22569 | 0.990496 |
| ILMN_48994 | Cbs | 1.395316 | -0.3392 | -0.34681 | 0.3392 | 0.346809 | -1.39532 | 0.990333 |
| ILMN_70295 | Dock6 | 0.337892 | -0.14082 | -0.15189 | 0.14082 | 0.151885 | -0.33789 | 0.990253 |
| ILMN_68478 | Leprel1 | 0.554055 | -0.31683 | -0.13977 | 0.316827 | 0.139773 | -0.55405 | 0.990187 |
| ILMN_68736 | Rab40b | 1.057837 | -0.25631 | -0.3126 | 0.256305 | 0.312595 | -1.05784 | 0.990163 |
| ILMN_70349 | Hspb1 | 1.623773 | -0.40407 | -0.53105 | 0.404074 | 0.531048 | -1.62377 | 0.989953 |
| ILMN_69714 | Gas7 | 2.151464 | -1.24383 | -0.73613 | 1.243835 | 0.736129 | -2.15146 | 0.989911 |
| ILMN_49693 | Gpx7 | 0.472111 | -0.17292 | -0.20954 | 0.172919 | 0.209541 | -0.47211 | 0.989726 |
| ILMN_60484 | Serpina3n | 0.74164 | -0.17599 | -0.21199 | 0.175989 | 0.211988 | -0.74164 | 0.989681 |
| ILMN_48530 | Swap70 | 0.438916 | -0.21876 | -0.1946 | 0.218759 | 0.1946 | -0.43892 | 0.989388 |
| ILMN_48179 | Ifitm6 | 0.628808 | -0.29162 | -0.28733 | 0.291623 | 0.287326 | -0.62881 | 0.989112 |
| ILMN_56934 | Ptges2 | 0.368671 | -0.1791 | -0.16667 | 0.179104 | 0.166674 | -0.36867 | 0.989013 |
| ILMN_66879 | Lingo1 | 0.995876 | -0.22939 | -0.26901 | 0.229388 | 0.269008 | -0.99588 | 0.988853 |
| ILMN_62037 | Zfp61 | 0.602912 | -0.13867 | -0.1689 | 0.138672 | 0.168897 | -0.60291 | 0.988764 |
| ILMN_61591 | Myh14 | 1.884044 | -0.758 | -0.87438 | 0.758002 | 0.87438 | -1.88404 | 0.988412 |
| ILMN_48846 | Mbp | 3.174381 | -1.64318 | -1.41215 | 1.64318 | 1.412151 | -3.17438 | 0.988345 |
| ILMN_61213 | Pja2 | 0.54123 | -0.1607 | -0.22797 | 0.160701 | 0.227968 | -0.54123 | 0.987805 |

| | | | | | | | | |
|---|---|---|---|---|---|---|---|---|
| ILMN_50141 | Camk2n1 | 2.104289 | -0.4751 | -0.63878 | 0.475102 | 0.638781 | -2.10429 | 0.987758 |
| ILMN_56539 | Slc13a3 | 0.960586 | -0.36637 | -0.44858 | 0.36637 | 0.448585 | -0.96059 | 0.987544 |
| ILMN_53466 | Chd6 | 0.506475 | -0.28571 | -0.21413 | 0.285712 | 0.214133 | -0.50648 | 0.987145 |
| ILMN_63176 | Camk2g | 0.867561 | -0.20679 | -0.15857 | 0.206791 | 0.158574 | -0.86756 | 0.986685 |
| ILMN_63705 | Gadd45a | 0.992869 | -0.48884 | -0.46958 | 0.488842 | 0.469585 | -0.99287 | 0.986583 |
| ILMN_52973 | Socs5 | 1.117396 | -0.2389 | -0.3165 | 0.238899 | 0.316502 | -1.1174 | 0.986392 |
| ILMN_54579 | Cspg4 | 0.717346 | -0.15291 | -0.1879 | 0.152912 | 0.187899 | -0.71735 | 0.986348 |
| ILMN_63299 | Rcn2 | 0.300591 | -0.1262 | -0.1452 | 0.126197 | 0.145205 | -0.30059 | 0.986324 |
| ILMN_50820 | Pik3ip1 | 0.691546 | -0.39426 | -0.29635 | 0.394265 | 0.296347 | -0.69155 | 0.986245 |
| ILMN_49961 | Tenm3 | 0.937817 | -0.35838 | -0.44947 | 0.358376 | 0.44947 | -0.93782 | 0.98602 |
| ILMN_53457 | Cabp2 | 0.472332 | -0.20493 | -0.23026 | 0.204934 | 0.230261 | -0.47233 | 0.985837 |
| ILMN_64601 | Ephx1 | 0.691564 | -0.31636 | -0.33745 | 0.316357 | 0.337452 | -0.69156 | 0.985647 |
| ILMN_66945 | S100a16 | 1.312002 | -0.81678 | -0.41788 | 0.816784 | 0.417883 | -1.312 | 0.985519 |
| ILMN_61454 | Gjc3 | 1.277384 | -0.52735 | -0.62988 | 0.527353 | 0.629876 | -1.27738 | 0.984943 |
| ILMN_67098 | Hsd17b8 | 0.338193 | -0.1855 | -0.15763 | 0.185495 | 0.157632 | -0.33819 | 0.984534 |
| ILMN_48324 | Sbds | 0.95934 | -0.4738 | -0.47121 | 0.473797 | 0.471213 | -0.95934 | 0.984438 |
| ILMN_64613 | Ntng1 | 0.915651 | -0.54775 | -0.38464 | 0.54775 | 0.384642 | -0.91565 | 0.984411 |
| ILMN_50322 | Map1lc3a | 0.612286 | -0.20661 | -0.29141 | 0.20661 | 0.291413 | -0.61229 | 0.984323 |
| ILMN_61374 | Arhgap12 | 0.340517 | -0.18375 | -0.16224 | 0.18375 | 0.162239 | -0.34052 | 0.984023 |
| ILMN_64243 | Cntn1 | 1.000261 | -0.3005 | -0.46529 | 0.300503 | 0.465289 | -1.00026 | 0.982935 |
| ILMN_63421 | Kcnmb4 | 1.218446 | -0.30485 | -0.51268 | 0.304845 | 0.512679 | -1.21845 | 0.982887 |
| ILMN_51080 | Col5a2 | 1.940938 | -0.58372 | -0.90918 | 0.583725 | 0.909182 | -1.94094 | 0.982537 |
| ILMN_66097 | Slc9a3r2 | 0.349734 | -0.15221 | -0.18094 | 0.15221 | 0.180937 | -0.34973 | 0.981856 |
| ILMN_60885 | Gabbr1 | 0.623019 | -0.22913 | -0.31556 | 0.229126 | 0.315562 | -0.62302 | 0.981734 |
| ILMN_49570 | Mia | 0.353353 | -0.1749 | -0.18129 | 0.174898 | 0.181286 | -0.35335 | 0.981688 |
| ILMN_53898 | Grk4 | 0.929991 | -0.29637 | -0.4517 | 0.296366 | 0.451697 | -0.92999 | 0.981684 |
| ILMN_56170 | Acsl3 | 1.504282 | -0.28579 | -0.32464 | 0.285788 | 0.324639 | -1.50428 | 0.981379 |
| ILMN_50723 | Sgca | 1.089486 | -0.69514 | -0.24803 | 0.695143 | 0.248029 | -1.08949 | 0.981329 |

| | | | | | | | | |
|---|---|---|---|---|---|---|---|---|
| ILMN_51104 | Aldh7a1 | 0.324873 | -0.17396 | -0.16602 | 0.173962 | 0.166015 | -0.32487 | 0.980332 |
| ILMN_68043 | Fam132a | 1.075395 | -0.20011 | -0.21957 | 0.20011 | 0.219566 | -1.0754 | 0.980098 |
| ILMN_65342 | Clk1 | 0.885357 | -0.53448 | -0.42319 | 0.534484 | 0.423195 | -0.88536 | 0.979235 |
| ILMN_53709 | Cmtm8 | 0.735985 | -0.12554 | -0.21424 | 0.125539 | 0.214241 | -0.73599 | 0.978874 |
| ILMN_68066 | Lnx1 | 0.340947 | -0.19688 | -0.17207 | 0.196884 | 0.172071 | -0.34095 | 0.978537 |
| ILMN_56373 | Atp1b2 | 2.587743 | -0.43385 | -0.67157 | 0.433845 | 0.671569 | -2.58774 | 0.978459 |
| ILMN_61541 | Lrrn2 | 0.691199 | -0.20376 | -0.34357 | 0.203761 | 0.343566 | -0.6912 | 0.978001 |
| ILMN_61050 | Ythdc1 | 0.399741 | -0.25645 | -0.1803 | 0.256448 | 0.180296 | -0.39974 | 0.977897 |
| ILMN_60705 | Pnisr | 0.611362 | -0.16863 | -0.29968 | 0.16863 | 0.299683 | -0.61136 | 0.977066 |
| ILMN_66203 | Gas2 | 0.777389 | -0.19668 | -0.36991 | 0.196679 | 0.369906 | -0.77739 | 0.976431 |
| ILMN_55909 | Aplp1 | 3.194083 | -1.80168 | -1.69989 | 1.801679 | 1.699893 | -3.19408 | 0.976143 |
| ILMN_48800 | Dpy19l1 | 0.77078 | -0.47953 | -0.38186 | 0.479533 | 0.381863 | -0.77078 | 0.975916 |
| ILMN_66383 | Sfxn5 | 0.662088 | -0.44933 | -0.1501 | 0.449327 | 0.150098 | -0.66209 | 0.975651 |
| ILMN_48420 | Thbs2 | 1.484524 | -0.36726 | -0.72033 | 0.367261 | 0.72033 | -1.48452 | 0.974388 |
| ILMN_66793 | Smim22 | 0.425039 | -0.21289 | -0.24032 | 0.212891 | 0.24032 | -0.42504 | 0.974206 |
| ILMN_52287 | Adhfe1 | 1.018982 | -0.65081 | -0.50789 | 0.650807 | 0.507885 | -1.01898 | 0.974078 |
| ILMN_67905 | Rgs3 | 0.962378 | -0.41311 | -0.54721 | 0.413111 | 0.547208 | -0.96238 | 0.974021 |
| ILMN_63500 | Zfp612 | 0.407167 | -0.23886 | -0.21964 | 0.238865 | 0.219643 | -0.40717 | 0.973796 |
| ILMN_54685 | Asrgl1 | 1.510989 | -0.92615 | -0.79259 | 0.92615 | 0.792592 | -1.51099 | 0.973602 |
| ILMN_51872 | Gpt | 0.55928 | -0.16607 | -0.29502 | 0.166073 | 0.295018 | -0.55928 | 0.973525 |
| ILMN_55706 | C1s | 1.171874 | -0.17112 | -0.26556 | 0.171122 | 0.265563 | -1.17187 | 0.973292 |
| ILMN_66745 | Ift81 | 0.678855 | -0.34163 | -0.3881 | 0.341632 | 0.3881 | -0.67885 | 0.973199 |
| ILMN_63225 | Taf15 | 0.28847 | -0.17906 | -0.15251 | 0.179058 | 0.152512 | -0.28847 | 0.972489 |
| ILMN_50918 | Rilpl1 | 0.886287 | -0.4531 | -0.51235 | 0.453096 | 0.512346 | -0.88629 | 0.972024 |
| ILMN_61402 | Ptprn | 0.64 | -0.4285 | -0.31704 | 0.428497 | 0.317036 | -0.64 | 0.971224 |
| ILMN_52684 | Col5a3 | 1.329996 | -0.81978 | -0.7219 | 0.819783 | 0.721901 | -1.33 | 0.971191 |
| ILMN_61722 | Sirt4 | 0.268724 | -0.17302 | -0.14079 | 0.173017 | 0.140791 | -0.26872 | 0.970968 |
| ILMN_50313 | Fank1 | 0.305505 | -0.15944 | -0.17821 | 0.159437 | 0.178212 | -0.3055 | 0.970913 |

| | | | | | | | | |
|---|---|---|---|---|---|---|---|---|
| ILMN_58657 | Trim45 | 1.124426 | -0.52821 | -0.66256 | 0.528212 | 0.662562 | -1.12443 | 0.970885 |
| ILMN_66452 | Phlda1 | 0.28362 | -0.11645 | -0.16685 | 0.116448 | 0.166845 | -0.28362 | 0.970304 |
| ILMN_62203 | Kcnk2 | 1.48101 | -0.20312 | -0.30175 | 0.203122 | 0.30175 | -1.48101 | 0.970261 |
| ILMN_48078 | Pdk2 | 1.148226 | -0.26585 | -0.57652 | 0.265855 | 0.576518 | -1.14823 | 0.969721 |
| ILMN_54786 | Map3k4 | 0.601584 | -0.40136 | -0.30919 | 0.401364 | 0.309186 | -0.60158 | 0.969705 |
| ILMN_50272 | Ttc39a | 0.371865 | -0.16279 | -0.2224 | 0.162794 | 0.222397 | -0.37186 | 0.96922 |
| ILMN_50783 | Papss1 | 0.891342 | -0.31726 | -0.51733 | 0.317263 | 0.517333 | -0.89134 | 0.969208 |
| ILMN_66756 | Cpxm2 | 0.681773 | -0.24157 | -0.39534 | 0.24157 | 0.395336 | -0.68177 | 0.969201 |
| ILMN_64013 | Mterfd3 | 0.575695 | -0.24679 | -0.34564 | 0.246788 | 0.345642 | -0.57569 | 0.968654 |
| ILMN_68863 | Pfkm | 1.57663 | -0.23611 | -0.2344 | 0.236111 | 0.2344 | -1.57663 | 0.968455 |
| ILMN_65644 | Pde9a | 0.839791 | -0.16474 | -0.39971 | 0.164742 | 0.399706 | -0.83979 | 0.968038 |
| ILMN_52471 | Prss23 | 2.072873 | -0.62104 | -1.16799 | 0.621041 | 1.16799 | -2.07287 | 0.967731 |
| ILMN_60483 | Cldn19 | 3.538925 | -0.44506 | -0.71731 | 0.445063 | 0.717308 | -3.53893 | 0.967588 |
| ILMN_61221 | Sdc2 | 1.261628 | -0.1464 | -0.38596 | 0.1464 | 0.385964 | -1.26163 | 0.966764 |
| ILMN_62327 | Wdr60 | 0.506755 | -0.33732 | -0.27617 | 0.33732 | 0.276172 | -0.50676 | 0.966577 |
| ILMN_57086 | Slc44a1 | 1.932215 | -0.4587 | -1.02135 | 0.458705 | 1.021346 | -1.93221 | 0.966339 |
| ILMN_50840 | Rai2 | 0.5837 | -0.22819 | -0.35453 | 0.22819 | 0.354532 | -0.5837 | 0.966203 |
| ILMN_68665 | Txndc15 | 0.787069 | -0.53901 | -0.41904 | 0.539007 | 0.419043 | -0.78707 | 0.965988 |
| ILMN_55428 | Csrp2 | 1.940364 | -0.22117 | -0.4422 | 0.221173 | 0.442197 | -1.94036 | 0.965969 |
| ILMN_64277 | Mboat2 | 1.571466 | -0.77987 | -0.97091 | 0.779871 | 0.970913 | -1.57147 | 0.965898 |
| ILMN_65301 | Gpx2 | 0.901734 | -0.31427 | -0.53795 | 0.314268 | 0.537955 | -0.90173 | 0.965816 |
| ILMN_60583 | Gtf3c1 | 0.871775 | -0.5271 | -0.52099 | 0.527099 | 0.520988 | -0.87177 | 0.964797 |
| ILMN_70164 | Cxcl12 | 1.281015 | -0.15287 | -0.2338 | 0.152866 | 0.233803 | -1.28102 | 0.964678 |
| ILMN_60327 | Armc1 | 0.306346 | -0.12961 | -0.19081 | 0.129611 | 0.190807 | -0.30635 | 0.964513 |
| ILMN_65756 | Extl2 | 0.455248 | -0.35347 | -0.16423 | 0.353469 | 0.164231 | -0.45525 | 0.96364 |
| ILMN_64766 | Ndufa10l1 | 0.300159 | -0.15976 | -0.18871 | 0.159759 | 0.188708 | -0.30016 | 0.963345 |
| ILMN_50988 | Pithd1 | 0.741508 | -0.29297 | -0.46364 | 0.292973 | 0.46364 | -0.74151 | 0.963085 |
| ILMN_58724 | Hmgcr | 1.165786 | -0.48244 | -0.73454 | 0.482442 | 0.734539 | -1.16579 | 0.962902 |

| | | | | | | | | |
|---|---|---|---|---|---|---|---|---|
| ILMN_63261 | Aspa | 0.315719 | -0.14853 | -0.2007 | 0.148526 | 0.200704 | -0.31572 | 0.962898 |
| ILMN_64984 | Pde6d | 0.628999 | -0.41562 | -0.36534 | 0.415618 | 0.365341 | -0.629 | 0.962752 |
| ILMN_63999 | Tspan12 | 1.174036 | -0.87669 | -0.57688 | 0.87669 | 0.576881 | -1.17404 | 0.962304 |
| ILMN_66930 | Lipe | 0.638244 | -0.31533 | -0.408 | 0.315328 | 0.408 | -0.63824 | 0.962215 |
| ILMN_160783 | Cd99 | 0.635349 | -0.50152 | -0.21823 | 0.501519 | 0.21823 | -0.63535 | 0.961635 |
| ILMN_48754 | Mbtps1 | 0.339805 | -0.21417 | -0.20717 | 0.21417 | 0.207169 | -0.3398 | 0.961325 |
| ILMN_57400 | Gpr182 | 0.305684 | -0.19479 | -0.18551 | 0.194793 | 0.185514 | -0.30568 | 0.961206 |
| ILMN_61581 | Gemin2 | 0.466155 | -0.2324 | -0.3014 | 0.232403 | 0.301403 | -0.46616 | 0.96088 |
| ILMN_54143 | Rbm10 | 0.286479 | -0.16571 | -0.1819 | 0.165713 | 0.181899 | -0.28648 | 0.96059 |
| ILMN_56965 | Lztr1 | 0.294097 | -0.20271 | -0.17087 | 0.202706 | 0.170872 | -0.2941 | 0.960074 |
| ILMN_60796 | Pon2 | 0.432049 | -0.26035 | -0.27316 | 0.260345 | 0.273155 | -0.43205 | 0.959762 |
| ILMN_53475 | Hpdl | 0.741304 | -0.49567 | -0.44608 | 0.495669 | 0.44608 | -0.7413 | 0.959355 |
| ILMN_52725 | Tmeff2 | 2.812565 | -0.47797 | -1.41982 | 0.477968 | 1.419815 | -2.81257 | 0.959038 |
| ILMN_60058 | Pim3 | 0.674003 | -0.34835 | -0.44243 | 0.34835 | 0.442428 | -0.674 | 0.958904 |
| ILMN_58363 | Plagl1 | 0.247279 | -0.16312 | -0.15248 | 0.16312 | 0.152483 | -0.24728 | 0.958092 |
| ILMN_64993 | Mcoln1 | 0.295815 | -0.14701 | -0.19595 | 0.147008 | 0.195955 | -0.29581 | 0.958031 |
| ILMN_69134 | Tgfb2 | 1.348734 | -0.40721 | -0.8363 | 0.407211 | 0.836304 | -1.34873 | 0.957445 |
| ILMN_64092 | Mrps35 | 0.263678 | -0.145 | -0.17435 | 0.144999 | 0.174351 | -0.26368 | 0.957302 |
| ILMN_54466 | Prkar1a | 0.378839 | -0.30362 | -0.17021 | 0.303623 | 0.170205 | -0.37884 | 0.957158 |
| ILMN_48827 | Tfip11 | 0.366016 | -0.22699 | -0.23741 | 0.22699 | 0.237408 | -0.36602 | 0.956174 |
| ILMN_53275 | Opn4 | 0.28809 | -0.17653 | -0.18787 | 0.176531 | 0.187872 | -0.28809 | 0.956059 |
| ILMN_61653 | Porcn | 0.514093 | -0.21217 | -0.34442 | 0.212173 | 0.344419 | -0.51409 | 0.955206 |
| ILMN_55333 | Cd82 | 0.297147 | -0.23478 | -0.15248 | 0.234781 | 0.152484 | -0.29715 | 0.954806 |
| ILMN_54140 | Gabarapl2 | 0.471932 | -0.22382 | -0.32094 | 0.223825 | 0.320936 | -0.47193 | 0.954699 |
| ILMN_60306 | Cspg5 | 0.914515 | -0.53598 | -0.61269 | 0.535984 | 0.612694 | -0.91452 | 0.954478 |
| ILMN_62183 | Gadd45b | 0.552552 | -0.42487 | -0.30379 | 0.424873 | 0.303789 | -0.55255 | 0.954471 |
| ILMN_48162 | Spa17 | 0.793317 | -0.51402 | -0.51448 | 0.514019 | 0.514482 | -0.79332 | 0.954363 |
| ILMN_57380 | Dbndd2 | 1.829505 | -0.59799 | -1.18463 | 0.597995 | 1.184631 | -1.8295 | 0.954329 |

| | | | | | | | | |
|---|---|---|---|---|---|---|---|---|
| ILMN_62814 | Csad | 1.119739 | -0.66042 | -0.75056 | 0.66042 | 0.750561 | -1.11974 | 0.954258 |
| ILMN_60456 | Son | 0.27449 | -0.20858 | -0.15538 | 0.208581 | 0.155381 | -0.27449 | 0.953989 |
| ILMN_161842 | Ppp1r1b | 1.854326 | -0.19535 | -0.21343 | 0.195351 | 0.213425 | -1.85433 | 0.953823 |
| ILMN_61980 | Rhbdf1 | 0.408915 | -0.14434 | -0.27002 | 0.144343 | 0.27002 | -0.40891 | 0.953818 |
| ILMN_61216 | Khdrbs3 | 0.684328 | -0.29854 | -0.46628 | 0.298538 | 0.46628 | -0.68433 | 0.953745 |
| ILMN_59243 | Prepl | 0.233449 | -0.15063 | -0.15339 | 0.150632 | 0.153387 | -0.23345 | 0.95325 |
| ILMN_70245 | Tspan6 | 0.608535 | -0.14548 | -0.36686 | 0.14548 | 0.366865 | -0.60854 | 0.953215 |
| ILMN_67199 | Obp3 | 0.249846 | -0.16757 | -0.16158 | 0.167574 | 0.161581 | -0.24985 | 0.952924 |
| ILMN_64748 | Ndrg2 | 3.23491 | -0.24336 | -0.57538 | 0.243361 | 0.57538 | -3.23491 | 0.952709 |
| ILMN_62739 | Camlg | 0.240102 | -0.18491 | -0.13705 | 0.184911 | 0.137052 | -0.2401 | 0.95226 |
| ILMN_66651 | Plekhb1 | 2.923639 | -0.39621 | -1.48356 | 0.396205 | 1.483559 | -2.92364 | 0.951608 |
| ILMN_52336 | Abat | 0.766703 | -0.17167 | -0.45986 | 0.171666 | 0.459861 | -0.7667 | 0.951586 |
| ILMN_56457 | Ndufv2 | 0.253646 | -0.1718 | -0.16561 | 0.171803 | 0.165606 | -0.25365 | 0.951495 |
| ILMN_60579 | Nudt6 | 0.443559 | -0.25512 | -0.30684 | 0.255122 | 0.306845 | -0.44356 | 0.951135 |
| ILMN_49445 | Prickle1 | 1.284204 | -0.52098 | -0.88575 | 0.520983 | 0.885752 | -1.2842 | 0.950941 |
| ILMN_54589 | Eml2 | 1.303367 | -0.89431 | -0.85199 | 0.894313 | 0.851986 | -1.30337 | 0.950665 |
| ILMN_49883 | Piga | 0.379278 | -0.24198 | -0.25752 | 0.241978 | 0.257523 | -0.37928 | 0.95026 |
| ILMN_62489 | Hdac11 | 2.958958 | -0.41028 | -1.54298 | 0.410281 | 1.542977 | -2.95896 | 0.950054 |
| ILMN_63557 | Fbxo36 | 0.494046 | -0.29939 | -0.34139 | 0.299388 | 0.341385 | -0.49405 | 0.950003 |
| ILMN_56185 | Tmem98 | 1.497531 | -0.60432 | -1.04221 | 0.604315 | 1.042206 | -1.49753 | 0.949569 |
| ILMN_57894 | Dpysl5 | 0.345344 | -0.18478 | -0.24493 | 0.184782 | 0.244931 | -0.34534 | 0.948949 |
| ILMN_65986 | Kctd13 | 0.431623 | -0.20597 | -0.3064 | 0.205967 | 0.306399 | -0.43162 | 0.948923 |
| ILMN_50342 | Mob2 | 0.224193 | -0.14356 | -0.15424 | 0.14356 | 0.154241 | -0.22419 | 0.948657 |
| ILMN_52250 | Prpsap2 | 0.54033 | -0.3671 | -0.36283 | 0.367104 | 0.362834 | -0.54033 | 0.948564 |
| ILMN_57817 | Ubxn11 | 0.300507 | -0.2538 | -0.14801 | 0.253802 | 0.148006 | -0.30051 | 0.948292 |
| ILMN_53767 | Spata22 | 0.529499 | -0.45143 | -0.26778 | 0.451432 | 0.267782 | -0.5295 | 0.946275 |
| ILMN_68026 | Usp53 | 0.586036 | -0.39825 | -0.40465 | 0.398251 | 0.40465 | -0.58604 | 0.945633 |
| ILMN_66312 | Baz2b | 0.792967 | -0.52551 | -0.55657 | 0.525508 | 0.556572 | -0.79297 | 0.944984 |

| | | | | | | | | |
|---|---|---|---|---|---|---|---|---|
| ILMN_66143 | Sgcd | 0.415123 | -0.16504 | -0.29812 | 0.165044 | 0.298125 | -0.41512 | 0.944644 |
| ILMN_67028 | Fut9 | 0.406326 | -0.2661 | -0.28933 | 0.266097 | 0.289332 | -0.40633 | 0.943803 |
| ILMN_56866 | Nthl1 | 0.383615 | -0.23511 | -0.27871 | 0.235114 | 0.27871 | -0.38362 | 0.943495 |
| ILMN_51069 | Map4k3 | 0.358363 | -0.19142 | -0.2645 | 0.191415 | 0.2645 | -0.35836 | 0.943439 |
| ILMN_62833 | Pgf | 0.658207 | -0.27611 | -0.48002 | 0.27611 | 0.480016 | -0.65821 | 0.943366 |
| ILMN_67627 | Pdp2 | 0.316268 | -0.21419 | -0.22368 | 0.214193 | 0.223678 | -0.31627 | 0.943141 |
| ILMN_63965 | Cttn | 0.315382 | -0.14596 | -0.23391 | 0.14596 | 0.233908 | -0.31538 | 0.942232 |
| ILMN_60775 | Clcc1 | 0.795931 | -0.6489 | -0.49156 | 0.648897 | 0.491558 | -0.79593 | 0.941772 |
| ILMN_63795 | Eif2ak3 | 0.328755 | -0.15125 | -0.24451 | 0.15125 | 0.244508 | -0.32876 | 0.941735 |
| ILMN_49215 | Ivns1abp | 0.660324 | -0.52212 | -0.42488 | 0.522116 | 0.424884 | -0.66032 | 0.941716 |
| ILMN_48076 | Ncl | 0.490319 | -0.4357 | -0.23887 | 0.435698 | 0.238866 | -0.49032 | 0.941701 |
| ILMN_59153 | Igfbp3 | 2.082734 | -0.17205 | -0.15984 | 0.172047 | 0.159841 | -2.08273 | 0.941571 |
| ILMN_56719 | Ybx3 | 0.594336 | -0.29382 | -0.44425 | 0.293821 | 0.444245 | -0.59434 | 0.941568 |
| ILMN_66695 | Rer1 | 0.295534 | -0.24456 | -0.17985 | 0.24456 | 0.179845 | -0.29553 | 0.941187 |
| ILMN_51807 | Ttc30a1 | 0.368233 | -0.20281 | -0.27685 | 0.202812 | 0.276853 | -0.36823 | 0.940566 |
| ILMN_54533 | Wbp1 | 0.521151 | -0.32751 | -0.38534 | 0.327506 | 0.385336 | -0.52115 | 0.940515 |
| ILMN_55168 | B3gnt1 | 0.465491 | -0.22901 | -0.35082 | 0.229012 | 0.35082 | -0.46549 | 0.940281 |
| ILMN_69740 | Atp1b3 | 0.408226 | -0.30935 | -0.27906 | 0.309345 | 0.279061 | -0.40823 | 0.939962 |
| ILMN_62813 | Ninj2 | 1.615356 | -0.50527 | -1.14746 | 0.505268 | 1.147461 | -1.61536 | 0.939809 |
| ILMN_69576 | Nim1k | 0.345277 | -0.27688 | -0.22537 | 0.276884 | 0.225371 | -0.34528 | 0.939316 |
| ILMN_57557 | Txnip | 0.823477 | -0.40131 | -0.6254 | 0.401314 | 0.6254 | -0.82348 | 0.939026 |
| ILMN_48339 | Mup5 | 0.413905 | -0.31595 | -0.2857 | 0.315946 | 0.285699 | -0.4139 | 0.938497 |
| ILMN_63761 | Slitrk6 | 2.257098 | -0.67606 | -1.60944 | 0.676064 | 1.609445 | -2.2571 | 0.937826 |
| ILMN_58642 | Map1lc3b | 0.348656 | -0.23875 | -0.25703 | 0.238754 | 0.257027 | -0.34866 | 0.937735 |
| ILMN_57620 | Zdhhc1 | 0.415743 | -0.28507 | -0.30709 | 0.285067 | 0.307089 | -0.41574 | 0.937434 |
| ILMN_54828 | Zfp287 | 0.282368 | -0.2485 | -0.16499 | 0.248501 | 0.164993 | -0.28237 | 0.936368 |
| ILMN_48331 | Bbs2 | 0.608514 | -0.37034 | -0.47012 | 0.370341 | 0.47012 | -0.60851 | 0.93523 |
| ILMN_58594 | Tecta | 1.736602 | -0.6765 | -1.32152 | 0.676503 | 1.321515 | -1.7366 | 0.934945 |

| | | | | | | | | |
|---|---|---|---|---|---|---|---|---|
| ILMN_63913 | Lrig1 | 0.31106 | -0.13814 | -0.24101 | 0.138143 | 0.241009 | -0.31106 | 0.934663 |
| ILMN_62209 | Med25 | 0.364839 | -0.18257 | -0.28522 | 0.182573 | 0.285222 | -0.36484 | 0.934578 |
| ILMN_67903 | Car2 | 3.300326 | -1.02925 | -2.4257 | 1.02925 | 2.425702 | -3.30033 | 0.934282 |
| ILMN_58400 | Atraid | 0.421814 | -0.19141 | -0.32915 | 0.191411 | 0.329153 | -0.42181 | 0.933817 |
| ILMN_56168 | Hbp1 | 0.362379 | -0.24905 | -0.27619 | 0.249053 | 0.276193 | -0.36238 | 0.933365 |
| ILMN_68489 | Banp | 0.34028 | -0.16234 | -0.27022 | 0.162344 | 0.270215 | -0.34028 | 0.931546 |
| ILMN_58046 | Poldip2 | 0.326707 | -0.16792 | -0.26065 | 0.167917 | 0.260648 | -0.32671 | 0.931384 |
| ILMN_50144 | Lrrc8d | 0.383122 | -0.31564 | -0.26706 | 0.315643 | 0.267057 | -0.38312 | 0.931301 |
| ILMN_52202 | Dync2li1 | 0.42273 | -0.33218 | -0.30996 | 0.332175 | 0.309956 | -0.42273 | 0.93023 |
| ILMN_51112 | Slc22a17 | 1.204944 | -0.89212 | -0.91761 | 0.892119 | 0.917615 | -1.20494 | 0.929789 |
| ILMN_69297 | Maged2 | 0.502105 | -0.48391 | -0.2466 | 0.483907 | 0.246598 | -0.50211 | 0.929155 |
| ILMN_69429 | Fam19a5 | 0.801163 | -0.36957 | -0.64463 | 0.36957 | 0.644634 | -0.80116 | 0.928818 |
| ILMN_68518 | Mapk1ip1 | 0.615321 | -0.52036 | -0.43084 | 0.520359 | 0.430839 | -0.61532 | 0.928464 |
| ILMN_52809 | Pax3 | 0.833426 | -0.47972 | -0.67735 | 0.479725 | 0.677347 | -0.83343 | 0.928184 |
| ILMN_51508 | Pkig | 0.359176 | -0.24727 | -0.28626 | 0.247269 | 0.286262 | -0.35918 | 0.92723 |
| ILMN_69940 | Reck | 1.865832 | -0.63478 | -1.45509 | 0.634782 | 1.455093 | -1.86583 | 0.926913 |
| ILMN_66191 | Rnase4 | 1.891119 | -0.86079 | -1.54627 | 0.860793 | 1.546268 | -1.89112 | 0.925751 |
| ILMN_48334 | Grip2 | 1.283719 | -0.39466 | -0.99481 | 0.394662 | 0.994814 | -1.28372 | 0.924768 |
| ILMN_62000 | Sh3tc2 | 0.825902 | -0.30109 | -0.66131 | 0.301088 | 0.661307 | -0.8259 | 0.924241 |
| ILMN_63894 | Snrnp70 | 0.348598 | -0.1361 | -0.28286 | 0.136102 | 0.282858 | -0.3486 | 0.92372 |
| ILMN_68813 | Snx13 | 0.379807 | -0.19033 | -0.31683 | 0.190329 | 0.316835 | -0.37981 | 0.923476 |
| ILMN_49072 | Egfl6 | 0.774028 | -0.6934 | -0.53936 | 0.693402 | 0.539357 | -0.77403 | 0.92291 |
| ILMN_61585 | Park7 | 0.297226 | -0.20129 | -0.24567 | 0.201287 | 0.245672 | -0.29723 | 0.922454 |
| ILMN_61671 | Krt8 | 0.893838 | -0.3061 | -0.71555 | 0.3061 | 0.715548 | -0.89384 | 0.922383 |
| ILMN_49202 | Gxylt1 | 0.309041 | -0.2409 | -0.24404 | 0.240897 | 0.244042 | -0.30904 | 0.922211 |
| ILMN_49004 | Lgi4 | 3.53074 | -1.00322 | -2.75176 | 1.003218 | 2.751757 | -3.53074 | 0.921062 |
| ILMN_68125 | Pum1 | 0.274917 | -0.24152 | -0.20326 | 0.241518 | 0.203257 | -0.27492 | 0.919783 |
| ILMN_69723 | Sult5a1 | 1.400629 | -0.93232 | -1.19035 | 0.932319 | 1.190354 | -1.40063 | 0.918579 |

| | | | | | | | | |
|---|---|---|---|---|---|---|---|---|
| ILMN_51918 | Ephb6 | 1.605997 | -0.61276 | -1.33549 | 0.612758 | 1.335487 | -1.606 | 0.918479 |
| ILMN_59966 | Irf2bp1 | 0.413137 | -0.20717 | -0.35463 | 0.207167 | 0.354634 | -0.41314 | 0.918238 |
| ILMN_58274 | MGC95210 | 0.314857 | -0.27803 | -0.2391 | 0.278029 | 0.239102 | -0.31486 | 0.916677 |
| ILMN_52209 | Asb8 | 0.311399 | -0.25558 | -0.25248 | 0.255579 | 0.252477 | -0.3114 | 0.915452 |
| ILMN_66938 | Tubgcp5 | 0.212218 | -0.15474 | -0.18072 | 0.154741 | 0.180716 | -0.21222 | 0.915265 |
| ILMN_53311 | Fam214a | 1.289121 | -0.6605 | -1.12898 | 0.660504 | 1.128976 | -1.28912 | 0.914693 |
| ILMN_59664 | Notch4 | 0.382665 | -0.32309 | -0.30711 | 0.323093 | 0.307105 | -0.38267 | 0.914571 |
| ILMN_51414 | Smpd1 | 0.619033 | -0.50406 | -0.50946 | 0.504056 | 0.509465 | -0.61903 | 0.914103 |
| ILMN_60666 | Ivd | 0.43369 | -0.40726 | -0.31586 | 0.407259 | 0.315856 | -0.43369 | 0.913952 |
| ILMN_53337 | Fundc2 | 0.370826 | -0.29451 | -0.30993 | 0.29451 | 0.309934 | -0.37083 | 0.913647 |
| ILMN_68712 | Tcf7l1 | 0.689865 | -0.42383 | -0.61087 | 0.423832 | 0.610871 | -0.68987 | 0.912935 |
| ILMN_69178 | Chpf | 0.948955 | -1.01129 | -0.42474 | 1.011286 | 0.424738 | -0.94895 | 0.912365 |
| ILMN_68361 | Mettl14 | 0.293021 | -0.14628 | -0.25993 | 0.146281 | 0.259932 | -0.29302 | 0.911881 |
| ILMN_67682 | Ppcdc | 0.333056 | -0.22104 | -0.29593 | 0.221041 | 0.29593 | -0.33306 | 0.911214 |
| ILMN_54426 | Arsk | 0.382162 | -0.16133 | -0.33441 | 0.161325 | 0.334406 | -0.38216 | 0.911203 |
| ILMN_52846 | Baalc | 1.470599 | -0.60277 | -1.28801 | 0.602772 | 1.288005 | -1.4706 | 0.910246 |
| ILMN_52426 | Fgfr3 | 0.376226 | -0.21355 | -0.33934 | 0.213553 | 0.339336 | -0.37623 | 0.909766 |
| ILMN_60149 | Fjx1 | 0.954474 | -0.38612 | 0.180982 | 0.386124 | -0.18098 | -0.95447 | 0.909711 |
| ILMN_57440 | Cpz | 0.363358 | -0.26742 | -0.32076 | 0.267423 | 0.320764 | -0.36336 | 0.909295 |
| ILMN_53665 | Serpine2 | 0.628685 | -0.47911 | -0.55105 | 0.47911 | 0.551047 | -0.62869 | 0.908943 |
| ILMN_70135 | Hexim2 | 0.428548 | -0.43013 | -0.30472 | 0.430126 | 0.304716 | -0.42855 | 0.907379 |
| ILMN_66636 | Acbd5 | 0.496908 | -0.52091 | -0.31621 | 0.520907 | 0.31621 | -0.49691 | 0.907298 |
| ILMN_53021 | Tdrd7 | 0.318091 | -0.18691 | -0.2909 | 0.186914 | 0.290903 | -0.31809 | 0.907146 |
| ILMN_70001 | Vkorc1 | 0.556043 | -0.19095 | -0.48259 | 0.190953 | 0.482588 | -0.55604 | 0.906721 |
| ILMN_56587 | Wnt6 | 0.506405 | -0.49216 | -0.38368 | 0.49216 | 0.383678 | -0.50641 | 0.906542 |
| ILMN_54969 | Csrp1 | 2.288624 | -1.48362 | -2.10371 | 1.483618 | 2.103709 | -2.28862 | 0.905542 |
| ILMN_59974 | Rbm46 | 0.529997 | -0.23017 | -0.47857 | 0.230166 | 0.478571 | -0.53 | 0.905491 |
| ILMN_56270 | Dvl1 | 0.914776 | -0.36111 | -0.81599 | 0.361105 | 0.815989 | -0.91478 | 0.905424 |

| | | | | | | | | |
|---|---|---|---|---|---|---|---|---|
| ILMN_58763 | Arhgef12 | 0.290371 | -0.15986 | -0.26759 | 0.159856 | 0.267585 | -0.29037 | 0.905417 |
| ILMN_57624 | Mlycd | 0.426709 | -0.42156 | -0.32115 | 0.421555 | 0.321153 | -0.42671 | 0.905106 |
| ILMN_56650 | Arfgap2 | 0.357947 | -0.38123 | -0.22654 | 0.381227 | 0.226537 | -0.35795 | 0.904973 |
| ILMN_55980 | Gstp1 | 0.975592 | -0.63264 | -0.90093 | 0.632635 | 0.900928 | -0.97559 | 0.904682 |
| ILMN_48049 | LOC306766 | 0.43785 | -0.19819 | -0.39992 | 0.198186 | 0.399921 | -0.43785 | 0.904103 |
| ILMN_55681 | Inppl1 | 0.653057 | -0.4514 | -0.61066 | 0.451399 | 0.610659 | -0.65306 | 0.901321 |
| ILMN_56108 | Lrrc17 | 0.752673 | -0.3301 | -0.69505 | 0.330103 | 0.695049 | -0.75267 | 0.901018 |
| ILMN_52926 | Rabep1 | 0.63131 | -0.60593 | -0.51513 | 0.605927 | 0.51513 | -0.63131 | 0.900886 |
| ILMN_69233 | Ppfibp2 | 1.045335 | -1.16764 | -0.57557 | 1.16764 | 0.575569 | -1.04534 | 0.900878 |
| ILMN_59969 | Inpp5f | 0.396813 | -0.36145 | -0.34408 | 0.361454 | 0.344078 | -0.39681 | 0.898884 |
| ILMN_63079 | Syf2 | 0.260942 | -0.14884 | -0.24901 | 0.148843 | 0.249006 | -0.26094 | 0.8986 |
| ILMN_70333 | Thumpd1 | 0.303478 | -0.24683 | -0.28023 | 0.246826 | 0.280225 | -0.30348 | 0.897653 |
| ILMN_50863 | Agt | 4.106979 | -0.44443 | 0.4709 | 0.444434 | -0.4709 | -4.10698 | 0.897533 |
| ILMN_65512 | Tfdp2 | 0.987901 | -1.1088 | -0.6 | 1.108795 | 0.600001 | -0.9879 | 0.89745 |
| ILMN_54906 | Fam98a | 0.422562 | -0.35518 | -0.38814 | 0.35518 | 0.388144 | -0.42256 | 0.896645 |
| ILMN_59287 | Nfib | 1.143737 | -0.36604 | 0.245553 | 0.366036 | -0.24555 | -1.14374 | 0.895473 |
| ILMN_58852 | Nr4a2 | 0.801491 | -0.80614 | -0.6559 | 0.806136 | 0.655901 | -0.80149 | 0.895373 |
| ILMN_62715 | Zfp523 | 0.479737 | -0.55542 | -0.23953 | 0.555418 | 0.239528 | -0.47974 | 0.895191 |
| ILMN_63786 | Odc1 | 1.54088 | -0.51119 | 0.336871 | 0.51119 | -0.33687 | -1.54088 | 0.894853 |
| ILMN_59897 | Ppp1r36 | 1.464292 | -1.07456 | -1.41046 | 1.074557 | 1.41046 | -1.46429 | 0.89448 |
| ILMN_51536 | Dcp1b | 0.2964 | -0.24876 | -0.27682 | 0.248756 | 0.276825 | -0.2964 | 0.894168 |
| ILMN_65976 | Dynlrb2 | 0.306383 | -0.33941 | -0.21313 | 0.339407 | 0.213129 | -0.30638 | 0.893986 |
| ILMN_48166 | Aldh1a1 | 3.674375 | -0.36355 | 0.437624 | 0.363548 | -0.43762 | -3.67437 | 0.893518 |
| ILMN_48065 | Itih3 | 2.24726 | -0.1795 | 0.239547 | 0.179498 | -0.23955 | -2.24726 | 0.892568 |
| ILMN_63177 | Igf2 | 2.439964 | 0.173766 | -0.23393 | -0.17377 | 0.233929 | -2.43996 | 0.89068 |
| ILMN_69751 | Ucn2 | 0.621656 | -0.55428 | -0.5803 | 0.554277 | 0.580296 | -0.62166 | 0.890457 |
| ILMN_56354 | Lars | 0.209346 | -0.20305 | -0.18672 | 0.203047 | 0.186721 | -0.20935 | 0.88972 |
| ILMN_69106 | Srp19 | 0.26736 | -0.25293 | -0.2429 | 0.252929 | 0.242899 | -0.26736 | 0.889635 |

| | | | | | | | | |
|---|---|---|---|---|---|---|---|---|
| ILMN_61414 | Sema4g | 1.493402 | -0.38001 | 0.317995 | 0.380012 | -0.31799 | -1.4934 | 0.888869 |
| ILMN_58686 | Wsb1 | 0.300092 | -0.18581 | -0.30101 | 0.185809 | 0.301007 | -0.30009 | 0.888543 |
| ILMN_49569 | Kcnc2 | 1.61391 | -0.23522 | 0.266356 | 0.235218 | -0.26636 | -1.61391 | 0.888178 |
| ILMN_54818 | Rhpn1 | 1.339572 | -0.4201 | -1.25124 | 0.420098 | 1.251244 | -1.33957 | 0.887716 |
| ILMN_57996 | St3gal4 | 1.311214 | -0.63058 | -1.3002 | 0.63058 | 1.300196 | -1.31121 | 0.887612 |
| ILMN_58793 | Ly6g6e | 1.719475 | -0.56639 | 0.407301 | 0.566389 | -0.4073 | -1.71948 | 0.887215 |
| ILMN_68994 | Hspb6 | 0.772838 | -0.34143 | 0.192693 | 0.341432 | -0.19269 | -0.77284 | 0.887137 |
| ILMN_50148 | Psmc1 | 0.397075 | -0.4486 | -0.29704 | 0.448597 | 0.297036 | -0.39708 | 0.886608 |
| ILMN_55504 | Sparc | 1.119268 | -0.29636 | 0.249844 | 0.296359 | -0.24984 | -1.11927 | 0.886016 |
| ILMN_62734 | Acot8 | 0.24995 | -0.18328 | -0.25224 | 0.183278 | 0.252244 | -0.24995 | 0.885729 |
| ILMN_62790 | Chi3l1 | 1.656743 | -0.23194 | 0.279576 | 0.231944 | -0.27958 | -1.65674 | 0.885418 |
| ILMN_51519 | Gprc5b | 2.704582 | -0.86692 | 0.648274 | 0.866922 | -0.64827 | -2.70458 | 0.885284 |
| ILMN_69708 | Ubl3 | 0.435672 | -0.16168 | -0.42215 | 0.161683 | 0.422153 | -0.43567 | 0.885253 |
| ILMN_51972 | Armcx1 | 1.097648 | -0.36147 | 0.268674 | 0.361471 | -0.26867 | -1.09765 | 0.883925 |
| ILMN_53433 | Sdhc | 0.315238 | -0.20022 | -0.32375 | 0.200221 | 0.323745 | -0.31524 | 0.883556 |
| ILMN_58184 | Asgr1 | 2.026775 | -0.33906 | 0.382971 | 0.339055 | -0.38297 | -2.02677 | 0.883488 |
| ILMN_59402 | Chst9 | 0.350363 | -0.2695 | -0.35572 | 0.269504 | 0.355724 | -0.35036 | 0.88338 |
| ILMN_54990 | Zfp282 | 0.395114 | -0.48054 | -0.2315 | 0.480538 | 0.231496 | -0.39511 | 0.882968 |
| ILMN_53272 | Ngb | 0.375077 | -0.44243 | -0.26742 | 0.442426 | 0.267416 | -0.37508 | 0.882149 |
| ILMN_58183 | S100a6 | 1.449354 | -0.21996 | 0.268208 | 0.219959 | -0.26821 | -1.44935 | 0.881685 |
| ILMN_70000 | Ptgds | 3.259062 | -0.23552 | 0.429972 | 0.235516 | -0.42997 | -3.25906 | 0.881426 |
| ILMN_50582 | Zmynd10 | 0.403167 | -0.42918 | -0.35644 | 0.429176 | 0.356439 | -0.40317 | 0.880819 |
| ILMN_67134 | Dcakd | 0.872173 | -0.57952 | -0.90938 | 0.579521 | 0.909377 | -0.87217 | 0.880257 |
| ILMN_52871 | Srpk2 | 0.481601 | -0.25424 | -0.49944 | 0.254244 | 0.499445 | -0.4816 | 0.879358 |
| ILMN_49169 | Vamp2 | 0.737709 | -0.18047 | 0.171805 | 0.180468 | -0.1718 | -0.73771 | 0.879171 |
| ILMN_57099 | Xrcc6 | 0.249628 | -0.29005 | -0.19818 | 0.290047 | 0.198183 | -0.24963 | 0.878243 |
| ILMN_49058 | Smim14 | 0.677272 | -0.8244 | -0.47601 | 0.824396 | 0.476006 | -0.67727 | 0.877198 |
| ILMN_52836 | Thnsl2 | 0.607994 | -0.37044 | -0.64367 | 0.370441 | 0.643668 | -0.60799 | 0.876678 |

| | | | | | | | | |
|---|---|---|---|---|---|---|---|---|
| ILMN_58860 | Tmprss7 | 0.324349 | -0.15653 | -0.33755 | 0.156532 | 0.337548 | -0.32435 | 0.876475 |
| ILMN_60157 | Gpr19 | 0.595824 | -0.73113 | -0.41862 | 0.731126 | 0.418624 | -0.59582 | 0.87573 |
| ILMN_63943 | LOC498460 | 0.416697 | -0.51486 | -0.28638 | 0.514856 | 0.286376 | -0.4167 | 0.875329 |
| ILMN_61545 | Cx3cl1 | 0.846627 | -0.41492 | 0.236248 | 0.41492 | -0.23625 | -0.84663 | 0.875092 |
| ILMN_68170 | Srpk3 | 0.514691 | -0.55252 | -0.47687 | 0.552519 | 0.476873 | -0.51469 | 0.87467 |
| ILMN_52687 | Acot7 | 0.813184 | -0.65547 | -0.85833 | 0.65547 | 0.858326 | -0.81318 | 0.874556 |
| ILMN_57073 | Plp1 | 0.780398 | -0.3856 | 0.219338 | 0.385595 | -0.21934 | -0.7804 | 0.874227 |
| ILMN_50763 | Itga7 | 3.066619 | -0.8345 | 0.7852 | 0.834496 | -0.7852 | -3.06662 | 0.873077 |
| ILMN_48356 | Mcee | 0.450297 | -0.55197 | -0.33757 | 0.551966 | 0.337567 | -0.4503 | 0.872865 |
| ILMN_58155 | Ogn | 3.025819 | 0.413048 | -0.52193 | -0.41305 | 0.521933 | -3.02582 | 0.871941 |
| ILMN_70122 | Ano4 | 1.891353 | -1.05205 | -2.03701 | 1.05205 | 2.037011 | -1.89135 | 0.871482 |
| ILMN_64681 | Igfbp6 | 0.697563 | -0.15862 | 0.172999 | 0.158619 | -0.173 | -0.69756 | 0.870032 |
| ILMN_52681 | Kcnb1 | 1.254588 | -0.44044 | 0.354648 | 0.44044 | -0.35465 | -1.25459 | 0.869494 |
| ILMN_49364 | Pigq | 0.665381 | -0.57014 | -0.71324 | 0.570141 | 0.713238 | -0.66538 | 0.869451 |
| ILMN_53766 | Mfap4 | 1.420806 | -0.66531 | 0.416819 | 0.665308 | -0.41682 | -1.42081 | 0.869321 |
| ILMN_55417 | Scnn1a | 0.401896 | -0.34744 | -0.43239 | 0.347443 | 0.432386 | -0.4019 | 0.868404 |
| ILMN_51228 | Mme | 1.377739 | -0.54851 | 0.401925 | 0.548509 | -0.40192 | -1.37774 | 0.868377 |
| ILMN_57698 | Reln | 1.067384 | -0.22508 | 0.26973 | 0.22508 | -0.26973 | -1.06738 | 0.865181 |
| ILMN_50326 | Brinp2 | 0.452667 | -0.5992 | -0.26455 | 0.599198 | 0.264548 | -0.45267 | 0.865138 |
| ILMN_64015 | Slc25a17 | 0.463795 | -0.22545 | 0.141279 | 0.225449 | -0.14128 | -0.4638 | 0.864632 |
| ILMN_55604 | Fat3 | 0.873528 | -0.33355 | 0.261381 | 0.333552 | -0.26138 | -0.87353 | 0.864312 |
| ILMN_60298 | Golga2 | 0.612633 | -0.78928 | -0.45463 | 0.789279 | 0.45463 | -0.61263 | 0.864286 |
| ILMN_60499 | Lrp11 | 0.985249 | -0.15472 | -0.92097 | 0.154723 | 0.92097 | -0.98525 | 0.863728 |
| ILMN_59575 | Ermn | 3.993838 | -1.47312 | 1.19574 | 1.473119 | -1.19574 | -3.99384 | 0.863447 |
| ILMN_69046 | Mog | 4.972703 | -0.97007 | 1.243811 | 0.970067 | -1.24381 | -4.9727 | 0.863406 |
| ILMN_54984 | Prrx2 | 0.696628 | -0.2228 | 0.20281 | 0.222798 | -0.20281 | -0.69663 | 0.863108 |
| ILMN_68931 | Ptk2 | 0.940038 | -0.55641 | 0.284019 | 0.556407 | -0.28402 | -0.94004 | 0.862415 |
| ILMN_66374 | Lmo4 | 0.885517 | -0.49354 | 0.273578 | 0.493542 | -0.27358 | -0.88552 | 0.861321 |

| | | | | | | | | |
|---|---|---|---|---|---|---|---|---|
| ILMN_56280 | Il16 | 0.914023 | -0.36388 | 0.282177 | 0.363881 | -0.28218 | -0.91402 | 0.86102 |
| ILMN_51759 | Gdf1 | 0.666129 | -0.15914 | 0.181792 | 0.15914 | -0.18179 | -0.66613 | 0.860959 |
| ILMN_57699 | Cyp4b1 | 0.264221 | -0.27098 | -0.28111 | 0.270983 | 0.28111 | -0.26422 | 0.86029 |
| ILMN_66294 | Pam | 1.37501 | -0.37078 | 0.395083 | 0.370777 | -0.39508 | -1.37501 | 0.858993 |
| ILMN_54063 | Entpd2 | 1.946166 | 0.318726 | -0.33072 | -0.31873 | 0.330723 | -1.94617 | 0.858744 |
| ILMN_65264 | Olfml2b | 1.116743 | 0.200122 | -0.36271 | -0.20012 | 0.362707 | -1.11674 | 0.858559 |
| ILMN_69434 | Chchd10 | 0.653646 | -0.13323 | 0.173497 | 0.133231 | -0.1735 | -0.65365 | 0.858313 |
| ILMN_49640 | Ddit4 | 1.051303 | -0.22736 | 0.28936 | 0.22736 | -0.28936 | -1.0513 | 0.856173 |
| ILMN_48761 | Lect1 | 3.295582 | 0.597862 | -1.25157 | -0.59786 | 1.251565 | -3.29558 | 0.856028 |
| ILMN_64063 | Slc6a13 | 1.544595 | -0.23231 | 0.379755 | 0.232315 | -0.37975 | -1.54459 | 0.855962 |
| ILMN_58912 | Pygm | 1.762849 | -0.33126 | 0.46536 | 0.331264 | -0.46536 | -1.76285 | 0.855928 |
| ILMN_50593 | Thrsp | 2.592179 | 0.389345 | -0.26068 | -0.38935 | 0.260677 | -2.59218 | 0.855903 |
| ILMN_65901 | Ppap2b | 0.59189 | -0.37643 | 0.18469 | 0.376432 | -0.18469 | -0.59189 | 0.855861 |
| ILMN_67775 | Atp13a4 | 1.004446 | -0.3563 | 0.317534 | 0.356303 | -0.31753 | -1.00445 | 0.855029 |
| ILMN_61557 | Gldn | 3.45339 | 0.649635 | -0.90523 | -0.64964 | 0.905235 | -3.45339 | 0.85344 |
| ILMN_55839 | Zfp775 | 0.330413 | -0.46048 | -0.14653 | 0.460482 | 0.146527 | -0.33041 | 0.853085 |
| ILMN_53099 | Abcb9 | 0.752201 | -0.22912 | 0.234442 | 0.229118 | -0.23444 | -0.7522 | 0.852307 |
| ILMN_54221 | Tyro3 | 2.560529 | -0.54029 | 0.726271 | 0.540293 | -0.72627 | -2.56053 | 0.851466 |
| ILMN_67316 | Tm9sf4 | 0.334027 | -0.17272 | -0.38769 | 0.172723 | 0.387693 | -0.33403 | 0.851242 |
| ILMN_55031 | Tnnc1 | 0.642616 | -0.75942 | -0.66152 | 0.759421 | 0.661516 | -0.64262 | 0.851235 |
| ILMN_70398 | Macrod1 | 1.008101 | -0.26711 | -1.07077 | 0.267107 | 1.070769 | -1.0081 | 0.850436 |
| ILMN_66726 | Ptn | 2.705863 | -0.60165 | -2.8071 | 0.601652 | 2.807095 | -2.70586 | 0.85008 |
| ILMN_69605 | Pcbp4 | 1.53229 | -0.84026 | -1.8016 | 0.840258 | 1.801601 | -1.53229 | 0.849478 |

**Appendix 3. Cell Surface Receptors with Known Ligands Identified as More Highly Expressed in Activated OPCs as compared to Non-activated OPCs, from Moyon et al., 2015 Dataset.**

| Agilent Array ID | Gene Symbol | $Log_2$ Fold Change | adj.P.Val | Known Ligands |
|---|---|---|---|---|
| A_55_P2045007 | Hrh1 | 0.879083 | 0.045517 | histamine |
| A_55_P2033425 | Grm5 | 0.469783 | 0.039461 | L-glutamic acid, L-aspartic acid, L-serine-O-phosphate, NAAG and L-cysteine sulphinic acid |
| A_51_P511015 | Fzd9 | 0.880167 | 0.035839 | Wnt |
| A_55_P2002557 | Srebf1 | 0.790624 | 0.035013 | A series of oxysterols are natural ligands |

| | | | | |
|---|---|---|---|---|
| A_51_P156274 | Ltbr | 1.163964 | 0.0314 | LIGHT (*TNFSF14*, O43557), lymphotoxin β2α1 heterotrimer (LTA, LTB, Q06643, P01374) |
| A_51_P404077 | Fzd2 | 0.684819 | 0.029232 | Wnt-5a |
| A_55_P2003053 | Dct | 0.718064 | 0.026886 | 5-hydroxytryptamine |
| A_52_P110052 | Darc | 0.709832 | 0.024579 | CXCL5 (CXCL5, P42830), CXCL6 (CXCL6, P80162), CXCL8 (CXCL8, P10145), CXCL11 (CXCL11, O14625), CCL2 (CCL2, P13500), CCL5 (CCL5, P13501), CCL7 (CCL7, P80098), CCL11 (CCL11, P51671), CCL14 (CCL14, Q16627), CCL17 (CCL17, Q92583) |
| A_55_P2007964 | Cx3cr1 | 1.610647 | 0.020778 | Cx3cl1 |
| A_55_P1961466 | Dct | 0.874146 | 0.020673 | 5-hydroxytryptamine |
| A_66_P118329 | Ntrk3 | 0.739135 | 0.018645 | 10+ ligands |
| A_55_P2185332 | Il17rc | 0.821857 | 0.018184 | IL-17A |
| A_55_P2025078 | Csf1r | 2.182575 | 0.01347 | IL4, M-CSF |
| A_55_P2064043 | Cd44 | 1.086395 | 0.012072 | (-)-adrenaline (-)-noradrenaline |
| A_52_P354744 | Slc2a3 | 1.019572 | 0.010191 | [3H]2-deoxyglucose |
| A_52_P192426 | Tnfrsf1a | 1.180514 | 0.008784 | TNF, lymphotoxin-α |
| A_55_P2057777 | Fgfr1 | 0.947437 | 0.008597 | FGF-1 (FGF1, P05230), FGF-2 (FGF2, P09038), FGF-4 (FGF4, P08620) > FGF-5 (FGF5, P12034), FGF-6 (FGF6, P10767 |

| | | | | |
|---|---|---|---|---|
| A_55_P2006792 | Ntrk2 | 0.769007 | 0.008143 | BDNF (BDNF, P23560), neurotrophin-4 (NTF4, P34130) > neurotrophin-3 (NTF3, P20783) |
| A_52_P317393 | Gpr56 | 1.082123 | 0.007508 | collagen III, transglutaminase |
| A_55_P2159710 | Acvr1 | 0.739323 | 0.007368 | Activin-A |
| A_55_P2051099 | Tnfrsf1a | 1.347615 | 0.006373 | TNF, lymphotoxin-α |
| A_51_P345649 | Pdgfrα | 1.150499 | 0.00535 | PDGFα |
| A_55_P1991985 | Ptprs | 0.964322 | 0.003744 | chondroitin sulphate proteoglycan 3 (NCAN, O14594), netrin-G3 ligand (LRRC4B, Q9NT99) |
| A_55_P2068892 | Il6ra | 1.52813 | 0.002956 | IL6 |
| A_55_P2000439 | Ptprz1 | 2.159583 | 0.001322 | contactin-1 (CNTN1, Q12860), pleiotrophin (PTN, C9JR52) |
| A_51_P507053 | Slc38a1 | 1.891604 | 0.000515 | [14C]alanine, [3H]alanine |
| A_51_P110759 | Slc1a1 | 2.05887 | 0.00044 | [3H]ETB-TBOA (Binding) pKd 6.5 [47] - Rat, [3H]L-aspartic acid, [3H]D-aspartic acid |
| A_51_P170463 | Gpr17 | 2.862208 | 0.000424 | cysteinyl-leukotrienes (CysLTs), uracil nucleotides (Proposed, 1 publication) |
| A_55_P2008061 | Itpr2 | 2.225311 | 0.00028 | cytosolic Ca2+, IP3 |
| A_52_P597634 | Fzd1 | 1.796602 | 0.000197 | Wnt-1, Wnt-2, Wnt-5a, Wnt-3a, Wnt-7b |
| A_52_P665675 | Abca1 | 2.06571 | 0.000179 | bihelical apoA-I mimetic peptide 5A |
| A_55_P2051414 | Axl | 1.698749 | 0.000172 | 10+ known endogenous ligands |
| A_51_P131408 | Tnfrsf12a | 2.881712 | 1.26E-05 | TWEAK |

**Appendix 3 R code used for bioinformatic analyses in**

**Chapter 3**

**Huang, Jarjour et al., 2011, Illumina Bead Chip Data Analysis**

```
#Install Bioconductor and analysis packages

source("https://bioconductor.org/biocLite.R")

biocLite()

biocLite("limma")

library(limma)

require(limma)

biocLite("affy")

library(affy)

require(affy)

biocLite("beadarray")

library(beadarray)

require(beadarray)

#set working directory

setwd("C:\\Users\\Cat\\Documents\\scrm misc\\Illumina
Analysis\\aIllumina_Analysis_start_07012017")

getwd()

#Read in targets file which defines the names of the arrays,

targets <- readTargets("targets.txt")

targets <- readTargets("targets.txt", row.names="SampleName")

# Read in background corrected Illumina bead chip data

BSData <- readBeadSummaryData(dataFile = "GSE24821_non-
normalized.txt.gz",

     ProbeID = "ID_REF", skip = 4, columns = list(exprs =
"AVG_Signal", Detection = "Detection Pval"),

          illuminaAnnotation="illuminaRatv1")

# Extract expression values from Illumina bead chip data

bd<- exprs(BSData)

#Boxplot of data

png("boxplot_pre-norm_illumina.png")

boxplot(log2(bd), las=2, range=1.5, col=c(rep("yellow",3),
rep("orange",3), rep("red",3)))

dev.off()
```

```
#Convert expression data to matrix
d_log_matrix <- as.matrix(bd)
## Desity plot of data
png("density_post_norm_illumina.png")
plot (density(d_log_matrix[,1]), col="yellow")
lines (density(d_log_matrix[,2]), col="yellow")
lines (density(d_log_matrix[,3]), col="yellow")
lines (density(d_log_matrix[,4]), col="orange")
lines (density(d_log_matrix[,5]), col="orange")
lines (density(d_log_matrix[,6]), col="orange")
lines (density(d_log_matrix[,7]), col="red")
lines (density(d_log_matrix[,8]), col="red")
lines (density(d_log_matrix[,9]), col="red")
dev.off()
##MA plots
#d28_1 vs d28_2
png("mva.pairs_norm_transform_none_illumina_replicates.png")
mva.pairs(bd[, c(1,3)])
dev.off()
#d28_1 vs d5_1
png("mva.pairs_norm_transform_none_illumina_different_times.pn
g")
mva.pairs(bd[, c(1,4)])
dev.off()
##hierarchical clustering of post norm data
hc<-hclust(as.dist(1-cor(d_log, method="pearson")),
method="average")
png("hclust_post_norm_illumina.png")
plot(hc)
dev.off()
# Quantile Normalise Illumina bead chip dta
BSData.qnorm <- normaliseIllumina(BSData, method = "quantile",
transform = "none")
d <- exprs(BSData.qnorm)
```

```
## Principal Component Analysis for Quantile Normalised
Activated and Non-activated OPC Data

# Install package used to generate plot

biocLite("scatterplot3d")

require(scatterplot3d)

library("scatterplot3d")

#Perform Principal Component Analysis using prcomp function

pca <- prcomp(t(d), scale=T)

#Specify which arrays belong to each sample group by numbering

pca_names <- c(1,2,3,4,1,2,3)

#Generate scatter plot showing variation between arrays for
principal components 1,2 and 3 with arrays coloured by sample
group

png("scatter3D_PCA_act_vs_nonact_norm.png")

s3d<-scatterplot3d(pca$x[,1:3], pch=19,
color=c(rep("green",4),rep("dark green",3)))

s3d.coords <- s3d$xyz.convert(pca$x[,1:3])

text(s3d.coords$x, s3d.coords$y, labels = pca_names,pos = 3,

offset = 0.5)

dev.off()

# Check data object created using prcomp (an object of class
prcomp), contains the correct information

names(pca)

# Calculate eigenvalues by raising the standard deviation for
each principal component to the power of 2

eig <- (pca$sdev)^2

# Calculate the variance captured by each principal component
using the eigenvalues

variance <- eig*100/sum(eig)

# Calculate the cumulative variances of the principal
components using the variance

cumvar <- cumsum(variance)

eig.pca <- data.frame(eig = eig, variance = variance,

                      cumvariance = cumvar)

# Check eigenvalue, variance and cumulative variance
calculations were successful

head(eig.pca)
```

```
#Use the function summary() to extract the eigenvalues and
variances from an object of class prcomp.

pca_eigenval_var <- summary(pca)

pca_eigenval_var

# Visualise the importance of principal components (PCs) by
generating a bar plot.

png("PCA_hj_plot.png")

barplot(eig.pca[, 2], names.arg=1:nrow(eig.pca),

       main = "Variances",

       xlab = "Principal Components",

       ylab = "Percentage of variances",

       col ="steelblue")

dev.off()

# Generate table of eigenvectors for each feature(Entrez gene
RNA or control probe)

rotations <- pca$rotation

write.table(rotations,file="PCA_act_vs_nonact.txt",
quote=F,sep="\t",col.names=NA)

# Differential Gene Expression Analysis Using Limma

# Extract expression values from normalised data

d <- exprs(BSData.qnorm)

#Define groups within the set of arrays

groups <-
c('d28','d28','d28','d5','d5','d5','d14','d14','d14')

design <- model.matrix(~0+factor(groups))

colnames(design) <- levels(factor(groups))

#Differential Gene Expression Analysis using Limma

fit <- lmFit(d, design)

cont.dif <- makeContrasts(

           d28.vs.d5 = "d28-d5",

           d28.vs.d14 = "d28-d14",

           d14.vs.d5 = "d14-d5",

           d14.vs.d28 = "d14-d28",

           d5.vs.d14 = "d5-d14",

           d5.vs.d28 = "d5-d28",
```

```
                    levels=design)
fit2 <- contrasts.fit(fit, cont.dif)

fit2 <- eBayes(fit2)

# get results for all contrasts:

topTable28.vs.5<-topTable(fit2, adjust="BH", n=nrow(d),
coef="d28.vs.d5")

topTable28.vs.14<-topTable(fit2, adjust="BH", n=nrow(d),
coef="d28.vs.d14")

topTable14.vs.5<-topTable(fit2, adjust="BH", n=nrow(d),
coef="d14.vs.d5")

topTable14.vs28<-topTable(fit2, adjust="BH", n=nrow(d),
coef="d14.vs.d28")

topTable5.vs.14<-topTable(fit2, adjust="BH", n=nrow(d),
coef="d5.vs.d14")

topTable5.vs.28<-topTable(fit2, adjust="BH", n=nrow(d),
coef="d5.vs.d28")

TiptopTable<-cbind(topTable28.vs.5, topTable28.vs.14,
topTable14.vs.5, topTable14.vs28, topTable5.vs.14,
topTable5.vs.28)

write.table(TiptopTable,file="Illumina_data_limma_output_02112
016.txt", quote=F,

sep="\t",col.names=NA)
```

```
#Install Bioconductor and analysis packages

source("https://bioconductor.org/biocLite.R")

biocLite()

biocLite("limma")

library(limma)

require(limma)

biocLite("affy")

library(affy)

require(affy)


#Set working directory

setwd("C:\\Users\\Cat\\Documents\\scrm misc\\Agilent
analysis\\Agilent analysis start 16032016")

getwd()


#Read in targets file which defines the names of the arrays,

targets <- readTargets("targets.txt")

targets <- readTargets("targets.txt", row.names="SampleName")


#Read in mean foreground (F532 Mean) and background (B532
Mean) values

Data<-read.maimages(targets, path=getwd(),columns=list(E =
"F532 Mean", Eb = "B532 Mean"),green.only=TRUE)


#Generate boxplot from foreground values

png("boxplot_test_15122016.png")

boxplot(log(Data$E,2), las=2, range=1.5,
names=targets$SampleName, col=c( rep("blue",3),
rep("orange",4), rep("red",4),

rep("green",4), rep("dark green",3)))

dev.off()



#Convert foreground values to log2 transformed matrix

Data_E_matrix <- as.matrix(Data$E,2)
```

```
#Generate density plot of foreground values
png("density_plot_all_data_pre_background_correct.png")
plot (density(log(Data_E_matrix[,2])), col="blue", xlim=c(4,
12))
lines (density(log(Data_E_matrix[,1])), col="blue")
lines (density(log(Data_E_matrix[,3])), col="blue")
lines (density(log(Data_E_matrix[,4])), col="orange")
lines (density(log(Data_E_matrix[,5])), col="orange")
lines (density(log(Data_E_matrix[,6])), col="orange")
lines (density(log(Data_E_matrix[,7])), col="orange")
lines (density(log(Data_E_matrix[,8])), col="red")
lines (density(log(Data_E_matrix[,9])), col="red")
lines (density(log(Data_E_matrix[,10])), col="red")
lines (density(log(Data_E_matrix[,11])), col="red")
lines (density(log(Data_E_matrix[,12])), col="green")
lines (density(log(Data_E_matrix[,13])), col="green")
lines (density(log(Data_E_matrix[,14])), col="green")
lines (density(log(Data_E_matrix[,15])), col="green")
lines (density(log(Data_E_matrix[,16])), col="dark green")
lines (density(log(Data_E_matrix[,17])), col="dark green")
lines (density(log(Data_E_matrix[,18])), col="dark green")
dev.off()

#Generate MA plots from foreground values

#Activated OPC replicate 2 vs Activated OPC replicate 3
png("mva.pairs_foreground_act2_vs_act3_16122016.png")
mva.pairs(Data_E_matrix[,c(13,14)])
dev.off()

#Activated OPC replicate 2 vs Non-activated OPC replicate 1
png("mva.pairs_foreground_act2_vs_Nonact1.png")
mva.pairs(log(Data_E_matrix,2)[,c(13,16)])
```

```
dev.off()

#Activated OPC replicate 2 vs Neonatal OPC replicate 1
png("mva.pairs_foreground_act2_vs_nOPC1.png")
mva.pairs(log(Data_E_matrix,2)[,c(13,1)])
dev.off()

#Generate boxplot from background features
png("boxplot_background_15122016.png")
boxplot(log(Data$Eb,2), las=2, range=1.5,
names=targets$SampleName, col=c( rep("blue",3),
rep("orange",4), rep("red",4),
rep("green",4), rep("dark green",3)))
dev.off()

#Convert background values to log2 transformed matrix
Data1_Eb_matrix <- as.matrix(Data$Eb,2)

#Density plot of background values
png("density_plot_all_data_background_probes.png")
plot (density(log(Data1_Eb_matrix[,2])), col="blue", xlim=c(4,
12))
lines (density(log(Data1_Eb_matrix[,1])), col="blue")
lines (density(log(Data1_Eb_matrix[,3])), col="blue")
lines (density(log(Data1_Eb_matrix[,4])), col="orange")
lines (density(log(Data1_Eb_matrix[,5])), col="orange")
lines (density(log(Data1_Eb_matrix[,6])), col="orange")
lines (density(log(Data1_Eb_matrix[,7])), col="orange")
lines (density(log(Data1_Eb_matrix[,8])), col="red")
lines (density(log(Data1_Eb_matrix[,9])), col="red")
lines (density(log(Data1_Eb_matrix[,10])), col="red")
lines (density(log(Data1_Eb_matrix[,11])), col="red")
lines (density(log(Data1_Eb_matrix[,12])), col="green")
lines (density(log(Data1_Eb_matrix[,13])), col="green")
lines (density(log(Data1_Eb_matrix[,14])), col="green")
```

```
lines (density(log(Data1_Eb_matrix[,15])), col="green")
lines (density(log(Data1_Eb_matrix[,16])), col="dark green")
lines (density(log(Data1_Eb_matrix[,17])), col="dark green")
lines (density(log(Data1_Eb_matrix[,18])), col="dark green")
dev.off()


#Perform background correction by subtracting background values from foreground values
backCorMatrix <- backgroundCorrect.matrix(matrixE, matrixEb, method="auto", offset=0)
##This generates a matrix of background corrected probes in which some values are negative
##Negative values cannot be logged to make MA plots etc
##find out the lowest value in backCorMatrix
min(backCorMatrix)
#[1] -19994.54
#Therefore add 20,000 to the pre-background corrected values
backCorMatrix <- backgroundCorrect.matrix(matrixE, matrixEb, method="auto", offset=20000)


##Density Plot Post Background Corrected values
png("density_plot_all_data_Background_corrected_16122016.png")
plot (density(log(backCorMatrix[,2])), col="blue", xlim=c(4, 12))
lines (density(log(backCorMatrix[,1])), col="blue")
lines (density(log(backCorMatrix[,3])), col="blue")
lines (density(log(backCorMatrix[,4])), col="orange")
lines (density(log(backCorMatrix[,5])), col="orange")
lines (density(log(backCorMatrix[,6])), col="orange")
lines (density(log(backCorMatrix[,7])), col="orange")
lines (density(log(backCorMatrix[,8])), col="red")
lines (density(log(backCorMatrix[,9])), col="red")
lines (density(log(backCorMatrix[,10])), col="red")
lines (density(log(backCorMatrix[,11])), col="red")
lines (density(log(backCorMatrix[,12])), col="green")
lines (density(log(backCorMatrix[,13])), col="green")
```

```
lines (density(log(backCorMatrix[,14])), col="green")
lines (density(log(backCorMatrix[,15])), col="green")
lines (density(log(backCorMatrix[,16])), col="dark green")
lines (density(log(backCorMatrix[,17])), col="dark green")
lines (density(log(backCorMatrix[,18])), col="dark green")
dev.off()


#Generate boxplot from background corrected values
png("boxplot_background_corrected_16122016.png")
boxplot(log(backCorMatrix,2), las=2, range=1.5,
names=targets$SampleName, col=c( rep("blue",3),
rep("orange",4), rep("red",4),
rep("green",4), rep("dark green",3)))
dev.off()


#Quantile Normalisation
Data2<- normalizeBetweenArrays(Data1, method="quantile")


# Hierarchical Clustering of Activated and Non-activated OPC
data
###hierarchical clustering
hc<-hclust(as.dist(1-cor(Data2$E, method="pearson")),
method="average")
png("hclust_act_vs_nonact_post_norm.png")
plot(hc)
dev.off()


## Principal Component Analysis for Quantile Normalised
Activated and Non-activated OPC Data
# Install package used to generate plot
biocLite("scatterplot3d")
require(scatterplot3d)
library("scatterplot3d")
#Perform Principal Component Analysis using prcomp function
pca <- prcomp(t(Data2$E), scale=T)
#Specify which arrays belong to each sample group by numbering
```

```
pca_names <- c(1,2,3,4,1,2,3)

#Generate scatter plot showing variation between arrays for
principal components 1,2 and 3 with arrays coloured by sample
group

png("scatter3D_PCA_act_vs_nonact_norm.png")

s3d<-scatterplot3d(pca$x[,1:3], pch=19,
color=c(rep("green",4),rep("dark green",3)))

s3d.coords <- s3d$xyz.convert(pca$x[,1:3])

text(s3d.coords$x, s3d.coords$y, labels = pca_names,pos = 3,

offset = 0.5)

dev.off()


# Check data object created using prcomp (an object of class
prcomp), contains the correct information

names(pca)

# Calculate eigenvalues by raising the standard deviation for
each principal component to the power of 2

eig <- (pca$sdev)^2

# Calculate the variance captured by each principal component
using the eigenvalues

variance <- eig*100/sum(eig)

# Calculate the cumulative variances of the principal
components using the variance

cumvar <- cumsum(variance)

eig.pca <- data.frame(eig = eig, variance = variance,

                      cumvariance = cumvar)

# Check eigenvalue, variance and cumulative variance
calculations were successful

head(eig.pca)

#Use the function summary() to extract the eigenvalues and
variances from an object of class prcomp.

pca_eigenval_var <- summary(pca)

pca_eigenval_var


# Visualise the importance of principal components (PCs) by
generating a bar plot.

png("PCA_moyon_plot.png")

barplot(eig.pca[, 2], names.arg=1:nrow(eig.pca),
```

```
        main = "Variances",
        xlab = "Principal Components",
        ylab = "Percentage of variances",
        col ="steelblue")
dev.off()


# Generate table of eigenvectors for each feature(Entrez gene
RNA or control probe)
rotations <- pca$rotation
write.table(rotations,file="PCA_act_vs_nonact.txt",
quote=F,sep="\t",col.names=NA)


## Differential Gene Expression Analysis
#Define groups within the set of arrays:
groups <-
c('Activated_OPCs','Activated_OPCs','Activated_OPCs','Activate
d_OPCs','Nonactivated_OPCs','Nonactivated_OPCs','Nonactivated_
OPCs')
#Define comparisons:
design <- model.matrix(~0+factor(groups))
colnames(design) <- levels(factor(groups))


#Differential Gene Expression Analysis using Limma
d <- Data_quantilenorm
fit <- lmFit(d, design)
cont.dif <-
makeContrasts(Activated_OPCs.vs.Nonactivated_OPCs="Activated_O
PCs-Nonactivated_OPCs", levels=design)
fit2 <- contrasts.fit(fit, cont.dif)
fit2 <- eBayes(fit2)



# get results:
limma_table <- topTable(fit2, adjust="BH", n=nrow(d),
coef="Activated_OPCs.vs.Nonactivated_OPCs")
#order limma table by rowname
```

```
limma_table <- limma_table[
order(as.numeric(row.names(limma_table))),]

#add columns for IDs and Gene Names

limma_table["GeneName"] <- All_rownames$GeneName

limma_table["ID"] <- All_rownames$ID

#average replicate probes for the same gene

limma_table_avereps <- avereps(limma_table, ID=limma_table$ID)


#write table of limma output

write.table(limma_table_avereps,file="Limma_output_act.vs.nona
ct_avereps.txt", quote=F,

sep="\t",col.names=NA)
```